



Fibroblast uptake of prostate cancer vesicles

Alex Cocks

Thesis submitted for the degree
DOCTOR OF PHILOSOPHY

Division of Cancer and Genetics
School of Medicine
Cardiff University

2019

Declaration

The work has not been submitted in substance for any other degree or award at this or any other university or place of learning, nor is being submitted concurrently in candidature for any degree or other award.

Signed..... (candidate) Date.....

STATEMENT 1

This thesis is being submitted in partial fulfilment of the requirements for the degree of PhD.

Signed..... (candidate) Date.....

STATEMENT 2

This thesis is the results of my own independent work/investigation, except where otherwise stated.

Other sources are acknowledged by explicit references. The views expressed are my own.

Signed..... (candidate) Date.....

STATEMENT 3

I hereby give consent for my thesis, is accepted, to be available online in the University's Open Access repository and for inter-library loan, and for the title and summary to be made available to outside organisations.

Signed..... (candidate) Date.....

STATEMENT 4: PREVIOUSLY APPROVED BAR ON ACCESS

I hereby give consent for my thesis, is accepted, to be available online in the University's Open Access repository and for inter-library loans after expiry of a bar on access previously approved by the Academic Standards & Quality Committee.

Signed..... (candidate) Date.....

Acknowledgements

Firstly, I would like to thank Tenovus Cancer Care for funding my research. This project would not have been possible without their support.

Thank you to my main supervisor, Professor Aled Clayton, for all of his help and guidance throughout the project. I would like to thank my co-supervisors, Professor Arwyn Jones and Dr Peter Watson, and their teams in the schools of Pharmacy and Biosciences for their valuable contributions to the project. I am also grateful for the extra assistance given to me during my PhD, particularly from Dr Jason Webber, Professor Rachel Errington and Dr Zsuzsanna Tabi.

All of my lab friends and colleagues deserve a thank you for putting up with me all this time and helping me with some of my experiments. Thanks to Dr Alex Shephard, “Dr” Vincent Yeung, Miss Sara Veiga, Miss Amy Codd, and Mr Mark Gurney for being the father of the lab, as well as Thea, Lauren, Francesca, Muireann, Kate, Andreia, Marie, Rachel HJ, Dimitris, and everyone else from the labs at Velindre Cancer Centre and the Tenovus building, UHW.

I want to thank my parents and grandparents for being supportive of my seemingly never-ending time as a student, and Becky and Jon for letting me write at their house to escape mum and dad. A big thank you to Irina for all of her support, and to all my friends at Cardiff University and beyond for keeping me relatively sane over the past three years.

And a final thank you to Javier Uceda Fernandez. Javi was a good friend of mine who we lost in August of 2018. His energy and spirit were of great inspiration and help to me throughout my PhD.

Summary

Prostate tumours are typically accompanied by an aberrantly activated stroma, populated by myofibroblastic cells. These stromal cells support angiogenesis, and tumour growth in preclinical models. The tumour-derived factors responsible for the onset of stromal myofibroblasts remains poorly defined, but the secretion of transforming growth factor beta-1 (TGF β 1) is strongly implicated in the differentiation of various precursors, such as fibroblasts.

Like other epithelial cancers, prostate cancer cells secrete small extracellular vesicles, these carry TGF β 1 on their outer surface, and can deliver to fibroblasts, driving their differentiation into myofibroblasts. Unlike stimulation with soluble TGF β 1, the vesicle generated myofibroblast is analogous to those naturally occurring at the cancer site. The vesicle form of TGF β 1 delivery therefore is TGF β 1 dependent yet the phenotype arising is distinct from that driven by soluble TGF β 1. This observation suggests that vesicles are likely to co-deliver other factors to the fibroblast that collectively generate the in vivo-like myofibroblast differentiation response. Because uptake of acquired vesicles is documented as important in many other biological systems, we hypothesised that vesicle entry into fibroblasts was an important aspect of vesicle-mediated communication, and relevant for the differentiation response.

The aim of this project was to define the uptake process of prostate cancer vesicles by fibroblasts, to determine the intracellular fate of the vesicles once internalised, and the importance of cell entry in the complex differentiation process. To achieve this, we developed labelling techniques to fluorescently tag vesicles and used these to monitor vesicle uptake and intracellular trafficking in fibroblasts by fluorescence microscopy and flow cytometry.

Prostate cancer vesicles can be flexibly fluorescently labelled with the novel maleimide linked Alexa dyes. Using Alexa labelled vesicles, we found that fibroblast uptake primarily occurs through Clathrin-mediated endocytosis, and we reveal a role for vesicle-cell surface interaction in the uptake process. The vesicles were observed in early endocytic compartments, then transit through maturing endosomes reaching lysosomes within 2 hours of cellular uptake. Vesicle labelling with intraluminal fluorescent dyes revealed the requirement of vesicle

internalisation by fibroblasts to occur prior to luminal cargo delivery to the cell cytosol, and this escape occurs before the vesicles reach lysosomes. Vesicle internalisation by fibroblasts is independent of the TGF β 1 mediated stimulation of the cell and occurs even if fibroblast differentiation is blocked.

This study concludes that prostate cancer vesicles can deliver their intraluminal contents to fibroblasts after clathrin dependent vesicle endocytosis, but before reaching the lysosome. Any effect the intraluminal cargo has on the fibroblast phenotype would be independent of the TGF β 1 mediated effects.

Publications

Roberts-Dalton, HD., Cocks, A., Falcon-Perez, JM., Sayers, EJ., Webber, JP., Watson, P., Clayton, A., Jones, AT. 2017. Fluorescence labelling of extracellular vesicles using a novel thiol-based strategy for quantitative analysis of cellular delivery and intracellular traffic: *Nanoscale*, v. 9, p. 13693-13706.

Théry, C., Witwer, K.W., et al. 2018. Minimal information for studies of extracellular vesicles 2018 (MISEV2018): a position statement of the International Society for Extracellular Vesicles and update of the MISEV2014 guidelines: *Journal of Extracellular Vesicles*, v. 7, p. 1535750.

Witwer, K.W., et al. 2019. Biological membranes in EV biogenesis, stability, uptake, and cargo transfer: an ISEV position paper arising from the ISEV membranes and EVs workshop. *In preparation*.

Cocks, A., Clayton, A., et al. 2019. Endocytosis and intracellular trafficking of prostate cancer small extracellular vesicles in fibroblasts. *In preparation*.

Presentations

Oral presentation, **Runner up prize** – Division of Cancer and Genetics (DCG) day 2016, Cardiff University, UK

Image presentation, **Highly commended** – Images of Research 2016, Cardiff University, UK

Poster presentation – United Kingdom Extracellular Vesicle (UKEV) forum 2016, Oxford Brookes University, UK

Poster presentation – Postgraduate research (PGR) day 2017, Cardiff University, UK

Oral presentation – Cardiff Institute of Tissue Engineering and Repair (CITER) annual scientific meeting 2017, Cardiff University, UK

Seminar – DCG seminar series 2017, Cardiff University, UK

Oral presentation, **Best oral presentation** – UKEV 2017, University of Birmingham, UK

Poster presentation – International Society of Extracellular Vesicles (ISEV) annual meeting 2018, Barcelona, Spain

Oral presentation – UKEV 2018, University of Sheffield, UK

Grants

WM Thomas fund, £200 – Travel grant to attend ISEV2018 annual meeting, Barcelona, Spain, May 2018

Table of contents

Chapter 1- Introduction	1
1.1. Tumour microenvironment in solid cancer	2
1.1.1. Prostate cancer	2
1.1.2. Components of the tumour microenvironment	4
1.1.3. Cancer associated fibroblasts	7
1.1.4. Myofibroblast differentiation	8
1.2. Small extracellular vesicles	10
1.2.1. Defining EVs	11
1.2.2. Biogenesis and composition	13
1.2.3. Isolation of sEVs	18
1.2.4. Role of sEVs in cancer	19
1.2.5. Cancer sEVs induce myofibroblast differentiation	21
1.3. Cellular uptake and intracellular fate of sEVs	23
1.3.1. Evidence for delivery of sEV cargo	23
1.3.2. Endocytosis	25
1.3.3. Intracellular trafficking.....	29
1.3.4. Tools to monitor sEV uptake.....	32
1.3.5. Endocytosis of sEVs.....	34
1.3.6. Intracellular fate of sEVs	36
1.4. Hypothesis and aims	38
Chapter 2 – Materials and methods	39
2.1. Cell culture	40
2.1.1. Monolayer cell culture	40
2.1.2. CELLline bioreactors for DU145 cells	40
2.1.3. Fluorescence microscopy of fibroblasts.....	41
2.2. sEV isolation	42
2.2.1. Bioreactor supernatant collection	42
2.2.2. Sucrose cushion ultracentrifugation.....	42
2.3. sEV characterisation.....	43
2.3.1. Bicinchoninic acid protein assay	43
2.3.2. Nanoparticle tracking analysis	43
2.3.3. Western blot	44
2.3.4. Immunophenotyping plate assay.....	45
2.3.5. Cryo-electron microscopy	45
2.4. Detection of sEVs	47

2.4.1. Fluorescent labelling	47
2.4.2. Detection of fluorescent sEVs	48
2.4.3. Monitoring dye loss from sEVs	48
2.5. Uptake of sEVs	49
2.5.1. Detection of cellular uptake of fluorescent sEVs	49
2.5.2. Pharmacological inhibition	50
2.5.3. siRNA transfection	50
2.5.4. Quantitative polymerase chain reaction	51
2.5.5. Cell viability assays	53
2.5.6. Bacmam transfections	53
2.5.7. Time-lapse microscopy	53
2.5.8. Endocytic probes.....	54
2.5.9. Antibody labelling of sEVs.....	55
2.6. Assessment of sEV functional effects on fibroblasts	55
2.6.1. Fibroblast differentiation	55
2.6.2. Quantification of secreted HGF	55
2.7. Image and statistical analysis.....	56
Chapter 3 – Characterisation of DU145 derived small extracellular vesicles	59
3.1. Introduction	60
3.2. DU145 derived sEV characterisation	61
3.2.1. Vesicle morphology.....	61
3.2.2. Vesicle size distribution and purity assessment	65
3.2.3. Vesicle protein profiling	66
3.2.4. Functional potency assay - induction of myofibroblast differentiation	71
3.3. Discussion.....	74
Chapter 4 – Cellular uptake of DU145 derived small extracellular vesicles	78
4.1. Introduction	79
4.2. Fluorescent labelling of sEVs.....	81
4.2.1. Detection of labelled vesicles	81
4.2.2. Effect of labelling on myofibroblast differentiation	88
4.3. Detection of DU145 sEV uptake in fibroblasts.....	90
4.4. Endocytosis of DU145 sEVs.....	96
4.4.1. Evidence for endocytosis of DU145 sEVs.....	96
4.4.2. Pharmacological inhibition of uptake	99
4.4.3. siRNA mediated inhibition of uptake	103
4.5. Comparison of DU145 and LNCaP sEV uptake.....	108
4.6. Discussion.....	111

Chapter 5- Intracellular trafficking of small extracellular vesicles.....	118
5.1. Introduction	119
5.2. Trafficking kinetics of sEVs.....	120
5.2.1. Uptake kinetics of sEVs compared to endosomal probes.....	120
5.2.2. Time-lapse microscopy of intracellular trafficking of sEVs	123
5.3. Endosomal localisation of sEVs in fibroblasts	127
5.3.1. Co-localisation of sEVs with Bacmam labelled endocytic compartments	127
5.3.2. Colocalisation of DU145 sEVs with endosomal probes	131
5.4. Tracking intraluminal sEV contents.....	135
5.4.1. Fluorescent labelling of sEV lumen	136
5.4.2. Characterisation of luminally labelled sEVs	140
5.4.3. Uptake of labelled sEVs.....	146
5.4.4. Dual-labelled sEVs.....	154
5.4.5. Uptake of dual-labelled sEVs	156
5.4.6. Tracking sEV intraluminal dye escape.....	160
5.5. Discussion.....	164
Chapter 6- Modulation of small extracellular vesicle uptake by fibroblasts	171
6.1. Introduction	172
6.2. Effect of endocytosis inhibitors on sEV induced myofibroblast differentiation.....	174
6.3. Blockade of sEV surface Integrins	181
6.3.1. RGD peptide mediated blocking of sEV uptake by fibroblasts	181
6.3.2. Detection of integrin subunits on sEV surface.....	183
6.3.3. Integrin antibody blockade of sEV internalisation by fibroblasts	187
6.4. Discussion.....	191
Chapter 7- General discussion	196
7.1. Summarising discussion	197
7.2. Future directions.....	202
References	205

Figures and tables

Figure 1.1: The tumour microenvironment.....	6
Figure 1.2: TGF β 1-mediated cancer cell-fibroblast crosstalk.....	9
Figure 1.3: sEV composition.....	17
Figure 1.4: Mechanisms of endocytosis.....	27
Figure 1.5: The endosomal system.....	31
Table 2.1: Primary antibodies.....	46
Table 2.2: siRNA sequences for knockdown of endocytic regulators.....	51
Table 2.3: List of materials.....	57
Figure 3.1: Cryo-EM of sucrose cushion purified DU145 derived sEV isolates.....	63
Figure 3.2: Size distribution of DU145 derived sEVs.....	67
Table 3.1: Particle and protein concentrations of DU145 derived sEVs...	68
Figure 3.3: Western blot characterisation of DU145 derived sEVs versus DU145 cells.....	69
Figure 3.4: Immunophenotyping plate assay for detection of DU145 derived sEV tetraspanins.....	70
Figure 3.5: Morphology of primary lung fibroblasts.....	72
Figure 3.6: Myofibroblast differentiation induced by DU145 derived sEVs.....	73
Figure 3.7: Schematic summary of chapter 3.....	77
Figure 4.1: Dose and treatment time optimisation of DU145 derived sEVs with Alexa dyes.....	82
Figure 4.2: Chosen treatment conditions for Alexa labelling of DU145 derived sEVs.....	83
Figure 4.3: Effect of N-acetyl-L-cysteine (NaLc) on Alexa labelling of DU145 derived sEVs.....	84
Figure 4.4: Visualisation of DU145 sEVs labelled with Alexa dyes.....	86
Figure 4.5: NTA of DU145 sEVs labelled with Alexa dyes.....	87
Figure 4.6: Effect of Alexa labelling on DU145 sEV induced myofibroblast differentiation.....	89
Figure 4.7: Staining patterns of fibroblasts treated with Alexa594-sEVs	92
Figure 4.8: Optimisation of Alexa594-sEV treatment dose for fibroblast uptake studies.....	93
Figure 4.9: Optimisation of Alexa594-sEV treatment time for fibroblast uptake studies.....	94
Figure 4.10: Use of flow cytometry to detect DU145 sEV uptake by fibroblasts.....	95
Figure 4.11: Temperature dependent uptake of DU145 sEVs by fibroblasts.....	97
Figure 4.12: Movement of Alexa633-sEVs in fibroblasts.....	98
Figure 4.13: Effect of pharmacological endocytosis inhibitors on fibroblast viability.....	101
Figure 4.14: Effect of pharmacological inhibitors on DU145 sEV uptake by fibroblasts.....	102
Figure 4.15: Confirmation of target mRNA knockdown by qPCR.....	105
Figure 4.16: Confirmation of target protein knockdown by Western blot.....	106
Figure 4.17: Effect of siRNAs on fibroblast viability and uptake of DU145 sEVs.....	107

Figure 4.18: Comparative uptake of DU145 derived sEVs versus LNCaP derived sEVs by fibroblasts.....	109
Figure 4.19: Co-localisation of DU145 derived sEVs and LNCaP derived sEVs following uptake by fibroblasts.....	110
Figure 4.20: Schematic summary of chapter 4.....	113
Figure 5.1: Fibroblast uptake kinetics of Alexa488-sEVs versus endocytic probes.....	122
Figure 5.2: Clustering of Alexa633-sEVs in fibroblast.....	124
Figure 5.3: 72 hour time-lapse of Alexa633-sEV signal in fibroblast.....	126
Figure 5.4: Co-localisation of Alexa594-sEVs and Bacmam transduction reagents in fibroblasts.....	129
Figure 5.5: Antibody staining of endosomal compartments in fibroblasts.....	130
Figure 5.6: Co-localisation of Alexa594 sEVs and Tf488 over time in fibroblasts.....	133
Figure 5.7: Co-localisation of Alexa594 sEVs and Dx488 over time fibroblasts.....	134
Figure 5.8: Dosing of intraluminal dyes for sEV labelling.....	138
Figure 5.9: Signal of chosen doses of intraluminal dyes for sEV labelling.....	139
Figure 5.10: Visualisation of sEVs labelled with intraluminal dyes.....	143
Figure 5.11: NTA of sEVs labelled with intraluminal dyes.....	144
Figure 5.12: Monitoring loss of intraluminal dyes from sEVs over time..	145
Figure 5.13: Fibroblast uptake of sEVs labelled with intraluminal dye...	148
Figure 5.14: Staining patterns of fibroblasts treated with sEVs labelled with intraluminal dyes.....	149
Figure 5.15: Co-localisation of SYTO-sEVs and Mitotracker in fibroblasts.....	150
Figure 5.16: Co-localisation of Alexa488-sEVs and Mitotracker in fibroblasts.....	151
Figure 5.17: Fibroblast uptake inhibition of sEVs labelled with intraluminal dyes.....	153
Figure 5.18: Co-localisation of dual-labelled sEVs.....	157
Figure 5.19: Fibroblast uptake of CFSE-Alexa594-sEVs.....	158
Figure 5.20: Fibroblast uptake of SYTO-Alexa594-sEVs.....	159
Figure 5.21: Detection of SYTO-Alexa594-sEVs by time-lapse microscopy.....	162
Figure 5.22: Monitoring fibroblast uptake of SYTO-Alexa594-sEVs by time-lapse microscopy.....	163
Figure 5.23: Schematic summary of chapter 5.....	167
Figure 6.1: Fibroblast stimulation with a reduced Du145 derived sEV dose.....	177
Figure 6.2: Effect of endocytic inhibitors on sEV induced onset of α SMA expression in fibroblasts.....	178
Figure 6.3: Effect of endocytic inhibitors on sEV induced production of HGF by fibroblasts.....	179
Figure 6.4: Effect of TGF β neutralising antibody on sEV uptake by fibroblasts.....	180
Figure 6.5: RGD mediated blockade of DU145 derived sEV internalisation by fibroblasts.....	182

Figure 6.6: Detection of integrin subunits on DU145 derived sEVs by immunophenotyping plate assay.....	185
Figure 6.7: Dosing of anti-integrin antibodies for detection saturation of DU145 derived sEV integrins by immunophenotyping plate assay.....	186
Figure 6.8: Anti-integrin antibody mediated blockade of DU145 derived sEV internalisation by fibroblasts.....	189
Figure 6.9: Anti-CD9 mediated blockade of DU145 derived sEV internalisation by fibroblasts.....	190
Figure 6.10: Schematic summary of chapter 6.....	195
Figure 7.1: Schematic summary - Endocytosis and intracellular processing of prostate cancer derived sEVs by fibroblasts.....	201

Abbreviations

αSMA	Alpha-smooth muscle actin
ADT	Androgen deprivation therapy
ALIX	Apoptosis-linked gene 2-interacting Protein X
ANOVA	Analysis of variance
BCA	Bicinchoninic acid
BPH	Benign prostatic hyperplasia
BSA	Bovine serum albumin
cDNA	Complementary deoxyribonucleic acid
Cal	Calcein AM
CD	Cluster of differentiation
CDE	Caveolin dependent endocytosis
CFSE	Carboxyfluorescein diacetate succinimidyl ester
CME	Clathrin mediated endocytosis
Cryo-EM	Cryogenic electron microscopy
CTR	Control
D₂O	Deuterium oxide
DAPI	4',6-diamidino-2-phenylindole
DMEM	Dulbeccos' Modified Eagle's Medium
DNA	Deoxyribonucleic acid
DRE	Digital rectal examination
DTT	Dithiothreitol
Dx	Dextran
Dye CTR	Control for free dye
ECM	Extracellular matrix
EE	Early endosome
EEA	Early endosome antigen
EIPA	5-(N-Ethyl-N-isopropyl) amiloride
ELISA	Enzyme-linked immunosorbent assay
EM	Electron microscopy
ER	Endoplasmic reticulum
ESCRT	Endosomal sorting complex required for transport
EV	Extracellular vesicle
FBS	Foetal bovine serum
FBS^{ev}	Extracellular vesicle depleted foetal bovine serum
GAPDH	Glyceraldehyde 3-phosphate dehydrogenase
GFP	Green fluorescent protein
HGF	Hepatocyte growth factor
HRP	Horseradish peroxidase
HSP	Heat shock protein
HSPG	Heparan sulphate proteoglycan
ILV	Intraluminal vesicle
ISEV	International Society of Extracellular Vesicles
LAMP	Lysosomal associated membrane protein
LDS	Lithium dodecyl sulphate
LE	Late endosome
mRNA	Messenger ribonucleic acid
miRNA	Microribonucleic acid
MFI	Mean fluorescent intensity
MHC	Major histocompatibility complex

MMP	Matrix metalloproteinase
MSC	Mesenchymal stem cell
MV	Microvesicle
MVB	Multi vesicular body
NTA	Nanoparticle tracking analysis
PAK1	P21 activated kinase 1
PBS	Phosphate buffered saline
PCa	Prostate cancer
PCR	Polymerase chain reaction
PFA	Paraformaldehyde
PIN	Prostatic intraepithelial neoplasia
PMSF	Phenylmethane sulfonyl fluoride
PSA	Prostate specific antigen
qPCR	Quantitative polymerase chain reaction
R18	Octadecyl rhodamine B chloride
RFP	Red fluorescent protein
RIPA	Radioimmunoprecipitation assay
RNA	Ribonucleic acid
RPMI	Roswell Park Memorial Institute
siRNA	Short interfering ribonucleic acid
SDS	Sodium dodecyl sulphate
SEC	Size exclusion chromatography
SEM	Standard error of the mean
sEV	Small extracellular vesicle
SNARE	Soluble N-ethylmaleimide-sensitive factor attachment protein receptors
SYTO	SYTO RNASelect green fluorescent cell stain
TAM	Tumour associated macrophage
Tf	Transferrin
TGFβ	Transforming growth factor β
TME	Tumour microenvironment
TRF	Time resolved fluorescence
TSG	Tumour susceptibility gene
VEGF	Vascular endothelial growth factor
WST	Water soluble Tetrazolium

Chapter 1- Introduction

1.1. Tumour microenvironment in solid cancer

Cancer is one of the leading causes of death in the developed world. In the UK, cancer accounts for more than a quarter of deaths each year (CRUK, 2016a).

Cancer can be characterised by generally accepted features, including genomic instability, uncontrolled proliferation, induction of angiogenesis, immune evasion, invasion and metastasis (Hanahan and Weinberg, 2011).

Prostate cancer (PCa) is the most common cancer in British males, and is responsible for more than 10,000 deaths per year in the U.K (CRUK, 2016b). Risk of developing disease increases with age (Leitzmann and Rohrmann, 2012), and with an ever-ageing population, PCa is likely to become a greater burden on health services in the coming years.

1.1.1. Prostate cancer

The prostate is a small organ in males, located at the base of the bladder surrounding the urethra. The prostate glands secrete fluid which contributes to semen, and the organ helps to expel semen during ejaculation through contraction (Kumar and Majumder, 1995). Many small epithelial glands are present in a uniform pattern, but during the progression of cancer, the disrupted tissue architecture and glands become more irregular in shape and size. Histology of a prostate biopsy is used to score the grade of disease (Gleason score), the classification of cancer based on these scores is used as a prognostic marker for PCa (Gleason and Mellinger, 1974). In aggressive disease, metastasis from the primary tumour site can occur, most commonly to bone (Bubendorf et al., 2000), which is incurable and leads to increased morbidity.

Besides age, the most strongly associated risk factors for PCa are race and family history of disease, and less established factors, such as diet and exercise (Leitzmann and Rohrmann, 2012). Prostatic intraepithelial neoplasia (PIN) is a condition characterised by the abnormal appearance and proliferation of intraepithelial cells. PIN is also a significant risk factor for development of PCa and is considered a precursor to malignant disease (Montironi et al., 2000).

Current methods used to diagnose PCa are problematic, some due to lack of accuracy, and others due to their invasiveness. Prostate epithelial cells secrete a

protein called prostate specific antigen (PSA). PSA has been used as a screening tool for PCa since the 1980s. However, PSA levels generally increase with age (Oesterling et al., 1993), and are also increased in other conditions such as benign prostatic hyperplasia (BPH) (Stamey et al., 1987). Furthermore, PCa can present with normal PSA levels (Nishio et al., 2003). This lack of specificity shows PSA is not ideal for detecting PCa and highlights the need for a more specific diagnostic method. Digital rectal examination (DRE) is often used when cancer is suspected to detect nodules on the prostate, as an additional tool to determine whether there are any obvious abnormalities. PSA and DRE together are not enough to definitively diagnose PCa, so prostate tissue biopsy is usually carried out to give a more accurate diagnosis. Tissue samples are graded based on the Gleason scoring system (Gleason and Mellinger, 1974), with a high score of 8-10 considered an aggressive cancer, with a poor prognosis. PSA and Gleason score are used to classify patients by risk of treatment failure (Hernandez et al., 2007). Tissue biopsy, is an invasive test and can give false negative results if the diseased tissue is missed during biopsy, and since current liquid biopsy are insufficient to diagnose disease, there is an interest in developing an accurate and non-invasive diagnostic marker (Tian et al., 2018).

In early stage disease in which the cancer is confined to the primary tumour site, monitoring of the disease is often sufficient, alternatively patients can undergo radical prostatectomy (Murphy et al., 1994), although side effects such as impotence and incontinence can occur. In metastatic disease, prostatectomy is no longer helpful. Radiotherapy is an alternative treatment course, in which the prostate is targeted with high energy x-rays, 3D conformal radiotherapy being a popular tool, which allows the radiation beams to target the prostate more specifically, thus inflicting less damage to surrounding tissues (Heidenreich et al., 2014). In PCa, testosterone is known to stimulate proliferation in cancer cells and promote tumour growth (Ahmad et al., 2008). Androgen deprivation therapy (ADT), through orchiectomy or treatment with anti-androgen agents remain widely used tools for slowing cancer growth, particularly in aggressive disease (Rove and Crawford, 2014). Though ADT can be initially effective in slowing tumour growth, castration resistance develops, when the tumour continues to grow despite the ADT (Chandrasekar et al., 2015). Chemotherapy is used in

patients with advanced disease and castrate resistance. Docetaxel is a widely used cytotoxic drug used in PCa, which shows survival benefits (Tannock et al., 2004), it binds microtubules in dividing cells preventing mitosis (Pienta, 2001), hence hair loss is a common side effect.

In prostate tumour tissue, in addition to the population of proliferative cancer cells, there is a reactive environment containing other cells which work to aid tumour growth and survival, termed the tumour microenvironment (TME). To better understand PCa progression, and identify future targets for diagnosis and therapy, it is important to appreciate the role of the TME in the disease pathology.

1.1.2. Components of the tumour microenvironment

In healthy tissues, all cell types in the tissue stroma work synergistically to maintain the local microenvironment and contribute to the functioning of the epithelial glands. Conversely, cells which usually preserve homeostasis in health, have been shown to support tumour survival and growth in cancer (Wang et al., 2017). Figure 1.1 depicts the cells that are part of the tumour microenvironment and are involved in supporting disease progression (Prajapati and Lambert, 2016).

In a growing tumour, the high number of malignant cells need an increased blood supply to satisfy their nutrient requirements; an inhibition of angiogenesis in a tumour is capable of halting growth (Holmgren et al., 1995). This need for new vessel formation leads to induction of persistent angiogenesis in tumours (Folkman et al., 1971). Tumour vasculature is abnormal in both structure and function (Jain, 2005); branching is chaotic, and the vessel lumen is uneven and leaky. Vessel leakiness raises the interstitial fluid pressure, resulting in uneven blood flow and distribution of nutrients, furthermore drug delivery to the tumour is impaired. Aberrant vasculature is accompanied by a low pericyte coverage, this is associated with poor prognosis (O'Keeffe et al., 2008). Tumours also drive lymphangiogenesis, and again this is linked to poor outcome (Alitalo, 2011). Abnormal blood flow is well characterised in aggressive tumours, and anti-angiogenic therapy is often used in treatment of cancer (Cao et al., 2011), bevacizumab, an anti-VEGF antibody based therapy, for example is used in the treatment of colorectal cancer (Hurwitz et al., 2004), though is associated with a number of side effects.

Introduction

Local adipose cells contribute to cancer progression (Wang et al., 2017), secreting pro-inflammatory factors, recruiting immune cells and supporting angiogenesis (Gilbert and Slingerland, 2013). Increased adiposity in obesity enhances the role of adipose cells, thus increasing the risk of aggressive disease in the obese.

Recruitment of immune cell is key step in cancer progression. The immune system usually fights infection and destroys damaged cells, however in neoplastic growths, this is not always the case. Immune evasion and inflammation in the TME are now considered hallmarks of cancer (Hanahan and Weinberg, 2011). In the TME, macrophages, which usually digests damaged tissue, convey a cancer promoting phenotype, and are termed tumour associated macrophages (TAMs) (Qian and Pollard, 2010). TAMs secrete factors to promote angiogenesis (Lin et al., 2006), aid tumour invasion (Condeelis and Pollard, 2006), and even drive chemoresistance (Challagundla et al., 2015; Shree et al., 2011). The tumour interacts with other immune cells to promote immunosuppression in order for the tumour to evade immune responses. For example, recruitment of regulatory T cells (Tregs) via tumour chemokines (Curiel et al., 2004), results in reduced survival (Bates et al., 2006), likely through immunosuppression (Hsieh et al., 2012).

In tumours, there is increased extracellular matrix (ECM) deposition, as a result, tumour tissue is often stiffer than its healthy counterpart (Weigelt and Bissell, 2008). Elevated desmoplasia increases interstitial pressure within the tumour tissue, inhibiting nutrient distribution, and causing cell necrosis (Brown et al., 2004). The physical barrier created through ECM deposition contributes to drug resistance (Miyamoto et al., 2004). High expression of matrix metalloproteinases (MMPs), enzymes which carry out ECM remodelling, in the TME correlate with poor outlook in cancer (Bergamaschi et al., 2008). It is believed that overexpression of MMPs may help degrade the basement membrane enabling tumour invasion and metastasis (Lu et al., 2011). ECM deposition and MMP secretion in the TME is carried out in particular by tumour associated myofibroblasts (DeClerck, 2000; Lagacé et al., 1985). These fibroblasts orchestrate tissue remodelling and this loss of architecture in cancer is considered a vital, rate limiting step in disease progression.

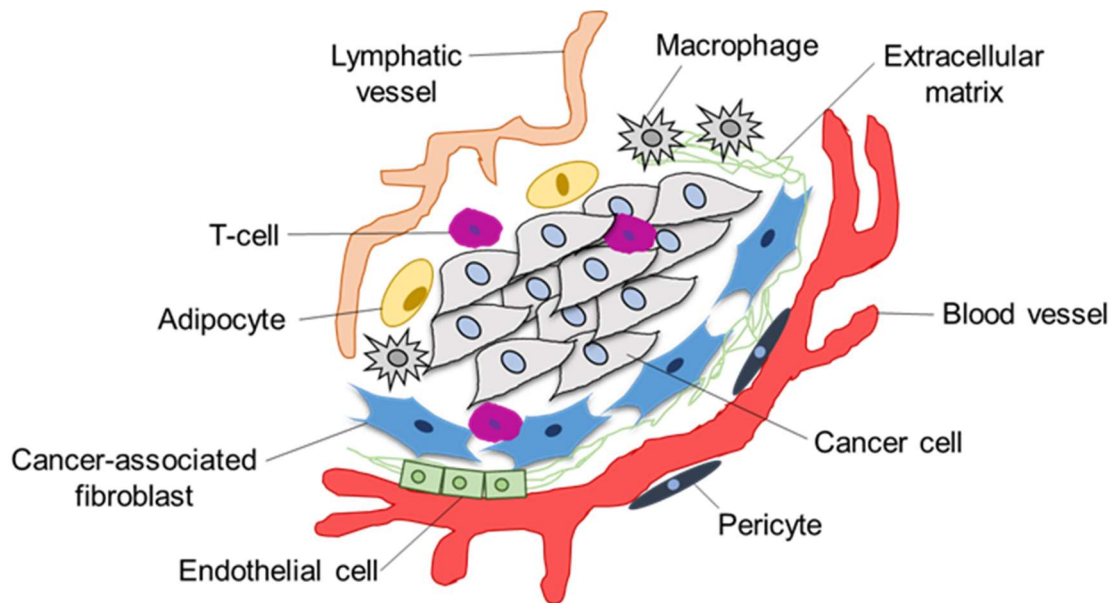


Figure 1.1. The tumour microenvironment. A schematic illustration of the components of the tumour microenvironment in solid cancers, cancer cells educate and are supported by local cells to aid tumour growth and survival. Cancer associated fibroblasts can be seen at the leading edge of the tumour (adapted from Prajapati and Lambert, 2016).

1.1.3. *Cancer associated fibroblasts*

Fibroblasts are elongated cells of mesenchymal origin, thin and spindle-like, identified by the intermediate filament protein Vimentin (Franke et al., 1978). In health, the fibroblast is a quiescent cell, becoming activated to be involved in wound healing (Gabbiani et al., 1971). In wound healing, fibroblasts act to repair the injury through promotion of angiogenesis, ECM deposition and contraction, then after the wound is healed, the number of activated myofibroblasts falls as they undergo apoptosis (Tomasek et al., 2002). In tumours, activated myofibroblasts are present (Lagacé et al., 1985), though in contrast to the wound healing cells, the myofibroblasts present in tumours are considered to be in a persistent wound healing state as they are present in large numbers and do not return to their quiescent state (Dvorak, 1986).

In healthy prostate tissue, stromal smooth muscle cells are abundant (Tuxhorn et al., 2002), and there are few fibroblasts (Rønnov-Jessen et al., 1996); in contrast, the reactive stroma present in tumours contains many more fibroblasts. The smooth muscle cells in PCa stroma are replaced by myofibroblasts, characterised by dual expression of Vimentin and α smooth muscle actin (α SMA) (Tuxhorn et al., 2002). Cancer associated myofibroblasts have been identified in prostate (Olumi et al., 1999), breast (Rønnov-Jessen et al., 1996), colon cancer (Martin et al., 1996) and others, this phenotype is indicative of solid cancer stroma. The myofibroblast phenotype is present in prostatic intraepithelial neoplasia (PIN) lesions (Tuxhorn et al., 2002), though in a smaller proportion to those present in a high Gleason score cancer. Since PIN is thought to be a precursor to PCa (Montironi et al., 2000), myofibroblast differentiation probably occurs very early in the progression of cancer. A high stroma ratio in tumours is linked to poor prognosis in cancer (Moorman et al., 2012; Yanagisawa et al., 2007).

The presence of myofibroblasts and association with aggressive disease is well documented. These cells are not just bystanders of the tumour's growth, but actively work to promote cancer progression (Olumi et al., 1999). Cancer myofibroblasts increase invasiveness of cancer cells (Dimanche-Boitrel et al., 1994), due to the various factors the activated cells produce. Cancer myofibroblasts are the principal source of vascular endothelial growth factor

(VEGF) in the TME (Fukumura et al., 1998), and they secrete hepatocyte growth factor (HGF) (De Wever et al., 2004), together they promote endothelial cell proliferation (Xin et al., 2001). HGF also stimulates proliferation and motility in epithelial cells (Bhowmick et al., 2004). MMP production by activated fibroblasts degrades the ECM, increasing tumour invasiveness (Boire et al., 2005). Myofibroblasts are found at the leading edge of the tumour, and ECM deposition provides tracks for cancer cells to aid invasion (Gaggioli et al., 2007).

1.1.4. Myofibroblast differentiation

Tumour promoting myofibroblasts are of unclear physiological origin within the prostate, they may originate from multiple sources, such as: resident fibroblasts (Desmoulière et al., 1993), as well as endothelial cells (Zeisberg et al., 2007), mesenchymal stem cells (Chowdhury et al., 2015), and epithelial cells (Petersen et al., 2003). These activated myofibroblasts exhibit a pro-tumoural phenotype, which is induced by the cancer cells (Rønnov-Jessen and Petersen, 1993).

Fibroblasts can undergo phenotypic change following stimulation by growth factors. Transforming growth factor beta-1 (TGF β 1), secreted by cancer cells (Rønnov-Jessen and Petersen, 1993), is an important inducer of differentiation, and in PCa, TGF β 1 is required for generating a tumour supporting stroma (Verona et al., 2007). TGF β 1 binds TGF β type II receptor, which recruits TGF β type I receptor and initiates SMAD signalling, SMAD complexes translocate to the nucleus where they act as transcription factors, driving myofibroblast differentiation (Verona et al., 2007). α SMA negative fibroblasts become contractile α SMA positive myofibroblasts, indicating differentiation has occurred (Rønnov-Jessen and Petersen, 1993). These TGF β 1 stimulated fibroblasts are now capable of supporting the tumour promoting functions already discussed. The crosstalk between cancer cell and fibroblast is schematically presented in figure 1.2 (Erdogan and Webb, 2017).

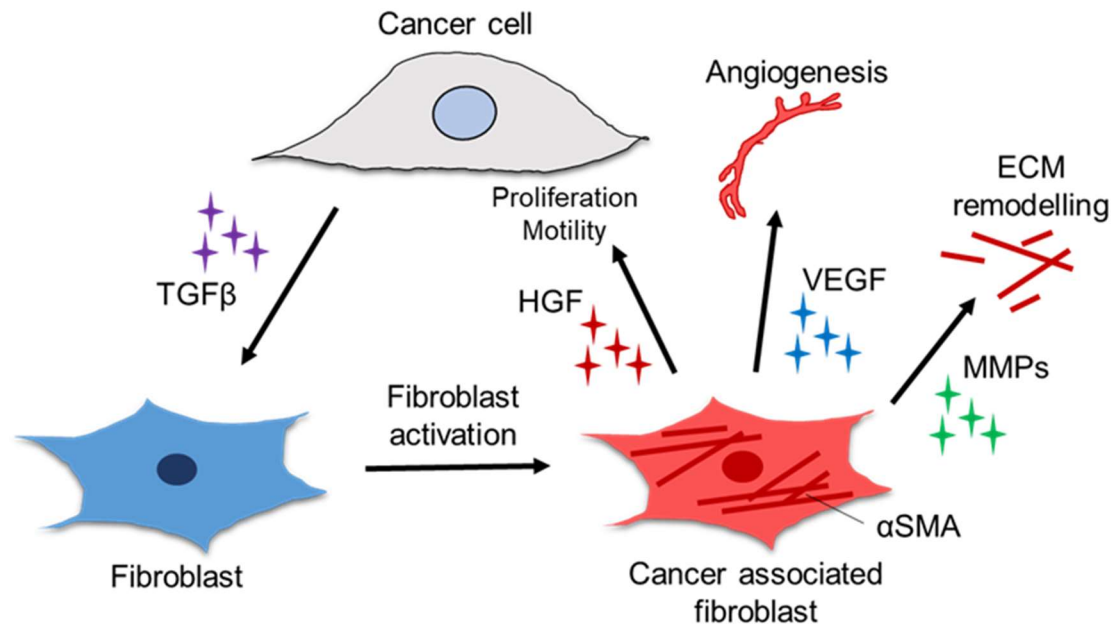


Figure 1.2. TGFβ1-mediated cancer cell-fibroblast crosstalk. TGFβ1 secreted by cancer cells can stimulate fibroblasts, generating alpha-smooth muscle actin (αSMA) positive myofibroblasts. These activated fibroblasts secrete various factors, promoting extracellular matrix (ECM) remodelling, tissue angiogenesis, and proliferation and motility of the cancer cells. Through these actions, cancer-associated fibroblasts support the growth and survival of tumours (adapted from Erdogan and Webb, 2017).

Although TGF β 1 triggers myofibroblast differentiation, it has been demonstrated that soluble TGF β 1 alone fails to generate the disease promoting phenotype in stromal fibroblasts (Webber et al., 2015b), whereas stimulation of fibroblasts with TGF β 1-positive PCa derived small extracellular vesicles (sEVs) is able to induce the phenotype which facilitates tumour growth and angiogenesis. This reveals a key role for PCa sEVs in the progression of cancer.

1.2. Small extracellular vesicles

sEVs are cell derived nanovesicles of 30-150nm in diameter (Pan et al., 1985; Raposo et al., 1996; van Niel et al., 2001). An early visualisation of these vesicles by electron microscopy was noted in the cartilage tissue of mice in the 1960's (Anderson, 1969). In the 1980s, these vesicles were named exosomes (Johnstone et al., 1987), and were found to originate from multivesicular bodies (MVBs) within the cell. Exosomes were first identified in maturing red blood cells, as a means of Transferrin receptor disposal (Harding et al., 1983). Later, B lymphocyte derived vesicles were found to play a role in antigen presentation (Raposo et al., 1996), revealing that exosomes may be key components to cell signalling and not just a means of removing waste. Following on from these early studies, sEV secretion has been demonstrated in many cell types, including dendritic cells (Zitvogel et al., 1998), fibroblasts (Richards et al., 2017), mesenchymal stem cells (Lai et al., 2011), epithelial cells (van Niel et al., 2001), and notably, tumour cells (Wolfers et al., 2001). sEVs are also present in most biological fluids (Keller et al., 2011).

In addition to MVB derived exosomes, sEVs, are also reported to be secreted directly from the plasma membrane (Booth et al., 2006). Furthermore, cells secrete larger vesicles up to 1000nm in size (Hess et al., 1999; Trams et al., 1981), mostly of plasma membrane origin. The nomenclature describing these vesicles is somewhat confusing, with many terms having been used to describe vesicles sized between 30-1000nm (Gould and Raposo, 2013).

1.2.1. *Defining EVs*

Nomenclature

Cell derived vesicles are principally viewed as derived from either endosomal or plasma membrane origin. Often, the term extracellular vesicle (EV) is used as a blanket term to describe all secreted vesicles, regardless of their size or origin. Whilst exosomes are described as the sEVs formed in MVBs, the term is almost universally used to describe sEVs in general, since there is currently no way to distinguish them from plasma membrane derived sEVs. Cells secrete other large vesicles >200nm which shed directly from the plasma membrane, as microvesicles (MVs) (Heijnen et al., 1999), also called ectosomes (Hess et al., 1999), apoptotic bodies have also been described (Hristov et al., 2004). The term exosome has also been used to describe these larger vesicles (Trams et al., 1981). As of 2014, exosome was the most popular term used to describe EVs (Lötvall et al., 2014).

Recently, the International Society for Extracellular Vesicles (ISEV) set out guidelines in order to normalise the terminology used to name EVs (Théry et al., 2018). Since it remains challenging to identify the exact origin of an isolated population of vesicles, the position paper proposes that EVs <200nm be termed small extracellular vesicles, and EVs >200nm large extracellular vesicles. Herein, the sEVs isolated and used in this study shall therefore be referred to as sEVs, not exosomes, as their exact subcellular origin cannot be determined.

EV characterisation

As studies with EVs typically require isolation of the vesicles from the cell supernatant/bodily fluid, characterisation of EV preparations should be carried out to assess the degree of isolation/purification which has been achieved. Demonstration of successful EV isolation increases the confidence in any results attributed to EVs (Lötvall et al., 2014).

Evaluation of EV proteins is an important characterisation step, since many proteins are enriched in EVs (Raposo and Stoorvogel, 2013), and this can be shown by standard protein detection methods, such as Western blot, enzyme-linked immunosorbant assay (ELISA) and flow cytometry. Demonstrating absence of proteins not associated with EVs is often used as further evidence for separation of

the vesicle from the parent cell. Calnexin, an endoplasmic reticulum (ER) protein, is factor not typically found on EVs, because it is not present in MVBs or on the plasma membrane, and is not detectable by Western blot in high quality vesicle isolates (Wolfers et al., 2001). Presence of Calnexin for example, would indicate contamination of the isolates by intracellular constituents. Online databases are available, collating EV characterisation data from hundreds of primary papers (Kalra et al., 2012; Kim et al., 2015), although the quality of vesicle isolates varies considerably across studies, as do the methods of isolation and analysis. One should approach such databases with some caution with regards to the validity of some findings.

Visualisation of vesicles by electron microscopy (EM) provides both evidence of vesicle shaped structures, and the presence/absence of large aggregated and non-vesicular material. Previously, EM revealed sEVs had a cup shaped morphology and this was considered characteristic of the vesicles (Raposo et al., 1996). The cup shape was later found to be an artefact of the sample fixation procedure for EM, likely due to osmotic damage, and the true spherical shape of the vesicle is retained and can be seen when the sample is prepared using cryo-EM techniques (Conde-Vancells et al., 2008), or variations such as high pressure freezing. Using immuno-EM can reveal expression of EV related proteins (Théry et al., 2006).

Whilst EM allows counting of both vesicle number and vesicle size within a given area, this can be biased since it only samples a relatively small number of vesicles and therefore may not be representative of the whole population. Nanoparticle tracking analysis (NTA) is an alternate method for quantifying the size and concentration of vesicles in solution (Dragovic et al., 2011; Soo et al., 2012). EVs exhibit Brownian motion in solution, and their velocity in suspension is related to their size. Using optical approaches, EVs in suspension are illuminated and scatter light. EV movement (seen by the movement of the scattered light) is tracked by the NTA software. NTA software generates data detailing the concentration of vesicles in solution, and the size of every detected particle which can be plotted as a histogram to provide a size distribution across the whole sample (Dragovic et al., 2011; Soo et al., 2012). A limitation however of light scattering based techniques is particles <50nm in size are difficult to detect. These very small sized vesicles in a sample are therefore likely to be underestimated. Although conventional flow

cytometry is not sensitive enough to detect individual sEVs, high resolution alternatives are being explored to allow for sophisticated high throughput analysis of single vesicles (Nolte-'t Hoen et al., 2012).

1.2.2. Biogenesis and composition

Biogenesis and secretion

EVs originate from MVBs and direct plasma membrane budding; secretion of EVs by cells has been described through both of these mechanisms (Muralidharan-Chari et al., 2009), and there are likely other routes of manufacture of less well characterised vesicles, or vesicle-like structures. Although sEV generation through plasma membrane budding has been described (Booth et al., 2006), this biogenesis pathway is difficult to distinguish from the MVB mechanism, since MVBs eventually fuse with the plasma membrane to release their sEVs and so in effect become part of the plasma membrane themselves. Moreover, the most defined and discussed mechanism for sEV biogenesis is through MVB formation and release (Raposo and Stoorvogel, 2013).

Following early endosome formation, late endosomes arise from endosome maturation (Stoorvogel et al., 1991). Here, MVBs are created, as intraluminal vesicles (ILVs) form from inward budding of the endosome membrane into the endosome lumen. MVBs often fuse with lysosomal compartments, however different subsets of MVBs are likely to exist (Colombo et al., 2014), and some subsets are destined to fuse with the plasma membrane to release these sEVs as exosomes, into the extracellular space (Raposo et al., 1996; Verweij et al., 2018).

Generation of ILVs is largely driven by a large group of proteins from the endosomal sorting complex required for transport (ESCRT). The components of the ESCRT work together to: recruit endosomal membrane proteins and vesicle associated cargo, initiate inward budding of the membrane, and scission of the vesicle, forming an ILV (Hanson and Cashikar, 2012). Ceramide dependent ILV production independent of ESCRT proteins has also been described (Trajkovic et al., 2008), though the ESCRT independent mechanisms are less well defined.

After ILV production, MVBs destined for the plasma membrane are transported under the regulation of Rab proteins (Stenmark, 2009). Secretion of sEVs can be

perturbed through knockdown of some of these proteins. sEV secretion by cells is inhibited by knockdown of Rab11b, Rab35 (Yeung et al., 2018), Rab27a and Rab27b (Bobrie et al., 2012b; Ostrowski et al., 2010). Inhibition of one of these Rab proteins may result in a partial reduction in sEV secretion, sEVs may be being secreted by MVBs regulated by different Rab proteins, or a significant number through plasma membrane budding. Yeung et al found that knockdown of Rab35, but not Rab11b in PCa cells rendered the remaining vesicles incapable of driving myofibroblast differentiation, suggesting that Rab proteins may regulate distinct sub-populations of vesicles (Yeung et al., 2018). Soluble N-ethylmaleimide-sensitive factor attachment protein receptors (SNAREs) play a fundamental role in membrane-membrane fusion (Bonifacino and Glick, 2004), and are involved in fusion of the plasma membrane with lysosomes (Rao et al., 2004), and MVB-plasma membrane fusion has been recently been shown to be dependent on the presence of SNAREs (Verweij et al., 2018).

Cells do not all secrete sEVs to the same degree. Some cell types secrete more vesicles than others, MSCs have been shown to secrete more sEVs than THP1 or HEK cells (Yeo et al., 2013). Vesicle production is increased in cancer cells relative to their healthy counterparts (Yu et al., 2006), as well as in cells submitted to stress, such as heat (Clayton et al., 2005) or hypoxia (King et al., 2012). These data presenting changes in dynamics of vesicle output demonstrate that sEV biogenesis and secretion is a highly regulated process, and sEVs are secreted to suit the needs of the parent cell.

Composition

sEVs are formed of a lipid bilayer, similar in some respects to the parent cell plasma membrane. They are made up of diverse composition, with proteins and lipid containing molecules in the sEV membrane, and a number of cytosolic molecules in the vesicle lumen. Examples of sEV contents and their topography are represented graphically (figure 1.3) (Clayton, 2012).

Early studies of EVs revealed a series of proteins expressed on their membranes (figure 1.3). The tetraspanins CD9 (Théry et al., 1999), CD63 and CD81 (Escola et al., 1998) are group of transmembrane proteins found on sEVs, and are often used as markers, however these are found on the cell surface and on MVs so cannot be

described as sEV specific markers. Other markers commonly found on sEVs are the ESCRT related proteins, ALIX and TSG101 (Théry et al., 2001), and the endosomal related lysosomal associated membrane proteins (LAMPs) LAMP1 (Wolfers et al., 2001) and LAMP2 (Escola et al., 1998), evidence of the endosomal origin of sEVs. Major histocompatibility complex (MHC) class I and class II are cell surface proteins involved in antigen presentation, these are also expressed on sEV membranes (Lamparski et al., 2002; Raposo et al., 1996), uncovering a role for sEVs in immune regulation. In addition to proteins found in most sEV population, sEVs also express proteins specific to their parent cell. Epithelial cell derived sEVs carry the marker epithelial cell surface antigen (EpCAM) (Mathivanan et al., 2010; Runz et al., 2007). The aggressiveness of a cancer cell is also relevant in generating the sEV proteome, as Peinado et al showed when they found that malignant melanoma cells secrete sEVs expressing the oncogenic MET protein up to 20-fold higher than those from a non-malignant origin (Peinado et al., 2012). sEVs from cancer cells also carry integrins (Hoshino et al., 2015; Webber et al., 2014), a family of adhesion proteins overexpressed in cancer (Desgrosellier and Cheresch, 2010).

Less is known about sEV lipids, though enrichment of a number of membrane components has been noted. sEVs are enriched in cholesterol, phosphatidylserine (PS), sphingomyelin and ceramide, the molecule implicated in an ESCRT independent MVB formation mechanism (Llorente et al., 2013; Trajkovic et al., 2008; Wubbolts et al., 2003). Lipid composition, like protein content, varies between sEV of different cellular origin (Skotland et al., 2019).

Within the sEV lumen are an assortment of encapsulated molecules (figure 1.3). One particular growing interest is in sEV nucleic acids. sEVs are known to carry messenger ribonucleic acid (mRNA) and micro RNA (miRNA) (Skog et al., 2008; Valadi et al., 2007). Interestingly, even mitochondrial DNA has been reported to be carried by sEVs (Sansone et al., 2017b). The ability of sEVs to transfer nucleic acids to recipient cells has made this field an area of increased attention. Enzymes are also present in sEVs. Calcein acetoxymethyl (Calcein AM) becomes fluorescent following hydrolysis by intracellular esterases (Weston and Parish, 1990); sEVs become fluorescent when treated with Calcein AM (Clayton et al., 2003; Gray et al., 2015), indicating that esterases are incorporated into sEVs. Acetylcholinesterase, an enzyme of the neurotransmitter acetylcholine, was reported to be in EVs in an

early study (Johnstone et al., 1987). Importantly, these contents are protected within the vesicles; protein is protected from proteolytic cleavage (Klibi et al., 2009) and RNA is protected from RNase digestion (Keller et al., 2011), ensuring their stability in the extracellular space. This makes sEVs desirable as drug delivery vehicles, with artificial loading of sEVs with therapeutic cargo being explored (Vader et al., 2016). However, in cells infected with pathogens, sEV loading is hijacked, resulting in the addition of cargo such as bacterial toxins (Abrami et al., 2013) and virus miRNA (Pegtel et al., 2010).

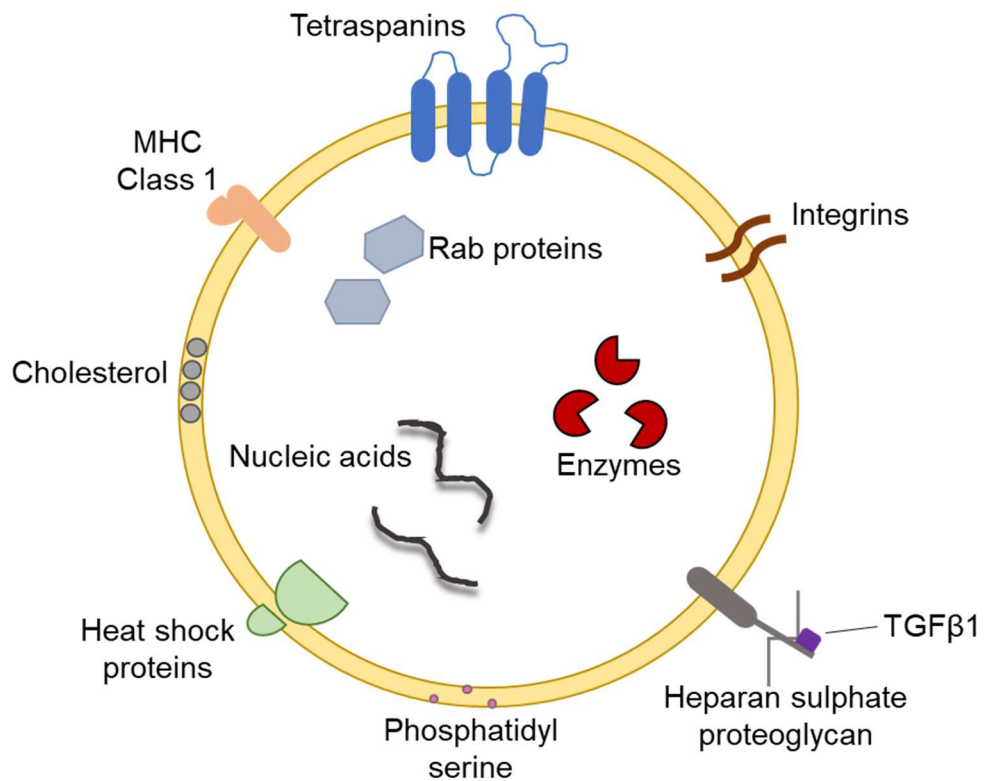


Figure 1.3. sEV composition. Small extracellular vesicles (sEVs) are nanometre sized vesicles made up of a lipid bilayer, enriched with cholesterol, and phosphatidyl serine. Membrane associated proteins are present, such as tetraspanins (CD9/CD63/CD81), integrins, MHC molecules etc. The sEV also contains an assortment of intraluminal cargo, including various RNA species (adapted from Clayton, 2012).

1.2.3. Isolation of sEVs

In early studies of sEVs, tissue culture supernatant underwent serial centrifugation steps to clear the fluid of cells and cellular debris, followed by high speed ultracentrifugation at 100,000g which is sufficient to pellet sEVs (Johnstone et al., 1987). Further separation of sEVs from co-sedimented protein aggregates is achieved through floatation of the sEVs on a sucrose gradient. Raposo et al showed that sEVs float at a density of roughly 1.1-1.2g/mL (Raposo et al., 1996). A protocol involving ultracentrifugation of sEVs on a 30% sucrose Deuterium oxide (D₂O), with a corresponding density of 1.21g/mL) was developed as a practical method for purification and concentration of sEVs from cultured dendritic cells (Lamparski et al., 2002). Combined with tangential flow filtration, the method allowed high quality sEV isolation whilst avoiding vesicle pelleting. Alternatively, sEV-containing sucrose can be diluted and undergo a second ultracentrifugation step to pellet the sEVs and wash off the sucrose. Although now a widely used technique for sEV isolation, there are reports of diverse vesicle populations in these preparations (Bobrie et al., 2012a), as well as aggregation and possible damage of sEVs after high speed centrifugation (Linares et al., 2015), likely to affect the vesicle function. Furthermore, Alternative isolation methods have also been developed to attempt to optimise the isolation and higher purification of sEVs.

Iodixanol has been proposed as an alternative to sucrose for density gradient ultracentrifugation (Optiprep™), and has been shown to produce highly purified sEVs (Lobb et al., 2015; Van Deun et al., 2014). This protocol requires preparation of a step-gradient with multiple iodixanol densities laid on top of one another. Currently, there are a number of commercially available isolation kits available, designed to be fast and practical. ExoQuick™ and Total Exosome Isolation™ precipitation kits work by mixing the kits with sEV containing solutions, and leaving overnight, allowing sEVs to precipitate. These use a straightforward protocols, apparently yielding high quantities of sEVs, but have been reported to also precipitate contaminants (Van Deun et al., 2014). With prior knowledge of sEV surface protein expression, antibody coated beads can be used to capture sEVs (Clayton et al., 2001), which can then be analysed by flow cytometry, whilst attached to the beads. Whilst use of antibodies allows specific capture of the desired sEVs, sub-populations of sEVs negative for the target protein will be

excluded from analysis, therefore proteomic analysis associated with the beads may not necessarily be truly representative of the whole sEV population.

Tangential flow filtration (TFF) is a method used to concentrate small particles in solution by pumping the particle containing fluid across a porous membrane with a small size cut off, thus removing excess fluid and retaining the particles. TFF has been used in the concentration of sEVs from MSCs (Haraszti et al., 2018), showing promise, though being a purely size based capture of vesicles this may also retain sEV sized contaminants. Plasma is a challenging fluid to isolate sEVs from because it is a very viscous fluid loaded with lipoproteins, which can be of similar size and density to sEVs (Théry et al., 2006), in this case ultracentrifugation is unsuitable for generating purified vesicles. In the absence of ultracentrifuge induced protein aggregate and vesicle aggregate formation, size exclusion chromatography (SEC) was reported to isolate sEVs whilst removing a significant portion of lipoproteins (Böing et al., 2014), though it now appears that a combination of SEC and a density gradient is required to remove lipoproteins (Karimi et al., 2018).

There are now various methods for sEV isolation, and choosing a suitable protocol should depend upon what the sEVs are required for post-isolation and what type of fluid the sEV is to be isolated from. How attainable a high-quality preparation is in terms of the degree of concentration and purification achieved should also be considered. sEV purity can be calculated by measuring a preparation's particle to protein (P:P) ratio, by measuring the concentration of vesicles in solution and dividing this by the protein concentration (Webber and Clayton, 2013). A high P:P ratio indicates a highly pure preparation of sEVs, though protein load per vesicle can be variable depending on the cell of origin. Alternatively, EV quality can be assessed by other measures, such as protein to lipid ratios (Osteikoetxea et al., 2015). For any isolation procedure used, accurate reporting of methods is important for replication and study (Théry et al., 2018), and preparations of sEVs should be well characterised (see section 1.2.1.).

1.2.4. Role of sEVs in cancer

Since the discovery that sEVs from B lymphocytes act as antigen presenting vesicles, inducing responses in T cells (Raposo et al., 1996), sEVs have been found to play functional roles in a diverse range of settings in health and disease (Yáñez-

Mó et al., 2015). Inhibition of sEV secretion in cancer cells reduces tumour growth (Bobrie et al., 2012b; Yeung et al., 2018), and the interactions of cancer sEVs with the tumour microenvironment has been well documented (Webber et al., 2015a).

Cancer derived sEVs have a peculiar role in regulating the immune system, with a large amount of data supporting both immune activation by sEVs, but also immunosuppression (Barros et al., 2018). One such example of sEV mediated immune evasion is a marked decrease of NKG2D expression in natural killers (NK) cells and CD8⁺ T cells in response to stimulation by TGFβ1 positive cancer sEVs (Clayton et al., 2008), reducing the ability of the lymphocytes to kill. Apoptosis of tumour reactive CD8⁺ T cells induced by cancer sEV stimulation has also been noted (Wieckowski et al., 2009). In contrast, others have shown that cancer sEVs induce anti-tumour effects in CD8⁺ T cells through antigen presentation (Wolfers et al., 2001), and they can promote tumour killing function in NK cells (Gastpar et al., 2005). The contrasting roles of cancer sEVs in immune regulation may underline the diverse phenotypes exhibited by sEVs secreted by different cancers/cell line sources. More research needs to be conducted to better understand this relationship between cancer sEV and the immune response to cancer.

Tumour growth is reliant upon angiogenesis to meet its needs (Holmgren et al., 1995). In tumours, sEV secretion is known to be increased during hypoxia, regulated by hypoxia-inducible factor (HIF) expression (King et al., 2012). Indeed, cancer sEVs are now believed to be involved in driving tumour supporting angiogenesis through direct endothelial cell stimulation, and through activation of vessel supporting cells. Many groups have shown evidence of endothelial cell activation and proliferation, dependent upon sEV surface markers (Nazarenko et al., 2010), and through delivery of angiogenic proteins (Sheldon et al., 2010; Skog et al., 2008) and mRNA (Hong et al., 2009). In addition, endothelial activation is also achieved through stimulation by TME cells themselves stimulated by cancer sEVs. TAMS (Bardi et al., 2018) and tumour associated fibroblasts (Webber et al., 2015b) notably secrete angiogenic factors following cancer sEV induction. The clear part cancer sEVs play in promoting angiogenesis make this an attractive target for therapy (Ludwig and Whiteside, 2018).

Away from the primary tumour site, cancer sEVs are being unmasked as drivers of pre-metastatic niche formation. In concurrence with the “seed and soil” theory, there is data indicating that cancers metastasise to areas prepared by sEVs.

Melanoma sEVs prepare distant sites for metastasis, through education of bone marrow progenitor cells and promoting vascular leakiness in lung, bone and brain (Peinado et al., 2012), enabling invasion of cancer cells; similarly, this is seen in lymph nodes (Hood et al., 2011). Interestingly, the organotropism of the sEV itself appears to be determined by its expression of specific integrins on the sEV surface (Hoshino et al., 2015), making it attracted to certain organs. These data underline how important cancer sEVs are, not just within the TME, but beyond at distant sites.

Besides the effect cancer sEVs have on the TME, cancer cells can be altered by other cells in the TME through sEV stimulation. sEVs from MSC cells can increase tumour growth through induction of expression of angiogenic factors in the tumour cells (Zhu et al., 2012). On the other hand, MSC derived MVs are shown to inhibit tumour growth (Bruno et al., 2013), pointing to potential differences between actions of EVs of distinct sizes and origins. Fibroblast derived sEVs activate NOTCH3 signalling pathways in breast cancer cells, leading to expansion of therapy resistant cancer cells (Boelens et al., 2014). sEV mediated drug resistance is another phenomenon within the TME, which occurs through various mechanism, not just stromal cell to cancer cell directed. Cisplatin treated ovarian cancer cells increase resistance in bystander cells in a sEV dependent manner (Samuel et al., 2018). Remarkably, cisplatin treated cells secrete sEVs loaded with cisplatin, perhaps as a protective mechanism (Safaei et al., 2005).

1.2.5. Cancer sEVs induce myofibroblast differentiation

The presence of myofibroblasts in solid cancers, and their role in tumour growth and survival has been known for many years (Olumi et al., 1999; Rønnov-Jessen and Petersen, 1993; Tuxhorn et al., 2001). More recently, sEVs from PCa cells were found to initiate myofibroblast differentiation in fibroblasts (Webber et al., 2010). Since then, this sEV driven phenotype has been described in various solid cancers, with sEVs stimulating cells of distinct origins (Atay et al., 2014; Cho et al., 2012; Chowdhury et al., 2015; Gu et al., 2012).

Following the finding that TGF β 1 not only existed in a soluble form, but was also bound the surface of DU145 (PCa cell line) sEVs (Clayton et al., 2007), and that TGF β 1 had a known role in myofibroblast differentiation (Rønnov-Jessen and Petersen, 1993), the distinctions between sTGF β 1 and sEV associated TGF β 1 in myofibroblast differentiation was explored. PCa sEV induced fibroblast to myofibroblast differentiation is dependent upon TGF β 1, which induces SMAD signalling (Webber et al., 2010). sEVs from a cell line considered less malignant (LNCaPs) fail to drive differentiation, these cells also express less TGF β 1 than DU145 cells (Webber et al., 2010). Differentiation could also be inhibited through TGF β 1 blockade. Whilst a TGF β 1 dependent process, the growth factor was found to be tethered to the vesicles by the Heparan sulphate proteoglycan (HSPG) Betaglycan, and this must remain intact for differentiation to occur. In an *in vivo* model with co-administered PCa cells and fibroblast, knockdown of Rab27a (thereby inhibiting sEV secretion) in the cancer cells inhibited tumour growth, demonstrating that the myofibroblasts generated by the sEVs are key for cancer progression (Webber et al., 2015b). sEV treated fibroblasts express the typical α SMA fibres, but in addition to this they also secrete various growth factors, including HGF and VEGF, meaning stimulated fibroblast conditioned media was capable of driving angiogenesis in a vessel formation assay (Webber et al., 2015b). Though sEV stimulated fibroblasts enhance tumour growth, and drive angiogenesis, these processes, and secretion of growth factors by the fibroblast can be attenuated by TGF β 1 blockade, however sTGF β 1 alone cannot support vessel formation, and actually inhibits tumour growth *in vivo* (Webber et al., 2015b).

Myofibroblast differentiation is TGF β 1 dependent, but since the sEV is required to drive the disease promoting phenotype seen in cancer, the sEV must be interacting with the fibroblast (or other cell type) in a distinct manner to sTGF β 1. sEV mediated myofibroblast differentiation appears to be a significant step in the progression of cancer, therefore uncovering the mechanism underlying the interaction is desirable. The cell surface interaction of the recipient cell with the HSPG bound TGF β 1 is important in this process. sEVs are also known to be taken up by recipient cells, and can deliver functional cargo to them (Valadi et al., 2007). An understanding of the uptake mechanism of PCa sEVs by fibroblasts may help

elucidate their role in myfibroblast differentiation and may also provide therapeutic targets to attenuate this differentiation stimulus.

1.3. Cellular uptake and intracellular fate of sEVs

The first evidence of a functional role for sEVs came in the form of a surface interaction between sEVs and T cells (Raposo et al., 1996). But since the discovery that sEVs are internalised by cells (Morelli et al., 2004) and that they can contain nucleic acids which is delivered to cells (Valadi et al., 2007), we now know that sEVs can communicate with cells through delivery of their cargo, and have begun to elucidate the mechanisms by which they are taken up and processed.

1.3.1. Evidence for delivery of sEV cargo

Since mRNA was shown to be transferred from sEVs to recipient cells (Valadi et al., 2007), there has been mounting evidence demonstrating that sEV derived nucleic acids can be delivered to cells, affecting gene expression. In several cancer models, sEV mediated interactions with cells implicate translation of sEV derived mRNA. Skog et al showed translation of a Glioblastoma sEV reporter mRNA in endothelial cells (Skog et al., 2008); Glioblastoma sEVs contain mRNA transcripts linked to angiogenesis, and these sEVs elicit an angiogenic response in endothelial cells, presenting the possibility that tumour promoting phenotypic changes in cells of the TME could be brought on through transfer of mRNA transcripts from cancer cells to non-cancerous cells. Indeed, other groups have reported on the phenotypic changes in cells potentially driven through sEV mRNA (Hong et al., 2009; Nazarenko et al., 2010). miRNA associated with sEVs are also reported for their role in directing phenotypic change in cells treated with sEVs (Donnarumma et al., 2017; Fabbri et al., 2012; Montecalvo et al., 2012; Valadi et al., 2007). Conveyance of the miRNA function however is reported through different mechanisms. Post-transcriptional regulation by miRNAs, the conventional miRNA function has been described in sEV miRNAs (Tian et al., 2014a; Zhou et al., 2014). In contrast, sEV miR-21/29a induced inflammatory responses in TAMs through toll-like receptor 8 binding (Fabbri et al., 2012), revealing an alternative mechanism for sEV miRNA action, and perhaps through a distinct delivery route. In parallel with the

emergence of sEV-miRNA function in disease, these nucleic acids are also being investigated as potential biomarkers (Salehi and Sharifi, 2018).

Another mechanism for functional delivery of sEV cargo is direct protein transfer to cells. PCa cells highly express the integrin $\alpha\beta6$, this integrin is packaged into sEVs, and can be transferred to $\alpha\beta6$ negative cells, localising to the cell surface and promoting cell migration (Fedele et al., 2015). Transfer of the epidermal growth factor receptor VIII (EGFRvIII) from vesicles to cells has also been described, the oncogenic activity of the receptor is also transferred to the cell (Al-Nedawi et al., 2008) Promotion of tumorigenesis through sEV protein transfer has been reported by various groups (Peinado et al., 2012; Singh et al., 2016; Skog et al., 2008).

Infections can lead to the hijacking of sEV loading, sEVs secreted by infected cells can deliver this pathogenic cargo to recipient cells. Epstein-Barr virus infected cells load their sEVs with viral miRNA and uptake of these sEVs by non-infected cells leads to miRNA mediated gene down-regulation (Pegtel et al., 2010). Transfer of bacterial toxins by sEVs has also been described (Abrami et al., 2013).

As the functional role of sEV cargo has become clearer in recent years, the idea to load sEVs with therapeutic molecules has become more prevalent. Small interfering RNA (siRNA) is a small RNA molecule suitable for sEV loading. Multiple groups have artificially loaded sEVs with siRNAs and demonstrated successful knockdowns in recipient cells (Alvarez-Erviti et al., 2011; Ohno et al., 2013; Pan et al., 2012), as well as demonstrate the ability of the sEV to penetrate biological obstacles such as the blood brain barrier (Alvarez-Erviti et al., 2011).

We do not yet have a good comprehension of how all these sEV contents can become functional in recipient cells, especially with extracellular and intracellular barriers to overcome. Endocytosis of sEVs and their processing has been described (Morelli et al., 2004), pointing to machinery which may be used by the sEVs to deliver their cargo. Understanding endocytosis and intracellular processing of sEVs may provide information on how sEVs deliver their contents to recipient cells. This knowledge will give us a greater comprehension of how sEVs convey their functions and help identify therapeutic targets in disease.

1.3.2. Endocytosis

Endocytosis is an important cellular process, it involves the internalisation of macromolecules which cannot pass through the plasma membrane. In simplistic terms, the plasma membrane invaginates inwards and pinches off, forming an internalised vesicle, termed endosome, containing any material taken up with extracellular fluid and the proteins present on the plasma membrane. In reality, endocytosis is a series of processes and can occur through various machineries (figure 1.4) (Mayor and Pagano, 2007)

Overview of endocytic pathways

Each endocytic route is defined by the proteins involved and the complexes formed. Some internalised materials are specific to an endocytic route, and some pathways are only seen in specialised cell types.

Phagocytosis is a receptor mediated means of internalisation in which the particle taken in is engulfed by plasma membrane extensions, this material is destined for degrading phagosomes (Swanson, 2008). This uptake pathway is dependent on PI3K activity, which can be blocked with Wortmannin, thus preventing phagocytosis (Wymann et al., 1996). Only specialised cells, namely macrophages, monocytes and neutrophils are capable of genuine phagocytosis, and this is dependent on actin polymerisation (Doherty and McMahon, 2009).

Macropinocytosis also involves large membrane protrusions into the extracellular space, engulfing material with the extracellular fluid, although macropinocytosis doesn't require ligand binding (Doherty and McMahon, 2009). PAK1 is one of key regulators of macropinocytosis (Dharmawardhane et al., 2000), and Na^+/H^+ exchange is also required; amilorides, potent Na^+/H^+ exchange inhibitors can block macropinocytosis (Ivanov, 2008).

Clathrin-mediated endocytosis (CME) involves internalisation of molecules through assembly of clathrin molecules in lattices, invaginating the plasma membrane and forming clathrin coated pits, pinching off to produce a clathrin coated vesicle, finally the vesicle is uncoated and deposits its contents into an early endosome (Kirchhausen, 2000). This is a receptor driven form of uptake. Like phagocytosis and macropinocytosis, CME is also dependent on actin polymerisation (Lamaze et al., 1997). Formation of the clathrin coated vesicle is

dependent on its scission from the plasma membrane by dynamin (Marks et al., 2001). Dynamin is also involved in clathrin independent endocytosis, notably in caveolin dependent endocytosis (CDE) (Nabi and Le, 2003). In CDE, intracellular vesicles are formed without clathrin coat forming lattices, instead there are cholesterol rich lipid rafts and caveolin proteins, forming caveolae (Doherty and McMahon, 2009). Inhibition of uptake dependent on lipid rafts is achievable through depletion of cholesterol (Parton and Simons, 2007). Lipid rafts are regions of the plasma membrane enriched with receptors and sphingolipids, and are associated with caveolin-1 (Cav1) in membrane invaginations, or oligomerised flotillin domains (Doherty and McMahon, 2009). Flotillin-1 (Flot1) containing lipid rafts are capable of endocytosis, independent of both clathrin and caveolin, and these are associated with endocytosis of glycosylphosphatidylinositol (GPI)-linked proteins (Glebov et al., 2006).

Other, less well-defined uptake machineries are also present. The clathrin-independent carrier (CLIC)/GPI enriched early endosomal compartment (GEEC) uptake pathway is a peculiar uptake pathway identified by its tubular invaginations in the plasma membrane (Kirkham et al., 2005), and its regulation by cdc42 (Chadda et al., 2007). CME can compensate for CLIC/GEEC interruption (Sabharanjak et al., 2002), masking the role of CLIC/GEEC in endocytosis. Further study on the more unknown of the uptake pathways will help us understand their specific role in endocytosis.

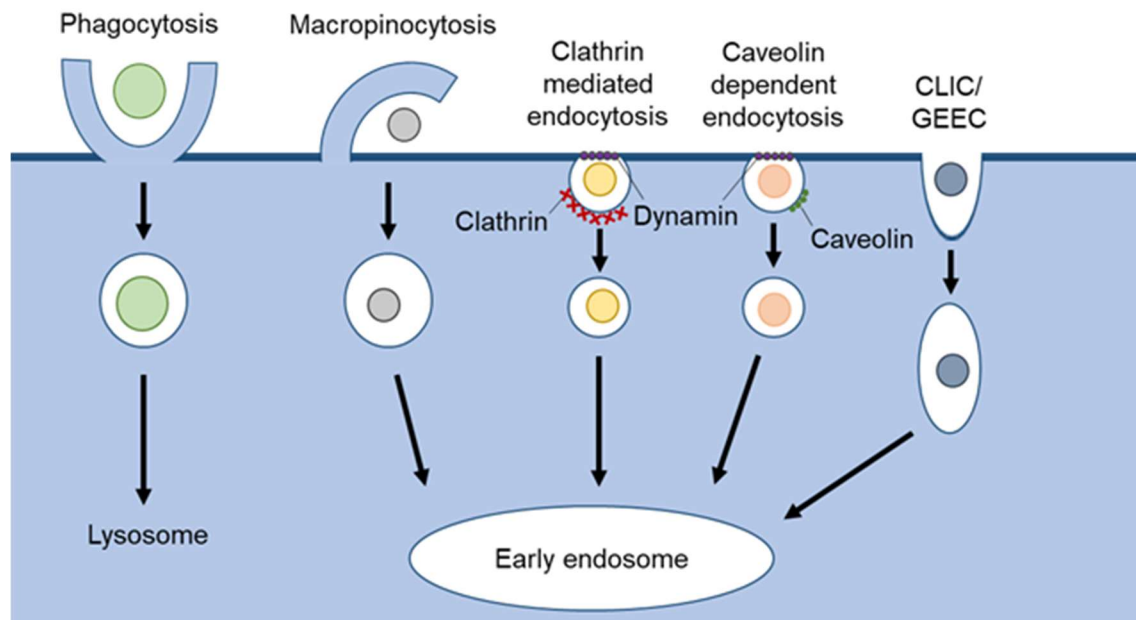


Figure 1.4. Mechanisms of endocytosis. Overview of the routes of endocytosis. Pathways involve distinct machinery to endocytose their material, typically delivering their contents to early endosomes. Large engulfment of extracellular material is possible through macropinocytosis and phagocytosis (in specialised cells). Dynamin dependent mechanisms exist, as Clathrin or Caveolin directed endocytosis. There are also less well characterised pathways, such as the CLIC/GEEC route for example (Adapted from Mayor and Pagano, 2007).

Determining the route of endocytosis

Traditionally, the route of endocytosis for a given internalised material is determined through pharmacological inhibition of specific pathways to identify the relevant route. Actin polymerisation is important for multiple endocytic pathways, and is inhibited by Cytochalasin D (Flanagan and Lin, 1980). Inhibition of a protein vital in so many endocytic pathways is limited in that it cannot identify a specific route of endocytosis. Dynamin function can be abrogated with the inhibitor Dynasore (Newton et al., 2006). Dynamin is known to be involved in both clathrin dependent and independent uptake (Marks et al., 2001; Nabi and Le, 2003). Inhibitors such as Dynasore should not be used to prove the role of a single pathway in uptake, unless corroborating data can also be provided. Many pharmacological inhibitors suffer from a lack of specificity for distinct endocytic pathways (Ivanov, 2008; Vercauteren et al., 2010), furthermore these inhibitors can be extremely cytotoxic (Vercauteren et al., 2010), but this is rarely considered. Knockdown of known regulators of specific endocytic pathways has been explored more recently, for determining the route of uptake (Al-Soraj et al., 2010; Payne et al., 2007; Vercauteren et al., 2011). siRNA targeted against clathrin heavy chain (CHC) will inhibit uptake of the CME specific transferrin (Tf), whereas this uptake is unaffected in cells treated with a Cav1 knockdown (Vercauteren et al., 2011), demonstrating the specificity of siRNAs, which is not attainable with an inhibitor such as Dynasore. Alternatively, generation of cell lines expressing fluorescent variants of endocytic regulators can define uptake route through co-localisation studies of internalised material with a fluorescent endocytic protein, e.g. Cav1 (Nanbo et al., 2013; Svensson et al., 2013).

Care should be taken when identifying endocytic pathways based on pharmacological inhibition alone, and additional studies with alternative methods would be beneficial. Endocytosis, through the pathways discussed, results in extracellular material being internalised by the cell, subsequently followed by intracellular sorting, and distribution to distinct cellular compartments.

1.3.3. *Intracellular trafficking*

Following uptake, internalised materials transit the endosomal system. The endosomal tract is formed of a series of maturing endosomes, identifiable by their expression of particular proteins. Sorting of the endocytic cargo in this system determines its fate (figure 1.5) (Huotari and Helenius, 2011).

Internalisation of material is quickly followed by fusion of the primary endosome with the early endosome (EE), the sorting centre at the cell periphery (Huotari and Helenius, 2011). From here endocytic cargo can be sorted and sent to the golgi apparatus, to lysosomes for degradation, or to recycling endosomes for exocytosis. The majority of internalised cargo is recycled back to the cell surface, transferrin (Tf) is a probe used for cargo sorted to recycling endosomes (Huotari and Helenius, 2011). EEs are slightly acidic (6.8-5.9) relative to the extracellular space (Maxfield and Yamashiro, 1987), this acidity increases in maturing endosomes bound for lysosomes (6.0-4.9), creating a better environment for hydrolytic reactions, and receptor-ligand decoupling (Huotari and Helenius, 2011). The family of Rab GTPases are key regulators in endosomal trafficking and maturation. Rab proteins are therefore used as markers to identify endosomes, Rab5 being a marker associated with the EE (Christoforidis et al., 1999). Endosomes move around the cell along microtubules (Nielsen et al., 1999), in a highly regulated system, although sorting of internalised cargo is not a particularly efficient process, as cargo taken up at the same time will gradually arrive at its destination over the course of hours (Kielian et al., 1986).

In maturing endosomes, Rab5, characteristic of the EE, is switched for Rab7 (Rink et al., 2005), these endosomes are now referred to as late endosomes (LEs). LEs are further characterised by expression of LAMP1, the presence of ILVs, plus the endosome lumen now contains various hydrolase enzymes (Huotari and Helenius, 2011). For LEs that do not become plasma membrane bound MVBs, they typically transfer their cargo to lysosomes. LEs can deliver their contents to lysosomes through membrane fusion (Luzio et al., 2007), thus it can be difficult distinguishing LEs from lysosomes, as they share many of the same proteins, notably LAMP1. In lysosomes, the pH can reach as low as 4.5 (Maxfield and Yamashiro, 1987), making it suitable for enzymatic degradation of the contents. Probes known to traffic to

lysosomes can be useful tools for determination of intracellular location of internalised materials. Dextran (Dx) is one such probe taken up and trafficked to lysosomes (Baravalle et al., 2005). Studying the effect of lysosomal localisation on a given cargo can be achieved through use of agents that raise the endosomal pH, impeding lysosomal function. The bafilomycins are a group of inhibitors which block V-ATPase activity, abrogating proton pumping thus raising the pH of the lysosome (Bowman et al., 1988), however these inhibitors also impair EE to LE cargo transfer (Baravalle et al., 2005) meaning results from use of these inhibitors can be challenging to interpret.

Endosomal trafficking is a complex process in which the cell decides the fate of internalised cargo. Pinpointing the destination of this cargo can provide evidence of whether it is degraded, but also how it may deliver information and educate the cell, through manipulation of the endosome system. In the uptake of viruses, delivery of viral genomes to the cell nucleus through endosomal escape is a well characterised process (Mudhakar and Harashima, 2009), which can occur through various mechanisms, including endosome membrane fusion and endosome disintegration. Studying sEV trafficking through this system may reveal the means of sEV cargo delivery and resulting phenotypic change in the cell.

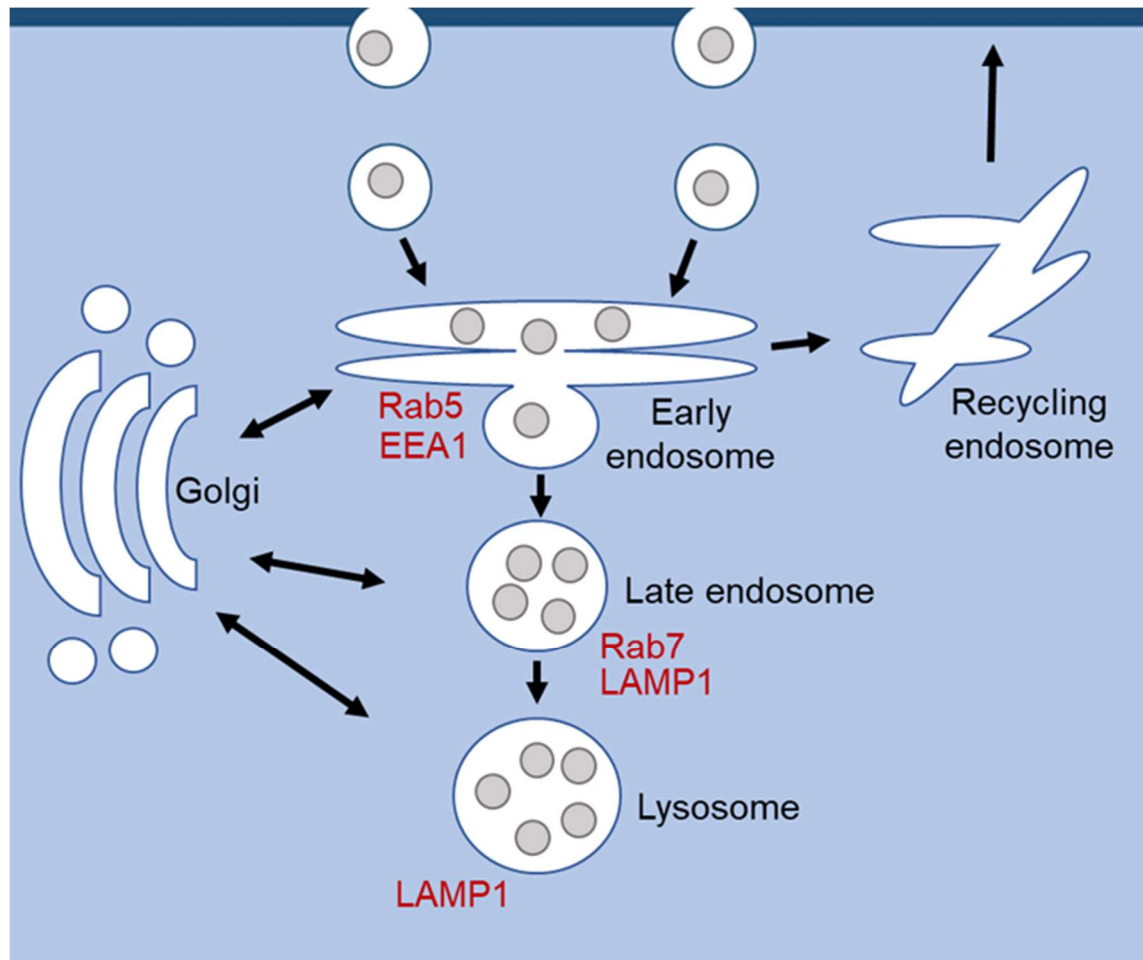


Figure 1.5. The endosomal system. Following endocytosis, cargo is typically delivered to early endosomes. Here cargo is sorted, recycling of material to the plasma membrane occurs, and endosome maturation ensues, in which early endosomes become late endosomes. Much of the material in the late endosome is bound for lysosomes, where degradation of the cargo takes place. Endosomal compartments can be characterised by the expression of particular proteins. Transport of proteins between the golgi network and the endosomal system also takes place (Adapted from Huotari and Helenius, 2011).

1.3.4. *Tools to monitor sEV uptake*

Visualising and tracking sEVs can clarify how they are taken up and traffic through cells, which is key to understanding the delivery of their contents, giving insights into their functions and how they may be employed as drug delivery vehicles or targeted therapeutically. The mechanisms behind these processes are now being elucidated through use of techniques to fluorescently label sEVs and monitor their interactions with cells. Typically, uptake of fluorescently labelled sEVs is monitored by fluorescence microscopy, the fluorescent signal can also be detected by flow cytometry (Morelli et al., 2004). There is an array of fluorescent dyes with distinct properties allowing them to bind to different parts of the vesicle.

As the quickest and simplest technique for labelling, addition of exogenous artificial dyes to sEVs is very widely used. Lipophilic dyes remain the most common. Lipophilic dyes insert themselves into the sEV membrane, and their fluorescent moiety allows their detection following uptake of the vesicle (Morelli et al., 2004), PKH dyes are widely used lipophilic dyes which are live cell stains, but have been used in a large number of sEV uptake studies (Christianson et al., 2013; Fedele et al., 2015; Fitzner et al., 2011; Frühbeis et al., 2013; Ohno et al., 2013; Pegtel et al., 2010; Peinado et al., 2012; Ronquist et al., 2016; Svensson et al., 2013). Other lipophilic dyes used to label sEVs include the carbocyanine dyes DiI (Nanbo et al., 2013), DiD (Tian et al., 2010) and DiO/DiR (Tian et al., 2014b), as well as octadecyl rhodamine B chloride (R18) (Pan et al., 2012) and FM4-64 (Wolf et al., 2015). Whilst labelling sEVs with lipophilic dyes is a straight forward procedure, usually involving simple incubation of dye with vesicle, their chemistry can make them problematic as sEV labels. PKH and DiI can form micelles/aggregates of size similar to sEVs (Morales-Kastresana et al., 2017; Pužar Dominkuš et al., 2018), meaning these dyes can give false-positive signals when used to detect sEV uptake. Flootation of PKH-sEVs may be sufficient to rid the sEVs of contaminating PKH particles (Pužar Dominkuš et al., 2018). Non-lipophilic dye alternatives may be more suitable for sEV labelling if they do not spontaneously form large fluorescent particles.

Carboxyfluorescein diacetate succinimidyl ester (CFDA-SE, also referred to as CFSE) is a dye which binds amine groups on proteins and has been used in sEV

labelling (Longatti et al., 2018; Morales-Kastresana et al., 2017; Pospichalova et al., 2015). Acetate groups on the CFSE molecule make it membrane permeable, although intracellular esterases cleave these groups decreasing permeability (Parish, 1999), therefore CFSE likely binds proteins on the sEV surface and proteins on the intraluminal membrane, with the dye being trapped within the sEV in the presence of intraluminal esterases. In contrast to the lipophilic dyes, CFSE does not form nano-particulate aggregates (Morales-Kastresana et al., 2017), though as a protein binding dye will bind to contaminating proteins in a sEV preparation. pHrodo is a protein binding dye with a twist. The fluorescent moiety in pHrodo becomes fluorescent at a low pH, indicative of phagosome pH, this has been used to confirm that sEVs could be taken up by phagocytosis in dendritic cells (Montecalvo et al., 2012). Dyes such as pHrodo can provide extra information on the intracellular location of sEVs following uptake. The presence of nucleic acids in sEVs has made them a target for fluorescence labelling, though to a lesser extent. SYTO 13, a membrane permeable compound which becomes highly fluorescent when bound to DNA/RNA enables detection of larger “microparticles” fluorescently (Ullal et al., 2010). SYTO RNASelect is more selective for RNA binding, and its delivery by sEVs to recipient cells has been demonstrated (Li et al., 2014; Singh et al., 2015), however SYTO RNASelect labelled sEVs themselves were undetectable by flow cytometry whereas PKH or CFSE labelled sEVs could be detected (Morales-Kastresana et al., 2017), which may be due to the strength of the SYTO RNASelect dye signal, or due to lack of RNA in the vesicle. Calcein AM is another membrane permeable dye, described in section 1.2.2, its fluorescence in sEVs shows it can permeate the membrane and be hydrolysed by intraluminal esterases (Clayton et al., 2003; Gray et al., 2015). Calcein labelled sEVs have rarely been used for cellular uptake studies (Samaeekia et al., 2018).

Stable cell lines genetically engineered to express a fluorescent molecule tagged to a protein known to be enriched on sEVs is a common method to produce fluorescent sEVs. Whilst addition of exogenous dyes to sEVs requires the isolation of the sEVs, or post-labelling purification to remove contaminants, cell lines secreting endogenously fluorescent sEVs circumvent this, making this method suitable for cell co-culture or *in vivo* studies where sEV isolation is not possible. Fluorescent sEV producing cell lines have also been utilised for monitoring sEV

secretion (Verweij et al., 2018). Proteins which are conserved and highly expressed on most sEV are ideal for attachment of fluorescent proteins. CD63, a sEV expressed tetraspanin is often targeted. sEVs produced from CD63-GFP cell lines have been used in cellular uptake studies (Heusermann et al., 2016; Koumangoye et al., 2011; Maida et al., 2016). This labelling method has some clear advantages over the addition of exogenous dyes, but it is not without its limitations. In generating these cell lines, it should be taken into account that overexpression of sEV proteins may alter the function of the sEV, sEV sub-populations which don't express the target protein will not be labelled and sEV output itself may be altered in the parent cell.

Since sEV contents have distinct intracellular fates (section 1.3.1), the cellular uptake and trafficking of a sEV dye will likely depend on which part of the vesicle they are conjugated to. Fluorescent sEVs have been a useful tool in clarifying how sEVs are taken up by recipient cells.

1.3.5. Endocytosis of sEVs

Addition of sEVs to cells results in the uptake of the sEVs, in a time dependent manner, with fluorescent sEVs appearing as punctate dots within the cell (Tian et al., 2010). Internalisation of sEVs by cells can be confirmed in several ways. Capturing z-stacks of fluorescent sEV treated cells, generating a 3D image of the cell, reveals that sEVs are within the cell, and not exclusively bound to the plasma membrane (Lai et al., 2015). Co-localisation of sEVs with fluorescently stained endosomal compartments is further evidence that sEVs can be taken up (Morelli et al., 2004). Acid stripping or trypsinisation of the cell surface can remove surface bound sEVs (Feng et al., 2010; Franzen et al., 2014). sEV uptake is inhibited by reducing the temperature during treatment of the cell (Franzen et al., 2014; Morelli et al., 2004), indicating the uptake process is an active energy requiring one. Endocytosis is possible through various mechanisms (Doherty and McMahon, 2009), and through many studies, sEV uptake has been reported in these mechanisms (Mulcahy et al., 2014).

Though phagocytosis is known to engulf large bodies such as bacteria or cell fragments, sEV uptake has been reported through this mechanism in phagocytic cells (Feng et al., 2010; Montecalvo et al., 2012). Similarly to phagocytosis,

macropinocytosis can engulf vesicles through membrane extensions into the extracellular space (Fitzner et al., 2011), however macropinocytosis is not a mechanism in specialised cells only and has been implicated in sEV uptake in numerous cell types (Costa Verdera et al., 2017; Nakase et al., 2015; Sagar et al., 2016). Other mechanisms of endocytosis have also been reported in sEV uptake. Both CME (Escrevente et al., 2011; Feng et al., 2010), and CDE (Nanbo et al., 2013) are involved in sEV uptake. Interestingly, knockdown, of Cav1 (a CDE related protein), actually increased sEV uptake in several cell lines (Svensson et al., 2013), maybe causing an upregulation of an alternative uptake pathway. Here, sEVs co-localised with the lipid raft marker Flotillin 1, showing a lipid raft-based uptake independent of caveolin (Svensson et al., 2013). Furthermore, sEV uptake is inhibited by disruption of lipid rafts through cholesterol depletion (Plebanek et al., 2015; Svensson et al., 2013). In the aforementioned studies on sEV endocytosis, this process has been described with diverse cancer model systems: endocytosis of cancer derived sEVs by the same cell type, in ovarian (Escrevente et al., 2011) and breast (Koumangoye et al., 2011) cancers, and monkey and mouse fibroblast cell lines to study internalisation of Glioblastoma sEVs (Svensson et al., 2013). However, the internalisation process of cancer derived sEVs has rarely been studied within the context of biologically relevant human cells present in the tumour microenvironment which are known to become activated by cancer derived sEVs. Pharmacological inhibition is frequently used to inhibit sEV uptake (Mulcahy et al., 2014). As mentioned in section 1.3.2, pharmacological inhibitors of uptake often do not specifically abrogate one endocytic mechanism. siRNAs downregulating specific endocytic regulators can help pinpoint routes of uptake for sEVs (Costa Verdera et al., 2017; Nanbo et al., 2013; Roberts-Dalton et al., 2017).

The protein profile of the sEV seems to be relevant for determining its cellular uptake, since protein stripping of the sEV surface inhibits internalisation (Escrevente et al., 2011). sEVs from a malignant cell line are more readily taken up by cells than those from a less aggressive cell line (Lázaro-Ibáñez et al., 2017), likely due to the difference in sEV surface proteins. On the other hand, malignant cell take up sEVs to a greater extent than less malignant cells (Parolini et al., 2009); in the central nervous system, oligodendrocyte sEVs are internalised by microglia

but less so in other local cell types (Fitzner et al., 2011), showing cell specificity for sEV uptake. These data indicate that the profile of the recipient cell surface is also important for determining uptake of sEVs. Integrins are a family of cell surface receptors which form heterodimers of α and β subunits (Humphries et al., 2006), these transmembrane proteins have been implicated in the uptake of sEVs, though the mechanisms are unclear. Obstruction of target cell integrins can inhibit sEV uptake, as can blockade of an integrin ligand (ICAM-1) on the sEV surface (Morelli et al., 2004), revealing a role for integrin-ligand binding in sEV uptake. sEVs containing the $\alpha\beta 3$ integrin counter receptor ADAM15 can block integrin mediated cell adhesion to matrix components, demonstrating that integrin mediated sEV-cell adhesion also plays functional roles other than aiding sEV uptake (Lee et al., 2012). Integrins themselves are also present on the sEV surface, and appear to be relevant in the adhesion to and uptake by cells (Wang et al., 2015). sEVs have also been shown to bind matrix components such as collagen and fibronectin in an integrin dependent manner (Clayton et al., 2004), perhaps enabling sEV capture by cells moving through the matrix, or by blocking cell migration. We do not yet fully understand the relationship between the sEV and recipient cell surfaces and how route of uptake is determined. Elucidating the mechanisms underlying cell specificity and route of uptake for sEVs will allow more accurate therapeutic targeting, but will also aid the development of sEV-based delivery vectors.

1.3.6. Intracellular fate of sEVs

Post-endocytosis, sEVs have been tracked within cells, to determine their intracellular fate, and monitor the delivery of their complex cargo. Parolini et al reported that sEV fusion can occur at the plasma membrane (Parolini et al., 2009). This fusion would release sEV cargo, notably nucleic acids, into the cytosol of the cell directly, and sEV proteins could be incorporated into the plasma membrane. However, EM investigations reveal sEVs intact in recipient cells within endocytic vesicles (Heusermann et al., 2016; Morelli et al., 2004; Svensson et al., 2013). Plasma membrane fusion is not an unreasonable theory, since sEV formation has been described through direct plasma membrane budding (Booth et al., 2006), though the mounting evidence showing uptake of sEVs would suggest uptake is more common than fusion.

sEVs in endocytic vesicles can be tracked microscopically. These endosomes are not stationary, but traffic through the cells along microtubules, seen in monkey kidney fibroblasts (Svensson et al., 2013). sEVs immediately co-localise with markers of early endosomes, demonstrated in various model systems with different recipient cells such as ovarian cancer cells (Escrevente et al., 2011), breast cancer cells (Koumangoye et al., 2011) and nasopharyngeal carcinoma cells (Nanbo et al., 2013), with this co-localisation decreasing after around 40 minutes (Nanbo et al., 2013), suggesting endosomal maturation as the sEVs are sorted into late endosomes. Late endosome marker Rab7 does indeed co-localise with sEVs (Nanbo et al., 2013), and sEVs were found to co-localise with lysosome marker LAMP1 in other studies (Escrevente et al., 2011; Koumangoye et al., 2011). sEVs are not transferred to organelles in the recipient cell such as the Golgi apparatus or ER (Escrevente et al., 2011; Tian et al., 2013). However, ER is known to wrap around endosomes (Friedman et al., 2013), and sEV containing endosomes do transit closely to the ER (Heusermann et al., 2016). Co-localisation of sEVs with CD71, a marker for recycling endosomes has also been reported, occurring 4 hours post-uptake, after co-localising with LAMP1 positive compartments (Koumangoye et al., 2011). Most studies reporting of sEV trafficking have sEVs reaching lysosomes, though reports of close interactions with ER and movement to recycling endosomes suggest there is some sorting of sEVs and potential material exchange in this system. There are also reports of blood brain barrier passage by sEVs (Alvarez-Erviti et al., 2011; Chen et al., 2016), and it is proposed that sEVs may cross this barrier through transcytosis, though there is little evidence so far to support transcytosis of sEVs.

How the sEV unloads its cargo, making it available to the recipient cell is poorly understood. mRNA can be translated in recipient cells within an hour after uptake (Lai et al., 2015), and sEV delivered luciferin is catalysed within minutes of sEV uptake (Montecalvo et al., 2012). These data reveal sEV cargo delivery occurs very rapidly. Fusion between the sEVs and the plasma membrane or early endosomal membrane are reasonable propositions as delivery mechanisms for sEV cargo. Indeed, sEV cargo delivery to the cytosol has been reported to be dependent upon functioning ESCRT components usually involved in MVB formation (Abrami et al.,

2013), though more research needs to be carried out to demonstrate the relevance of endosomal proteins for sEV cargo delivery to corroborate this finding.

1.4. Hypothesis and aims

PCa sEVs induce myofibroblast differentiation in fibroblasts, a key step in the progression of cancer. Modulation of cell behaviour brought about by delivery of sEV cargo has been demonstrated in various settings, though little is known about how PCa derived sEVs deliver their contents to cells within the tumour microenvironment. To this end, using primary human fibroblasts as a model cell for PCa derived sEV uptake, we sought to determine whether PCa derived sEVs delivered its contents to the fibroblast, driving phenotypic change.

Hypothesis: PCa derived sEVs are internalised and sorted by fibroblasts, delivering their intraluminal contents to the cell, in a process required for sEV-driven fibroblast stimulation.

The aims for this study were as follows:

- 1.** Develop a labelling protocol for the fluorescent detection of sEVs using a novel protein binding fluorescent dye. Then validate the use of the dye for cellular uptake studies with the sEVs.
- 2.** To detail the route of endocytosis of the sEV in the fibroblast and determine the subsequent intracellular fate of the sEV.
- 3.** To clarify the mechanisms of sEV cargo transfer to the fibroblasts, using diverse fluorescent dyes.
- 4.** Assess the relevance of sEV internalisation by the fibroblast in inducing phenotypic change within the cell.

Defining PCa sEV internalisation, trafficking and intraluminal cargo delivery in fibroblasts will give us a greater comprehension of the interaction between PCa cells and fibroblasts, as well as the role of sEVs in driving fibroblast activation. Moreover, elucidating the mechanism of sEV intraluminal cargo delivery is fundamental for understanding sEV-cell communication in cancer and other disease settings.

Chapter 2 – Materials and methods

2.1. Cell culture

2.1.1. Monolayer cell culture

The source of sEVs used in this study is the DU145 PCa cell line (ATCC, USA). These are human derived PCa cells taken from a brain metastasis (Stone et al., 1978). sEVs from these cells are known to induce myofibroblast differentiation in fibroblasts (Webber et al., 2010). Cells were cultured in RPMI-1640 media (Lonza, UK), supplemented with 10% FBS^{ev-} (Thermofisher Scientific, UK), 100µg/mL streptomycin (Lonza) and 100U/mL penicillin (Lonza). Cultured cells for sEV studies must have FBS depleted of sEVs, to prevent any bovine derived sEV mediated effects on cells (Shelke et al., 2014). Ultracentrifugation of FBS for 18 hours at 120,000g almost completely removes sEVs from the serum, this depleted serum is referred to as FBS^{ev-}. The sEV recipient cells used were AG02262 human lung fibroblasts (Coriell institute for medical research, USA); these primary fibroblasts were used in this study as a model cell in the tumour microenvironment. Fibroblasts were cultured in DMEM/F12 media (Lonza) and the same supplements as used with the DU145 cells. Cells were cultured in a 95% humidified incubator at 37°C and 5% CO₂. MycoAlert detection kits (Lonza) were used to test for Mycoplasma every 2 months.

For fibroblasts seeded for uptake or functional experiments, cells were growth arrested at 80% confluency for 24 hours prior to experiments through culture in FBS^{ev-} free media, to deplete the culture conditions of growth factors.

2.1.2. CELLine bioreactors for DU145 cells

For continuous culture of DU145 cells and production of sEVs for isolation, cells were grown in CELLine bioreactor flasks (Wheaton, USA). These flasks allow weekly collection of sEV concentrated supernatant. The flask contains two chambers separated by a 10kDa semipermeable membrane, allowing movement of nutrients and O₂/CO₂, but does not permit movement of sEVs. 1.2x10⁷ DU145 cells are initially seeded, into the smaller chamber, in 15mL DMEM/F12 with 5% FBS^{ev-} and penicillin/streptomycin, and the outer chamber contains 500mL DMEM/F12 with 5% FBS and penicillin/streptomycin in the absence of cells. The high volume of media maintains a colony of DU145 cells, whilst weekly collection of secreted sEVs are all contained within the 15mL cell supernatant. Use of these flasks for sEV

Materials and Methods

production is more cost-effective, is less labour intensive, and generates more highly concentrated sEV supernatants than regular monolayer cell culture (Mitchell et al., 2008). Large cell masses do form in these flasks however, therefore there is likely to be regions of hypoxia which would not be seen in monolayer cell culture.

2.1.3. Fluorescence microscopy of fibroblasts

For all brightfield and fluorescence microscopy, except for time-lapse microscopy experiments (see section 2.5.7), images were taken using an Axio Observer Z1 widefield microscope with Apotome (Zeiss, Germany) with a 20x objective lens or 63x objective lens with oil where stated. Green dyes were visualised using a 488nm laser, red dyes visualised using a 561nm laser, and DAPI was visualised using a 405nm laser. Apotome is a form of structural illumination and is a means of removing out of focus light. Images were saved and processed using Zen Blue software (Zeiss). Cell morphology of fibroblasts was examined by taking brightfield images.

For immunofluorescence, fibroblasts were seeded in 96 well glass-bottomed plates (Greiner Bio-One, Germany) at 10,000 cells per well and incubated until confluency reached $\approx 80\%$. In differentiation experiments, fibroblasts were treated (section 2.6.1), and were then fixed. Fibroblasts stained for endosomal markers were just fixed in culture once confluent. Cells were washed in PBS, then fixed in ice cold 1:1 acetone/methanol (100 μ L/well) for 5 minutes, fixative was then removed and wells were allowed to dry at room temperature. Cells were treated with 1% BSA/PBS as a blocking solution for 1 hour at room temperature before being washed in PBS again. Primary antibody (α SMA, EEA1 or LAMP1, see table 2.1) was then added to wells diluted in 0.1% BSA/PBS at a working concentration of 2 μ g/mL for 1 hour at room temperature. Cells were washed in phosphate buffered saline (PBS; Lonza) then treated with an Alexa488/594 conjugated goat anti-mouse secondary antibody (Thermofisher) at 10 μ g/mL in 0.1% BSA/PBS for 1 hour in the dark, at room temperature, then washed in PBS. Cell nuclei were stained in fixed cells using 4',6-diamidino-2-phenylindole (DAPI), a 14.3mM stock was diluted 1:50,000 times in PBS and added to wells for 5 minutes in the dark at

room temperature. Cells could then be visualised using Alexa488/594 and DAPI filters on the Axio Observer Z1.

In experiments where acetone/methanol fixation was unsuitable, paraformaldehyde (PFA) fixation was carried out where stated. 16% PFA (ThermoFisher) was freshly diluted in PBS generating a 4% PFA working concentration. PFA was added to washed cells for 15 minutes at room temperature. Cells were then washed and were ready for microscopy, following staining with DAPI. Where stated, in some situations cells were visualised live, DMEM/F12 was washed off cells, and this media was replaced with colourless FluoroBrite™ DMEM, an imaging compatible media, with little endogenous autofluorescent properties.

2.2. sEV isolation

2.2.1. Bioreactor supernatant collection

Once a week, the CELLline bioreactor cell supernatant is collected and replaced with 15mL of fresh media/supplements, the outer chamber is replaced with 500mL fresh media/supplements. The collected cell supernatant is centrifuged twice at 400g for 6 minutes, and once at 2000g for 15 minutes, this removes any cells and large particles from the media. The resulting media is filtered through a 0.22µm Millex GP syringe filter unit (Merck Millipore, UK). Filtered media is stored at -80°C.

2.2.2. Sucrose cushion ultracentrifugation

Centrifuged and filtered DU145 bioreactor media is defrosted and sEVs are isolated by sucrose cushion ultracentrifugation. Ultracentrifuge tubes (Beckman Coulter, USA) are loaded with sEV containing media, on top of 4mL of 30% sucrose/D₂O solution (Sigma-Aldrich, USA). Tubes are sealed and loaded into a SW32 swing rotor (Beckman Coulter), then spun at 100,000g for 90 minutes. The now sEV containing sucrose (usually 20mL) is collected and mixed with 79mL PBS, then loaded into new ultracentrifuge tubes. A second ultracentrifuge spin, in a fixed angle 70Ti rotor (Beckman Coulter) at 100,000g for 90 minutes pellets the

sEVs on the bottom of the tubes. All of the fluid in the tubes is discarded, sEVs are resuspended in 500 μ L PBS and stored in aliquots of 10 μ L and 30 μ L at -80°C.

2.3. sEV characterisation

2.3.1. *Bicinchoninic acid protein assay*

sEV protein is quantified using a micro bicinchoninic acid (BCA) protein assay kit (ThermoFisher Scientific). Bovine serum albumin (BSA) is used as the protein concentration standard. 2000 μ g/mL BSA is used as the highest concentration, and a 12-point serial dilution is carried out. 10 μ L of sEV is diluted in 70 μ L PBS (1:8 dilution). Absorbance values at 562nm of the sEV sample and standards were recorded in duplicate in a PHERAstar FS Microplate plate reader (BMG Labtech, Germany). sEV protein concentration was calculated based on the standard curve absorbance values of known BSA concentrations. sEV protein concentration was used as a surrogate for sEV quantity in experiments.

2.3.2. *Nanoparticle tracking analysis*

Nanometre sized particles (<1 μ m) can be analysed in solution using NTA. NTA uses the light scattering of particles to track their movement under Brownian motion to calculate particle size. Sample particles are detected through use of laser beams, beams are sent through the particle containing sample, the particles then scatter this light which can be detected by a camera. The NTA software tracks particle velocity, and the velocity of the particles is used to calculate the particle sizes, using the Stokes-Einstein equation. The size of every particle in the population is recorded and the concentration of particles/mL is plotted against size in nm as a histogram.

Before sEV samples were run on the NanoSight™ NS3000 (Malvern instruments, UK), 100nm latex beads (Malvern instruments) were first run to confirm correct calibration of the instrument. For sEVs/beads, samples were diluted in particle-free water (Fresenius Kabi, UK), then run at a constant flow rate using a NanoSight™ syringe pump (Malvern instruments) for 5 x 30 second captures at 25°C. Videos were captured with a sCMOS camera system (OrcaFlash 2.8, Japan), and the videos analysed using the NTA software v3.1. sEV concentration, size

Materials and Methods

distribution, mean and mode sizes were calculated by the software and exported as excel files, which were used to plot histograms on Prism 5 software (v5.03) for presentation.

2.3.3. Western blot

Cells were seeded at 1.5×10^5 per well in 6 well plates (Greiner Bio-One) and left till around 90% confluent. Cells were treated with specified conditions (e.g. siRNA transfections), and cell lysates were prepared using RIPA lysis buffer (Santa Cruz, USA). The buffer was made up of 1X protease inhibitor cocktail, 100mM Sodium orthovanadate, 200nM phenylmethane sulfonyl fluoride (PMSF) and 1X lysis buffer. Lysates were centrifuged for 10 minutes at 10,000g and 4°C to pellet insoluble material, then the supernatant was collected and stored at -80°C for later use.

Cell lysate or isolated sEVs were prepared for electrophoresis. 20µg (Calculated by Bradford protein assay; BioRad, UK) of samples were boiled in Sodium dodecyl sulphate sample buffer (Invitrogen, USA) with 20nM Dithiotheitol (DTT; Santa Cruz). NuPAGE™ precast 4-12% gels (Life Technologies, USA) were loaded with samples, and the molecular weight markers SeeBlue® Plus 2 precision stain and Magic Mark™ XP in separate lanes. An Intivtrogen PowerEase® 500 (Thermofisher) power system ran the gels in NuPAGE™ MOPS Sodium dodecyl sulphate (SDS) running buffer (Life Technologies). Gels were transferred onto a methanol activated polyvinylidene fluoride (PVDF) membrane (GE Life Sciences, UK), in a BioRad mini trans-blot electrophoretic transfer cell with 25mM Tris (Sigma Aldrich) and 192mM glycine (Sigma Aldrich), at ice cold conditions and 80V for 90 minutes. Membranes were blocked in 0.5% Tween®20 (Sigma Aldrich) and 5% milk powder (Marvel, UK) overnight at 4°C. 1µg/mL primary antibodies (table 2.1) were added to membranes at room temperature for 2 hours, then membranes were washed in 0.5% Tween®20/PBS for 3x5 minutes. 1:10,000 goat anti-mouse/rabbit Horseradish peroxidase (HRP) conjugate (Santa Cruz) was added to membranes for 1 hour at room temperature, then membranes were washed again for 3x5 minutes. Membranes were enhanced in a chemiluminescent substrate (Li-Cor, USA) and bands were detected using a C-Digit blot scanner (Li-Cor).

2.3.4. Immunophenotyping plate assay

For detection of protein on the sEV surface, immunophenotyping plate assays were carried out. 1 µg/mL sEV isolates were seeded onto a high protein bind ELISA strip 96 well plates (Greiner Bio-One, Germany), and incubated at 4°C overnight. Tris-based wash buffer (Perkin Elmer, USA) was used to wash wells 3 times. 1% BSA in PBS was added to wells for a 2 hour block at room temperature. Following 3 washes, 1 µg/mL primary antibody (table 2.1) in 0.1% BSA/PBS was added to wells for 2 hours at room temperature, then wells were washed 3 times again. Goat anti-mouse/rabbit (depending on species of primary antibody) biotinylated antibody (Perkin Elmer) was added to wells at 200ng/mL in 0.1% BSA/PBS for 1 hour at room temperature, then wells were washed 3 times. Europium streptavidin conjugate (Perkin Elmer), diluted 1:1000 in red assay buffer (Kaivogen), which provides some enhanced blocking properties, was added to wells for 45 minutes at room temperature, then wells were washed 6 times. Europium fluorescence intensifier (Kaivogen) was added to wells for 5 minutes at room temperature, then time resolved fluorescence (TRF) was measured in the plate using a PHERAstar FS Microplate reader (Webber et al., 2014).

2.3.5. Cryo-electron microscopy

Cryo-EM was carried out for visualisation of isolated sEVs. sEVs were added to glow-discharged holey carbon grids (Quantifoil, Germany) and then a Vitrobot (Maastricht instruments BV, The Netherlands) was used to vitrify the grids. A JEM-2200FS/CR transmission cryo-electron microscope (JEOL, Japan) imaged the samples at liquid nitrogen temperatures with an acceleration voltage of 200kV. All cryo-EM was performed by our collaborator Professor Juan Falcon-Perez (CIC bioGUNE, Spain). Analysis of exported tiff images using ImageJ was carried out to determine sizes and morphologies of structures in the cryo-EM field of views, and averages were plotted on graphs using Prism 5 software.

Materials and Methods

Primary antibody	Isotype	Company	Catalogue number	Application	Concentration (µg/mL)
ALIX	IgG ₁	Santa Cruz	Sc-166952	Western blot	1
TSG101	IgG _{2a}	Santa Cruz	Sc-7964	Western blot	1
Calnexin	IgG ₁	Santa Cruz	Sc-23954	Western blot	1
MHC1	IgG _{2a}	eBioscience	16-9983-85	Western blot	1
CD9	IgG _{2b}	R&D Systems	MAB1880	ELISA, uptake blockade	1-10
CD63	IgG ₁	AbD Serotec	MCA2142	ELISA	1
CD81	IgG ₁	BioRad	MCA1847EL	ELISA	1
TGFβ pan specific	Rabbit IgG	R&D Systems	AB-100-NA	Differentiation + uptake blockade	10
Integrin α ₃	IgG ₁	Merck Millipore	MAB1952Z	sEV ELISA + sEV uptake blockade	0.1-10
Integrin α ₆	Rat IgG _{2a}	R&D Systems	MAB13501	sEV ELISA	0.1-10
Integrin β ₁	IgG ₁	R&D Systems	MAB17781	sEV ELISA + sEV uptake blockade	0.1-10
Integrin β ₃	IgG ₁	Sigma Aldrich	MAB2023Z	sEV ELISA	0.1-10
AP2µ2	IgG ₁	BD Transduction Laboratories	611351	Confirmation of protein knockdown	1
CAV1	Rabbit IgG	Cell Signalling Technologies	D46G3	Confirmation of protein knockdown	1
FLOT1	IgG ₁	BD Transduction Laboratories	610821	Confirmation of protein knockdown	1
PAK1	Rabbit IgG	Cell Signalling Technologies	2602S	Confirmation of protein knockdown	1
αSMA	IgG ₁	Santa Cruz	Sc-32251	Fibroblast expression, fluorescence microscopy	2
EEA1	IgG ₁	BD Biosciences	610456	Fibroblast expression, fluorescence microscopy	2
LAMP1	IgG ₁	Santa Cruz	Sc-20011	Fibroblast expression, fluorescence microscopy	2

Table 2.1. Primary antibodies. All primary antibodies used for Western blots, ELISA-like plate assays and immunofluorescence, antibody isotypes, companies and catalogue numbers are shown.

2.4. Detection of sEVs

2.4.1. Fluorescent labelling

5-200 μ g/mL Alexa maleimide linked dye (Alexa; Thermofisher Scientific), e.g. Alexa488 (Thermofisher-Scientific, 2019) was added to a 30 μ L sEV sample, and made up to 50 μ L with PBS, this mixture was incubated for 0.5-5 hours in the dark at room temperature. sEV concentration was typically 2000-4000 μ g/mL, though this was subject to variation between isolations. Exosome Spin Columns MW3000 (Thermofisher) were prepared according to manufacturer's instructions, 650 μ L PBS was used to rehydrate the powder in the columns, for 15 minutes at room temperature. Excess PBS was removed by centrifugation of the column at 750g for 2 minutes. 50 μ L Alexa dye and sEV mixture was added to the top of the gel now formed in the column. The columns were centrifuged again, this time for 3 minutes, to pull through the labelled sEVs, leaving the unbound Alexa trapped in the column. The remaining solution contains sEVs labelled with Alexa (Alexa-sEVs). Experiments with controls for free dye used solution collected from a column in which Alexa only had been centrifuged through, in the absence of sEVs. These controls were used to demonstrate retention of the Alexa by the columns. Concentration of sEVs after the labelling process was estimated by measuring 1 μ L of labelled sEVs applied onto a NanodropTM 2000 Spectrometer (Thermo Scientific, UK). Concentrations calculated post-labelling were used as the basis for sEV doses, when treating fibroblasts.

sEVs were also labelled with SYTO RNASelect green fluorescent cells stain (Invitrogen), herein referred to as SYTO, CFSE (EBioscience, USA) and Calcein AM (Invitrogen), shortened to Cal. The labelling protocol for sEVs with SYTO, CFSE or Cal is the same as with the Alexa dyes, but with doses of 50-200 μ M CFSE, 10-40 μ M Cal and 50-200 μ M SYTO. For dual labelling experiments, sEVs were first labelled with an intraluminal dye by the described labelling protocol, then the collected labelled sEVs were then co-labelled with 200 μ g/mL Alexa594, again under the same labelling procedure.

2.4.2. Detection of fluorescent sEVs

For visualisation of fluorescently labelled sEVs, labelled sEVs were diluted 1:60 in PBS and added to wells of a 96 glass-bottomed plate for 1 hour at room temperature in the dark. Labelled sEVs could then be visualised stuck to the glass plate or floating in suspension. sEVs labelled with Alexa594 were visualised using the Alexa594 filter on the Axio Observer Z1 microscope, sEVs labelled with Alexa488, SYTO, CFSE or Cal were visualised using the Alexa488 filter.

Intensity of fluorescent sEVs was measured using a PHERAstar FS Microplate reader. Increasing doses of labelled sEVs diluted in PBS were added to wells of 96 well cell culture plates (Greiner Bio-One). Fluorescent intensity of sEVs labelled with Alexa488, CFSE, Cal or SYTO was measured using an Alexa488 optic module in the plate reader. Fluorescent intensity of controls for free dye were also measured.

2.4.3. Monitoring dye loss from sEVs

Loss of fluorescent dye from labelled sEVs in PBS was assessed by monitoring the fluorescent signal of the sEVs over time. Labelled sEVs were diluted 1:6 in PBS and added to high protein binding ELISA plates (Greiner Bio-One) at 100 μ L/well. The plate was incubated at room temperature in the dark for 1 hour, then was washed 3 times with a Tris-based buffer, and 100 μ L PBS was added to each well.

Fluorescent intensities were measured using the PHERAstar FS microplate reader with an Alexa488 optic module. Plates were then incubated, washed and measured again every hour for 6 hours to track fluorescent signal of sEVs over the time course. Separation of dye from sEV may result in movement of the dye into the surrounding PBS, therefore change in sEV signal following wash steps was used as a measure of sEV dye loss. In parallel, fluorescent signal was measured over 6 hours in wells not washed in PBS as a control for photobleaching effect arising from repeat measures.

2.5. Uptake of sEVs

2.5.1. Detection of cellular uptake of fluorescent sEVs

Fluorescence microscopy

Fibroblasts were seeded at 10,000 cells per well in 96 glass-bottomed plates (175µm thick glass) and cultured until 80% confluent. Cells were treated with labelled sEVs at stated doses and incubation times in DMEM/F12 free of FBS. For experiments when cells are fixed, sEV containing media is washed off the cells with PBS prior to fixation. For experiments conducted with live cells, DMEM/F12 is washed off and replaced with FluoroBrite™ DMEM. sEV containing fibroblasts are typically visualised on the Axio Observer Z1 microscope with a 63x/1.4 numerical aperture objective lens with oil. Alexa488, CFSE, Cal and SYTO labelled sEVs are visualised using an Alexa488 filter (Ex/Em = 493/520) and Alexa594 sEVs using an Alexa594 filter (Ex/Em = 590/619).

Flow cytometry

Fibroblasts were seeded in 24 well cell culture plates (Greiner Bio-One) at 40,000 cells/well and cultured until 80% confluent. Cells were treated with labelled sEVs at stated doses. Following treatment, cells were washed in PBS and stripped from the well surface using 200µL/well trypsin (Lonza) at 37°C until cells have detached from the plate (usually 5-10 minutes). Cell suspension was added to flow cytometry tubes (StemCell Technologies, Canada), then cells were pelleted by centrifugation at 400g for 6 minutes, washing off the trypsin. Pelleted cells were resuspended in 300µL PBS per tube and put on ice. Following calibration of the FACSverse cytometer (BD Biosciences, USA), using cytometry signalling and tracking (CST) beads (BD Biosciences), tubes were loaded, forward scatter and side scatter measurements are taken, and a gated population of cells considered live based on the scatter measurements. Fluorescent intensity of gated cells was measured until 1,000 cells have been measured (unless otherwise stated). 10,000 cells were initially measured, however this was reduced to 1,000 cells, to allow reduced sEV consumption for experiments. Mean fluorescent intensity (MFI) was used to represent the fluorescent intensity of the population.

2.5.2. Pharmacological inhibition

In experiments involving treatment of fibroblasts with sEVs and pharmacological inhibitors, cells were pre-treated with inhibitors for 30 minutes prior to sEV addition, to ensure endocytic blockade before addition of sEVs (Roberts-Dalton et al., 2017). All inhibitors were diluted in Dimethyl sulfoxide (DMSO) and working concentrations were diluted in DMEM/F12. Fibroblasts were washed with DMEM, then pre-incubated with inhibitors at stated doses for 30 minutes. Doses of inhibitors were derived from published reports, and to validate these we performed experiments to establish their toxicities. Cells were then treated with stated doses of sEVs in the continued presence of the inhibitors. Pharmacological inhibitors used were: Dynasore (EMD Millipore, USA), Cytochalasin D (Sigma Aldrich), EIPA (Sigma Aldrich) and Bafilomycin A1 (Sigma Aldrich). Heparin (Sigma Aldrich) was prepared as a stock concentration of 50mg/mL in purified water, working concentrations were diluted in DMEM/F12 for experiments, again cells were pre-treated for 30 minutes with Heparin before addition of sEVs.

2.5.3. siRNA transfection

siRNAs of the 4 targets (AP2 μ 2, Cav-1, Flot-1, PAK1) and GFP (used as an irrelevant siRNA control since GFP is not expressed in our cells) were previously used, validated in HeLa cells (Al Soraj et al., 2012; Roberts-Dalton et al., 2017) and custom made by Europhins MWG Operon, Germany. The target sequences are shown in table 2.1.

For transfections, fibroblasts were seeded in 6 well cell culture plates (Greiner Bio-One) at 150,000 cells/well and left overnight. On the day of transfection, 100nM siRNA in 185 μ L Opti-MEM[®] (Invitrogen) per well was made up and mixed via gentle inversion. 2 μ L Lipofectamine[™] (Invitrogen) was mixed with 13 μ L Opti-MEM per well. Diluted Lipofectamine was transferred to the diluted siRNA and mixed by gentle inversion and pipetting. This mixture was incubated for 30 minutes at room temperature. Cells were washed 3 times in Opti-MEM before addition of 800 μ L Opti-MEM per well. The siRNA-Lipofectamine mixture was added to the Opti-MEM containing wells drop by drop. Cells were incubated at 37°C for 4 hours, then 500 μ L of 30% FBS^{ev-}/Opti-MEM was added to each well.

Materials and Methods

Following incubation of cells for 48 hours (Roberts-Dalton et al., 2017), transfected cells were then used for mRNA/protein analysis or used for uptake experiments.

Target	Sequence
AP2 μ 2	GUGGAUGCCUUCGGGUCAdTdT
Cav-1	AGACGAGCUGAGCGAGAAGdTdT
Flot-1	UGAGGCCAUGGUGGUCUCCdTdT
PAK1	AUAACGGCCUAGACAUUCAdTdT
GFP	GGCUACGUCCAGGAGCGCAdTdT

Table 2.2. siRNA sequences for knockdown of endocytic regulators. List of protein targets for siRNA-mediated knockdown, with sequences

2.5.4. Quantitative polymerase chain reaction

To confirm knockdown of target mRNA by transfected siRNA, mRNA content in treated cells was assessed by quantitative polymerase chain reaction (qPCR) and compared target mRNA expression in cells treated with the target siRNA versus a GFP siRNA treated cell as a control. siRNA treated cells were lysed with 1mL TRI Reagent® (Sigma Aldrich) per well. Samples were then added to Eppendorf tubes and 200 μ L chloroform was added to each tube, and the solutions were mixed. Phenol and aqueous layers were separated through centrifugation of the tubes at 4°C, 16,000g for 20 minutes, then the aqueous colourless layer was extracted and mixed with ice cold isopropanol for precipitation of RNA, this mix was left for 24 hours, at -20°C. The following day, Isopropanol was removed through another centrifugation step, a 16,000g spin for 20 minutes at 4°C. RNA pellet was then resuspended in 1mL of 70% ethanol and spun again under the same centrifuge conditions. Ethanol was removed, fresh ethanol added, and the samples were centrifuged once again. This time the RNA pellets were allowed to air dry after ethanol removal, then pellets were dissolved in 11 μ L of RNase free molecular grade water.

Analysis of 1 μ L of dissolved RNA using a NanoDrop™ 2000 Spectrometer was used to calculate the purity of the RNA sample. Absorbance at 260nm indicates nucleic

Materials and Methods

acid quantity and absorbance at 280nm indicates protein quantity, the ratio between these absorbance values is used to determine the quality of RNA extraction. Ratios of 260:280nm >1.7 were required for RNA sample to be considered pure enough for reverse transcription. The Beer-Lambert equation takes the RNA extinction coefficient as 40 and uses the absorbance value measured to calculate the concentration of nucleic acid. 1µg of RNA is then added to a reverse transcription master mix. The master mix (Thermofisher) was made up of 2µL 10X reverse transcription buffer, 2µL 10X reverse transcription random primers, 1µL RNase inhibitor, 1µL Multiscribe™ reverse transcriptase and 0.8µL of deoxynucleotide triphosphate (dNTP) mix (with dATP/dCTP/dGTP/dTTP), the final volume of this mix with the RNA sample is 20µL. Reverse transcription was carried out using a S1000 thermal cycler (BioRad), the first incubation for primer annealing was for 10 minutes at 25°C. the next step, extension, was for 2 hours at 37°C. This step creates complementary DNA (cDNA), the reverse transcriptase enzyme is deactivated through incubation at 85°C for 5 minutes. Created cDNA is stored at -20°C.

In a 20µL PCR reaction, 1µL cDNA is mixed with 10µ TaqMan® universal master mix, 1µL TaqMan® custom gene expression assay primer and probe mixes (all from Thermofisher), and 8µL of water. A StepOnePlus™ real time PCR thermocycler (Thermofisher) was used for the PCR procedure. Heating steps were: 50°C for 2 minutes, 95°C for 15 seconds and 60°C for 1 minute, these were repeated for 40 cycles. The cycle threshold (C_T) value (number of cycles required to detect a fluorescent signal) was calculated to determine relative mRNA expression, GAPDH was used as a standard reference gene. C_T of GAPDH was subtracted from the target C_T , this generated the ΔC_T , allowing calculation of relative expression of the target gene by the equation $2^{-(\Delta C_T1 - \Delta C_T2)}$ where ΔC_T1 is the ΔC_T for the experimental target and ΔC_T2 is the ΔC_T for the control GAPDH samples. Negative controls for reverse transcription and PCR were done by using water as a sample in place of RNA/cDNA.

2.5.5. Cell viability assays

Orangu™ Cell counting solution (Cell guidance systems, UK) was used to determine viability of AG02262 fibroblasts. Orangu™ is a water-soluble tetrazolium salt (WST)-8 which exhibits a strong orange colour when reduced by viable cell dehydrogenase activity, and the number of living cells is related to the amount of orange dye formed. For a viability assay, cells were washed in media, then treated with 1:10 dilution of Orangu™ in DMEM/F12 for 1 hour at 37°C, then absorbance at 450nm was read on a PHERAstar FS microplate reader.

2.5.6. Bacmam transfections

CellLight® BacMam reagents (Thermofisher), were used to tag target proteins in live fibroblasts with red fluorescent protein (RFP) (Dolman et al., 2013). Fibroblasts were seeded at 150,000 cells/well and incubated overnight. Cells were treated with 1:200 of a BacMam reagent in DMEM/F12, reagents used were to fluorescently label early endosomes (Rab5-RFP), late endosomes (Rab7-RFP) or lysosomes (LAMP1-RFP). Following overnight treatment, the media was washed and replaced with FluoroBrite™ DMEM/F12, for live cell imaging, the cells would now be expressing the RFP-tagged proteins and could be visualised fluorescently. Fluorescence microscopy was carried on cells following Alexa488-sEV treatment.

2.5.7. Time-lapse microscopy

Time-lapse microscopy experiments were carried out on an Axiovert 100 widefield microscope (Zeiss) with a temperature and CO₂ controlled black box encasing the area around the plate (Solent Scientific, UK), creating an incubator like environment to maintain cells in incubator-like conditions. For experiments using this microscope, a 40x objective lens was used, and red dyes were visualised using a 633nm laser. Multi-dimensional acquisition software on the MetaMorph v7.8.13.0 program was used to set stage positions, experiment time course, and time points for image capture. Alexa633-sEVs were typically used for time-lapse experiments, unless otherwise stated, and cell morphology was tracked with brightfield imaging.

2.5.8. Endocytic probes

For comparison of uptake kinetics of sEVs versus Transferrin (Tf) and Dextran (Dx), fibroblasts were pulsed with 25µg/mL Alexa488-sEVs, 5µg/mL Tf-Alexa488 (Molecular Probes, USA) or 100µg/mL Dx-Alexa488 (Invitrogen) for 30 minutes, then washed in fresh media, the uptake was then “chased” for the stated time points, dosing and treatment time had been previously used for similar experiments in HeLa cells (Roberts-Dalton et al., 2017). Fibroblasts of 80% confluency were cultured prior to experiments. For microscopy experiments, cells were fixed in 4% PFA and visualised using the Axio Observer Z1, and for flow cytometry, cells were washed and trypsinised, then cooled to 4°C for analysis.

Co-localisation experiments of Alexa594-sEVs with Dx or Tf were used to determine intracellular location of sEVs post-uptake. Fibroblasts were treated with 100µg/mL Dx-Alexa488 for 2 hours, the cells were then washed, and the Dx was chased overnight, ensuring Dx loading of lysosomes. The following day, cells were treated with 25µg/mL Alexa594-sEVs for 30 minutes, then washed and chased for stated time points. For evaluation of early endosome localisation of sEVs, co-localisation of Alexa594-sEVs with Tf was measured. Fibroblasts were treated with 25µg/mL Alexa594-sEVs and 5µg/mL Tf-Alexa488 simultaneously for 30 minutes, washed, then chased for stated time points. Co-localisation was determined by the proportion of 594 signal overlapping 488 signal, a calculation of Mander’s coefficient using the JACoP plug-in on ImageJ (ImageJ, USA). This allowed us to determine the proportion of sEVs in early endosomes or lysosomes at given time points post-uptake.

Fibroblasts were treated with Mitotracker (Invitrogen) for determination of mitochondrial localisation of sEV delivered SYTO/Alexa488. Fibroblasts treated with 100nM Mitotracker in FluoroBrite™ DMEM for 1 hour, the cells were washed, then treated with 25µg/mL SYTO/Alexa488-sEVs for 1 hour. Cells were washed again and replaced with fresh FluoroBrite™ DMEM, then visualised fluorescently.

2.5.9. Antibody labelling of sEVs

sEVs were tagged with antibodies against surface proteins as an approach to inhibit cellular binding and uptake. Alexa633-sEVs were incubated with 10µg/mL of primary antibody over night at 4°C. Fibroblasts were treated with 25µg/mL Alexa-sEVs in the presence of blocking antibody for 1 hour at 37°C, then cells were washed, and trypsinised for measurement by flow cytometry. Antibodies used for these experiments were: anti-TGFβ, anti-CD9, anti-β1 (all R&D Systems) and anti-α3 (Merck Millipore; Table 2.1).

2.6. Assessment of sEV functional effects on fibroblasts

2.6.1. Fibroblast differentiation

AG02262 fibroblasts were seeded in a 96 well glass-bottomed plates at 10,000 cells per well, in DMEM/F12 media with supplements as described in section 2.1.1. Once the cells were around 80% confluent, they were growth arrested for 24 hours. Cells were treated with 200µg/mL (unless otherwise stated) DU145 sEVs or 1.5ng/mL sTGFβ1 in DMEM/F12 for 72 hours. Following the treatment, the cell conditioned media was frozen at -80°C, for later use in growth factor assays, and the cells were fixed in ice cold 1:1 acetone/methanol for 5 minutes. Alpha-smooth muscle actin (αSMA) expression in fibroblasts, a marker of myofibroblast differentiation (Desmoulière et al., 1993), was evaluated by staining of fixed cells with an αSMA antibody (Santa Cruz). Cells were visualised with an Axio Observer Z1 with apotome.

2.6.2. Quantification of secreted HGF

Fibroblast conditioned media was analysed for HGF quantity using DuoSet ELISA systems (R&D Systems). 1µg/mL HGF capture antibody in PBS was added to high protein binding ELISA strip 96 well plates, these plates were incubated at room temperature overnight. The plates were washed 3 times using a Tris-based buffer. Wells were then treated with 1% BSA/PBS for 2 hours at room temperature as a blocking step, then the wash step was repeated. 100µL defrosted fibroblast media was added to each well. In other wells a serial dilution of recombinant human HGF was added, with concentrations ranging from 0ng/mL to 8ng/mL in PBS, these

Materials and Methods

were used to generate a standard curve. Following a 2 hour treatment at room temperature, wells were washed again, then treated with 200ng/mL HGF detection antibody for 2 more hours, at room temperature, then washed. In a departure from manufacturer instructions, wells were treated with Europium-streptavidin conjugates in a 1:1000 dilution in red assay buffer for 45 minutes at room temperature, wells were then washed 6 times. Europium fluorescence intensifier was added to wells for 5 minutes, then the signal assessed by TRF on a PHERAstar FS microplate reader. Fluorescence values generated were used to quantify HGF expression extrapolated from the standard curve.

2.7. Image and statistical analysis

Quantification of sEV uptake in microscope images was carried out by measuring mean fluorescent intensity (MFI) of fields of view (divided by number of nuclei where stated), using ImageJ software V1.51n. Co-localisation analysis of microscopic images were performed using the JACoP plug-in with ImageJ software v1.51n, using program default thresholding, calculating Mander's coefficients of colour 1 over colour 2 (M1) or colour 2 over colour 1 (M2) (Dunn et al., 2011). Measurement of sEV clustering in fibroblasts overtime was evaluated by integrated morphometry analysis, calculating average fluorescent area size with auto-thresholding of light objects, using MetaMorph v7.8.13.0 software (Molecular Devices, USA).

1-way (with Tukey's post-test) and 2-way (Bonferroni post-test) Analysis of variance (ANOVA) tests were used in experiments with more than two experimental groups. Otherwise, experiments with two groups were analysed by Students T-test. ANOVAs and T-tests were performed using Prism-5 software v5.03 (GraphPad, USA). Data on graphs signifies mean +/- Standard error of the mean (SEM) from a representative experiment, unless otherwise stated. Significant P-values were deemed significant when $p < 0.05$. *= $p < 0.05$, **= $p < 0.01$, ***= $p < 0.001$.

All materials used can be seen in table 2.3.

Materials and Methods

Material	Company	Catalogue number	Material	Company	Catalogue number
DU145 cells	ATCC	HTB81	Alexa488 Maleimide	Life technologies	A10254
AG02262 Primary fibroblasts	Coriell	AG02262	Alexa594 Maleimide	Life technologies	A10256
RPMI 1640	Thermofisher	31870074	Alexa633 Maleimide	Life technologies	A20342
DMEM/F12	Lonza	BE04-687F	Exosome spin column MW3000	Life technologies	4484449
Penicillin-Streptomycin	Lonza	17602E	CFSE	EBioscience	65085084
L-Glutamine	Lonza	BE17605E	Calcein AM	Invitrogen	65085378
Foetal bovine serum	Thermo Scientific	11573397	SYTO RNASelect	Invitrogen	S32703
T75 flask	Greiner Bio One	658170	BCA protein assay kit	Thermofisher Scientific	23235
CELLline Bioreactor	Sigma-Aldrich	Z688045	100nm latex beads	Malvern Instruments	NTA4088
Acetone	GPR Rectapur	20065.327	Particle free water	Fresenius Kabi	3158589
Methanol	GPR Rectapur	85650.320	High protein bind ELISA strip 96 well plate	Greiner Bio One	756071
Paraformaldehyde	Life technologies	28906	Wash buffer	Perkin Elmer	1244114
Phosphate buffered saline	Sigma-Aldrich	D8537	Goat anti-mouse biotinylated secondary antibody	Perkin Elmer	NEF8-23001EA
Trypsin	Lonza	CC5012	Europium-Streptavidin	Perkin Elmer	1244360
96 well glass bottom plate	Greiner Bio One	655892	Red assay buffer	Kaivogen	4202
96 well plastic plate	Greiner Bio One	655930	Europium fluorescence intensifier	Kaivogen	4204
24 well plate	Greiner Bio One	662892	RGD peptide	Sigma-Aldrich	A8052
6 well plate	Greiner Bio One	657160	BSA	R&D Systems	5217
0.22µm Millex GP syringe filter unit	Merck Millipore	SLGP033RS	Chemi-luminescent substrate	LiCOR	92695000
Ultracentrifuge tubes	Beckman Coulter	344623	Flow cytometry tubes	StemCell technologies	38057
Sucrose	Sigma-Aldrich	S9378	Cytometry signalling and tracking beads	BD Biosciences	656504
D ₂ O	Sigma-Aldrich	151882	DMSO	Sigma-Aldrich	D2650
DAPI	Thermo Scientific	D1306	Dynasore	EMD Millipore	324410
FluoroBrite DMEM	Thermofisher	A1896701	Cytochalasin D	Sigma-Aldrich	C8273
Alexa488 goat anti-mouse secondary antibody	Thermo Scientific	A11001	EIPA	Sigma-Aldrich	A3085
Alexa594 goat anti-mouse secondary antibody	Thermo Scientific	R37121	Bafilomycin A1	Sigma-Aldrich	B1793
Opti-MEM	Invitrogen	31985047	Heparin	Sigma-Aldrich	H33393
Lipofectamine	Invitrogen	11668030	TRI reagent	Sigma-Aldrich	T9424

Materials and Methods

Material	Company	Catalogue number	Material	Company	Catalogue number
Chloroform	Amresco	0757	SeeBlue Plus 2 precision	Thermo Scientific	LC5925
Isopropanol	VWR	437423R	Magic Mark XP	Thermo Scientific	LC5602
Molecular grade water	Sigma-Aldrich	W4502	MOPS Buffer	Thermo Scientific	NP0001
TaqMan universal PCR master mix	Thermofisher	4304437	PVDF membrane	GE Life Sciences	10600023
Orangu Cell counting solution	Cell Guidance Systems	OR01-1000	Glycine	Sigma-Aldrich	G8898
CellLight BacMam Rab5 RFP	Thermofisher	C10587	Tris	Sigma-Aldrich	252859
CellLight BacMam Rab7 RFP	Thermofisher	C10589	Tween	Sigma-Aldrich	P9416
CellLight BacMam LAMP1 RFP	Thermofisher	C10597	Goat anti-mouse HRP secondary antibody	Santa Cruz Biotechnologies	Sc2005
RIPA lysis buffer system	Santa Cruz Biotechnology	Sc24948	Transferrin-Alexa488	Molecular Probes	T13342
Bradford protein assay kit	BioRad	5000001	Dextran-Alexa488	Invitrogen	D22910
DTT	Sigma-Aldrich	10197777001	Mitotracker	Invitrogen	M7512
SDS buffer	Invitrogen	NP000202	Recombinant human TGF β 1	Peptotech	10021C
NuPAGE precast 4-12% gel	Life technologies	NP0321BO X	HGF DuoSet ELISA kit	R&D Systems	DY294

Table 2.3. List of materials. A list of materials used in experiments.

Chapter 3 – Characterisation of DU145 derived small extracellular vesicles

3.1. Introduction

In cancer, tumour derived sEVs educate cells of the tumour microenvironment to promote growth and survival of the cancer (Webber et al., 2015a). The presence of cancer associated myofibroblasts is well documented in the tumour microenvironment (Kalluri, 2016), and induction of myofibroblast differentiation from fibroblasts (Webber et al., 2010), as well as mesenchymal stem cells for example (Chowdhury et al., 2015) by cancer derived sEVs has been uncovered and has been repeated across many cancer types. These studies collectively reveal a key role for cancer derived sEVs in microenvironment modulation and progression of cancer.

In this study we examine the cellular uptake of PCa derived sEVs by fibroblasts, in order to better understand sEV modes of action relating to stromal cell differentiation. The DU145 PCa cell line was the chosen source of sEVs for our experiments, sEVs from this cell line have been previously well characterised by the group and have been shown to play various tumour promoting roles, including induction of myofibroblast differentiation (Webber et al., 2010), and immune evasion (Clayton et al., 2007). sEVs have been widely studied in recent years for their potential to deliver numerous factors to recipient cells (Tkach and Théry, 2016), driving phenotypic change. Cellular uptake of sEVs, and delivery of both protein (Fedele et al., 2015) and nucleic acids (Valadi et al., 2007) by sEVs have been described, suggesting a well-regulated processing of sEVs by recipient cells following internalisation. Progress has been made on mapping out the uptake routes and intracellular fate of sEVs in various recipient cells. Here, internalisation and intracellular trafficking of DU145 derived sEVs was defined in primary fibroblasts, a cell type biologically relevant in the tumour microenvironment. Our recipient cells in this study were the AG02262 lung fibroblasts, primary human fibroblasts used as model cells for myofibroblast differentiation (Midgley et al., 2013; Webber et al., 2010), shown by the group previously to undergo differentiation following stimulation by DU145 PCa derived sEVs.

To understand the biological relevance of sEVs in functional studies, their isolation from their cell supernatant/ biological fluid is vital, in order to attribute results to the role of sEVs. In this study, sEVs were isolated through ultracentrifugation on a 30% sucrose/D₂O cushion, followed by a second ultracentrifugation step to wash

off the sucrose and pellet the sEVs. The International Society for Extracellular Vesicles (ISEV) has recently published guidelines for defining EVs by their characteristics (Théry et al., 2018). EVs can typically be characterised by their morphology, size and expression of specific proteins, ISEV guidelines strongly encourage explicit description of these features, to better define EVs being used in further experiments. We have employed a number of techniques to characterise sEVs isolated from DU145 cells, showing their morphology and size, assessing their purity, expression of marker proteins and their ability to drive myofibroblast differentiation in primary fibroblasts.

In this chapter, isolated sEVs from DU145 cells were subject to characterisation using diverse techniques, with the aim of demonstrating successful purification of DU145 derived sEVs through the sucrose cushion isolation method. Firstly, structures in a sEV sample were analysed by cryo-EM to determine the heterogeneity of the morphologies present. Light scattering and protein assays of sEVs were carried out to evaluate the purity of the preparations. Next, immunophenotyping plate assays and Western blotting were employed to reveal expression of particular sEV associated proteins. Finally, we assessed the ability of these sEVs to stimulate activation of primary fibroblasts, to confirm the known function of these sEVs. The data collected here will define our sEVs, in accordance to ISEV guidelines, and these sEVs will be used to monitor cellular uptake by fibroblasts in subsequent chapters.

3.2. DU145 derived sEV characterisation

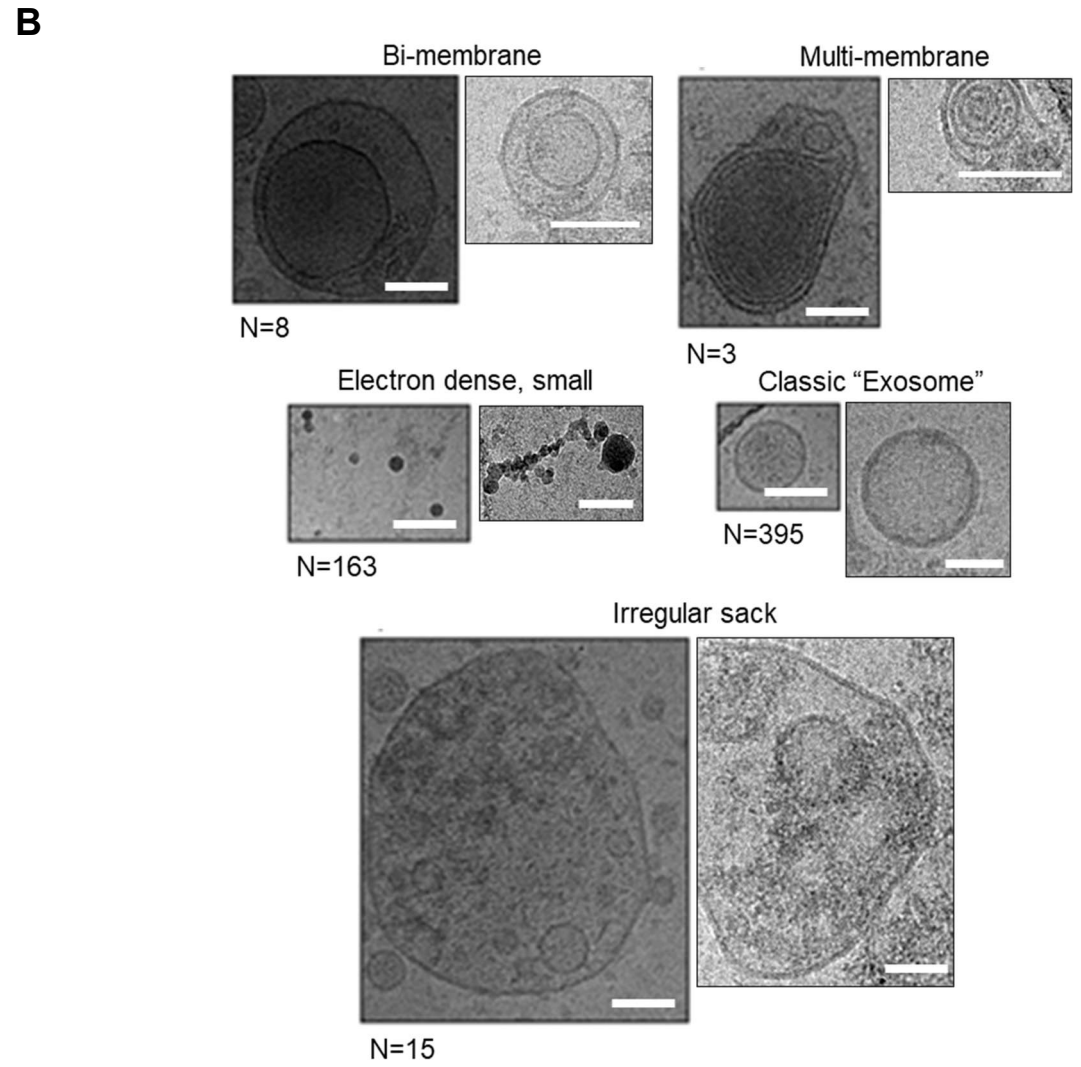
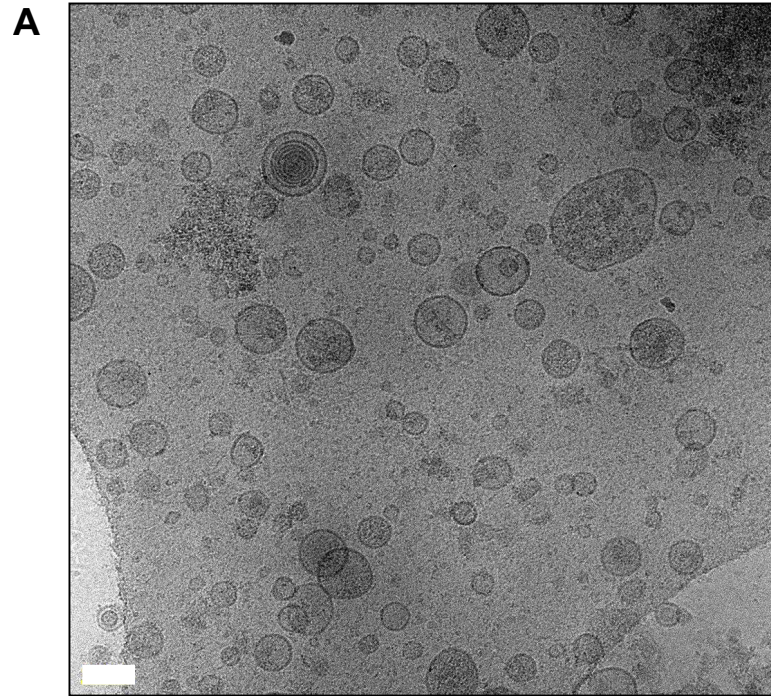
3.2.1. Vesicle morphology

The cells used to generate sEVs is the DU145 PCa cell line (ATCC, USA), derived from a brain metastasis. DU145 cells underwent continuous culture in bioreactors flasks described in section 2.2, the cell conditioned media is collected weekly and goes through serial centrifugation steps to remove dead cells and larger debris. Following filtration of the media through a 0.22µm filter, the sEV containing media is floated on a sucrose cushion, and the sEVs are then isolated by ultracentrifugation driven pelleting.

Results

Cryo-EM, which retains the native structure of sEVs (Conde-Vancells et al., 2008), was carried out by our collaborator (Professor Juan Falcon-Perez, CIC-bioGUNE, Spain) to examine the morphology of structures present in sEV isolates. This revealed a heterogenous population of vesicle like structures, electron dense bodies and other structures (Figure 3.1a). Figure 3.1b shows examples of distinct structures present in sEV isolates. The “classical exosome” or vesicle-like structure is the most common structure seen in the sEV preparation (figure 3.1c), representing 67% of the total structures counted. These vesicles are sized around 66nm (figure 3.1d), indicative of sEVs. Besides these, are numerous distinct morphologies (figure 3.1b). There are unusual structures seen, such as vesicles with two or more membrane layers (termed bi-membrane and multi-membrane structures) and large irregular sacks which appear to contain smaller vesicles. These structures are present in almost all fields of view, however, together they represent less than 5% of total structures counted in these images (figure 3.1c). The sizes of these structures varied greatly (figure 3.1d), with many of them measuring above the size range indicative of sEVs (200nm). More than a quarter of all structures present are very small electron dense particles (figure 3.1c), which appear to lack a lumen (figure 3.1a, b), and were typically around 22nm in diameter (figure 3.1d), in contrast to the larger structures which exhibit a membrane. The larger structures present contain a greater volume than the small vesicles (figure 3.1e), however these small vesicles have a much greater surface area to volume ratio, likely making them more biological relevant in terms of vesicle to cell surface interactions. The nature and origin of these structures is unexplained, though their presence suggests that the sEV isolation procedure is not perfect in generating entirely homogenous uni-lamellar sEV preparations.

Results



Results

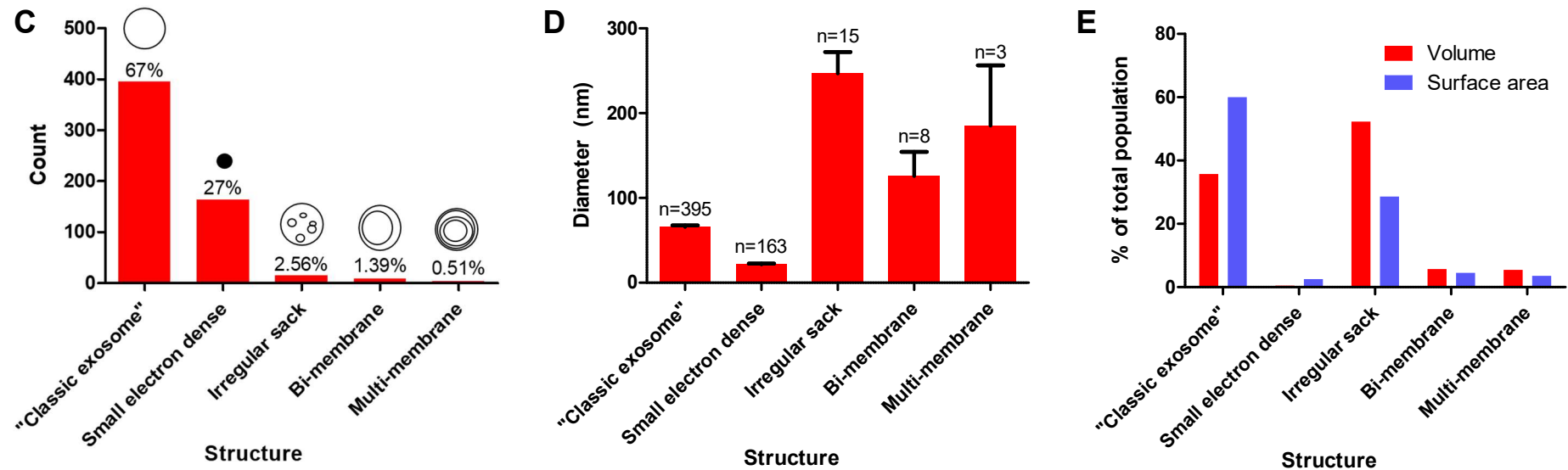


Figure 3.1. Cryo-EM of sucrose cushion purified DU145 derived sEV isolates. Cryo-EM was performed on a sample of isolated DU145 derived sEVs and structures were counted and classified. (A) Morphologies of structures visible in a DU145 sEV preparation, by cryo-EM. Scale bar = 100nm. (B) Examples of distinct structures seen in sEV isolates. Scale bar = 100nm. (C) Count of each structure type represented in the sEV preparation, with percentages each represents in the total count. Schematic representations of each respective structure are also shown. (D) Mean diameter (nm) of every structure counted in the sEV sample. (E) Volumes and surface areas of each structure, represented as their percentage of the whole population. Bars represent means +/- SEM. Data based on 584 structures counted across 40 fields of view from 1 sEV preparation. Cryo-EM was performed by Professor Juan Falcon-Perez, CIC-bioGUNE, Spain.

3.2.2. Vesicle size distribution and purity assessment

Nanoparticle tracking analysis (NTA) was performed to gain a size distribution of a typical sEV population. Diluted sEVs were subject to analysis by Nanosight under flow conditions. Following analysis by NTA software, distribution of particle sizes within a sEV population is plotted as a histogram, with size plotted against respective concentrations of particles at these sizes (figure 3.2). In concurrence with cryo-EM, the vast majority of particles detected by the Nanosight were below 200nm in size, falling into the range of small EVs as defined by ISEV (Théry et al., 2018), with the modal size around 100nm. The lower end of the distribution curve is steeper than the upper end, and with the very small particles seen by cryo-EM, it is possible that the NTA is unable to detect particles <50nm. The size distribution of the sEV isolate is typical of a DU145 sEV preparation subject to NTA (Yeung et al., 2018).

The BCA protein assay is routinely used to determine protein concentration of our sEV isolates. The protein concentration of the sample is determined by comparing the absorbance readout against a BSA standard. Protein concentration of a sEV preparation is typically given in µg/mL (table 3.1) and is used to normalise sEV quantity in later experiments. NTA also provides the sEV concentration of a preparation, in particles/mL (table 3.1). The particle and protein concentrations seen in table 3.1 show variation from preparation to preparation and can be affected by factors such as volume of supernatant used for an isolation, and number of cells in a bioreactor flask used to collect sEV containing media, but also operator dependent nuances. Using these two measures of concentration, the purity of sEVs, in terms of the number of detected particles per µg of protein, in a given sample can be assessed. The particle to protein (P:P) ratio calculation, see below, allows us to confirm the purity of the preparation procedure, with low P:P ratios indicative of protein contamination (Webber and Clayton, 2013).

Particles/mL ÷ µg/mL protein = Particles/µg protein (P:P ratio)

Examples of P:P ratios calculated in our sEV samples are shown in Table 3.1. Despite sizeable differences in particle and protein concentrations between preparations, P:P ratios are mostly above 1×10^{10} particle/µg protein, meaning they are considered to be of high purity, according to study examining P:P ratios (Webber and Clayton, 2013). Preparations with P:P ratios $< 1 \times 10^{10}$ particle/µg

protein were deemed impure (table 3.1, red). We would be cautious in using sEVs that had been deemed impure as they would have considerable contaminating protein, and these preparations were generally discarded. The high P:P ratios usually calculated in DU145 sEV preparations shows that the sucrose cushion method for isolation of sEVs produces samples of high purity.

3.2.3. Vesicle protein profiling

DU145 sEV isolates were next assessed for their expression of accepted sEV or “exosome” markers. Western blotting was carried out to compare the expression of the proteins ALIX, TSG101, MHC1 and Calnexin in DU145 cell lysate versus DU145 derived sEVs to look for enrichment in sEVs (Figure 3.3). As expected, ALIX, TSG101, MHC1 were all found to be enriched in the sEV lanes relative to the DU145 cell lysate, normalised for input protein quantity. TSG101 and MHC1 appeared as thick single bands, however ALIX in the sEV sample was peculiar in that the staining produced multiple bands; this suggests distinct isoforms of the protein, which we consistently observe in these sEVs, though the reason for this observation requires clarification. Calnexin, an ER protein, was not detected in the sEV lane, suggesting that the isolates are void of contaminating cellular material. Lack of detectable non-vesicular material in the Western blot is in agreement with the high purities determined by the P:P ratios and further assures that the sEVs isolation method is effective at removing soluble cell components.

The classical sEV-related tetraspanins, CD9, CD63 and CD81 were assessed in a semi-quantitative fashion, by immunophenotyping plate assay. 1µg of sEVs per well were added to sticky ELISA plates and subject to labelling with tetraspanin antibodies, and Europium was later attached for a TRF readout. DU145 derived sEVs were positive for all three of the tetraspanins (figure 3.4). CD9 was detected with the highest signal, followed by CD81 and CD63 respectively, and negligible signal in the isotype controls demonstrates the specific binding of the tetraspanin antibodies to their targets. The proteins expected to be expressed on the DU145 derived sEVs were all expressed, and Western blot analysis demonstrated enrichment of all the sEV markers in sEVs and a lack of contaminating materials.

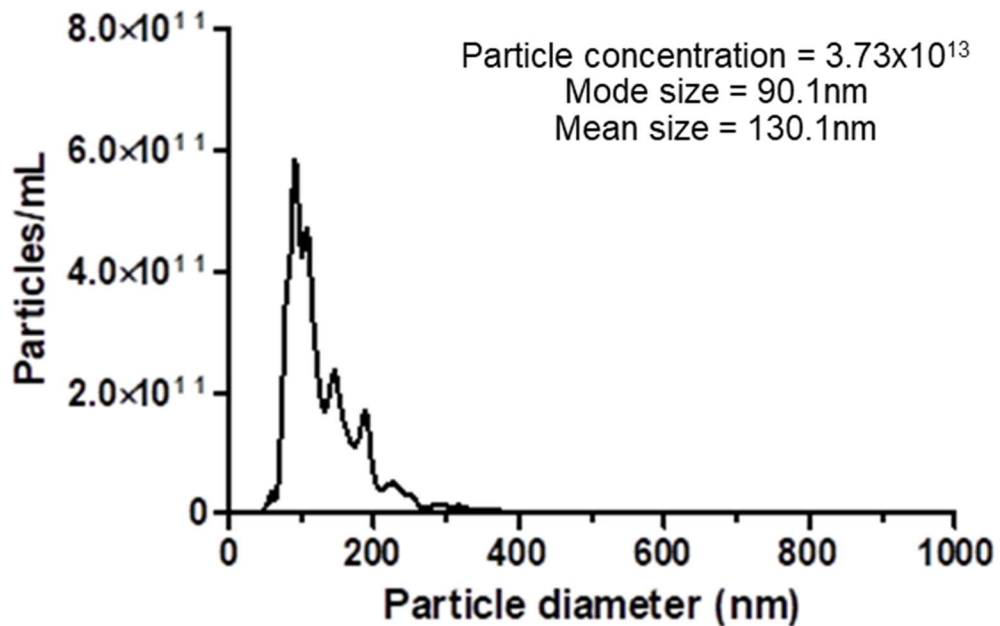


Figure 3.2. Size distribution of DU145 derived sEVs. NTA histogram demonstrating the size distribution of a typical sEV isolate. Histogram represents the concentration of analysed particles against their respective size in nm. Presented histogram is based on summary data from 5 videos, each video tracks particles across 749 frames over 30 seconds. Collected data also allows us to calculate the particle concentration of the sample, as well as the mode and mean sizes of the particles.

sEV preparation date	Particle concentration (particles/mL)	Protein concentration ($\mu\text{g/mL}$)	P:P ratio (Particles/ μg protein)
4/11/15	3.73×10^{13}	1760	2.12×10^{10}
3/12/15	8.31×10^{12}	903	9.2×10^9
21/3/16	4.59×10^{13}	1550	2.96×10^{10}
16/8/17	6.11×10^{13}	4273	1.43×10^{10}
29/11/17	6.42×10^{13}	1999	3.21×10^{10}
1/2/18	6.87×10^{13}	3286	2.09×10^{10}
11/6/18	6.49×10^{13}	3382	1.92×10^{10}
3/7/18	6.23×10^{13}	3917	1.59×10^{10}

Table 3.1. Particle and protein concentrations of DU145 derived sEVs. A summary of particle and protein concentrations (calculated by BCA protein assay and NTA respectively) of 8 separate sEV preparations, isolated by the sucrose cushion method. Particle and protein concentration variation between preparations is noted. Particle and protein concentrations are used to calculate the P:P ratio of the sEV samples, which can be used to assess preparation purity (Webber and Clayton, 2013). Red = sEV preparation deemed impure (P:P ratio $< 1 \times 10^{10}$).

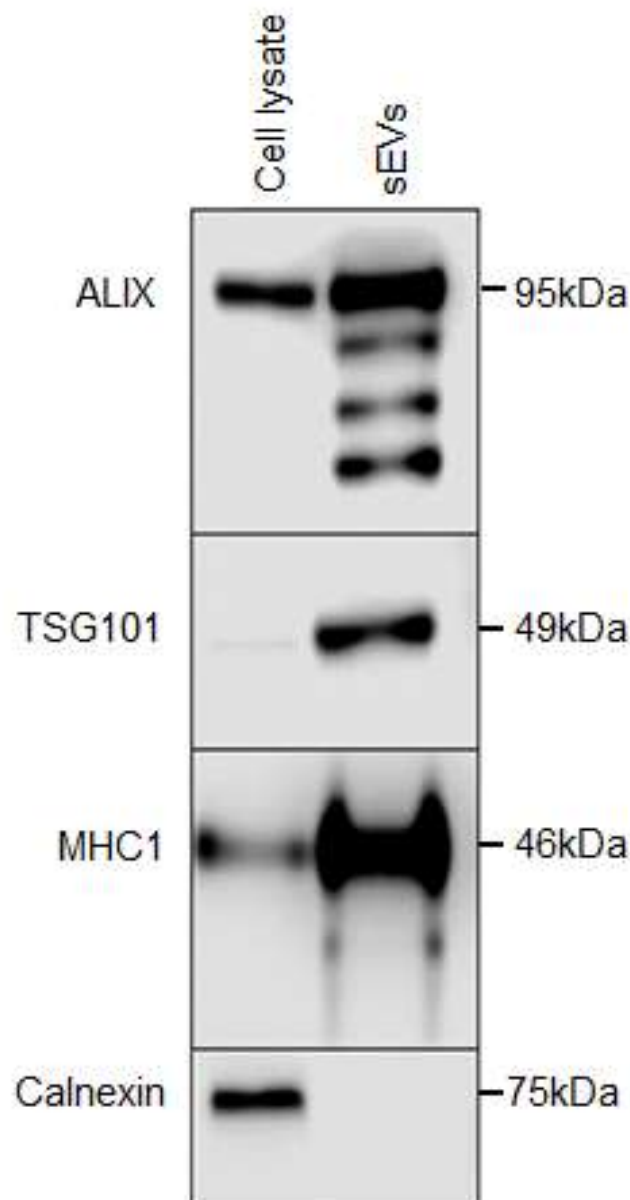


Figure 3.3. Western blot characterisation of DU145 derived sEVs versus DU145 cells. 20 μ g protein of DU145 cell lysate or DU145 derived sEVs were loaded into parallel lanes, and SDS-PAGE and Western blotting were performed, with primary antibodies as indicated. Western blotting revealed relative expression of ALIX, TSG101 and MHC1, as well as the endoplasmic reticulum marker not expected in sEV isolates, Calnexin.

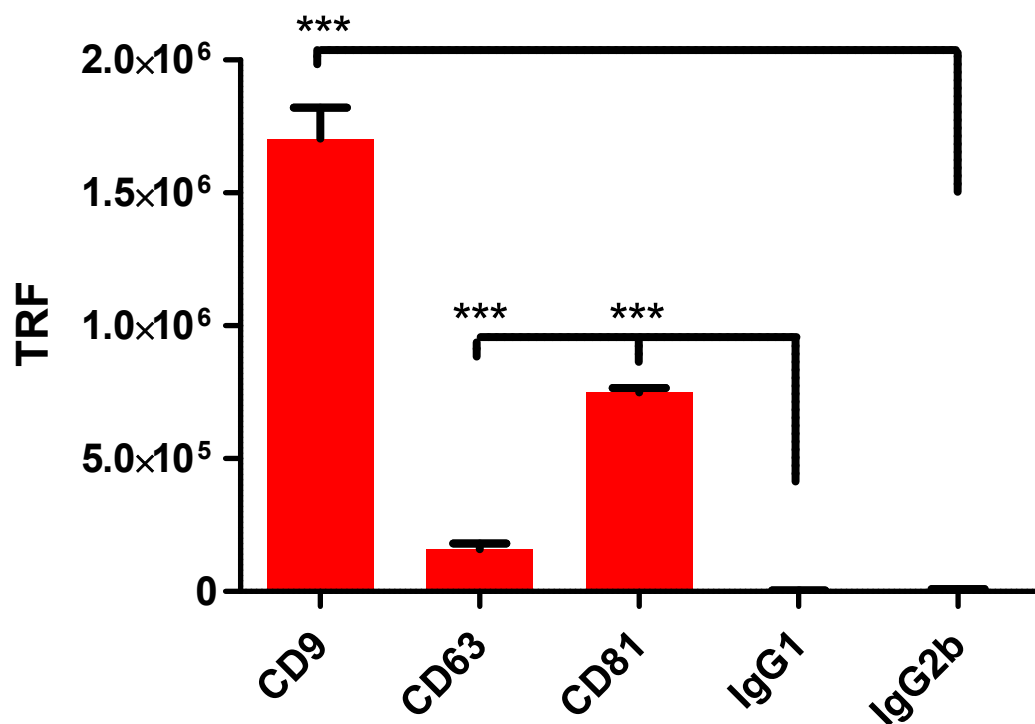


Figure 3.4. Immunophenotyping plate assay for detection of DU145 derived sEV tetraspanins. $1 \mu\text{g}/\text{well}$ sEVs were seeded onto high protein binding ELISA plates and analysed for the surface tetraspanins CD9, CD63 and CD81. Bars represent means \pm SEM, based on triplicate wells, *** $P < 0.001$, one-way ANOVA with Tukey's multiple comparison test.

3.2.4. Functional potency assay - induction of myofibroblast differentiation

Following characterisation of DU145 derived sEVs, we carried out myofibroblast differentiation experiments on primary fibroblasts using these isolated sEVs, to confirm their known functionality. Fibroblasts were cultured as described in section 2.1 and seeded in microscopy plates for differentiation experiments. Fibroblasts were treated with the known differentiation stimulating dose of 200 μ g/mL DU145 sEVs (Webber et al., 2010), equivalent dose of 1.5ng/mL sTGF β 1 to compare sEV and sTGF β 1 mediated effects, or control media, for 72 hours. Cell supernatant was then collected for HGF assays and cells were fixed in 1:1 acetone/methanol then stained for α SMA. The primary fibroblasts, which will be used in later uptake studies, are large elongated cells, spindle-like in shape, sometimes with filopodia protruding from the main cell body (figure 3.5).

Stimulated fibroblasts stained for α SMA were visualised by fluorescence microscopy (figure 3.6a). Fibroblasts treated with control media do not express α SMA, as quiescent fibroblasts are negative for α SMA (Rønnov-Jessen and Petersen, 1993). Fibroblasts treated with either DU145 sEVs or sTGF β 1 both exhibited the onset of α SMA stress fibres (figure 3.6a, zoom), indicative of an acquired myofibroblastic phenotype.

Collected supernatants were subjected to HGF DuoSet ELISA-like assay, with a Europium TRF readout. HGF was significantly detected in the supernatant of fibroblasts treated with sEVs compared to those treated with control media (figure 3.6b). sTGF β 1 did not elicit HGF secretion in the fibroblasts, as expected, underlining the clear differences in the myofibroblasts generated by DU145 derived sEVs versus sTGF β 1. These data show that PCa derived sEVs are capable of driving myofibroblast differentiation in fibroblasts, a rate-limiting step in cancer progression, in a manner distinct to sTGF β 1 alone, demonstrating the complexity of the sEV driven response.

Here, in the presence of DU145 derived sEVs, the fibroblasts behave as expected, as reported previously (Webber et al., 2010).

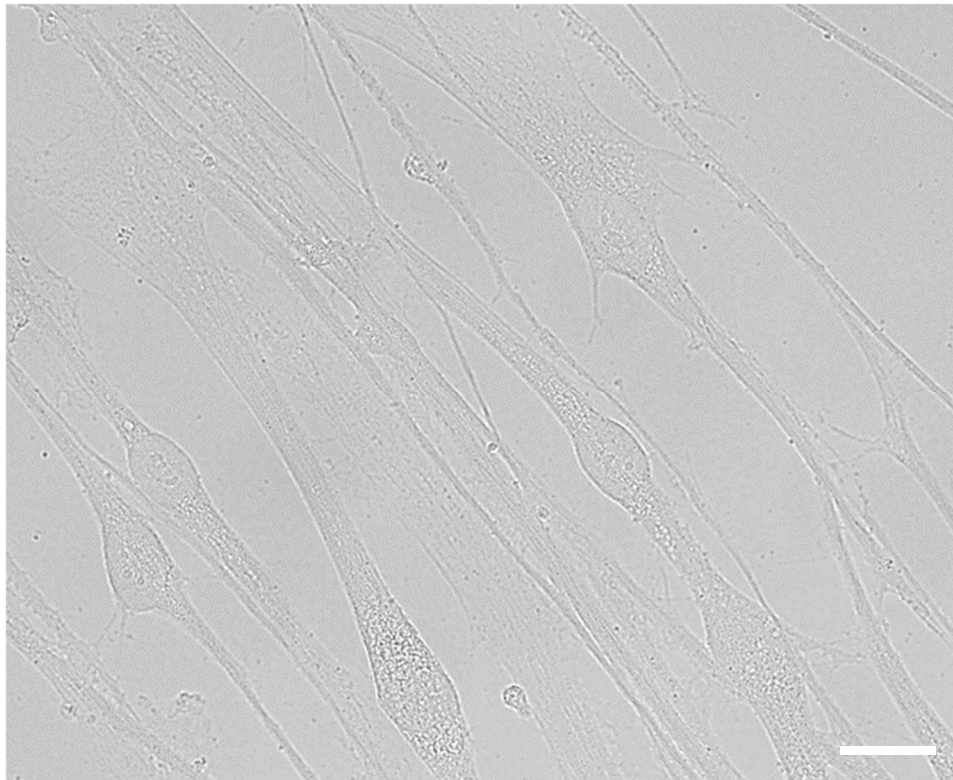


Figure 3.5. Morphology of primary lung fibroblasts. Monolayer of 1:1 acetone/methanol fixed fibroblasts, visualised by brightfield microscopy. Images captured by Axio Observer Z1, 63x lens used, scale bar = 20 μ m.

Results

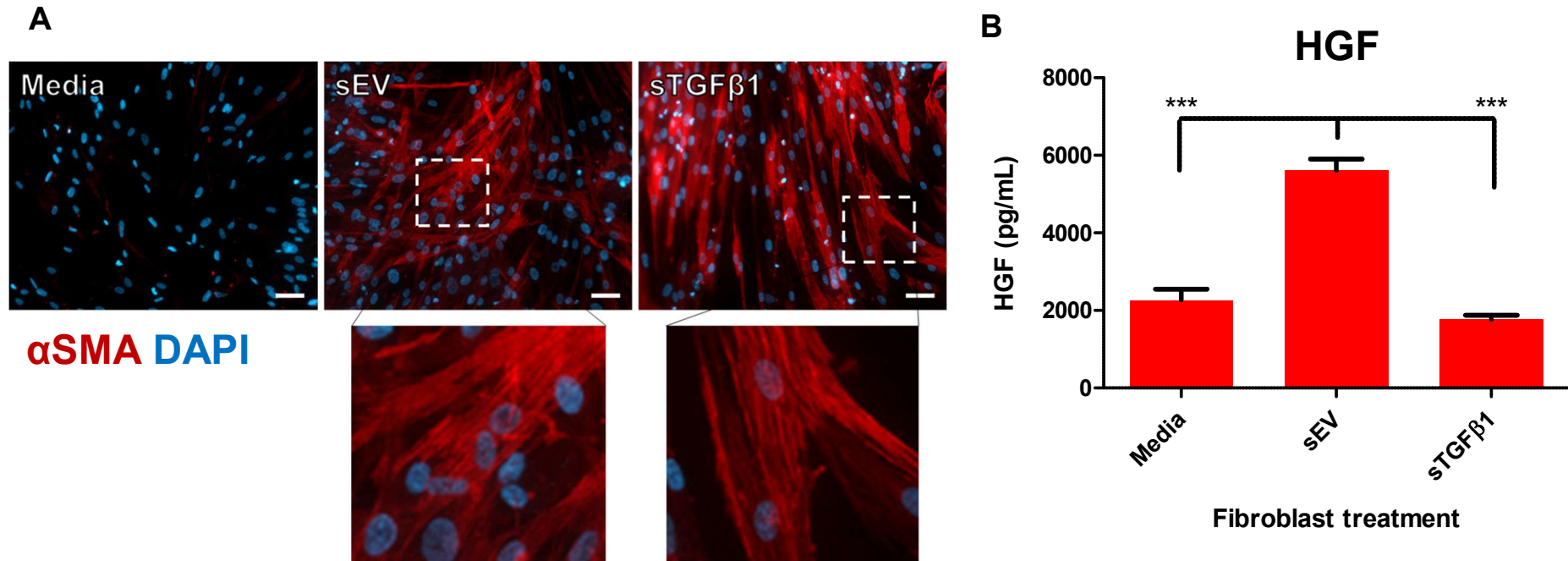


Figure 3.6. Myofibroblast differentiation induced by DU145 derived sEVs. (A) Fibroblasts were treated for 72hrs with 200µg/mL sEVs, 1.5ng/mL sTGFβ1 or control media, then conditioned supernatant was collected, and the cells were fixed. Cells were stained for αSMA (red), and nuclei were stained with DAPI (blue), and visualised by fluorescence microscopy. Examples at higher magnification show stress fibre structures. Representative images from 3 separate wells are shown. Images captured by Axio Observer Z1, 20x lens used, scale bar = 50µm (B) Cell supernatants were analysed by sandwich ELISA assay for levels of HGF secreted by conditioned fibroblasts, detected by time resolved fluorescence of Europium labelled HGF. bars represent means +/- SEM, based on triplicate wells, ***P<0.001, one-way ANOVA with Tukey's multiple comparison test.

3.3. Discussion

In this chapter, sEVs isolated from DU145 cells were characterised based on their size, morphology and protein content; their ability to drive a complex process of cellular differentiation to myofibroblasts. This data is schematically summarised in figure 3.7. The analysis seems to satisfy the definition of the vesicles isolated as sEVs, according to the ISEV guidelines (Théry et al., 2018). The data also presents evidence for both the quality of EVs used and to what extent results attributed to EVs can be believed. We demonstrated that sucrose cushion ultracentrifugation-based isolation of DU145 sEVs produces a population of vesicles mostly of sEV size and morphology, with particle to protein ratios indicative of low protein contamination. The isolates express the tetraspanins CD9, CD63 and CD81 on their surface, and are enriched in ALIX, TSG101 (indicating an endosomal origin of at least of subset of vesicles) and MHC1, whilst ER protein calnexin could not be detected. sEVs could also drive myofibroblast differentiation in primary fibroblasts in a manner distinct to sTGF β 1. Data shown here allows us to define our vesicle isolates as small extracellular vesicles of high purity, with protein markers indicative of the classic “exosome” termed vesicle (Lötvall et al., 2014).

Large numbers of \approx 100nm vesicles were identified by cryo-EM, similar to sEVs identified in other studies (Conde-Vancells et al., 2008; Zabeo et al., 2017). Yet there are other structures present with distinct appearances. Peculiar multi-membrane encased vesicle-like structures were present, as well as sacks of material >200nm, the presence of the larger structures is perhaps unexpected since sEVs were isolated based on their floatation characteristics, which should be distinct from sacks of that size. High speed ultracentrifugation is known to cause aggregation in sEV samples (Linares et al., 2015), therefore irregular shaped vesicles could be an artefact of the centrifugation process. Comparison of morphologies of sEVs isolated by centrifugation versus other methods may clarify this issue. However, large numbers of small electron dense particles were also present, the origin of these is unclear, though they are reminiscent of histone proteins (Jodoin and Hincke, 2018), which would indicate there is a degree of contamination in the sEV preparations. Given the complexity of bioreactor cultures, the input material is likely to contain an assortment of cell-derived debris. Others have similarly noted abnormal vesicular structures in their EM images,

Zabeo *et al* note that the majority of their vesicles appear like typical sEVs, but there are also a number of other structures present, including very long tubules (Zabeo et al., 2017). Like this study, the majority of the population is made up of sEV sized vesicles, but it is important to point out other structures, since they honestly reflect the contents of the sEV preparation. Most studies fail to present heterogeneity in sEV samples, therefore the presented analyses of sEVs are more often than not, poorly defined. It is important to discuss the presence of these other structures, since there is clearly production of structures of unknown origin by cells, but also, it points out problems in the process of sEV isolation/purification, as we see material in sEV isolates which should be excluded from the sEV fraction based on their sizes/densities. However, the uni-lamellar vesicle is the predominant structure, in terms of both the entities observed and in providing the overall surface area of secreted material, so it is a good representation of the sEV sample, despite the heterogeneity of structures present.

NTA was utilised to quantify sEV concentration and the size distribution of the population. Whilst the nature of the particles measured by NTA cannot be determined, the cryo-EM images compliment this by showing the proportion of particles that are in fact sEV-like vesicles. NTA does reveal that the vast majority of particles in a sEV sample are <200nm in size, however it is also likely under sampling particles <50nm since the lower end of the distribution curve is very steep and there many structures <50nm, clearly visible by cryo-EM which are not being captured by the Nanosight. Calculations of particle (NTA) and protein (BCA protein assay) concentrations allowed us to determine the purity of the sEV isolates. We could be confident that high P:P ratios in sEV preparations used in future experiments were low in contaminating protein, meaning that results we gathered from sEV could be attributed to sEVs with some assurance. Keeping in line with studies that have previously quantified exosomes by their protein concentration (Christianson et al., 2013; Hoshino et al., 2015; Peinado et al., 2012; Webber et al., 2010), this study will normalise sEVs used in experiments by their protein concentration measured by BCA protein assay, unless otherwise specified.

To further characterise the sEV isolates, expression of proteins known to be associated with sEVs was evaluated. DU145 sEVs were positive for CD9, CD63 and CD81, all standard sEV markers (Colombo et al., 2014), suggesting at least part of

Results

the vesicle population was expressing these proteins. Other markers, ALIX, TSG101 and MHC1 are all enriched in sEVs compared with DU145 cells, pointing to selective loading of proteins into the vesicles. ALIX and TSG101 are also markers of MVB formation, showing that at least a portion of the vesicle population are likely MVB derived, though sEVs of plasma membrane origin have also been reported (Booth et al., 2006). To further demonstrate the purity of the sEV isolates, we showed that an ER protein not expected to be in the sEV fraction (calnexin) was indeed not detectable, showing the effectiveness of clearance of non-vesicular material during the isolation process.

Cancer derived sEVs from various sources are known to induce myofibroblast differentiation (Atay et al., 2014; Cho et al., 2012; Chowdhury et al., 2015; Gu et al., 2012; Webber et al., 2010), this sEV driven response is characteristic of solid cancer progression. Here, we showed isolated DU145 derived sEVs can stimulate α SMA expression and production of HGF in primary fibroblasts, a biologically relevant cell type in solid tissues. This sEV mediated phenotypic change in the fibroblasts generates a myofibroblast distinct to that generated by sTGF β 1 alone, in agreement with previous findings by the group (Webber et al., 2010), showing that the differentiation process with DU145 sEVs is reproducible, and that our isolation process produces a population of vesicles which respond as expected according to previous studies.

Overall, sucrose cushion-based ultracentrifugation produces DU145 derived sEVs of high purity, enriched in sEV markers with an indication of the endosomal origin of at least part of the population. Various structures are present in these isolates however which reflects the heterogeneity of structures in the sEV preparations. This shows the limitation of the sEV isolation process, as we are currently unable to solely isolate the small vesicle-like structures from the rest of the observed morphologies.

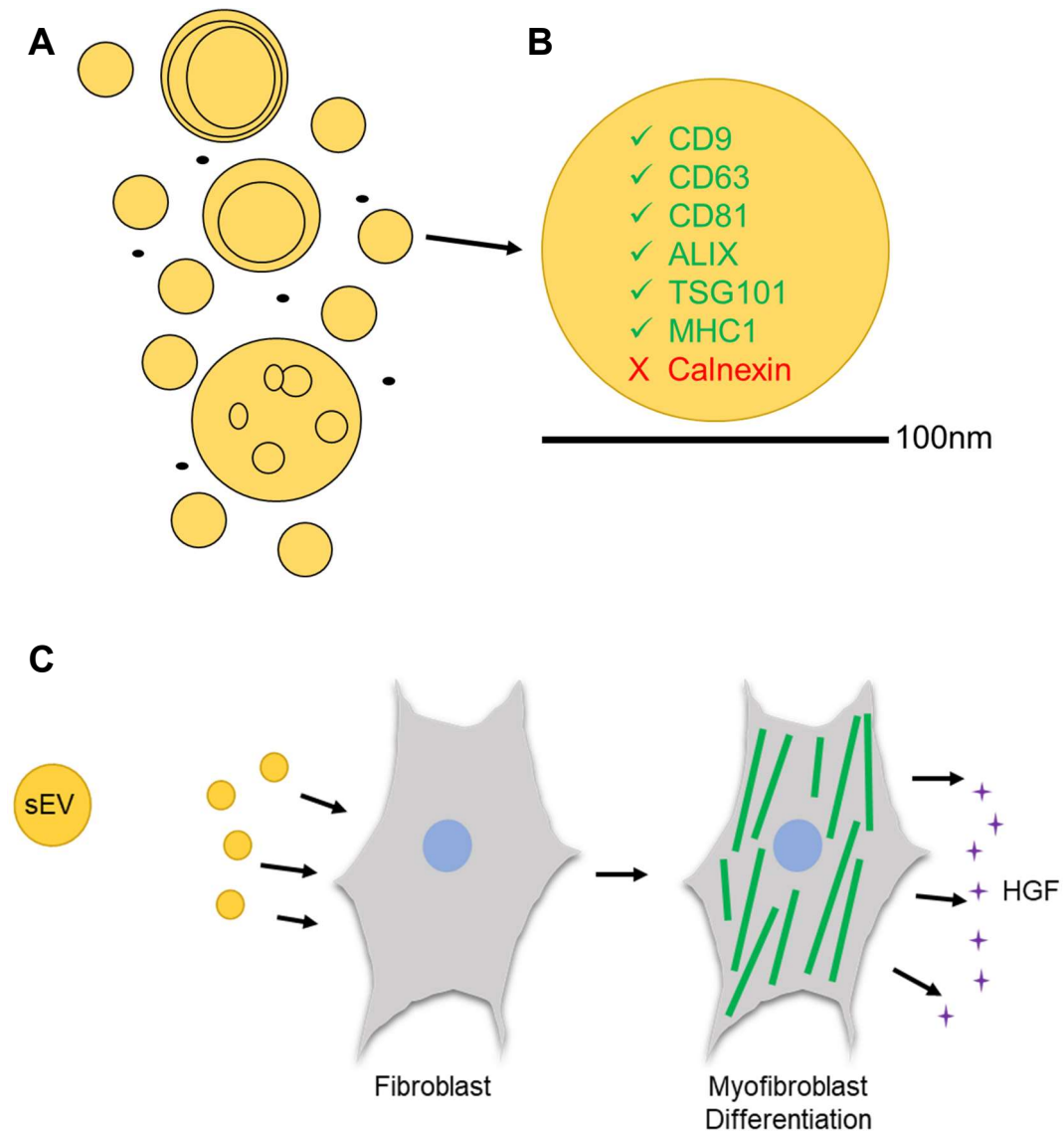


Figure 3.7. Schematic summary of chapter 3. Summary of the data collected in chapter 3. (A) The DU145 derived sEV isolates are a heterogeneous population of structures of various shapes and sizes, the most common structure is the single membrane vesicle. (B) Isolates express proteins indicative of sEVs, but lack contaminating soluble cellular material. (C) sEVs stimulate fibroblasts, inducing the onset of α SMA expression and secretion of HGF by the fibroblast.

Chapter 4 – Cellular uptake of DU145 derived small extracellular vesicles

4.1. Introduction

sEVs interact with cells at the plasma membrane and can undergo internalisation, delivering their membrane bound contents and intraluminal cargo to the recipient cell, driving phenotypic change. The delivery of this cargo has been implicated in the progression of cancer. Colorectal cancer derived sEVs deliver mRNA to endothelial cells which drives proliferation (Hong et al., 2009), key for angiogenesis of tumour tissue. miRNA delivery by cancer derived sEVs, inducing pro-metastatic inflammatory response in macrophages has also been described (Fabbri et al., 2012). Elucidating the machinery behind uptake of sEVs is therefore a logical target for cancer therapy, as evidence shows numerous pro-tumoural effects are governed by delivery of this intraluminal sEV cargo to recipient cells. In this chapter, the mechanism of DU145 derived sEV internalisation by fibroblasts was examined, a cell type relevant in the pathology of prostate cancer progression.

For tracking exosome uptake and intracellular trafficking, fluorescently tagging the sEV remains the easiest and most widely published method. Of the methods for fluorescently labelling exosomes, lipophilic dyes (mainly the PKH family) have been the most commonly used (Mulcahy et al., 2014), however there has recently been a desire to move away from these dyes due to them forming fluorescent particulates, of comparable size to sEVs (Lai et al., 2015), providing misleading information about sEV delivery. Fluorescent sEVs generated through genetically engineered cell lines, such as those with GFP-tetraspanin fusions (Heusermann et al., 2016) also have their limitations (section 1.3.4) and can be costly and time consuming to develop. In this study, we present a novel fluorescent tag, available in various colours, for rapid covalent labelling of sEVs. Maleimide linked-Alexa Fluor (Alexa) dyes are designed to covalently bind thiol groups on proteins. In this chapter we explored the utility of this alternative method of sEV labelling to study cellular uptake of sEVs. Alexa dyes were assessed for their ability to fluorescently label sEVs. Excess unbound Alexa dye would be separated from the sEVs using Exosome Spin Columns MW3000 (ThermoFisher); the fluorescent sEV labelling protocol is described in section 2.4.1.

sEV proteins are usually instrumental when the vesicles interact with cells (Clayton et al., 2011; Nazarenko et al., 2010; Peinado et al., 2012; Raposo et al., 1996), and they are vital for sEV internalisation (Escrevente et al., 2011). In PCa,

sEV mediated TGF β 1 delivery to fibroblasts is dependent on the HSPG Betaglycan (Webber et al., 2010). Since our proposed sEV label exploits thiol groups for protein binding, it is possible that this could impact sEV functionality in terms of the biological response of the fibroblast to the sEV. We felt it was important to examine the consequences of labelling in terms of sEV function, therefore we evaluated the effect of sEV labelling on the ability of the sEV to induce myofibroblast differentiation in the fibroblast model.

Internalised fluorescent sEVs are visualised by fluorescence microscopy, and the detection of their signal by flow cytometry of the cells allows for high-throughput quantification of sEV uptake (Barrès et al., 2010; Franzen et al., 2014; Morelli et al., 2004; Nakase et al., 2015). Detection of sEVs labelled with maleimide linked Alexa dyes following cellular uptake by fibroblasts was assessed by fluorescence microscopy and flow cytometry. Using these platforms for detection of internalised fluorescent sEVs, we then sought to pinpoint the specific route of endocytosis used by fibroblasts to take up the sEVs, as endocytosis is possible through various mechanisms (Mayor and Pagano, 2007). Defining the route used by PCa derived sEVs in fibroblasts would enable more accurate therapeutic targeting.

In summary, the aim of this chapter was to develop a sEV labelling approach to monitor internalisation in fibroblasts, and for the specific endocytic route to be defined.

4.2. Fluorescent labelling of sEVs

4.2.1. Detection of labelled vesicles

Initially, DU145 sEVs were treated for 1 hour with increasing doses of Alexa488 from 5 to 200 μ g/mL, and after removal of the unbound dye, the fluorescent intensity of the sEVs was measured using the PHERAstar FS microplate reader, using the Alexa488 optic module. These results showed a dose dependent relationship between dye concentration and fluorescent output, as expected. With the input of sEVs, saturation of the fluorescent signal was achieved at doses of 100 μ g/mL (figure 4.1a). At 200 μ g/mL, labelling marginally increases from 1 hour to 5 hour incubation times (figure 4.1b), surprisingly with a peak signal at 3 hours, however in the interest of developing a rapid labelling technique, further labelling experiments would continue with a 1 hour incubation. No free dye is detectable in post-spin solutions at any incubation time (figure 4.1b), suggesting that the dye does not form artificial aggregates greater than 3000Da in size (as these would be pulled through the spin column), at least up until 5 hours in PBS. At our chosen conditions, sEVs treated with 200 μ g/mL Alexa488 dye for 1 hour are highly fluorescent, detectable using a PHERAstar FS microplate reader, sEVs alone are not fluorescent, and there is no detectable free dye when 200 μ g/mL Alexa488 alone is spun through a spin column (figure 4.2), experiments using controls for free dye will be referred to as "Dye CTR". N-acetyl-L-cysteine (NaLc), a thiol containing compound (Parasassi et al., 2010) was added to the incubation process as a competitor of sEV thiol-maleimide binding. NaLc blocked Alexa488-sEV binding in a dose dependent manner, 1mM NaLc reduced the fluorescent signal of the sEVs by \approx 80% (figure 4.3), an indication that the majority of the Alexa-sEV labelling occurs via the maleimide-thiol bond.

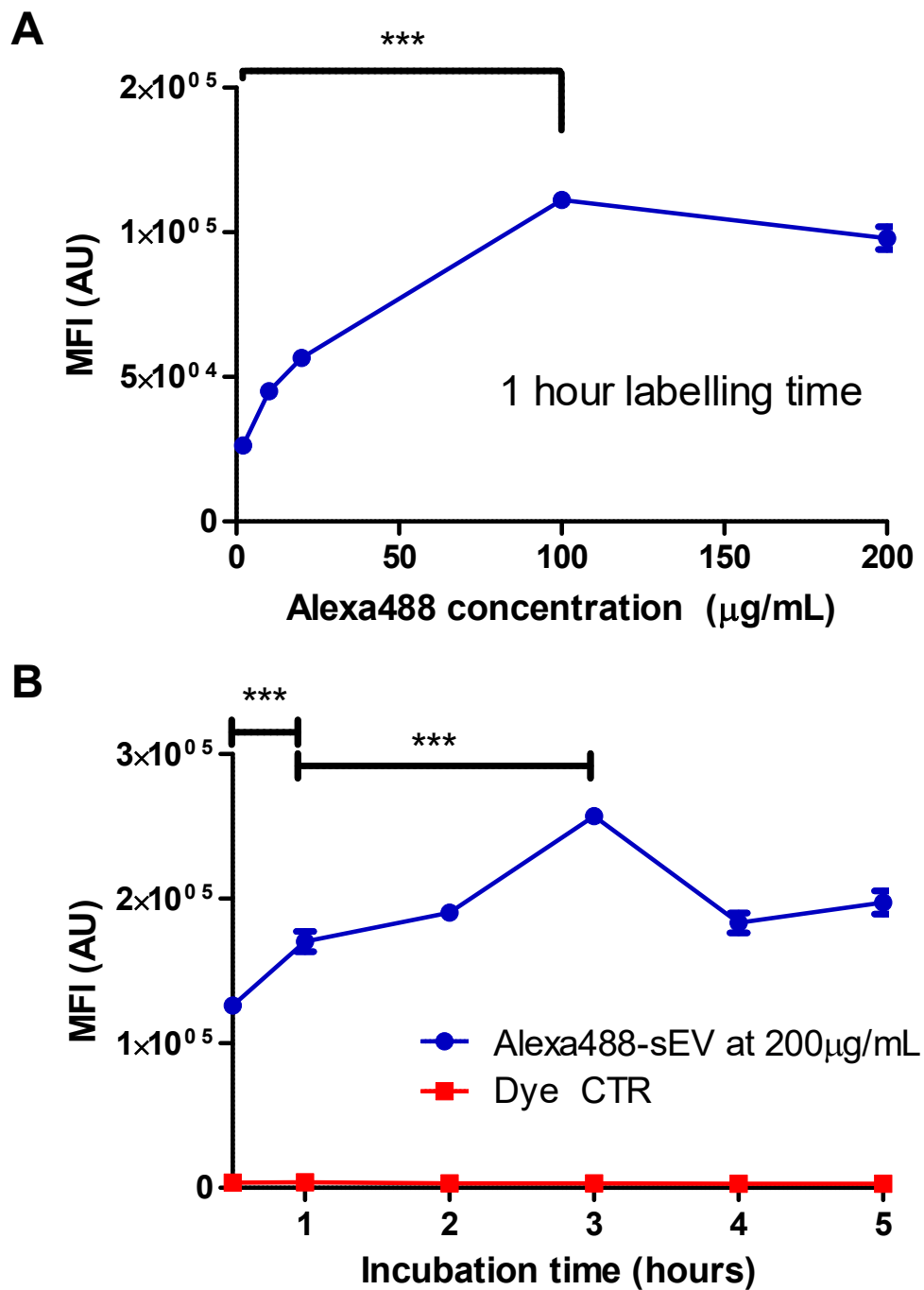


Figure 4.1. Dose and treatment time optimisation of DU145 derived sEVs with Alexa dyes. DU145 derived sEVs were incubated with (A) 5-200 $\mu\text{g/mL}$ Alexa488 for 1 hour, (B) 200 $\mu\text{g/mL}$ Alexa488 for 0.5-5 hours. Unbound dye was removed and labelled sEVs were diluted 1:6 in PBS and their mean fluorescent intensities measured using on a PHERAstar FS microplate reader with an Alexa488 optic module. Points on graphs represent means \pm SEM, based on triplicate wells, *** $P < 0.001$, one-way ANOVA with Tukey's multiple comparison test.

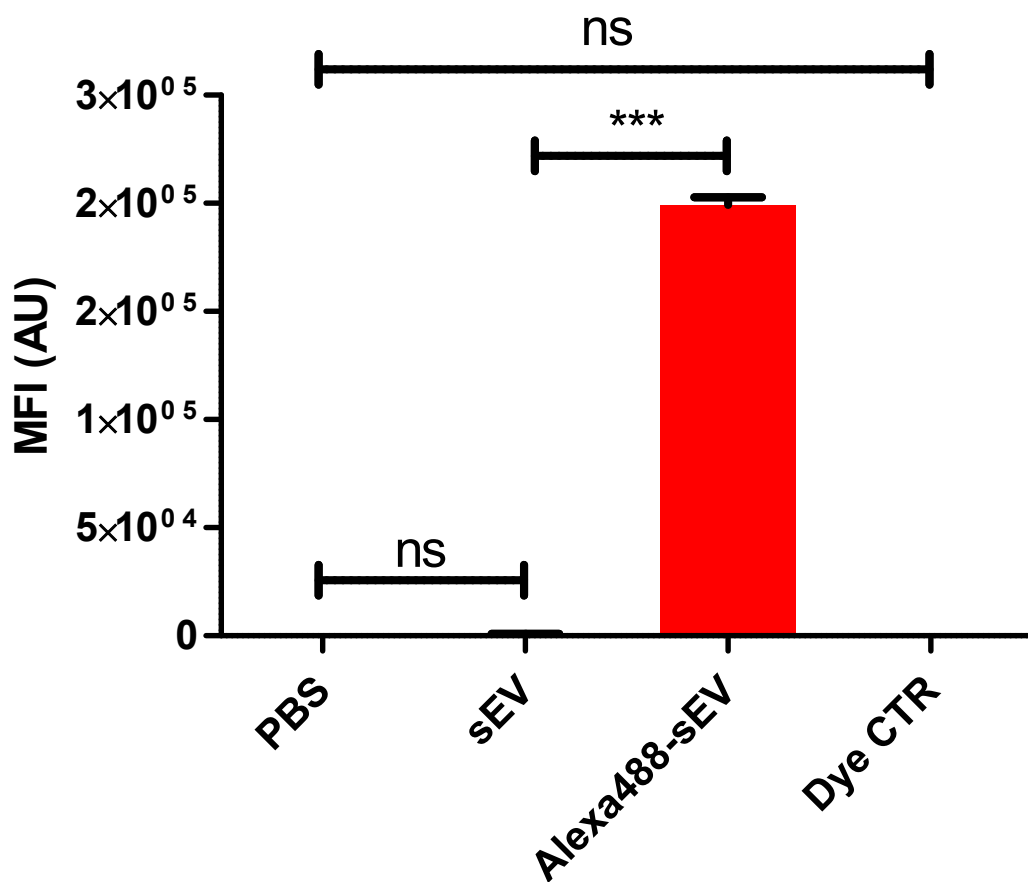


Figure 4.2. Chosen treatment conditions for Alexa labelling of DU145 derived sEVs. DU145 derived sEVs were incubated $200 \mu\text{g}/\text{mL}$ Alexa488 for 1 hour. Unbound dye was removed and labelled sEVs were diluted 1:6 in PBS and their mean fluorescent intensities measured using on a PHERAstar FS microplate reader with an Alexa488 optic module. Intensities of Alexa488-sEVs was compared with the control for free dye (Dye CTR) and unlabelled sEVs. Bars represent means \pm SEM, based on triplicate wells, *** $P < 0.001$, one-way ANOVA with Tukey's multiple comparison test.

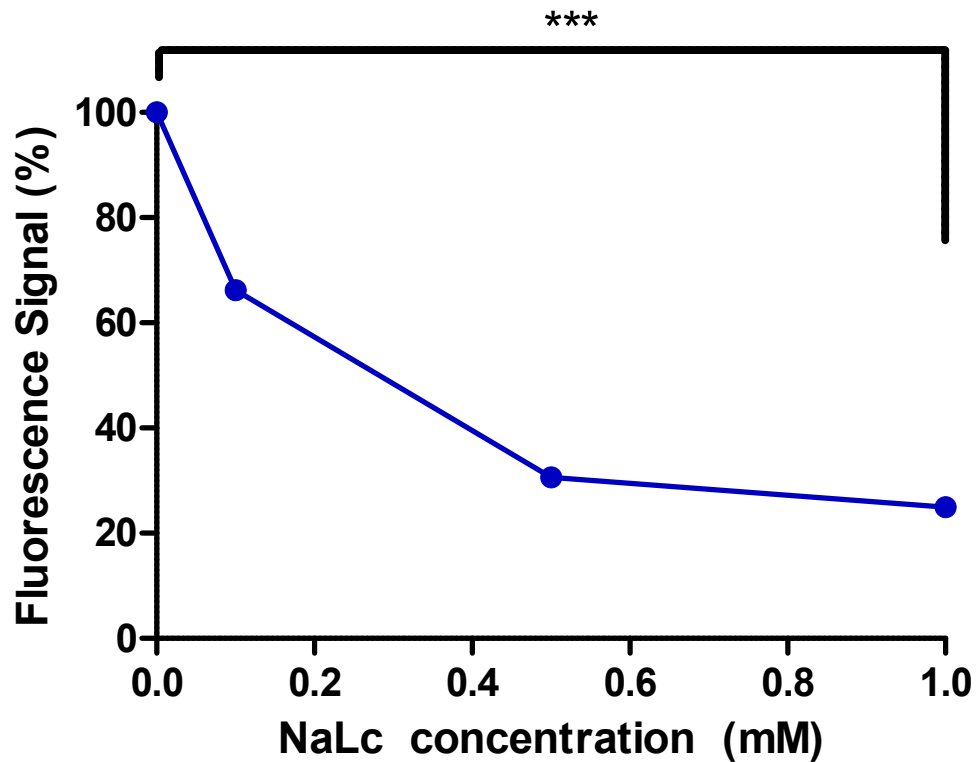


Figure 4.3. Effect of N-acetyl-L-cysteine (NaLc) on Alexa labelling of DU145 derived sEVs. DU145 derived sEVs were incubated 200 μ mL Alexa488 and 0-1mM NaLc for 1 hour. Unbound dye was removed and labelled sEVs were diluted 1:6 in PBS and their relative fluorescent intensities measured using on a PHERAstar FS microplate reader with an Alexa488 optic module. Bars represent means \pm SEM, based on triplicate wells, ***P<0.001, one-way ANOVA with Tukey's multiple comparison test.

Results

Alexa488 sEVs taken post-spin could be visualised by fluorescence microscopy using an Axio Observer Z1 microscope, when diluted 1:60 in PBS and added to wells of a 96 well glass bottomed plate (figure 4.4), sEVs appeared as small puncta floating in suspension. Fluorescent signal is likely linked to the sEVs since no puncta or signal of any sort can be visualised in Dye CTR wells.

Nanoparticle tracking analysis (NTA) of Alexa488-sEVs shows that the size profile of the sEV population is not grossly affected by Alexa labelling (figure 4.5a). In both the sEV and Alexa-sEV populations, the proportion of particles measured by NTA smaller than 200nm \approx 80%, indicative of the majority of the populations being within the size range of sEVs, and there is no significant difference between the respective modal sizes (figure 4.5b), so the dye does not alter the sizes of sEVs, since the most commonly sized particles in the populations are the same. As the labelling procedure involves diluting sEVs in PBS and spinning them through a column containing more PBS, concentration of sEVs is roughly halved (figure 4.5a). Negligible particles were detected in analysis of Dye CTR experiments (figure 4.5a), in agreement with figure 4.4, in which no fluorescent particles were detected in the absence of sEVs, meaning that the Alexa dye does not pass through the spin columns by itself in a way which would make it detectable by fluorescence microscopy or light scattering techniques.

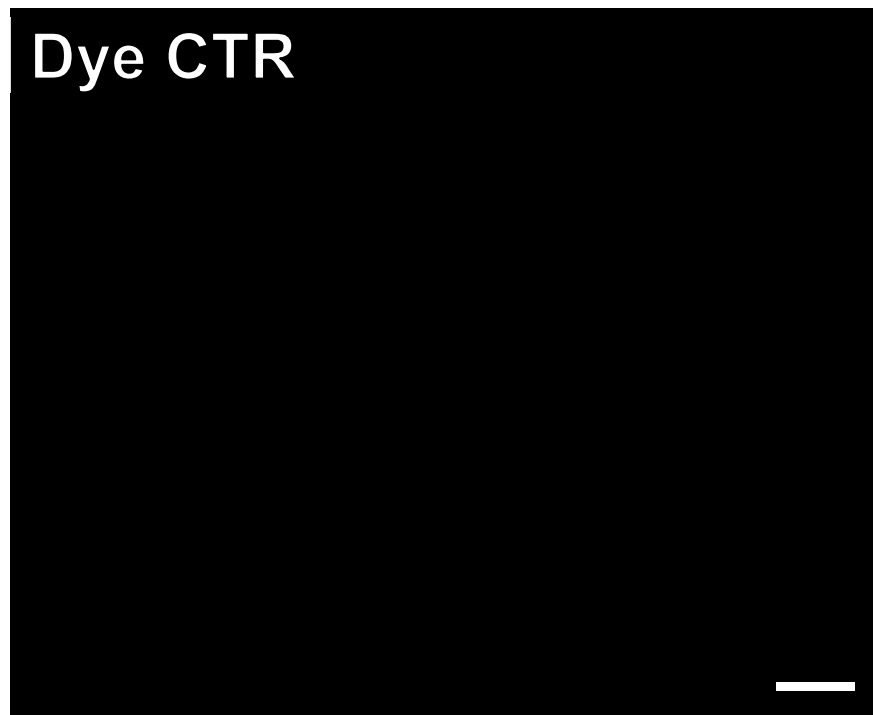
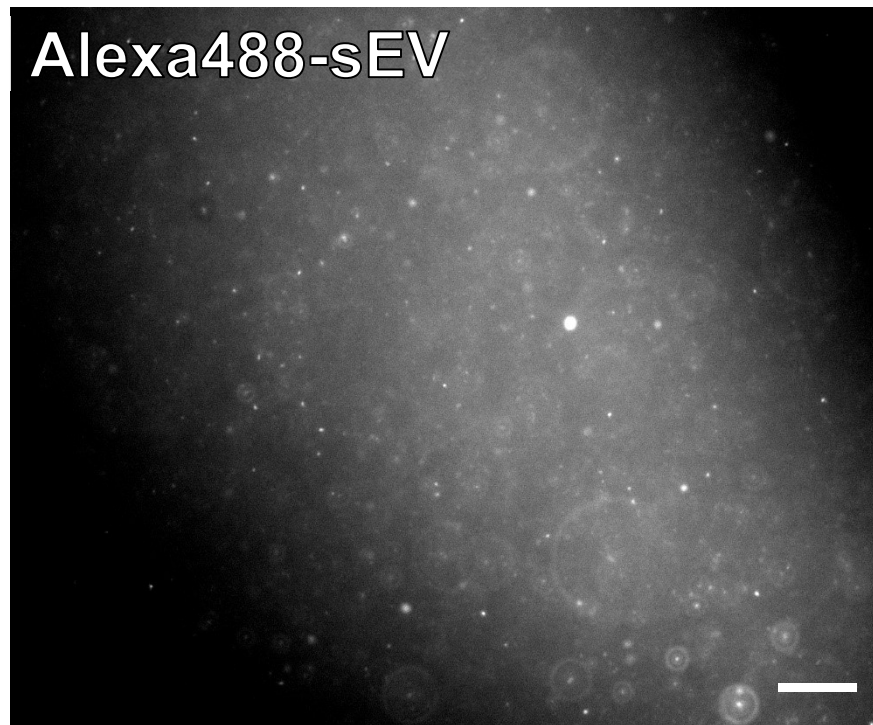


Figure 4.4. Visualisation of DU145 sEVs labelled with Alexa dyes. Alexa488-sEVs were diluted 1:60 PBS and added to microscopy plates for fluorescent visualisation, respective dye CTR fluorescence was also measured. Images were captured of sEVs floating in suspension. sEVs = white. Images captured by Axio Observer Z1, 63x lens used, Scale bar = 20 μ m. Images are representative from an experiment of 9 fields of view across 3 wells.

Results

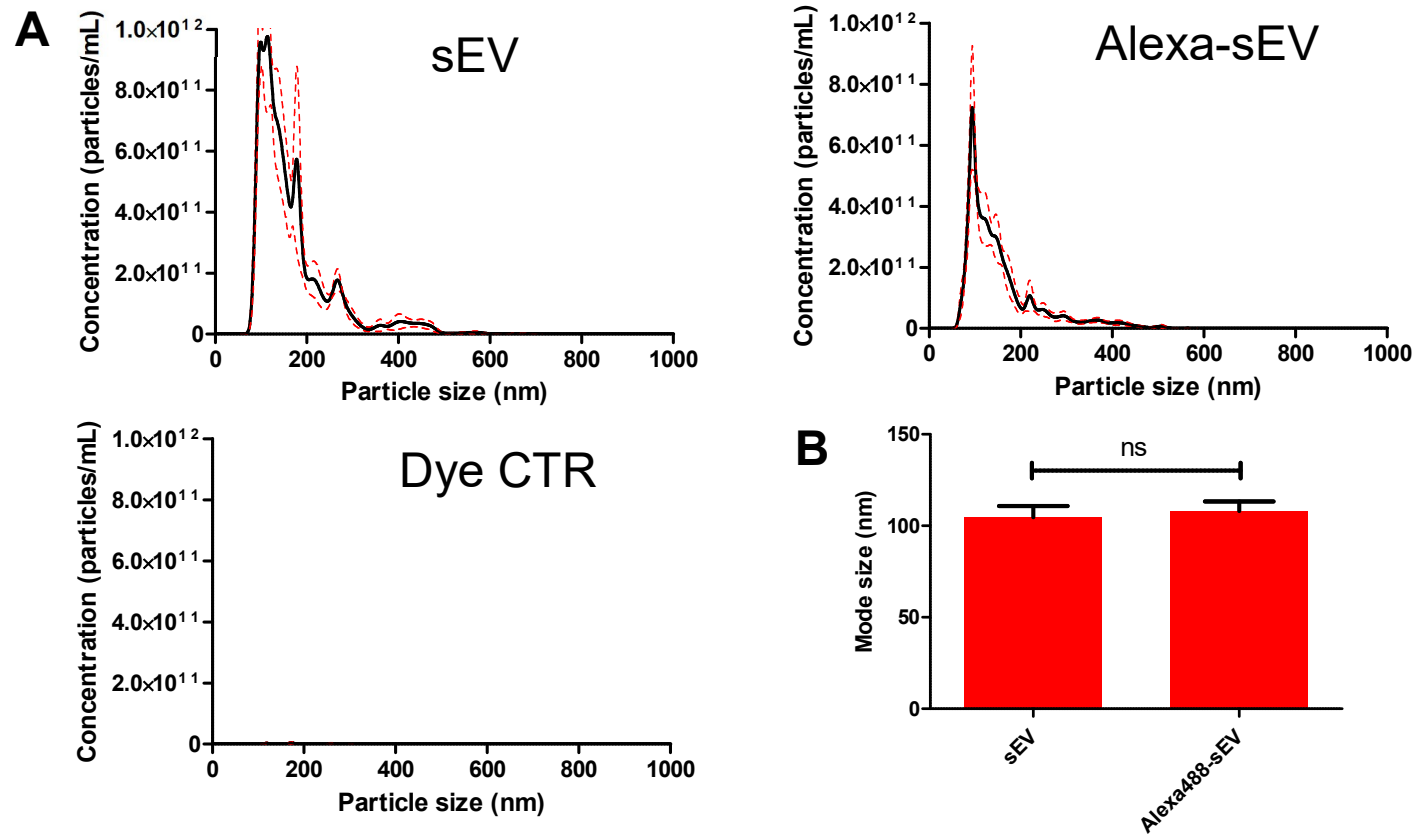


Figure 4.5. NTA of DU145 sEVs labelled with Alexa dyes. NTA histogram demonstrating the size distributions of sEV populations labelled with Alexa488 dye. Histogram represents the concentration of analysed particles against their respective size in nm. Presented histograms are an average of 5 measurements. (A) Histograms of particles detected in unlabelled DU145 derived sEV, Alexa488-sEV and Dye CTR samples. (B) Modal sizes of measured particles from the histograms in A. Bars represent means \pm SEM, based on the 5 measurements taken per sample, Students t-test tested for significant differences.

4.2.2. Effect of labelling on myofibroblast differentiation

As shown in section 3.2.6, DU145 sEVs induce phenotypic changes in fibroblasts, inducing the onset of α SMA expression and *de novo* production and secretion of HGF. Alexa488-sEVs were used in fibroblast stimulation experiments to assess the impact of Alexa labelling on differentiation function of the sEVs. Fibroblasts were hence treated with 200 μ g/mL of labelled or unlabelled sEVs for 72 hours, and α SMA expression and HGF secretion in stimulated fibroblasts were used as markers for sEV functionality.

Alexa labelling does not impede the DU145 sEVs ability to induce α SMA expression in fibroblasts (figure 4.6a). Fibroblast treated with either sEVs or Alexa488-sEVs differentiate into α SMA-positive myofibroblasts. Fibroblasts treated with a control for free dye in media do not undergo differentiation. Analysis of cell conditioned media by sandwich ELISA further reveals that HGF production by fibroblasts, a process unique to the sEV which sTGF β 1 does not drive, is also not perturbed by the conjugation of maleimide linked dye to the sEV surface (figure 4.6b). Again, a control for free dye does not stimulate HGF secretion by fibroblasts. The Alexa dye linked DU145 sEV is capable of driving differentiation in fibroblasts, akin to unconjugated sEVs, at least in its ability to generating myofibroblasts which secrete growth factors beneficial to tumour growth and survival.

Results

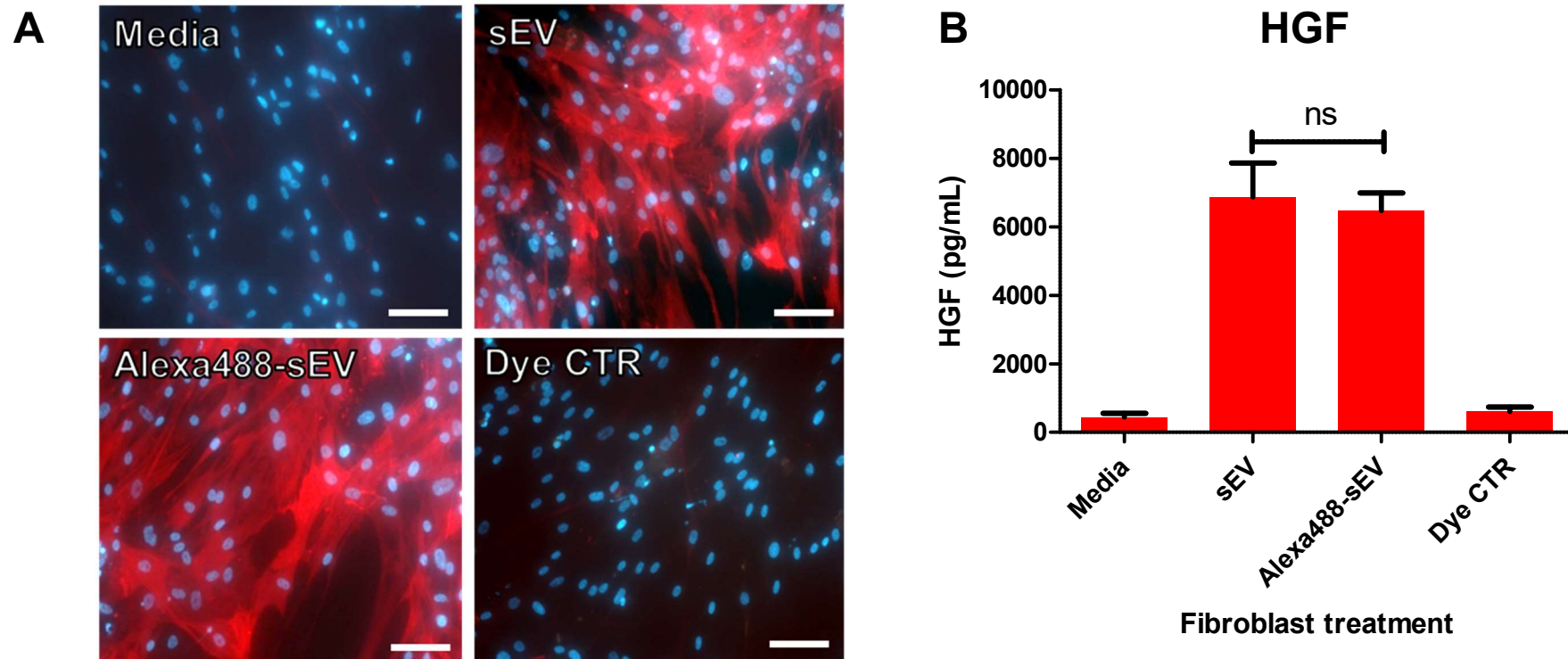


Figure 4.6. Effect of Alexa labelling on DU145 sEV induced myofibroblast differentiation. Fibroblasts were treated for 72hrs with control media, 200 μ g/mL sEVs, 200 μ g/mL Alexa488-sEVs or a control for free dye (Dye CTR), cell supernatants were collected, and cells were fixed. (A) Cells were stained with an antibody for α SMA (red) and nuclei were stained with DAPI (blue), images are representative of 9 fields of view taken across 3 wells. Images captured by Axio Observer Z1, 20x lens used, scale bar = 50 μ m. HGF levels were measured in collected cell conditioned media by sandwich ELISA. Bars represent means \pm SEM, based on triplicate wells, one-way ANOVA with Tukey's multiple comparison test.

4.3. Detection of DU145 sEV uptake in fibroblasts

Following optimisation and validation of sEV labelling with Alexa Fluor Alexa dyes, Alexa-sEVs was next tested for their capacity to be taken up by fibroblasts addition to fibroblast media. 200µg/mL of red Alexa594-sEVs (myofibroblast stimulation dose) in DMEM/F12 were added to fibroblasts for 1 hour. Following washing and fixation of the cells, red puncta are clearly visible by fluorescence microscopy, the vast majority of which appear overlaid in association with the fibroblasts (figure 4.7). However, some regions of the cells exhibit large fluorescent aggregates (figure 4.7, zoom, arrows), making it difficult to distinguish individual sEV containing compartments from one another, this is possibly due to oversaturating the cells with sEVs. Furthermore, persistent use of 200µg/mL Alexa-sEVs for uptake studies would rapidly deplete stocks of isolated sEVs, and since generating sEVs is a costly and time-consuming process, lowering doses of sEVs for experiments to reduce depletion of stocks would be desirable. Fibroblasts were next treated with 25-200µg/mL Alexa594-sEVs for 1 hour to assess detection of lower sEV doses in fibroblasts. Uptake was dependent on sEV dose (figure 4.8a), though clear red puncta were visible in all cells at the lowest dose of 25µg/mL (figure 4.8b). At this dose and treatment time, individual puncta are dispersed throughout the cells, without the appearance of large fluorescent aggregates. Cellular uptake of sEVs was also dependent on treatment time (figure 4.9a), the appearance of fluorescent aggregates become more common with the longer treatment times, particularly at 2 or more hours (figure 4.9b). sEVs are still detectable at 25µg/mL and 30 minutes of treatment, however Alexa-sEVs do not appear to label all fibroblasts (figure 4.9b). For future uptake studies, unless otherwise specified, an optimal fibroblast treatment of 25µg/mL Alexa-sEVs for 1 hour will be used.

Detection of Alexa-sEVs in fibroblasts was also possible by flow cytometry. Fibroblasts were treated with 25µg/mL green Alexa488-sEVs for 1 hour, then trypsinised and resuspended in PBS, to be used with the flow cytometer. A gated population of cells was based upon the forward and side scatter profiles, to eliminate cell fragments and large particulates from measurement (figure 4.10a). Alexa488-sEV treated fibroblasts are detectable, producing histograms of higher signal than untreated cells or cells treated with controls for free dye (figure 4.10b).

Results

There is a small tail in the Alexa488-sEV treated fibroblast histogram, representing a population of fibroblasts which are not fluorescent, meaning they have not taken up sEVs, though this is only roughly 6% of the population. There is no difference between the fluorescent signals in cells treated with a control for free dye and untreated cells. Fibroblasts can exhibit a strong green autofluorescence (Carter et al., 2018), giving untreated cells an apparent positive fluorescent signal.

Fibroblasts were treated with 25µg/mL of either Alexa488-sEV or red Alexa633-sEVs to compare the relative signal to noise ratios of the treated versus untreated cells. Since fibroblasts do not typically express red autofluorescence, Alexa633-sEV treated fibroblast histograms displayed a greater separation in signal from their control cells than Alexa488-sEV treated fibroblasts (figure 4.10c). Therefore, Alexa633-sEV treated fibroblasts exhibited a higher signal to noise ratio compared with Alexa488-sEV treated cells (figure 4.10d), the signal to noise ratio of the Alexa633 treatment was roughly 6-fold higher than the Alexa488 treatment. Histograms of Alexa488/633 signal was generated based on 10,000 cells (scaled down to 1000 cells in later experiments to reduce vesicle input requirements). For future experiments, Alexa633 dye was used to label sEVs for flow cytometry experiments unless otherwise stated. Herein, fluorescent intensity in fibroblasts associated with sEVs, detected by flow cytometry, will be used as a quantitative measure of the level of sEV uptake within the fibroblast population.

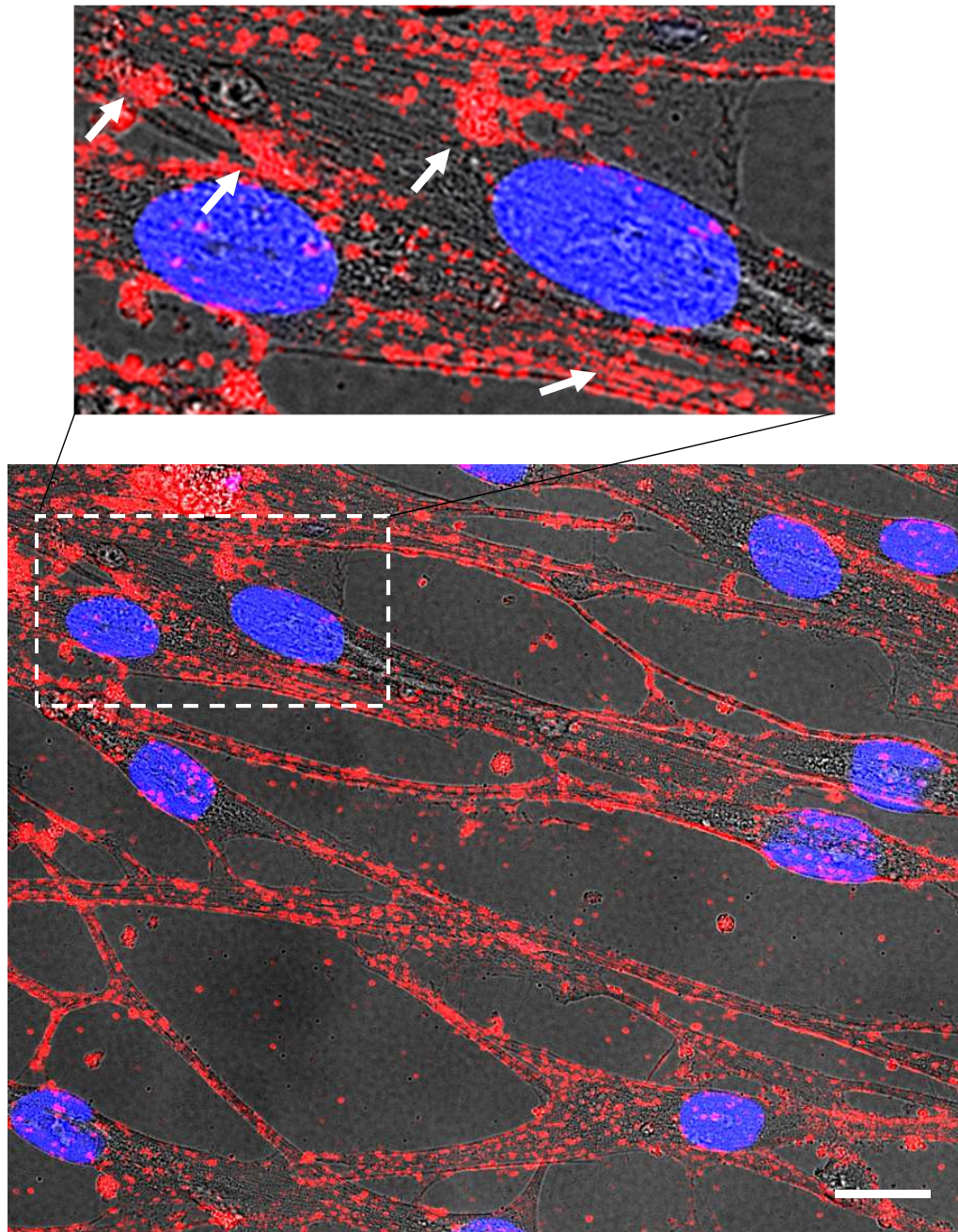


Figure 4.7. Staining patterns of fibroblasts treated with Alexa594-sEVs. Fibroblasts were treated with 200 μ g/mL Alexa594-sEVs for 1 hour. Fibroblasts were visualised for the staining pattern exhibited. White arrows in zoomed section point to areas of fluorescent aggregation. sEVs = red, DAPI = blue. Images captured by Axio Observer Z1, 63x lens used, scale bar = 20 μ m. Images are representative from an experiment of 9 fields of view across 3 wells.

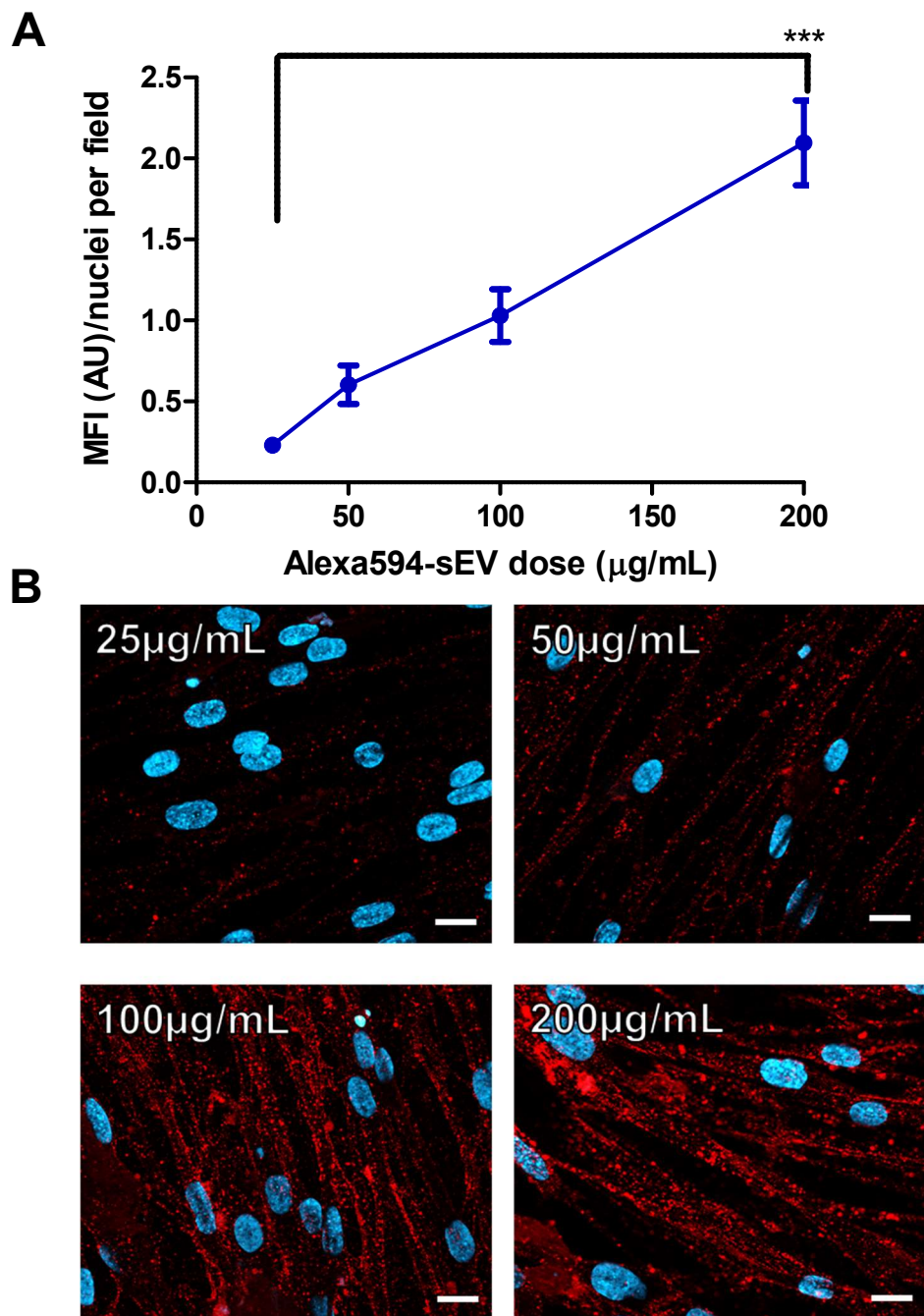


Figure 4.8. Optimisation of Alexa594-sEV treatment dose for fibroblast uptake studies. Fibroblasts were treated with 25-200 $\mu\text{g/mL}$ Alexa594-sEVs for 1 hour. Fibroblasts were visualised for the staining pattern exhibited. (A) Cells were visualised by fluorescence microscopy and their fluorescent intensities quantified by ImageJ, points on graphs represent means \pm SEM, based on 9 fields of view across 3 wells, *** $P < 0.001$, one-way ANOVA with Tukey's multiple comparison test. (B) Representative images of each treatment condition, sEVs = red, DAPI = blue. Images captured by Axio Observer Z1, 63x lens used, scale bar = 20 μm . Images are representative from an experiment of 9 fields of view across 3 wells.

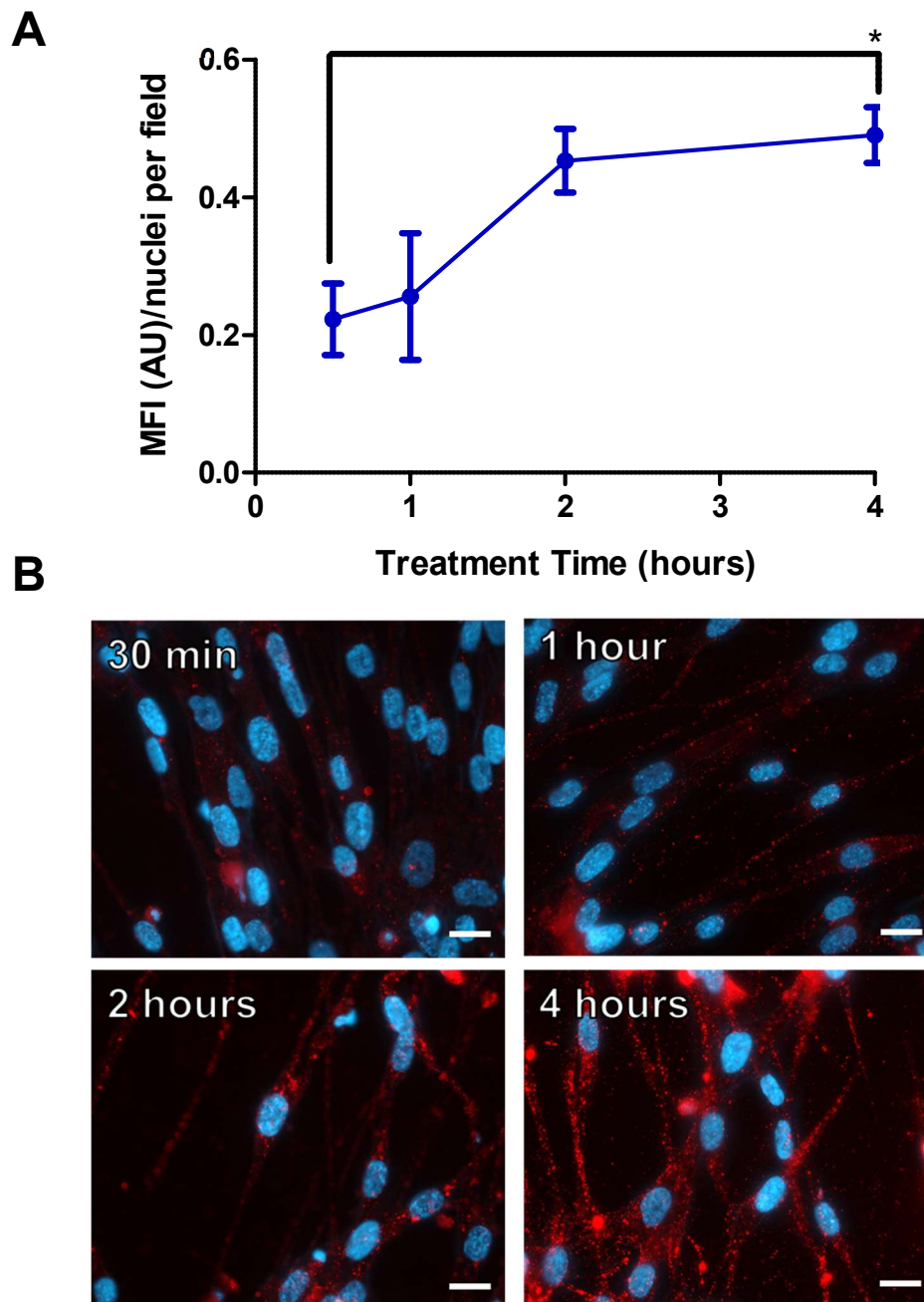


Figure 4.9. Optimisation of Alexa594-sEV treatment time for fibroblast uptake studies. Fibroblasts were treated with 25/ μ L Alexa594-sEVs for 0.5-4 hours. Fibroblasts were visualised for the staining pattern exhibited. (A) Cells were visualised by fluorescence microscopy and their fluorescent intensities quantified by ImageJ, points on graphs represent means \pm SEM, based on 9 fields of view across 3 wells, *** $P < 0.001$, one-way ANOVA with Tukey's multiple comparison test. (B) Representative images of each treatment condition, sEVs = red, DAPI = blue. Images captured by Axio Observer Z1, 63x lens used, scale bar = 20 μ m. Images are representative from an experiment of 9 fields of view across 3 wells.

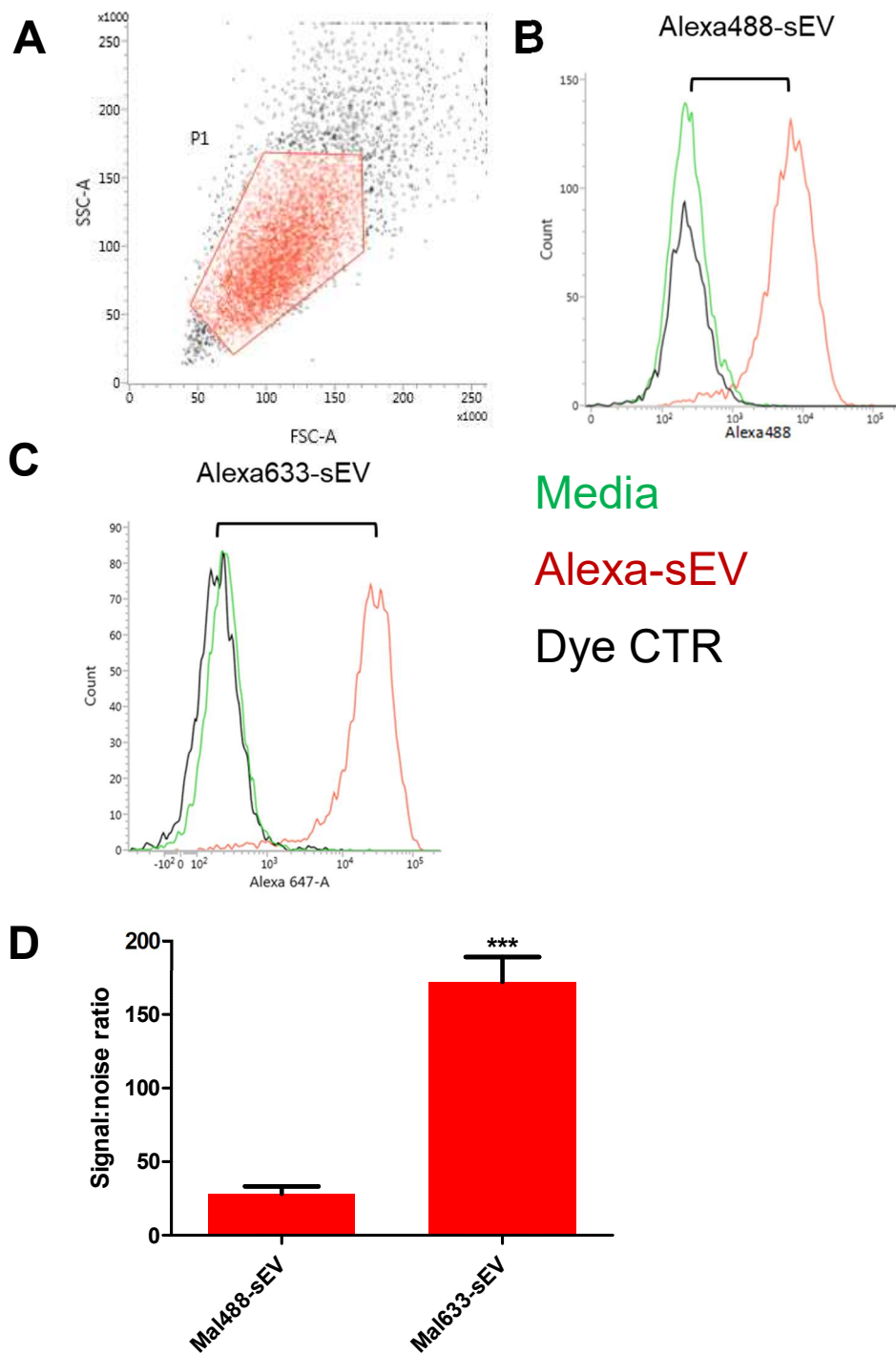


Figure 4.10. Use of flow cytometry to detect DU145 sEV uptake by fibroblasts. Fibroblasts were treated with 25/mL Alexa488/633-sEVs for 1 hour, then cells were prepared for flow cytometry. (A) Representation of the gated population for fluorescent intensity analysis, determined by forward and side scatter profiles of cells. (B) Detection of Alexa488-sEV treated (red) fibroblasts plotted as a histogram, in comparison with media treated (green) or control for free dye treated (black) cells. (C) Comparison of signal detection of the green Alexa488-sEV versus the red Alexa633-sEV in fibroblasts. (D) Signal to noise ratios of Alexa488-sEV versus the red Alexa633-sEV in fibroblasts, bars represent means \pm SEM, based on triplicate wells, Students t-test tested for significant differences, ***P<0.001.

4.4. Endocytosis of DU145 sEVs

4.4.1. Evidence for endocytosis of DU145 sEVs

sEV internalisation by cells has been described through various endocytic mechanisms (Mulcahy et al., 2014). Inhibition of this process through treatment of recipient cells at a reduced temperature indicates the endocytosis of the vesicle is energy requiring (Franzen et al., 2014). We treated fibroblasts with Alexa-sEVs at 37°C versus 4°C to determine whether there is evidence of endocytosis of the sEVs by fibroblasts. Treating fibroblasts with Alexa-sEVs at 4°C instead of 37°C abrogates their uptake (figure 11). When fluorescence images are overlaid with the brightfield, Alexa594-sEVs largely appear along the cell peripheries in 4°C treated cells (figure 4.11a, 4°C. zoom, white arrows), in contrast to the disperse appearance of sEVs throughout the 37°C treated cells (figure 4.11a, 37°C. zoom, white arrows). Acid stripping or trypsinisation is reported to remove any sEVs bound to the plasma membrane of a recipient cell (Feng et al., 2010; Franzen et al., 2014). Alexa-sEVs detected by flow cytometry (figure 4.10) should therefore be within the fibroblast, as trypsinisation of the cells occurs prior to the experiment. Flow cytometry reveals that the fluorescent signal of 4°C/Alexa633-sEV treated fibroblasts is almost entirely eliminated (figure 4.11b), suggesting that trypsinisation of the cells does strip them of surface bound sEVs, since any sEVs that may be present at the cell surface, as seen in figure 4.11a, are barely detectable by flow cytometry.

Time-lapse fluorescence microscopy reveals that sEVs are mobile when in association with the fibroblast, meaning they have been internalised and are not bound to the plasma membrane. Captured across an 8 second time course (figure 4.12, yellow/red arrow), sEVs move in straight trajectories, consistent with sEV movement along microtubules, likely within endosomes (Svensson et al., 2013).

DU145 sEVs are internalised by fibroblasts, and this is inhibited through reduction in temperature of the experimental conditions, suggesting the uptake process is an active energy requiring process for the fibroblast.

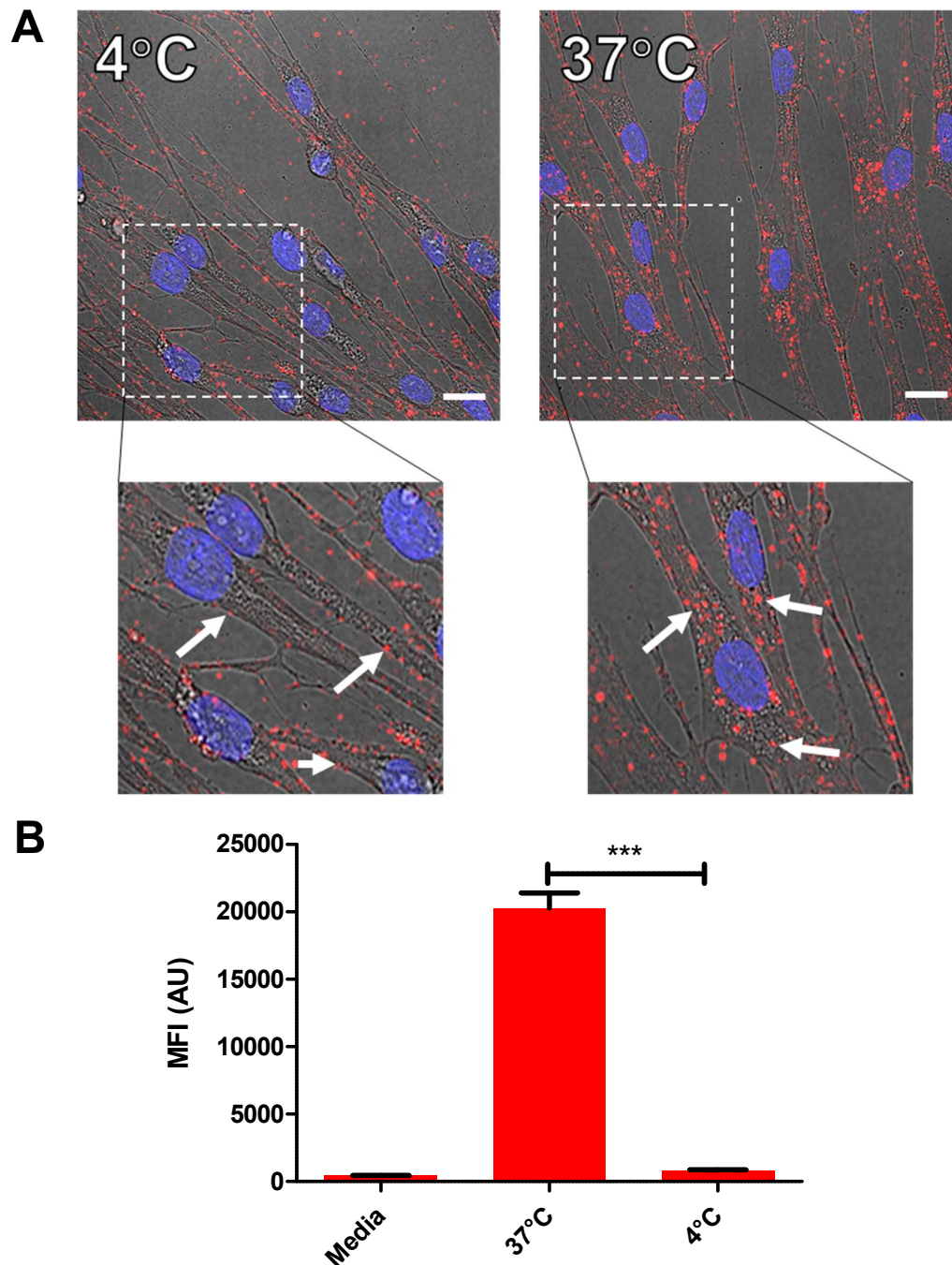


Figure 4.11. Temperature dependent uptake of DU145 sEVs by fibroblasts. Fibroblasts were treated with 25 μ mL Alexa594/633-sEVs for 1 hour at either 37°C or 4°C. (A) Fibroblasts were visualised for the staining pattern exhibited. White arrows in zoomed section point to areas of plasma membrane bound sEVs in the 4°C treatment, and intracellular sEVs in the 37°C treatment. Alexa594-sEVs = red, DAPI = blue. Images captured by Axio Observer Z1, 63x lens used, scale bar = 20 μ m. Images are representative from an experiment of 9 fields of view across 3 wells. (B) Fluorescent intensity of fibroblasts treated with Alexa633-sEVs at 37°C or 4°C was measured by flow cytometry. Bars represent means \pm SEM, based on triplicate wells, ***P<0.001, one-way ANOVA with Tukey's multiple comparison test.

Results

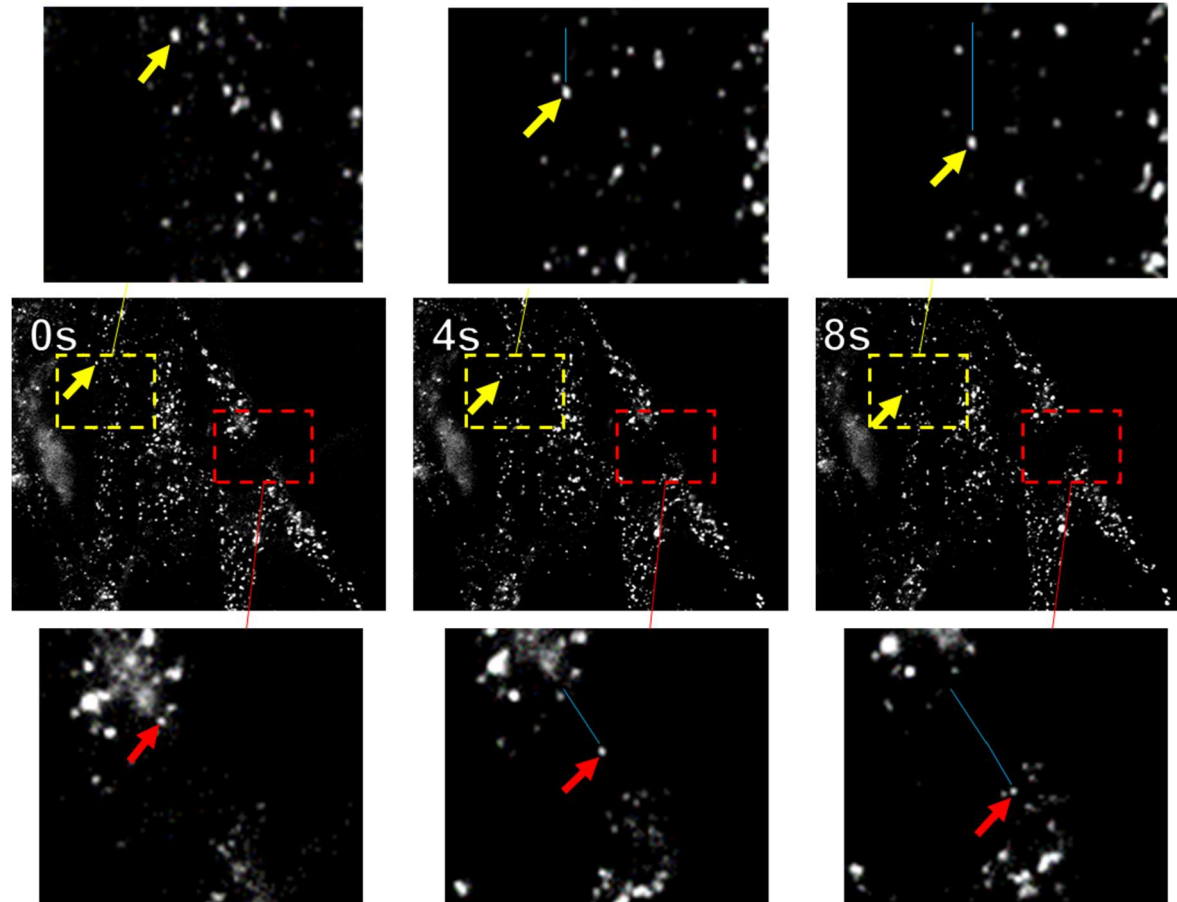


Figure 4.12. Movement of Alexa633-sEVs in fibroblasts. Fibroblasts were pulsed with 25 μ g/mL Alexa633-sEVs for 30 minutes, then sEVs washed off and 10 second time-lapses were conducted. Images were captured every second with an Axiovert 100 and a 40x lens, with the fibroblasts contained within an incubator-like black box. Alexa633-sEVs = white. In zoomed images, Red/yellow arrows point to sEVs moving in the fibroblast, blue lines represent the path of movement of the tracked sEVs. Images are representative images from an experiment of 9 fields of view across 3 wells.

4.4.2. Pharmacological inhibition of uptake

To pinpoint route of cellular uptake of DU145 derived sEVs in fibroblasts, pharmacological inhibitors of endocytosis were used. Pharmacological inhibitors were selected to target the common endocytic regulators and the most well characterised pathways. Actin, a filament protein important for cell structure and contraction, is implicated in numerous endocytic pathways (Doherty and McMahon, 2009). Cytochalasin D (CytoD) is a compound known to cause actin depolymerisation (Flanagan and Lin, 1980), thus is a standard inhibitor of endocytosis. Dynasore, inhibitor of dynamin function (Newton et al., 2006), abrogates both clathrin and caveolin coated vesicle formation. Macropinocytosis, another well characterised endocytic pathway is reliant upon Na^+/H^+ exchanger activity, which can be inhibited by ethyl-isopropyl amiloride (EIPA) (Hosogi et al., 2012). Inhibitors CytoD, Dynasore and EIPA were all assessed for their ability to block sEV uptake. Bafilomycin A1 (BafA), typically used to raise pH of endocytic compartments is also thought to affect endosome trafficking (Baravalle et al., 2005), therefore effect of endosomal transport inhibition on endocytosis would be gauged using BafA. Pharmacological inhibitors of uptake are often highly cytotoxic, and the cytotoxicity varies depending on the recipient cell (Vercauteren et al., 2010). Dosing of inhibitors was carried out on fibroblasts and cell viability measured to find a suitable dose, which does not kill the cells, allowing any perturbation of sEV uptake to be attributed to the specific inhibition and not the cytotoxicity of the drug. Heparin, a Heparin sulphate mimetic, blocks uptake of Glioblastoma sEVs (Christianson et al., 2013). Here Heparin was also evaluated as inhibitor of DU145 sEV uptake to assess the importance of cell/sEV surface interactions.

Pharmacological inhibition of endocytosis was carried out on the fibroblasts to expose the relevant molecular machinery used in uptake of DU145 sEVs and provide clues to the specific route of endocytosis. WST-8 cell viability assays were undertaken to identify doses of inhibitors which would not impact cell viability. Fibroblasts were treated with increasing doses of CytoD, Dynasore, EIPA or BafA for 24 hours, then cell viability was measured. Chosen doses: 100ng/mL CytoD, 10 μ g/mL Dynasore, 1 μ g/mL EIPA and 100ng/mL BafA were deemed not to impact the viability of the fibroblasts (figure 4.13a). All inhibitors were diluted in DMSO;

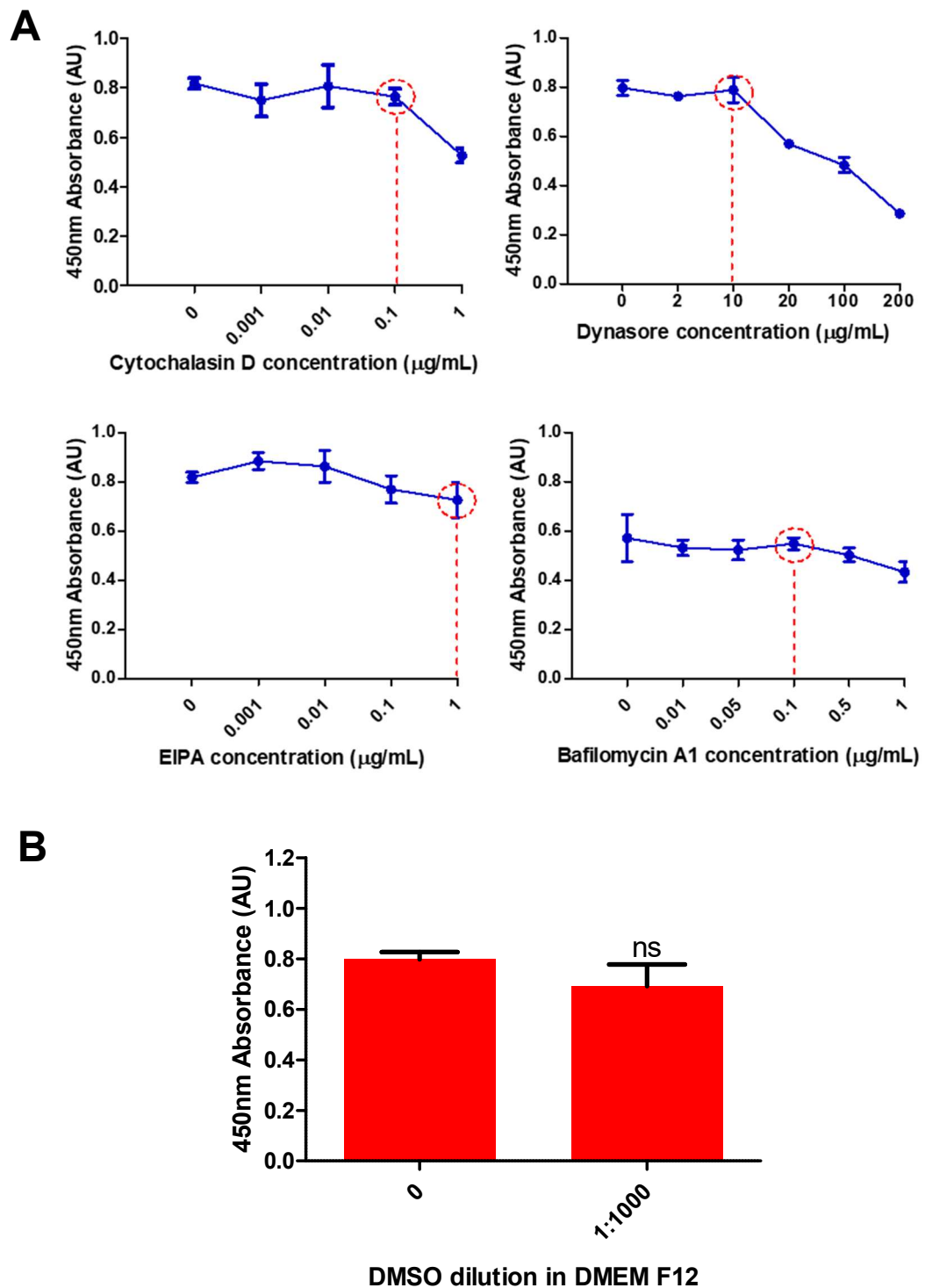
Results

the highest dilution of DMSO associated with an inhibitor in DMEM/F12 is 1:1000, DMSO itself does not impact cell viability at this dose (figure 4.13b). Chosen inhibitor doses, which did not affect cell viability were taken forward for use in sEV uptake studies.

Measured by flow cytometry, the actin depolymerising agent CytoD blocks uptake of almost 50% of Alexa633-sEVs (figure 4.14a). Macropinocytosis inhibitor EIPA modestly inhibited Alexa633-sEV uptake by around 20%, whereas Dynasore, an inhibitor of dynamin had a much greater impact, reducing uptake of sEVs by 60% (figure 4.14a). Surprisingly, pH raising and endosomal traffic blocking agent BafA also abrogated sEV uptake by 60% (figure 4.14a). These data reveal the importance of actin in internalisation of sEV containing endosomes, the role of dynamin, a scission protein involved in both Clathrin and Caveolin mediated pathways, and Na⁺/H⁺ exchange activity, though to a lesser extent. Targeting the internal endosomal trafficking network appears to perturb endocytosis.

The pharmacological inhibitors described here all impact in the internal machinery of the fibroblast to impede uptake, HS mimetic Heparin interrupts interactions between sEV and the recipient cell surface. Here, co-treatment of fibroblasts with Alexa633-sEVs and 50µg/mL Heparin (above concentration of Heparin used in other studies to perturb sEV internalisation (Christianson et al., 2013)) inhibited sEV uptake by 45% (figure 14b), demonstrating the role of the sEV/fibroblast surface interactions in sEV internalisation, in addition to the importance of the internal endocytic machineries of the fibroblast.

Effect of inhibitors CytoD, Dynasore, EIPA and Heparin on sEV uptake was also assessed by fluorescence microscopy (figure 4.14c). The images appear to show agreement with flow cytometry with regards to reduced uptake in the presence of Dynasore and Heparin, however significant differences between the treated/untreated conditions were not detected (figure 4.14d), suggesting that fluorescence microscopy is not as sensitive in gauging differences in sEV uptake compared to flow cytometry.



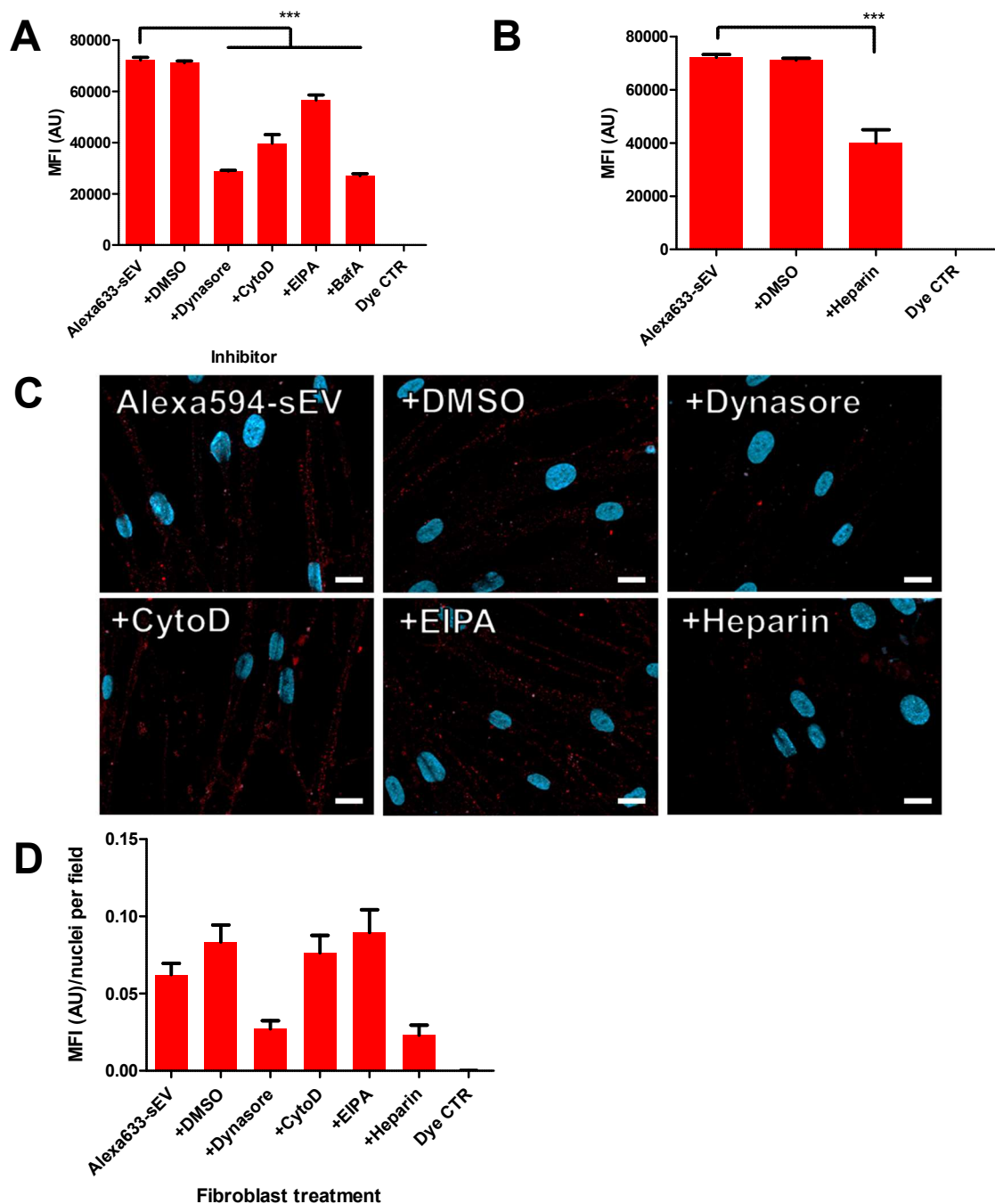


Figure 4.14. Effect of pharmacological inhibitors on DU145 sEV uptake by fibroblasts. Fibroblasts were treated with 25 μ g/mL Alexa594/633-sEVs for 1 hour with 100ng/mL CytoD, 10 μ g/mL Dynasore, 1 μ g/mL EIPA and 100ng/mL BafA, 50 μ g/mL Heparin or 1:1000 DMSO in DMEM F/12. Fluorescent intensity of fibroblasts treated with Alexa633-sEVs with (A) pharmacological inhibitors or (B) Heparin, was measured by flow cytometry. Bars represent means \pm SEM, based on triplicate wells, *** P <0.001, one-way ANOVA with Tukey's multiple comparison test. (C) Treated fibroblasts were visualised by fluorescence microscopy. Alexa594-sEVs = red, DAPI = blue. Images captured by Axio Observer Z1, 63x lens used, scale bar = 20 μ m. Images are representative from an experiment of 9 fields of view across 3 wells, (D) and their fluorescent intensities were quantified by ImageJ, bars represent means \pm SEM, based on 9 fields of view across 3 wells, one-way ANOVA with Tukey's multiple comparison test.

4.4.3. siRNA mediated inhibition of uptake

Inhibitors such as Dynasore or CytoD do not specifically block one endocytic route, furthermore specificity of inhibitors for their claimed target is often lacking (Vercauteren et al., 2010). Whilst pharmacological inhibitors are not sufficient to identify an exact route of endocytosis for sEVs, siRNA are available which target specific regulators of endocytosis, enabling a knockdown of a desired route of uptake (Al Soraj et al., 2012). The panel of siRNAs have been previously used to probe uptake of DU145 sEVs by HeLa cells (Roberts-Dalton et al., 2017), but they have not been employed in the fibroblasts before, therefore their efficacy for mRNA downregulation in fibroblasts was validated by qPCR, then protein knockdown by Western blot, before reporting on their effect on sEV uptake.

Fibroblasts were treated with siRNAs against AP2 μ 2 (Clathrin adaptor protein), CAV1 (Caveolin), PAK1 (Macropinocytosis), FLOT1 (Flotillin) or GFP as a transfection control, then knockdowns were validated at the mRNA and protein levels. All 4 targets (AP2 μ 2, CAV1, FLOT1, PAK1) were successfully knocked down at the mRNA level relative to the GFP control siRNA, reducing mRNA levels of the targets by 80%, 95%, 60% and 70% respectively (figure 15). Knockdown was then validated at the protein level by Western blot (figure 16). Clear protein knockdown was observed in CAV1 and PAK1 siRNA treated cells, whereas detection of AP2 μ 2 and FLOT1 proteins proved challenging, even in untreated cells. Furthermore, GAPDH staining of blots was often found to be inconsistent between experimental groups. It seems that solubilisation of membrane related proteins in these fibroblasts was difficult.

In contrast to pharmacological inhibitors, siRNAs were found to have no impact on the viability of the fibroblasts (figure 17a). Uptake of Alexa633-sEVs was then measured in siRNA treated cells by flow cytometry (figure 17b). Irrelevant GFP siRNA did not affect sEV uptake. Of all the targets, only knockdown of AP2 μ 2 (Clathrin adaptor protein subunit) inhibited uptake, achieving a 40% reduction in uptake. CAV1 knockdown did not perturb cellular uptake. Interestingly, PAK1 and FLOT1 knockdowns both, contrary to expectation, increased sEV internalisation significantly, by 36% and 43% respectively.

As with the pharmacological inhibitors, the effect of endocytic knockdowns on sEV uptake measured by fluorescence microscopy was also carried out. Representative

Results

images are shown in figure 4.17c, with differences between conditions difficult to see. Similarly, to figure 4.14d, significant differences between treated/untreated cells were not seen, with the exception of the FLOT1 knockdown, in which cellular uptake of sEVs was higher than in non-siRNA treated cells (figure 4.17d). Lack of sensitivity or sampling capacity of the fluorescence microscopy technique could explain our inability to observe significant differences in these experiments, in contrast to flow cytometry.

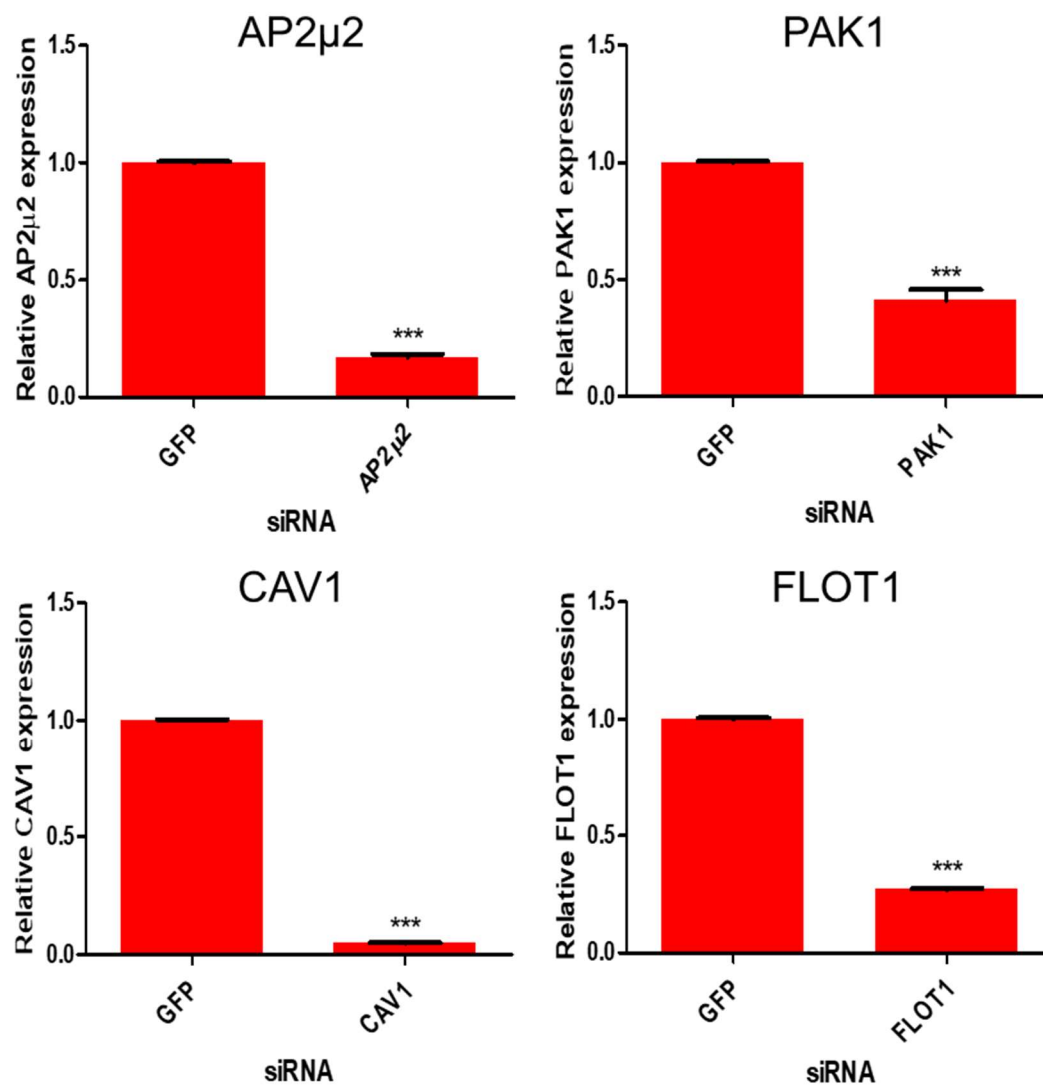


Figure 4.15. Confirmation of target mRNA knockdown by qPCR.

Fibroblasts were transfected with siRNAs against AP2 μ 2, CAV1, PAK1, FLOT1 and GFP and an siRNA control. qPCR was carried out to determine the relative expression of target mRNA in target siRNA versus GFP siRNA control treatments, with GAPDH as the internal control. Bars represent means \pm SEM, based on triplicate wells. Students t-test tested for significant differences, ***P<0.001.

Results

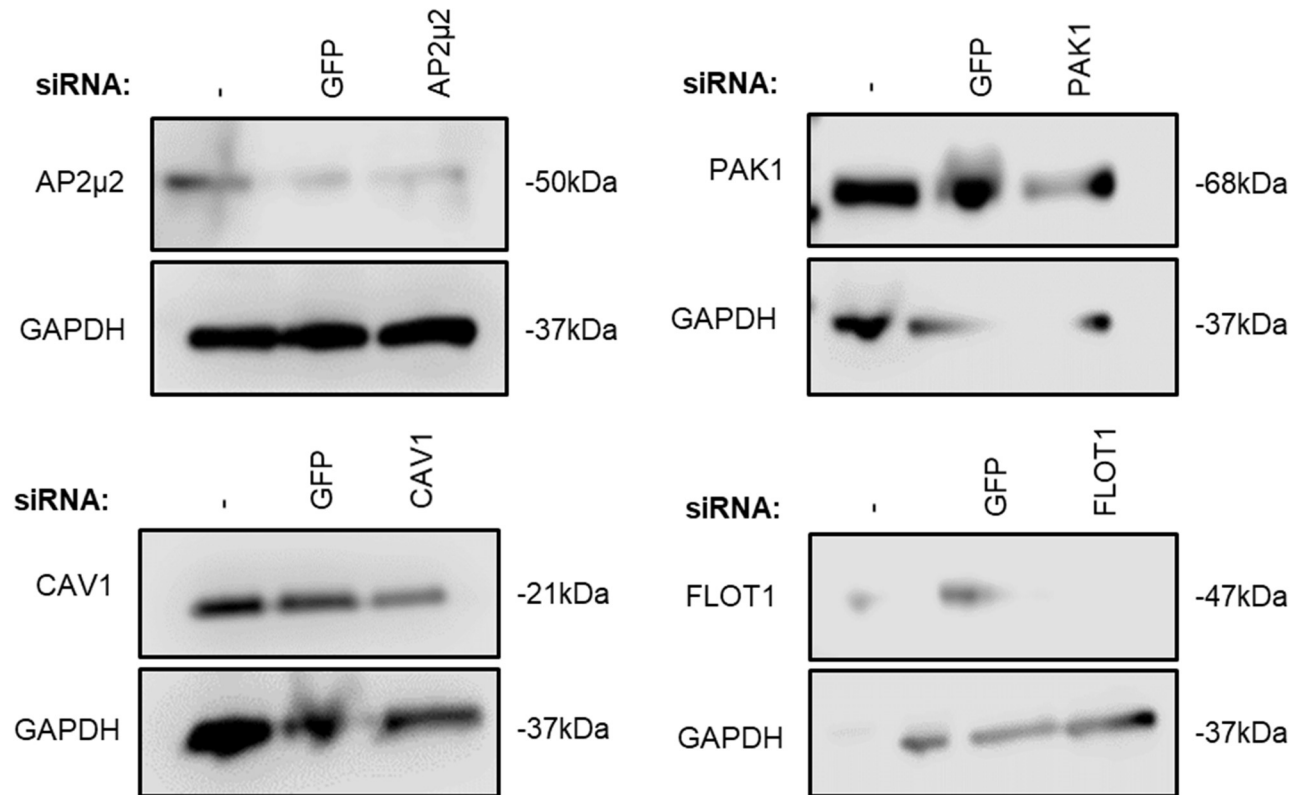


Figure 4.16. Confirmation of target protein knockdown by Western blot. Fibroblasts were transfected with siRNAs against AP2μ2, CAV1, PAK1, FLOT1 and GFP and an siRNA control. 20μg protein of cell lysates were loaded into parallel lanes, and SDS-PAGE and Western blotting were performed, with primary antibodies as indicated.

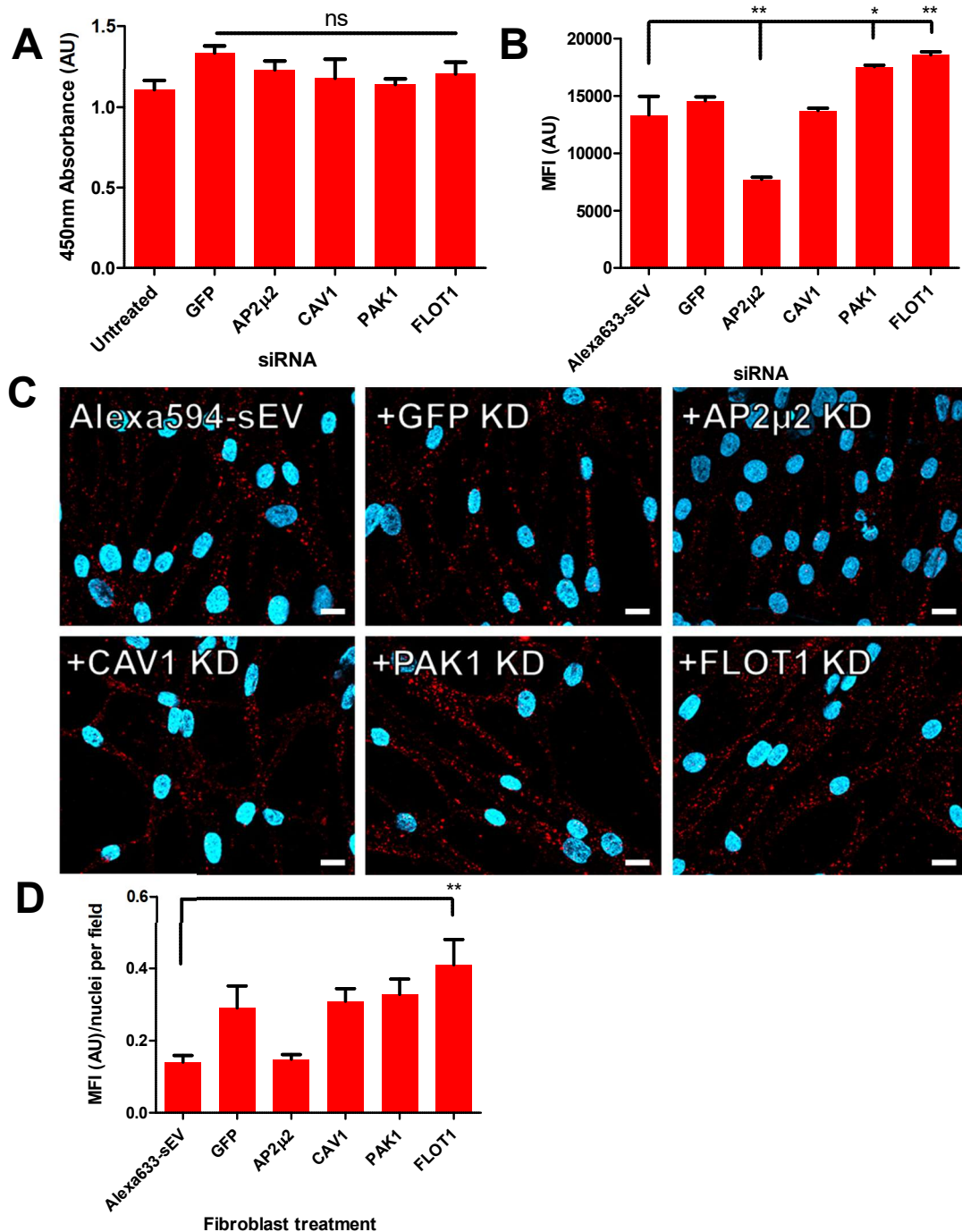


Figure 4.17. Effect of siRNAs on fibroblast viability and uptake of DU145 sEVs. (A) WST-8 assays were carried out on fibroblasts treated with siRNAs. Cells were treated with WST-8 for 1 hour, then absorbance of orange light (corresponding to viability) was measured at 450nm using the PHERAstar FS microplate reader. (B) siRNA transfected fibroblasts were treated with 25 μ g/mL Alexa633-sEVs for 1 hour, then fluorescent intensities assessed by flow cytometry. (C) Treated fibroblasts were visualised by fluorescence microscopy. Alexa594-sEVs = red, DAPI = blue. Images captured by Axio Observer Z1, 63x lens used, Scale bar = 20 μ m. Images are representative from an experiment of 9 fields of view across 3 wells, (D) and their fluorescent intensities were quantified by ImageJ. In all experiments, bars represent means \pm SEM, based on triplicate wells (or 9 fields of view over 3 wells for (D)), * P <0.05, ** P <0.01, one-way ANOVA with Tukey's multiple comparison test.

4.5. Comparison of DU145 and LNCaP sEV uptake

We showed that there is some interaction between the DU145 sEVs and fibroblasts as we could block uptake with Heparin, others have described the importance of sEV proteins in the vesicle's endocytosis (Christianson et al., 2013; Escrevente et al., 2011). In addition, PCa sEVs are more readily internalised if they are from a malignant cell line compared to a less aggressive one, and this is also correlated to their cancer promoting functionality (Lázaro-Ibáñez et al., 2017). We investigated whether fibroblasts would endocytose DU145 sEVs to a greater extent than LNCaP sEVs.

LNCaP sEVs were isolated using the same protocol used to isolate the DU145 sEVs, then both sEV populations were labelled with Alexa594. After a 1 hour treatment with 25µg/mL with one of the respective sEV populations, microscopic analysis showed a preferential uptake of DU145 sEVs by fibroblasts over LNCaP sEVs by a factor greater than 10 (figure 18).

Labelling DU145 sEVs with Alexa488, and LNCaP sEVs with Alexa594 allowed us to co-treat fibroblasts with both sEV populations simultaneously. As expected, DU145 sEVs appeared to be much more readily taken up, though LNCaP sEV uptake still occurred in the presence of the DU145 sEV (figure 19a). Co-localisation analysis revealed that almost 60% of LNCaP sEVs overlapped the DU145 sEV signal (figure 4.19b), meaning a majority of LNCaP sEVs are probably in the same endocytic compartment, or in very close association with DU145 sEVs.

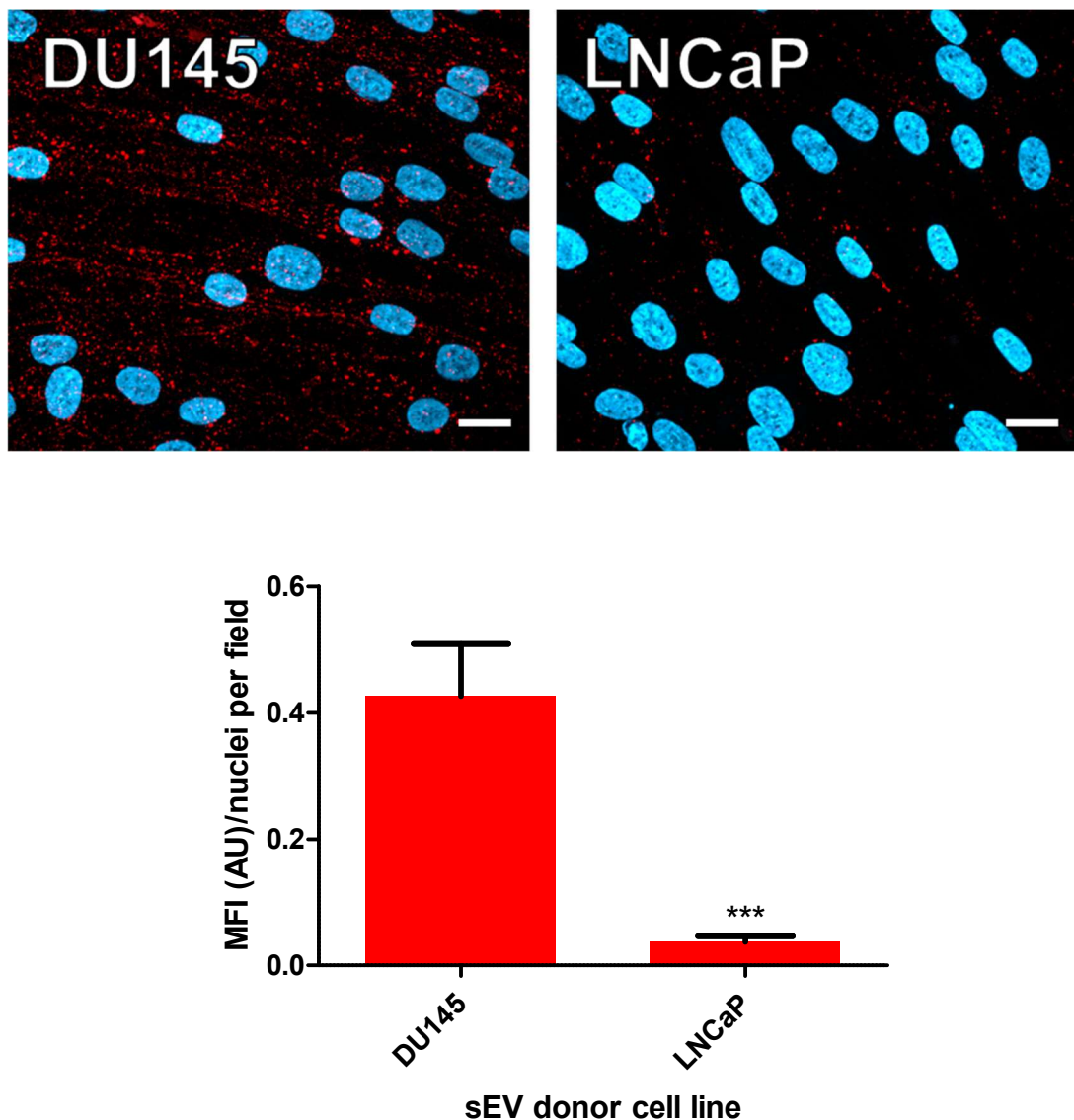


Figure 4.18. Comparative uptake of DU145 derived sEVs versus LNCaP derived sEVs by fibroblasts. Fibroblasts were treated with 25 μ g/mL DU145 Alexa594-sEVs or 25 μ g/mL LNCaP Alexa594-sEVs for 1 hour, then visualised by fluorescence microscopy. Alexa594-sEVs = red, DAPI = blue. Images captured by Axio Observer Z1, 63x lens used, scale bar = 20 μ m. Images are representative from an experiment of 9 fields of view across 3 wells for each condition. Fluorescent intensities of the two conditions were quantified by ImageJ. Bars represent means \pm SEM, based on 9 fields of view over 3 wells, *** P <0.001, Students t-test.

Results

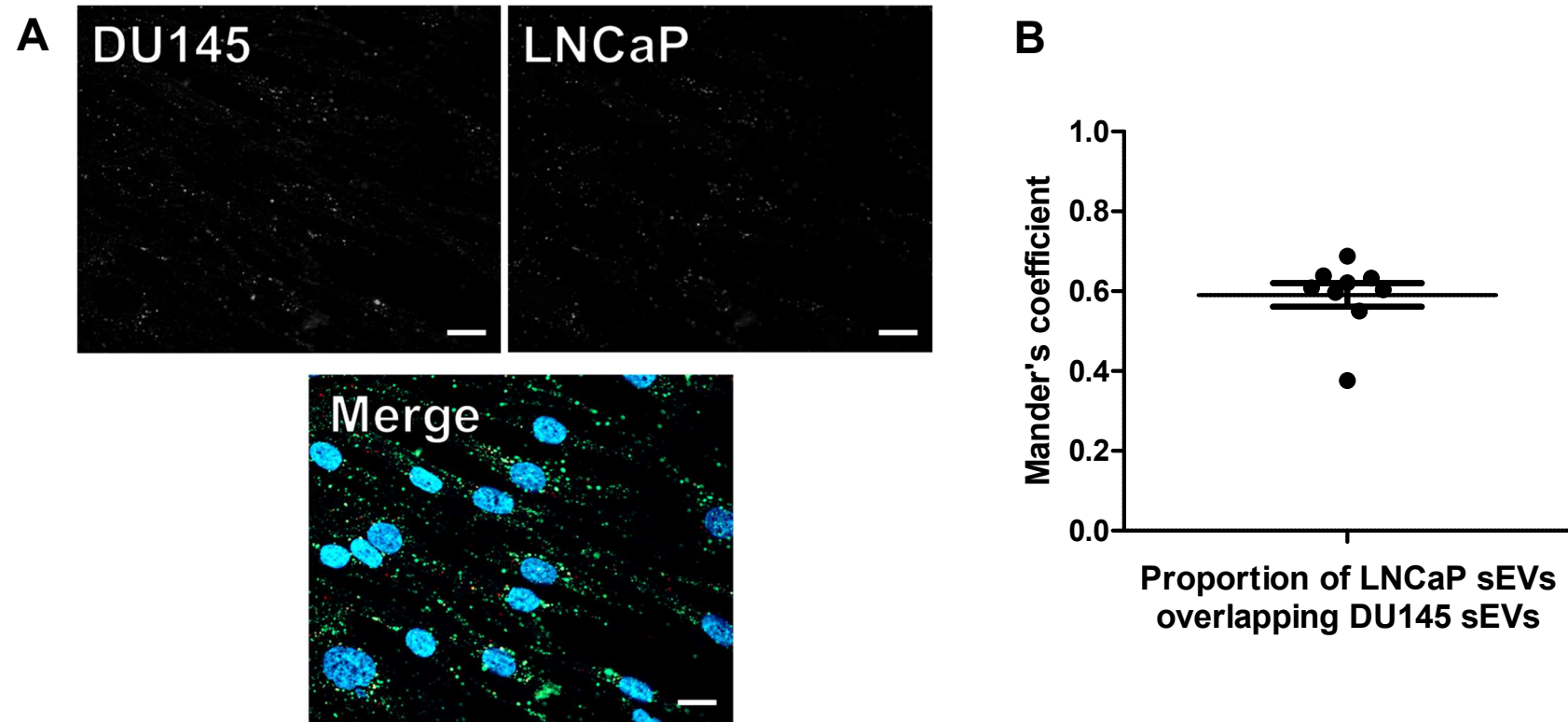


Figure 4.19. Co-localisation of DU145 derived sEVs and LNCaP derived sEVs following uptake by fibroblasts. Fibroblasts were treated with 25 μ g/mL DU145 Alexa488-sEVs and 25 μ g/mL LNCaP Alexa594-sEVs for 1 hour, (A) then visualised by fluorescence microscopy, images were captured for co-localisation analysis. DU145 sEVs = green, LNCaP sEVs = red, DAPI = blue. Images captured by Axio Observer Z1, 63x lens used, scale bar = 20 μ m. Images are representative from an experiment of 9 fields of view across 3 wells for each condition. (B) Mander's coefficient analysis to determine co-localisation of DU145 sEVs and LNCaP sEVs from fields of view taken in A, co-localisation was defined as proportion of red signal (LNCaP sEVs) associated with green signal (DU145 sEVs), measured by the JACoP plugin on the ImageJ software. Graph represent means \pm SEM of Mander's coefficients calculated, based on 9 fields of view across 3 wells.

4.6. Discussion

In this chapter, we examined internalisation of PCa derived sEVs by fibroblasts using sEVs fluorescently labelled with a novel maleimide linked Alexa dye. The main findings of this chapter are summarised in figure 4.20.

We explored the use of a novel maleimide linked Alexa dye to label sEVs for use in uptake studies. The Alexa Fluor maleimides were found to be robust sEV labelling dyes, available in multiple colours, making them suitable for various applications. The dyes produce a strong enough signal to allow fluorescent imaging of sEVs in suspension and following internalisation by primary fibroblasts. The molecular weight of the dye (Alexa488= 720.66MW) is such that it will be captured by the Exosome Spin Column in its unbound form, and hence free dye is removed. All fluorescent material used in uptake studies is therefore sEV-associated, or due to dye binding to macromolecular protein-containing aggregates. Acetylcysteine mediated inhibition of sEV-Alexa labelling supports the thiol-based targeting of the maleimides, and points to a covalent disulphide bonding between sEV and dye. 100% blockade of sEV-maleimide binding was not achieved however, higher doses of NaLc may have reduced the binding further, though we cannot rule out the possibility that some maleimide binds to the sEVs in a thiol independent manner.

Despite the protein binding nature of the dye, we did not observe an impact on the ability of the sEV to drive myofibroblast differentiation when labelled with the Alexa dye, suggesting sEV functionality is not impeded by this labelling process at least with respect to this particular phenotypic induction. The impact of sEV-dye labelling on sEV functionality is rarely considered, but important to study, as an alteration in function may reflect perturbed and non-natural uptake mechanisms. The Alexa dye does not spontaneously form large particulates, of similar size to sEVs, as seen with the widely used PKH dyes (Lai et al., 2015; Pužar Dominkuš et al., 2018), since no detectable dye comes through the 3000Da cut-off spin columns, reducing the likelihood of false positive signals associated with Alexa dyes, this was confirmed by measurement of fluorescent intensity of controls for free dye and by NTA. Overall, the Alexa Fluor maleimide dyes are proposed as easy to use labels to stain sEVs for use in uptake studies, they are versatile in their availability in different colours, do not appear to impact the size or functionality of the sEV and do not generate false positive signals post-clearance through spin columns. Use of

Alexa dyes in monitoring DU145 sEV uptake in HeLa cells has recently been published (Roberts-Dalton et al., 2017).

Fluorescence microscopy of the labelled sEVs in fibroblasts shows dispersed punctate staining with the appearance of fluorescent puncta, this quality of image will enable further studies monitoring intracellular sorting of the sEVs with the use of these dyes. Large aggregates of fluorophores were sometimes seen both within the fibroblast and externally (figure 7-9). Whilst these masses of fluorophore are unexplained, they could derive from multiple sources. Sorting of many sEVs into a single endocytic compartment could be a source of the appearance of aggregation, as the distance between the individual sEVs may fall below the resolution limit of light, thus giving the appearance of one large fluorescent particle. Aggregates of vesicles are known to form during high-speed ultracentrifugation (Linares et al., 2015), and may also be a source of the large fluorescent masses seen, particularly those seen in the extracellular space. A limitation of maleimide based labelling is that large contaminating protein structures will be labelled as well as sEVs, again a potential cause for the presence of large fluorescent materials within the sEV sample, though the use of a sucrose cushion during sEV isolation means the protein contaminants pulled into the sEV containing layer must be of similar size and density to the sEVs, therefore their presence should be limited in the sEV isolates. Alexa-sEV treated fibroblasts are also detectable fluorescently by flow cytometry. The large separation between the histograms of treated and untreated fibroblasts gives us room to detect interference of sEV uptake in future experiments, and use of far red dyes (Alexa633) to label sEVs exhibits a greater signal:noise ratio over green Alexa488 dye as it removes the green autofluorescent nature of the fibroblast from consideration. The high sampling capacity nature of flow cytometry allows us to quantify uptake in 1000s of cells rapidly, making this a robust method for analysing sEV uptake, and will be used to complement or replace analysis by microscopy in future experiments. Microscopy remains essential however for experiments identifying intracellular location of sEVs.

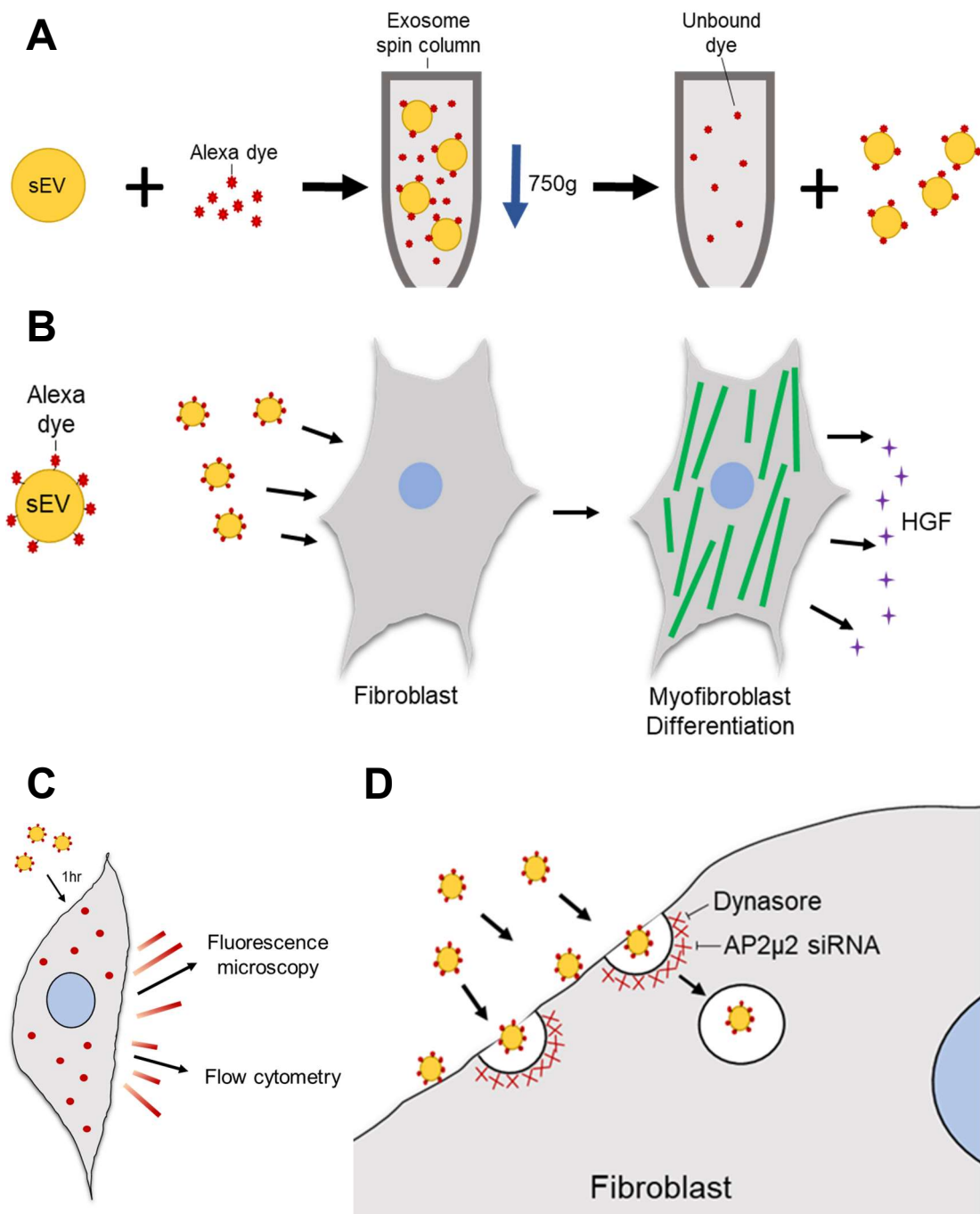


Figure 4.20. Schematic summary of chapter 4. Summary of the data collected in chapter 4. (A) sEVs can be fluorescently tagged with Alexa dyes and free dye can be removed. (B) Alexa labelling does not impede the myofibroblast differentiation function of the sEV. (C) Alexa-sEVs can be detected fluorescently in fibroblasts, by fluorescence microscopy and flow cytometry. (D) sEVs are taken up by fibroblasts primarily through Clathrin mediated endocytosis, shown by inhibition of uptake with Dynamin inhibitor Dynasore and AP2 μ 2 siRNA.

Results

It is challenging to determine the exact proportion of visible sEVs which have been internalised versus plasma membrane bound sEVs, without advanced 3-D imaging of the cell, though sEVs which are very mobile and move typically in straight lines are most likely internalised, since sEVs outside the cell would either be stuck to the plasma membrane or move under Brownian motion which would appear much more random. Co-localisation of sEVs with fibroblast internal markers would be further evidence of their uptake, this will be investigated in chapter 5. Our sEV movement was often stop and start, described previously by others (Tian et al., 2013) and since cells are known to sort cargo slowly (Kielian et al., 1986), the movement of sEVs in the fibroblast is in keeping with what is known of endosomal trafficking. Cell trypsinisation prior to flow cytometry may be a way to ensure measured sEVs are internal as this is thought to strip the cell surface of sEVs (Franzen et al., 2014). Indeed, fluorescent signal of fibroblasts treated at 4°C versus 37°C is almost entirely eradicated when measured by flow cytometry, whereas many sEVs are clearly visible using microscopy in which cells are not trypsinised, and sEVs appear in close association with the plasma membrane of the fibroblasts. Since the uptake process is temperature dependent, we believe that it is an active energy requiring one, this temperature dependent mechanism has been reported numerous times (Christianson et al., 2013; Escrevente et al., 2011; Tian et al., 2013).

Through complimentary use of pharmacological inhibitors and siRNAs against specific endocytic regulators, we were able to identify the key route of uptake for DU145 sEVs in fibroblasts. Actin polymerisation, fundamentally key to endocytosis (Galletta and Cooper, 2009), was blocked using CytoD, resulting in reduction of sEV uptake by almost 50%. EIPA only had a modest effect on uptake, macropinocytosis may therefore not play a large role in sEV uptake in fibroblasts. In contrast, Dynasore had a sizeable impact on uptake, indicating the role of dynamin in endocytosis, a protein involved in both Clathrin and Caveolin mediated uptake. Interestingly, BafA also blocked a high percentage of sEV uptake, though it is unclear whether the perturbation in uptake is due to the pH raising or endosomal maturation action of BafA. The decreased fluorescent signal is unlikely due to an effect of alteration of endosomal pH on fluorescence of the fluorophore, since the Alexa Fluor maleimide dyes are pH insensitive between pH 4-10 (Panchuk-Voloshina et al., 1999). None of the inhibitors achieved a 100% blockade in sEV

uptake. Continued tweaking of the inhibitor doses may have allowed us to increase the doses further before impacting cell viability, improving the impact on sEV uptake. Some of the targets are critical to normal cellular function, however full blockade of them may not be possible without a severe reduction in the viability of the population. Blockade of an uptake route may be compensated by another, uptake in the presence of Dynasore may still occur through macropinocytosis for example, supported by evidence that sEVs can be internalised via more than one route in a given cell (Costa Verdera et al., 2017; Tian et al., 2014a).

Knockdown of the protein AP2 μ 2 significantly abrogated sEV endocytosis. The knockdown of this Clathrin related protein, together with the Dynasore mediated inhibition demonstrates that uptake of DU145 sEVs by fibroblasts is primarily through Clathrin mediated endocytosis. Dynamin is also involved in caveolin dependent endocytosis, however knockdown of CAV1 showed no impact on uptake at all, meaning the role of dynamin is entirely related to CME in this instance. Surprisingly, knockdown of PAK1 and FLOT1 both lead to an increase in sEV uptake. The result seen with PAK1 was particularly unexpected because treatment with macropinocytosis inhibitor EIPA did slightly block uptake, whereas PAK1 knockdown has had the opposite effect. Whilst these results are so far unexplainable, perhaps their knockdowns are causing an upregulation of the other pathways, which could be tested by qPCR/Western blot, or using known probes of the other pathways. It has been shown that CAV1 for example can negatively regulate sEV uptake in mouse embryonic fibroblasts (Svensson et al., 2013), supporting this theory. The siRNAs allowed for a more accurate defining of the endocytic routes used by sEVs and did not affect cell viability. Although confirmation of our knockdowns at the mRNA was straightforward, Western blot analysis of these protein in the fibroblasts proved difficult, despite repeated attempts, high quality blots were not achievable for most targets, meaning we could not be certain of knockdown at the protein level. However, with the qPCR data, and that these siRNAs have been validated previously in HeLa cells (Roberts-Dalton et al., 2017), we were confident that they functioned as they were designed to, and that the poor protein knockdown confirmation was due to the difficulty of carrying out Western blots with these cells rather than the knockdowns themselves. The Western blots may have been challenging due to the solubility of

the target proteins in these cells, or simply due to the low abundance of the protein in the fibroblast, however we have not tested these theories.

Together, siRNA knockdown and pharmacological inhibition identify CME as the principal endocytic route for DU145 sEV uptake in fibroblasts. CME is not the main endocytic mechanism for DU145 sEV though in every recipient cell, we previously showed that DU145 uptake in HeLa cells is actually macropinocytosis driven (Roberts-Dalton et al., 2017). Furthermore, internalisation of cancer sEVs by fibroblasts has been described via different mechanisms too. Glioblastoma sEVs rely on lipid rafts, rich in Flotillin-1, and are independent of Clathrin Heavy Chain protein in mouse embryonic fibroblasts for their uptake (Svensson et al., 2013). Clearly, endocytosis of sEVs is dependent on both the origin of the recipient cell, but also the origin of the sEV. Uncovering the specific pathways for sEV uptake in different cell types will be a challenge for the EV field, but essential for allowing for more accurate therapeutic targeting of sEV uptake into target cells.

The protein content of the sEV surface is key for uptake to occur (Escrevente et al., 2011). Here we showed uptake could be significantly abrogated by Heparin, suggesting a role for HSPGs for sEV endocytosis, shown previously by others (Christianson et al., 2013). CME is a receptor mediated uptake route, so since we show DU145 sEVs are taken up by fibroblasts through this mechanism, the sEV surface proteins are clearly important. Our maleimide linked dyes bind sEV proteins, possible interference this has with endocytic route used by our sEVs is unclear; determining route of endocytosis using alternative dyes to the maleimide linked dye may reveal whether the Alexa dyes have any impact on route of uptake.

DU145 sEVs are detected in fibroblasts to a higher degree than the less malignant LNCaP sEVs. We do not know if the differences recorded are in fact due to increased uptake of the DU145 sEV, or that the LNCaP sEVs are not labelled as efficiently, resulting in uptake of unlabelled LNCaP vesicles. Though since LNCaP sEVs are detectable with the dye, and that discrepancies between uptake of PCA sEVs from distinct cell lines has been reported before (Lázaro-Ibáñez et al., 2017), it seems likely that the DU145 sEVs are just preferentially endocytosed. The big difference in extent of uptake between DU145 and LNCaP sEVs in the same recipient cell and under the same experimental conditions is very interesting and suggests that the protein content of the respective sEV surfaces must be pivotal in

regulating their internalisation. Analysis of DU145 and LNCaP cell surface proteins shows differential expression of many (Liu, 2000), such as positive expression of CD44, a marker of advanced prostate cancer (Liu et al., 1999), and CD55 (decay accelerating factor) on DU145 versus negative expression on LNCaP cells. Proteomic analysis and comparison of the two sEV populations may reveal differential expression of surface proteins relevant in the process of cellular uptake.

Movement of sEVs within the fibroblast post-uptake (figure 11), and the tendency for sEVs of different origin to co-localise into the same endosomal compartments (figure 19), illustrates that PCa sEVs begin to undergo sorting by the fibroblasts when they are internalised. Tracking the intracellular fate of the DU145 sEV will help uncover how cargo is delivered to the cell, which may provide more information on how the PCa sEVs interact with fibroblasts.

Chapter 5- Intracellular trafficking of small extracellular vesicles

5.1. Introduction

It is well established that sEVs can deliver diverse cargo to recipient cells. PCa derived sEVs transfer integrins to non-cancerous cells, which become expressed on the target cell surface (Fedele et al., 2015; Singh et al., 2016). As well as membrane proteins, cancer derived sEVs also deliver intraluminal cargo such as nucleic acids to recipient cells (Skog et al., 2008). Transfer of both protein and nucleic acids by sEVs suggest a complex processing of the vesicles by cells and potentially the degradation of the sEV with distinct components directed to different parts of the cell. Furthermore, the contents delivered to cells may become active within an hour of sEV treatment (Lai et al., 2015; Montecalvo et al., 2012), showing this delivery mechanism is surprisingly rapid. Rapid uptake can be visualised, with fluorescent sEVs detectable in cells within minutes of sEV addition (Feng et al., 2010; Tian et al., 2010), and after uptake, sEVs can be seen intact within endocytic compartments (Heusermann et al., 2016; Morelli et al., 2004; Svensson et al., 2013), meaning they are unlikely to transfer their contents to cells at the plasma membrane. Some groups have looked at sEV fate within recipient cells post-uptake and numerous studies have detailed intracellular trafficking of sEVs to late endocytic and lysosome-like compartments (Escrevente et al., 2011; Koumangoye et al., 2011; Nanbo et al., 2013). Fluorescently tracking sEVs following their uptake by cells may clarify where sEVs are sorted to and how they deliver their contents to the cells. Mapping out this cargo transfer could give us a greater understanding of fundamental sEV-cell interactions, and by studying this in our model system gain insights into how PCa derived sEVs communicate with fibroblasts.

Assessment of intracellular trafficking and luminal cargo delivery of DU145 derived sEVs in primary fibroblasts was the focus of this chapter. This was achieved through tracking of fluorescently tagged sEVs, firstly subcellular location of Alexa-sEVs post-uptake was investigated, then we examined use of alternative fluorescent dyes to probe delivery of intraluminal sEV cargo, and this aspect is particularly novel. Through these experiments, we aimed to increase our understanding of PCa derived sEV interactions with fibroblasts post-internalisation and expand our knowledge of luminal cargo delivery mechanics from sEVs to recipient cells.

5.2. Trafficking kinetics of sEVs

Before determining subcellular compartment localisation of DU145 derived sEVs following uptake by fibroblasts, we first monitored Alexa-sEV signal post-internalisation. We wanted to see whether sEVs were retained or perhaps ejected by the fibroblasts, since evidence of lysosome (Escrevente et al., 2011) and recycling endosome localisation (Koumangoye et al., 2011), even transcytosis (Chen et al., 2016) has been described for sEVs taken up by cells. Then we sought to identify any clear changes in the staining patterns of Alexa-sEVs over time, which could provide clues on the sorting or fate of the sEV.

5.2.1. Uptake kinetics of sEVs compared to endosomal probes

Firstly, sEV retention by fibroblasts was evaluated, to see whether sEVs would remain within the cells post-uptake. Signal for Alexa488-sEVs in fibroblasts over 4 hours was compared against the changes in signal over time of the endocytic probes transferrin (Tf) and dextran (Dx). Alexa488 conjugated Tf (Tf488), was used as a probe of recycling endosomes, and we expected it to be rapidly internalised, then recycled back to the plasma membrane and released (Mellman, 1996). Alexa488 conjugated Dx (Dx488), in contrast to Tf488, was expected to be retained by fibroblasts and localise to lysosomes (Baravalle et al., 2005). The fluorescent signal of Alexa488-sEVs over time versus these probes may indicate whether sEVs are recycled or retained by fibroblasts. To monitor sEV retention by fibroblasts, we employed a “pulse and chase” treatment approach. Fibroblasts were treated (or pulsed) for 30 minutes with 25 µg/mL Alexa488-sEVs, 5 µg/mL Tf488 or 100 µg/mL Dx488, then the wells were washed, and fresh media was added, cells were then incubated for 0-4 hours (chased) so we could track only the sEVs/probes that had been internalised and not inadvertently record continuous cellular uptake over the time course. Treated fibroblasts were visualised by fluorescence microscopy and the signal quantified in parallel experiments using flow cytometry.

Immediately following a 30 minute pulse, Tf488 was clearly visible inside fibroblasts (figure 5.1a), then as expected its signal deteriorated when the cells were chased prior to microscopy or flow cytometry; over the 4 hour time course, the Tf488 signal, measured by flow cytometry significantly fell (figure 5.1b), and little Tf488 could be seen in the cells (figure 5.1a). In contrast, Dx488 can be

clearly visualised in fibroblasts at 0 and 4 hours at similar levels post-uptake (figure 5.1c) and the fluorescent signal of the cells is not significantly different at 0 hours versus 4 hours, assessed by flow cytometry (figure 5.1d). Alexa488-sEVs do not appear to be recycled by fibroblasts, as signal does not decrease over the time course and Alexa488-sEVs are clearly visible in fibroblasts at 4 hours post-uptake (figure 5.1e). However, neither do they exhibit a comparable signal to D_x488. Flow cytometry reveals that over the time course, Alexa488-sEV signal dramatically increased over 3 hours (figure 5.1f), suggesting continued cellular uptake of sEVs after the wash step. Nevertheless, fibroblasts are likely retaining and not expelling the sEVs following uptake since the Alexa488-sEV signal does not fall during the 4 hour time course. Alternatively, this apparent retention of sEVs could be explained by a net balance of sEVs taken in versus those recycled; determining subcellular location of sEVs could determine whether this was in fact the case.

Results

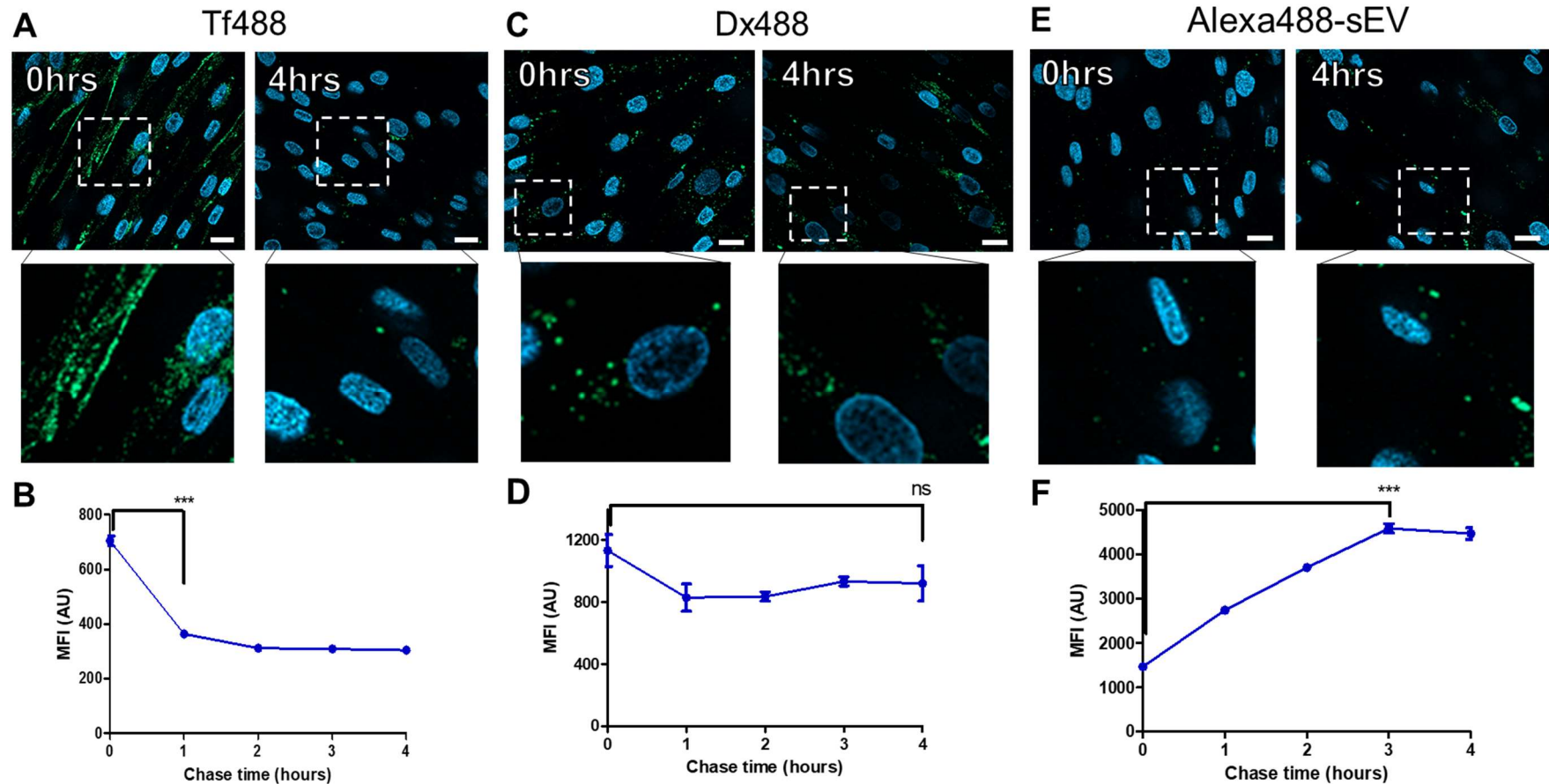


Figure 5.1. Fibroblast uptake kinetics of Alexa488-sEVs versus endocytic probes. Fibroblasts were pulsed with (A) 5 μ g/mL Tf488, (B) 100 μ g/mL Dx488 or (C) 25 μ g/mL Alexa488-sEVs, for 30 minutes, then chased for 0-4 hours. Expression of sEVs/probes were visualised by fluorescence microscopy and signal intensity measured by flow cytometry in parallel experiments. sEVs/endocytic probes = green, nuclei = blue. Images captured by Axio Observer Z1, 63x lens used, scale bar = 20 μ m. Points on graphs represent means \pm SEM, based on triplicate wells, ***P<0.001, one-way ANOVA with Tukey's multiple comparison test.

5.2.2. Time-lapse microscopy of intracellular trafficking of sEVs

After finding sEVs are retained by fibroblasts over 4 hours, we monitored sEV movement over this time by time-lapse microscopy to see how the staining pattern of sEVs changed, as changes could provide useful information on intracellular distribution/sorting of acquired sEVs. Fibroblasts were pulsed with 25µg/mL Alexa633-sEVs for 30 minutes, then wells were washed with fresh media and Fluorobrite DMEM was added to wells for imaging. Cells were incubated and simultaneously visualised using an Axiovert 100 (Zeiss) with a black box enclosure mimicking incubator conditions. Imaging was then carried out over a 4 hour time course to monitor sEV behaviour. Collected images were analysed using Integrated morphometry analysis (Metamorph v7.8.13.0) to calculate the size of fluorescent areas in fibroblasts; the size of the fluorescent areas would be related to how closely associated sEVs are within the endosomal system. Areas of positive fluorescent signal are highlighted in orange in figure 5.2a to signify areas used for analysis.

As seen previously, Alexa633-sEVs appear as punctate dots shortly after internalisation (figure 5.2a). Within 2 hours of uptake, the sizes of the surface areas of regions which were fluorescent in fibroblasts had significantly increased, and continued to increase through 4 hours (figure 5.2b). At 4 hours, clusters of Alexa633-sEVs are clearly visible in fibroblasts (figure 5.2a, zoom, white arrows). The increase in mean fluorescent area sizes in fibroblasts over time suggests that sEV are being sorted so that they are in close association, they are now close enough together that our microscope sees these as single fluorescent entities, rather than in nearby distinct endosomes, though the resolution limit of the microscope may mean we are overestimating how closely associated these sEVs are.

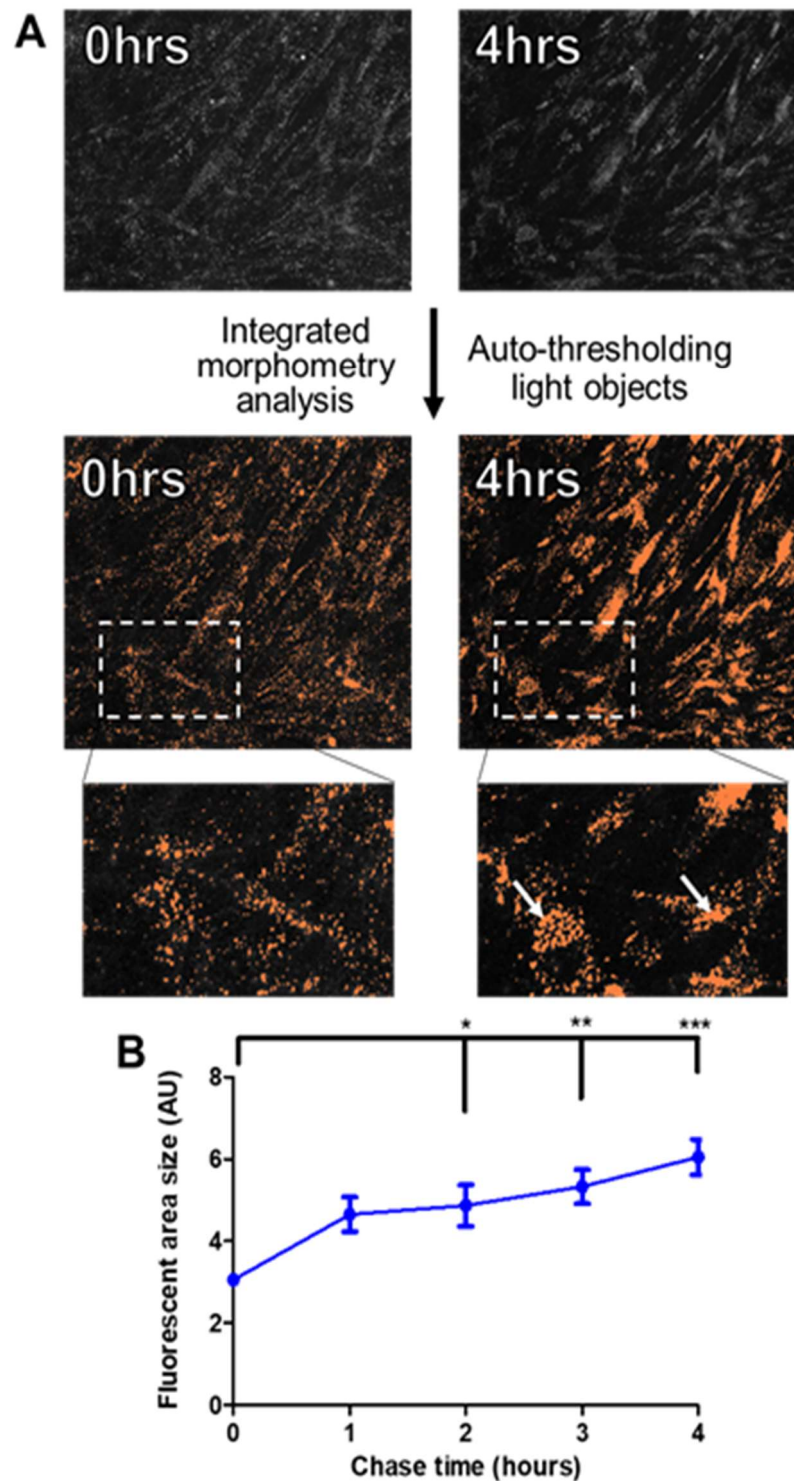


Figure 5.2. Clustering of Alexa633-sEVs in fibroblasts. Fibroblasts were pulsed with 25 μ g/mL Alexa633-sEVs for 30 minutes, then chased for 4 hours. Images were captured every hour for analysis, using an Axiovert 100 and a 40x lens. (A) Using Metamorph software, fields of view were auto-thresholded for light objects, shown in orange. (B) Integrated morphometry analysis was used to analyse light regions, mean fluorescent area sizes were plotted on a line graph. White arrows represent large fluorescent areas. Points on graphs represent means \pm SEM, based on 9 fields of view across 3 wells, *P<0.05, **P<0.01, ***P<0.001, one-way ANOVA with Tukey's multiple comparison test.

A fibroblast differentiation experiment typically takes 72 hours (Webber et al., 2010). If we extended the time course for the time-lapse experiments, we can see that fibroblasts are still fluorescent 72 hours post sEV treatment (figure 5.3a). Fluorescent signal of fibroblasts remains elevated at 72 hours, measured by flow cytometry (figure 5.3b), albeit slightly decreased from 48 hours post-sEV treatment. At 72 hours, very few clear puncta can be seen (figure 5.3a, zoom), and many cells exhibit a diffuse staining pattern. Due to lack of follow up experiments, it is unclear whether photo bleaching of the Alexa633 fluorophore occurred over this long time-lapse, with images taken every hour, or whether the patterns seen are due to further processing of the sEVs/ redistribution of the fluorophore following decoupling from the sEV.

We have demonstrated here that DU145 derived sEVs are retained by fibroblasts following uptake, and at the very least, the Alexa dye used to label the sEVs is still present in the fibroblast at 72 hours though the fate of the sEV, whether they remain structurally intact is unknown because fluorescent puncta are rare. We have evidence of the transit of sEV-containing compartments to a similar intracellular location by the fibroblasts, seen by small areas of fluorescent signal merging into larger areas (figure 5.2), indicating transit of sEVs through the endosomal system. Next, we investigated the specific subcellular location of sEVs during this intracellular sorting.

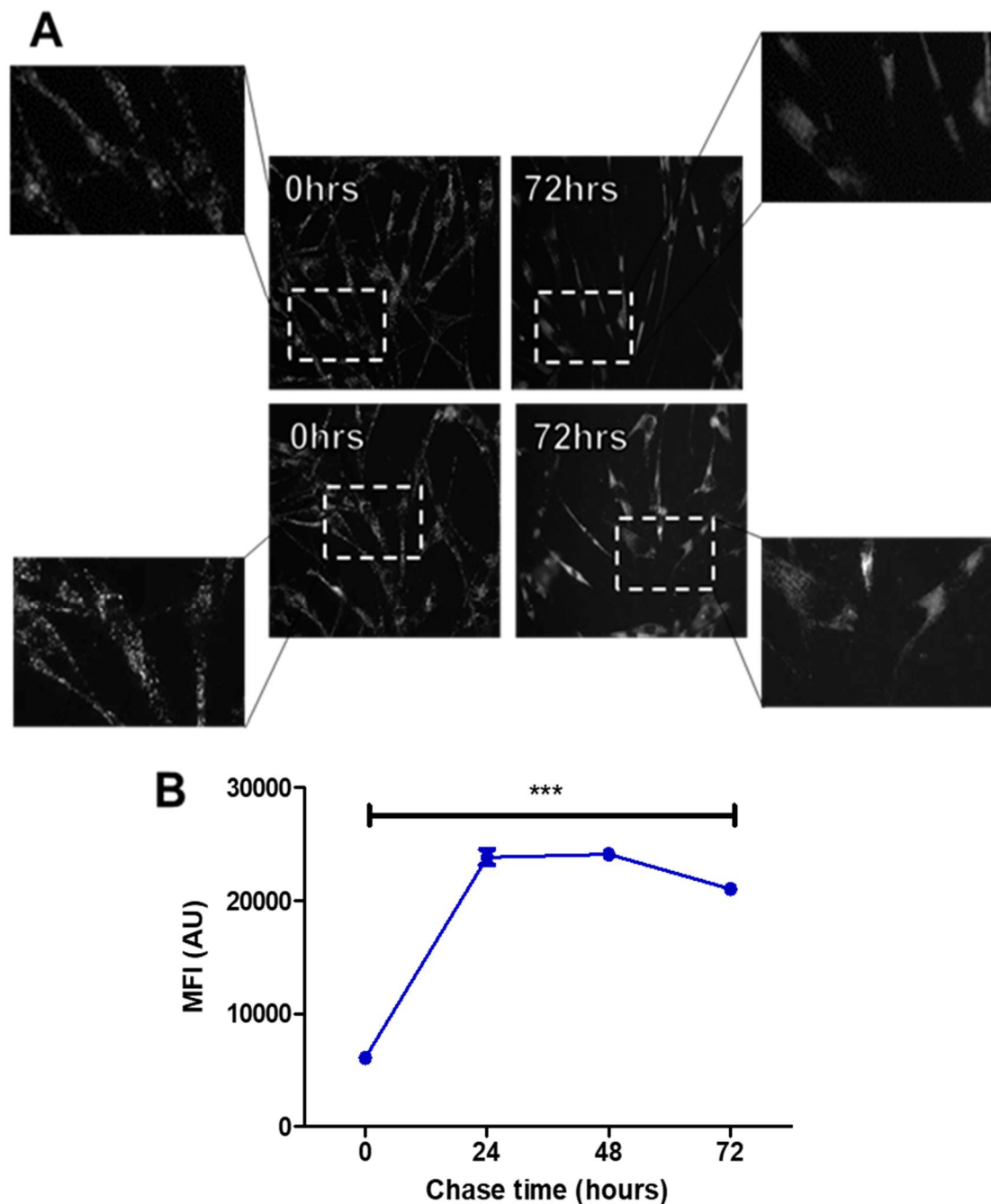


Figure 5.3. 72 hour time-lapse of Alexa633-sEV signal in fibroblasts. Fibroblasts were pulsed with 25 μ g/mL Alexa633-sEVs for 30 minutes, then chased for 72 hours. (A) Images were captured every hour with an Axiovert 100 and a 40x lens, with the fibroblasts contained within an incubator-like black box. sEVs = white. Images are representative images from an experiment of 9 fields of view across 3 wells. (B) Parallel experiment, measuring fluorescent signal of sEVs in fibroblasts. Points on the graph represent means \pm SEM, based on triplicate wells, *** P <0.001, one-way ANOVA with Tukey's multiple comparison test.

5.3. Endosomal localisation of sEVs in fibroblasts

Co-localisation analysis of sEVs with fluorescently labelled endocytic compartments was next carried out, in order to examine the route of intracellular transport of sEVs, to see if they transit towards lysosomes. We decided to track sEVs through the endosomal system, fluorescently labelling early endosomes, late endosomes and lysosomes for co-localisation with sEVs. These endosomal compartments are often fluorescently labelled through antibody staining of proteins characteristic of particular compartments (e.g. LAMP1 staining for LE/lysosomes). Antibody staining of endosomal compartments for sEV co-localisation may be unsuitable however, since at least a substantial proportion of sEVs are of an endosomal origin, and endosomal markers such as Rab5 (Christianson et al., 2013) and LAMP1 (Wolfers et al., 2001) are detectable in sEV isolates. Antibodies for endosomal proteins may therefore stain the internalised sEV itself, generating a false positive signal for the location of the sEV. CellLight® BacMam reagents (Thermofisher) are designed for fluorescent labelling of proteins in live cells (Dolman et al., 2013). They utilise a baculovirus to deliver a desired gene modified to include a red fluorescent protein (RFP) following translation in the target cell. Here, fibroblasts were transduced with CellLight reagents to express Rab5-RFP (EEs), Rab7-RFP (LEs) or LAMP1-RFP (lysosomes) and used for co-localisation analysis with sEVs. Subcellular location of sEVs was also examined through co-localisation with endocytic probes. These methods for fluorescent endosome labelling were assessed for their ability to effectively stain the fibroblasts and practicality in co-localisation experiments.

5.3.1. Co-localisation of sEVs with Bacmam labelled endocytic compartments

Bacmam reagents were ideal for co-localisation analysis as they permit specific tagging of endosomal markers in live cells. Fibroblasts were treated with 1:200 diluted Rab5-RFP (early endosome), Rab7-RFP (late endosome) or LAMP1-RFP (lysosome) transduction reagents in DMEM/F12 overnight prior to sEV addition. Following washing of cells in DMEM/F12, 25µg/mL Alexa488-sEVs were added to cells for 1 hour, then in the first instance Rab7 and LAMP1 transduced cells were chased for a further hour, as late endosome and lysosome localisation of sEVs was not expected following an hour only treatment. Cells were then visualised live using an Axio Observer Z1 microscope.

Results

Red-positive fibroblasts were identified with all three transductions, however the efficiency was very poor, most cells were positive for the Alexa488-sEV derived green signal only (figure 5.4). After 1 hour Alexa488-sEV treatment, co-localisation could be observed between sEVs and Rab5-RFP, seen as a yellow colour (figure 5.4a, zoom). 1 hour Alexa488-sEV treatment followed by a 1 hour chase revealed sEVs also co-localised with Rab7-RFP (figure 5.4b, zoom) and LAMP1-RFP (figure 5.4c, zoom), showing some evidence that sEVs can be found in early endosomes, late endosomes and lysosomes in fibroblasts after internalisation. The poor transduction efficiency in the fibroblast however meant quantification of co-localisation analysis could not generate significant data, and increasing the concentration of the reagent for fibroblast treatment to 1:20 in DMEM/F12 did not clearly improve this efficiency (data not shown).

Rab7 and LAMP1 tagging revealed the appearance of large ring-like structures (figure 5.4b-c, zoom, white arrows) in the fibroblasts; there was some concern that the transduction process had caused the formation of large artificial endosomes due to what is in essence an overexpression of the tagged proteins in transduced cells. LAMP1 staining in fibroblasts has been shown to appear punctate previously without the appearance of the ring-like structures (Falcón-Pérez et al., 2005). We therefore explored antibody labelling of early endosomes and lysosomes in untransduced fibroblasts to determine whether or not endosomes seen in fibroblasts were similar or different to their transduction positive counterparts. Fixed fibroblasts were labelled with EEA1 (early endosome antigen 1) or LAMP1 antibodies and visualised using an Axio Observer Z1 microscope with structural illumination. Figure 5.5 shows that the early endosomes and lysosomes do appear similar to those labelled with Bacmam transduction reagents. EEA1 labelling shows puncta dispersed throughout the cell (figure 5.5.a, zoom, white arrows), whereas LAMP1 staining reveals the appearance of similar ring-like structures as seen with LAMP1-RFP (figure 5.5b, zoom, white arrows). If the Bacmam is not creating the ring-like endosomal compartments, then the structures we observed are likely to be real, and not an artefact arising from overexpression of the proteins. Fibroblast endosomal compartments tagged with RFP using the Bacmam system appear to match those labelled with antibodies, however the transduction efficiency was poor, and this was not resolved, therefore co-localisation of sEV with endosomal probes was carried out.

Results

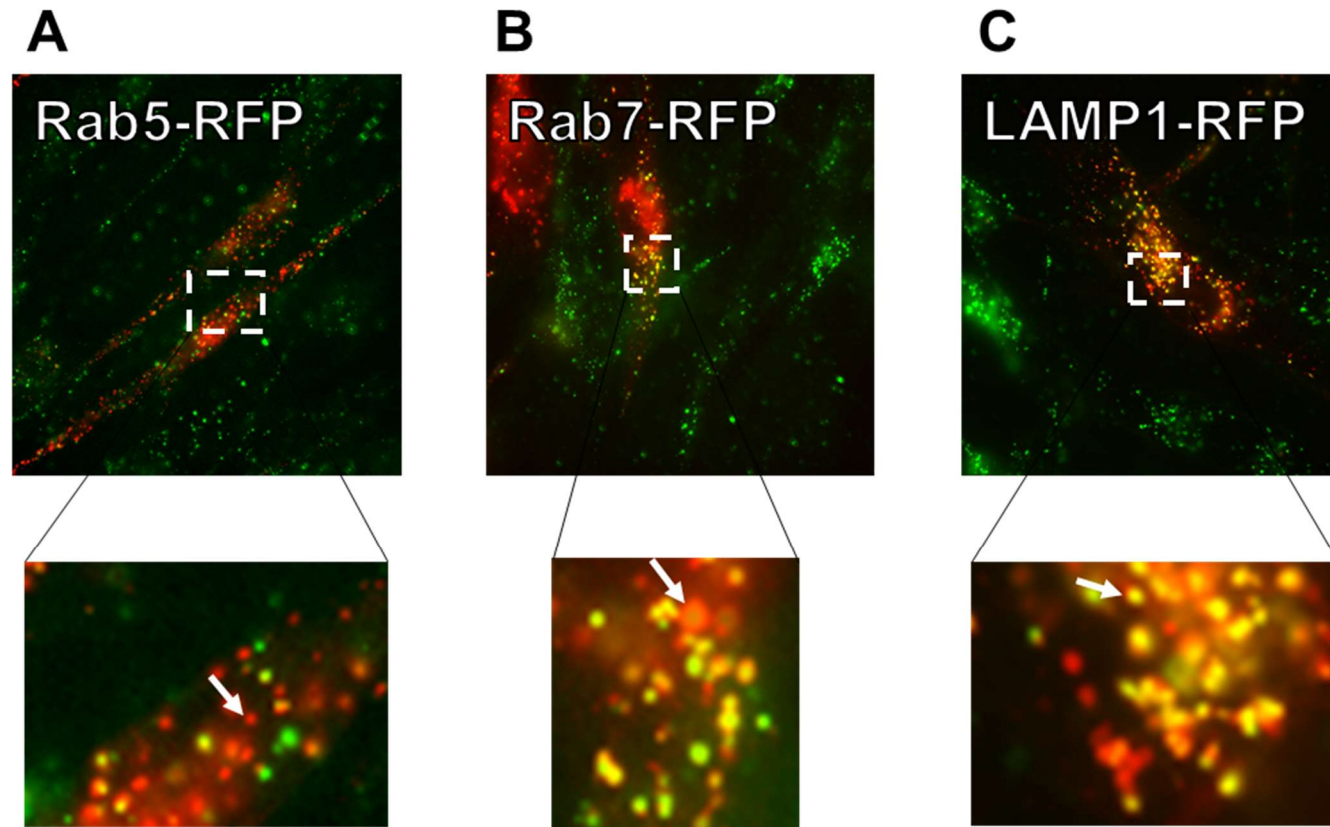


Figure 5.4. Co-localisation of Alexa594-sEVs and Bacmam transduction reagents in fibroblasts. Fibroblasts were treated with 1:200 (A) Rab5-RFP, (B) Rab7-RFP or (C) LAMP1-RFP Bacmam transduction reagents in DMEM/F12 for 18 hours. Fibroblasts were then treated with 25 μ g/mL Alexa488-sEVs for 1 hour, then chased for (A) 0 hours, (B) 1 hour and (C) 1 hour respectively. Images were captured to detect co-localisation between Bacmam reagents (red) and Alexa488-sEVs (green). White arrows indicate (A) distinct punctate staining and (B, C) ring-like structures. Images captured by Axio Observer Z1, 63x lens used. Images are representative from an experiment of 6 fields of view.

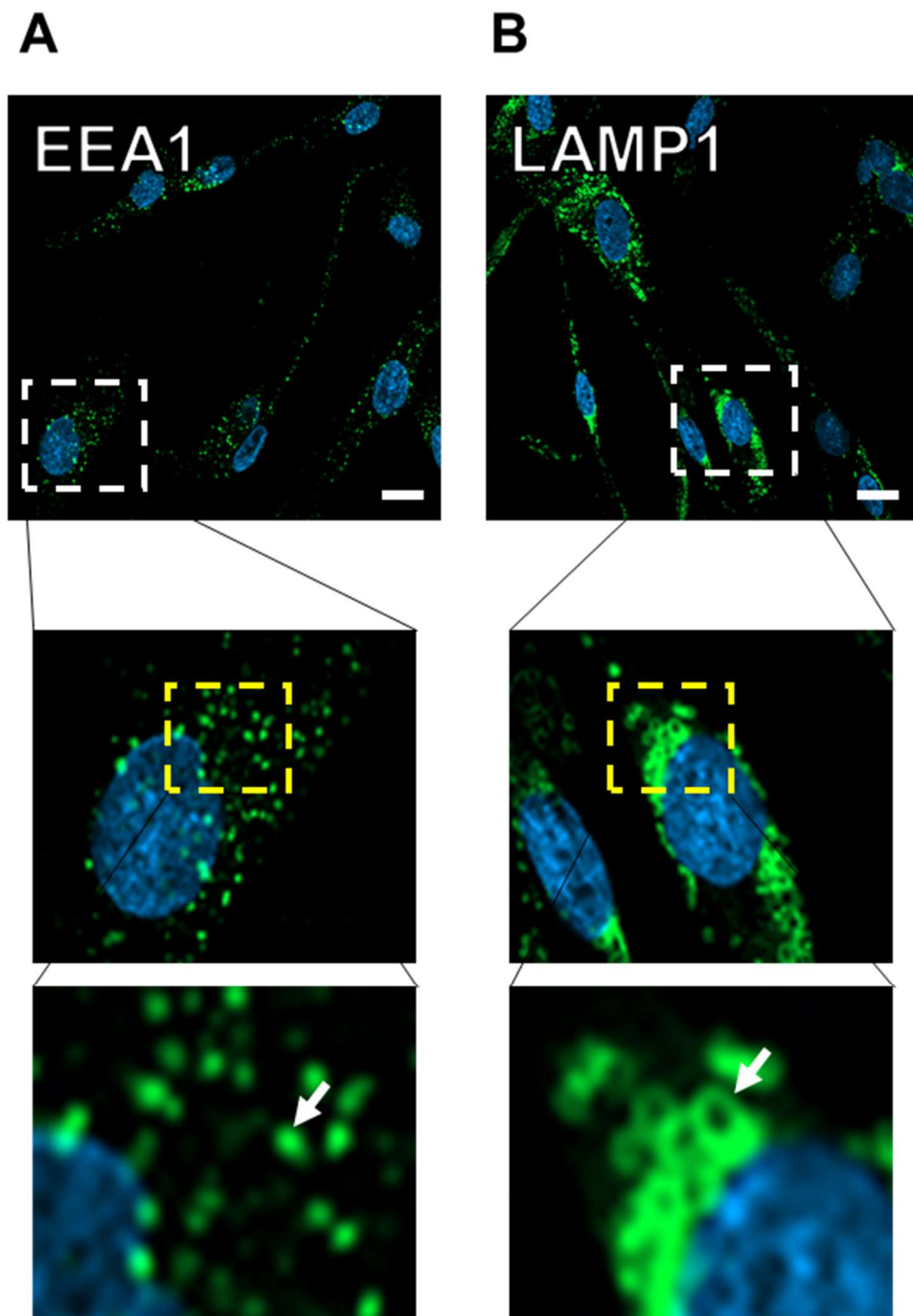


Figure 5.5. Antibody staining of endosomal compartments in fibroblasts. Fibroblasts were fixed and stained with antibodies for (A) EEA1 and (B) LAMP1. Images were captured for observation of endosomal structures. White arrows indicate (A) distinct punctate staining and (B) ring-like structures. Images captured by Axio Observer Z1, 63x lens used, scale bar = 20 μ m. Images are representative from an experiment of 9 fields of view across 3 wells.

5.3.2. Colocalisation of DU145 sEVs with endosomal probes

Endocytic probes were employed to determine subcellular localisation of DU145 derived sEVs through co-localisation analysis. Tf is recycled quickly following uptake, but is found in early endosomes, before being sorted to recycling endosomes then sent back to the plasma membrane (Mayle et al., 2012). Since we showed that sEVs are retained by fibroblasts, Tf488 was used to measure early endosome co-localisation of Alexa594-sEVs, as it was assumed the sEVs would not transit to recycling endosomes. Dx is known to be sorted to lysosomes (Baravalle et al., 2005), so would be used to determine lysosome localisation of sEVs.

For Tf co-localisation experiments, fibroblasts were co-treated with 25µg/mL Alexa594-sEVs and 5µg/mL Tf488 for 30 minutes, washed, then the cells were chased for 0-4 hours and co-localisation was measured. For lysosome localisation experiments, fibroblasts were pulsed with 100µg/mL Dx488 for 2 hours, then chased for 18 hours to ensure Dx488 has loaded the lysosomes (Roberts-Dalton et al., 2017), 25µg/mL Alexa594-sEVs were added to fibroblasts for 30 minutes, washed, and chased for 0-4 hours. Cells for Tf/Dx experiments were fixed with 4% PFA, since acetone/methanol fixation was unsuitable for these probes. Images were captured using an Axio Observer Z1 microscope, and images analysed using ImageJ.

Immediately following Alexa594-sEV/Tf488 co-treatment, sEVs can be seen co-localised with Tf488 (figure 5.6a, white arrows). Tf can be recycled within 15 minutes of addition to cells (Mayle et al., 2012), so even at this early time point (30 minute pulse), it is likely a portion of the Tf488 seen is already in or transiting to recycling endosomes. After a 1 hour chase, there is almost no detectable Tf488 remaining in the cells (figure 5.6b), suggesting it has been recycled to the plasma membrane. In contrast, fluorescent sEVs persist beyond 1 hour and hence results in a decrease in the degree of co-localisation between sEVs and Tf. At 4 hours, there is no significant difference in co-localisation from the 1 hour measurement (figure 5.6b). This data shows evidence of early endosome localisation for sEVs within 30 minutes of fibroblast treatment, and subsequent distinct sorting from Tf as the Tf is recycled back to the plasma membrane.

Alexa594-sEVs/Dx488 co-localisation after a 30 minutes sEV pulse is very rare (figure 5.7a), the Mander's coefficient at this time is close to 0, and this is not

significantly different after a 1 hour chase (figure 5.7b). Co-localisation then significantly increases at 2 hours through 4 hours, suggesting sEVs begin reaching lysosomes 2 hours after a 30 minute treatment (figure 5.7b). The fluorescent area sizes represented by clustering sEVs begins to significantly increase after a 2 hour chase (figure 5.2), this together with the Dx co-localisation data shows that sEVs appear to be grouping together into lysosomes at 2 hours post-treatment, and this continues through 4 hours.

sEVs have a 2 hour window of transport before they begin to reach lysosomes, we assume that they are then degraded here, hence the liberation of the sEV cargo may need to occur before the sEV reaches the lysosome. Next, we explored delivery of sEV luminal cargo and fate.

Results

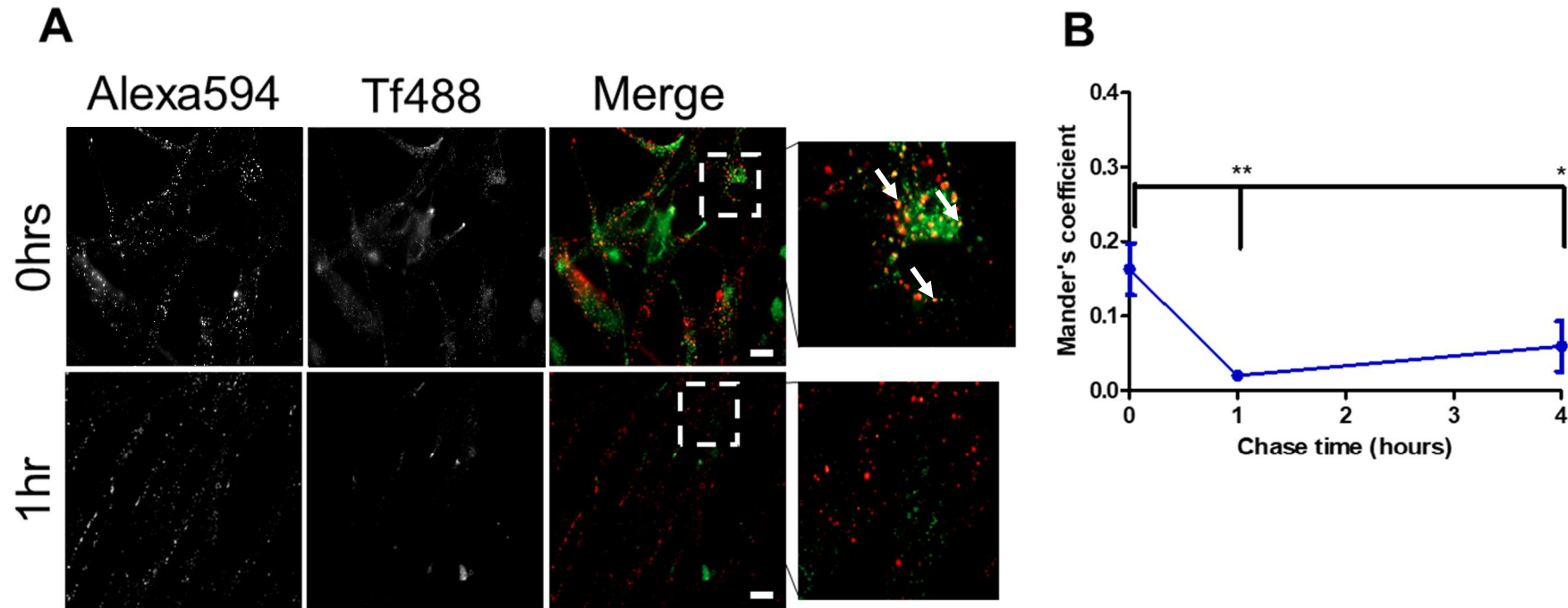


Figure 5.6. Co-localisation of Alexa594 sEVs and Tf488 over time in fibroblasts. Fibroblasts were pulsed with 25 μ g/mL Alexa594-sEVs and 5 μ g/mL Tf488 for 30 minutes, then chased for 0-4 hours. Images were captured at 0, 1 and 4 hours. (A) Images shown at 0 and 1 hours to visualise co-localisation between sEVs (red) and Tf (green), white arrows indicate co-localisation. Images captured by Axio Observer Z1, 63x lens used, scale bar = 20 μ m. (B) Mander's coefficient analysis to determine co-localisation of Alexa594-sEVs and Tf488, measured by the JACoP plugin on the ImageJ software, co-localisation was defined as the proportion of red signal (sEVs) associated with green signal (Tf). Points on graphs represent means \pm SEM of Mander's coefficients calculated, based on 9 fields of view across 3 wells, * P <0.05, ** P <0.01, one-way ANOVA with Tukey's multiple comparison test.

Results

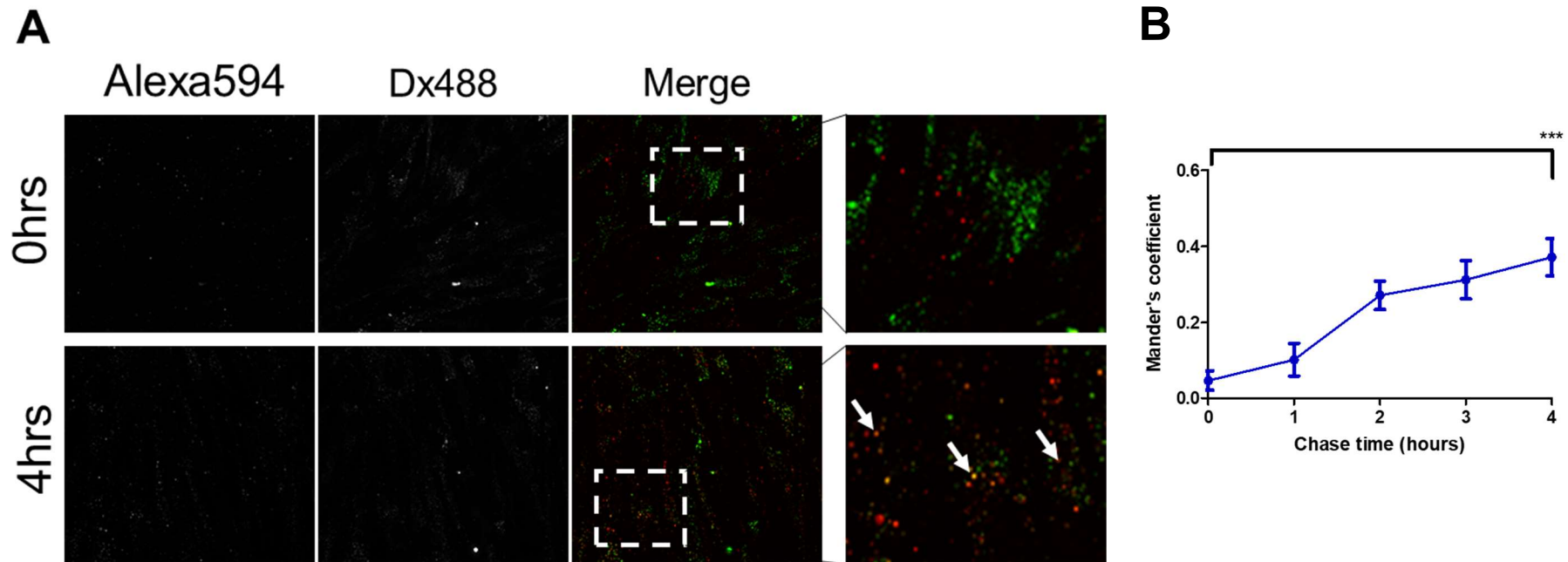


Figure 5.7. Co-localisation of Alexa594 sEVs and Dx488 over time fibroblasts. Fibroblasts were pulsed with 100µg/mL Dx488 for 2 hours, then pulsed for 18 hours. Fibroblasts were next treated with 25µg/mL Alexa594-sEVs for 30 minutes, then chased for 0-4 hours. Images were captured at hours 0-4. (A) Images shown at 0 and 4 hours to visualise co-localisation between sEVs (red) and Dx (green), white arrows indicate co-localisation. Images captured by Axio Observer Z1, 63x lens used, scale bar = 20µm. (B) Mander's coefficient analysis to determine co-localisation of Alexa594-sEVs and Dx488, measured by the JACoP plugin on the ImageJ software, co-localisation was defined as the proportion of red signal (sEVs) associated with green signal (Dx). Points on graphs represent means +/- SEM of Mander's coefficients calculated, based on 9 fields of view across 3 wells, **P<0.01, ***P<0.001, one-way ANOVA with Tukey's multiple comparison test.

5.4. Tracking intraluminal sEV contents

There is not currently a good understanding of how sEVs transfer their contents to recipient cells. To this end, we carried out labelling of DU145 derived sEVs using intraluminal fluorescent dyes to monitor the delivery of luminal cargo into fibroblasts.

With use of these alternative dyes, we wanted to track their staining patterns following sEV internalisation as a surrogate for sEV cargo delivery. Similarly, to Alexa labelling of sEVs, we optimised sEV labelling with chosen dyes to make the process simple and rapid, to allow for easy reproducibility. The fluorescent dyes chosen for sEV labelling were CFSE, Calcein AM (Cal) and SYTO RNASelect (SYTO). The selected dyes were chosen based on their membrane permeability, size, distinct chemistries and colour. The molecular weights of the dyes: 557.47 for CFSE, 994.87 for Cal and ≈ 800 for SYTO mean they are small enough that they can be captured in their unbound form with the Exosome Spin Columns used with Alexa-sEV labelling. All three of the dyes are membrane permeable, allowing them to label intraluminal contents in the sEV and are described in detail in sections 1.2.2 and 1.3.4. CFSE is a protein binding dye which will likely bind proteins on both the inner and outer leaflet of the sEV membrane, and may be trapped in the lumen if it is cleaved by intraluminal esterases (Parish, 1999). Cal permeates sEV membranes and becomes fluorescent upon cleavage by intraluminal esterases (Clayton et al., 2003). SYTO becomes highly fluorescent when bound to RNA molecules (Singh et al., 2015). All three of the dyes have been previously used to fluorescently label sEVs (Gray et al., 2015; Li et al., 2014; Morales-Kastresana et al., 2017), and all exhibit green fluorescence allowing their detection with the available instruments, such as the microscopes, flow cytometer and plate reader. Collectively, these dyes will be referred to as intraluminal dyes.

Optimisation and validation of sEV labelling with these three distinct dyes: CFSE, Cal and SYTO was performed, allowing easy and rapid sEV labelling. Then the staining patterns of fibroblasts treated with these labelled sEVs and the effect of uptake inhibition on their expression was assessed. Lastly, sEVs were co-labelled with both a green intraluminal dye and a red Alexa maleimide linked dye, demonstrating a simple method for dual-labelling sEVs with exogenous dyes. The

cellular uptake of the dual-labelled dyes was then carried out, to monitor co-localisation of the two dyes within the fibroblasts.

5.4.1. Fluorescent labelling of sEV lumen

Before use of labelled sEVs in cellular uptake experiments, we had to carry out optimisation and validation of the labelling of sEVs, with membrane permeable dyes to demonstrate their association with the vesicles and determine their stability, as carried out in chapter 4. The three selected dyes, CFSE, Cal and SYTO were first subject to detection and dosing experiments, to identify optimal doses for sEV labelling. The labelling protocol would be the same as Alexa labelling in chapter 4, where sEVs would be incubated with stated doses of dye for 1 hour and spun through Exosome Spin Columns to remove unbound dye from the solution. Labelled sEVs were then diluted in PBS, and fluorescent intensities were measured using a PHERAstar FS microplate reader, controls for free dye were also included.

DU145 sEVs were labelled with increasing doses of each dye for 1 hour at 37°C, this temperature was introduced for the labelling process as it was thought this would aid intraluminal esterase activity for CFSE and Cal cleavage. These dyes have all been previously used to label sEVs, sEVs had been tagged with 40µM CFSE (Morales-Kastresana et al., 2017), 10µM Cal (Gray et al., 2015) and 10µM SYTO (Li et al., 2014). Here we increased these doses for our sEVs in order to ensure close to saturating levels of labelling. Doses used were 50-200µM CFSE, 10-40µM Cal and 50-200µM SYTO. There was no significant increase in fluorescent intensity of sEVs with increase in CFSE dose suggesting a saturation point had already been reached (figure 5.8a), surprisingly, the highest dose of CFSE tested, 200µM produced the lowest signal. With doses of Cal, there was no significant difference between the lowest and highest doses (10µM vs 40µM; figure 5.8b). Similarly, to CFSE labelling, the highest dose of SYTO resulted in the lowest sEV signal detected (figure 5.8c), contrary to expectation. The highest tested doses would be used for sEV labelling, as they are, or at least are very close to, a saturating dose for fluorescence detection. Consistent saturation of sEV labelling would be difficult to achieve, due to the varying quantities of sEVs used in the labelling procedure.

These three selected labelling doses, 200µM CFSE, 40µM Cal and 200µM SYTO, allow fluorescent detection of DU145 derived sEVs significantly above background PBS levels (figure 5.9), measured using the PHERAstar FS microplate reader. There

Results

is also no detectable free dye above background fluorescence with any of the dyes, suggesting either the Exosome Spin Columns capture all the non-vesicular bound dye, or the dyes are not fluorescent in the absence of sEVs. SYTO-sEVs express the weakest fluorescent signal relative to background signal. SYTO-sEV fluorescent intensity was only $\approx 1.5x$ greater than background PBS signal, compared to $\approx 27.9x$ greater with Cal labelling, and $\approx 210.2x$ greater with CFSE labelling. Others have previously had difficulty detecting SYTO signal when staining EVs (Morales-Kastresana et al., 2017).

We successfully fluorescently labelled DU145 derived sEVs with the three selected intraluminal dyes. Labelled sEVs were fluorescently measurable above background levels in the absence of detectable free dye. We observed unexplained decreases in fluorescent signal with the highest doses used for CFSE and SYTO labelling, though with the variations in sEV dose which will be labelled in future experiments, it is unclear whether this dosing phenomenon we saw is applicable to any quantity of sEVs in the labelling reaction.

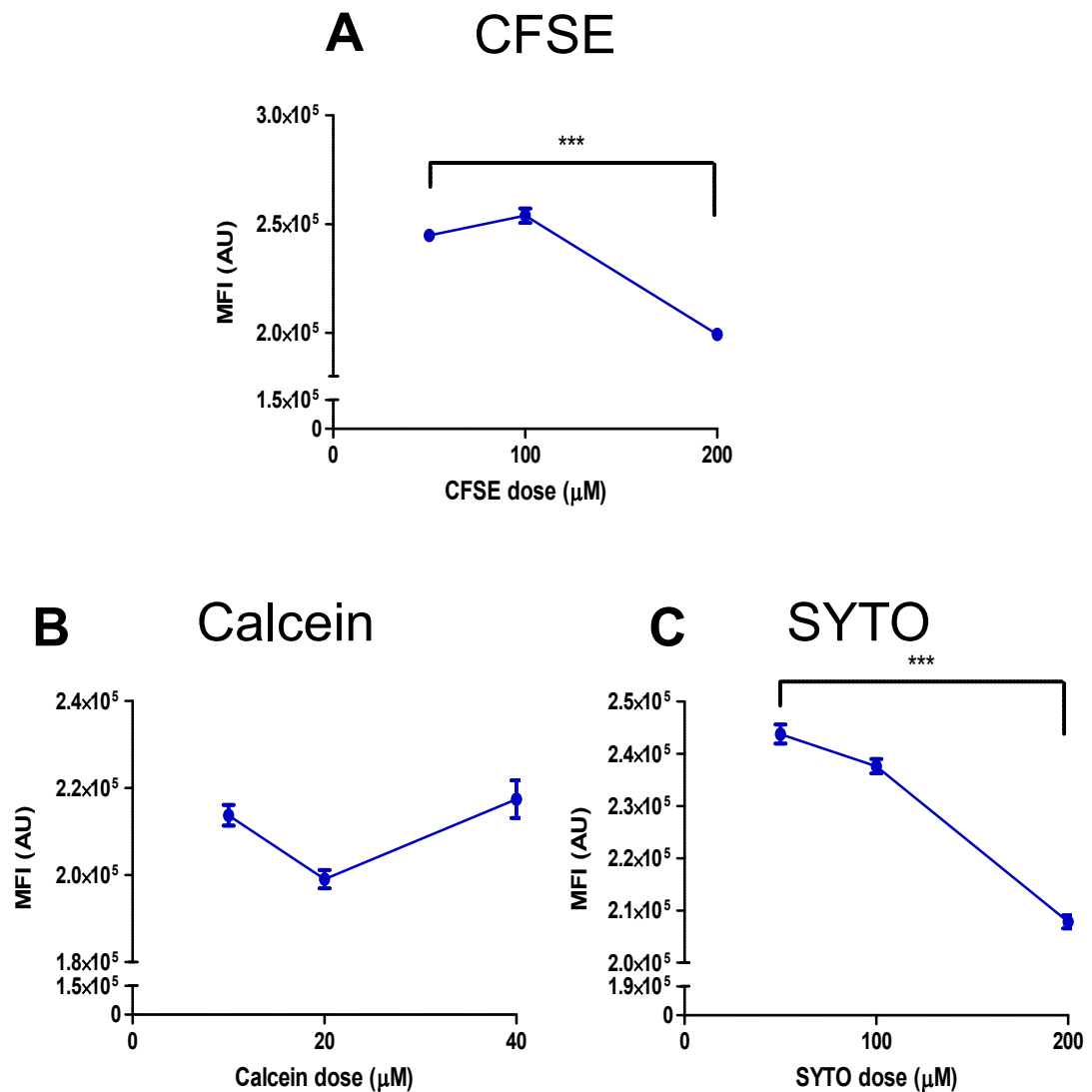


Figure 5.8. Dosing of intraluminal dyes for sEV labelling. DU145 derived sEVs were incubated with (A) 50-200 μM CFSE, (B) 10-40 μM Cal or (C) 50-200 μM SYTO for 1 hour at 37°C. Unbound dye was removed and labelled sEVs were diluted 1:6 in PBS and their mean fluorescent intensities measured using an Alexa488 optic module on a plate reader. Points on graphs represent means \pm SEM, based on triplicate wells, *** $P < 0.001$, one-way ANOVA with Tukey's multiple comparison test.

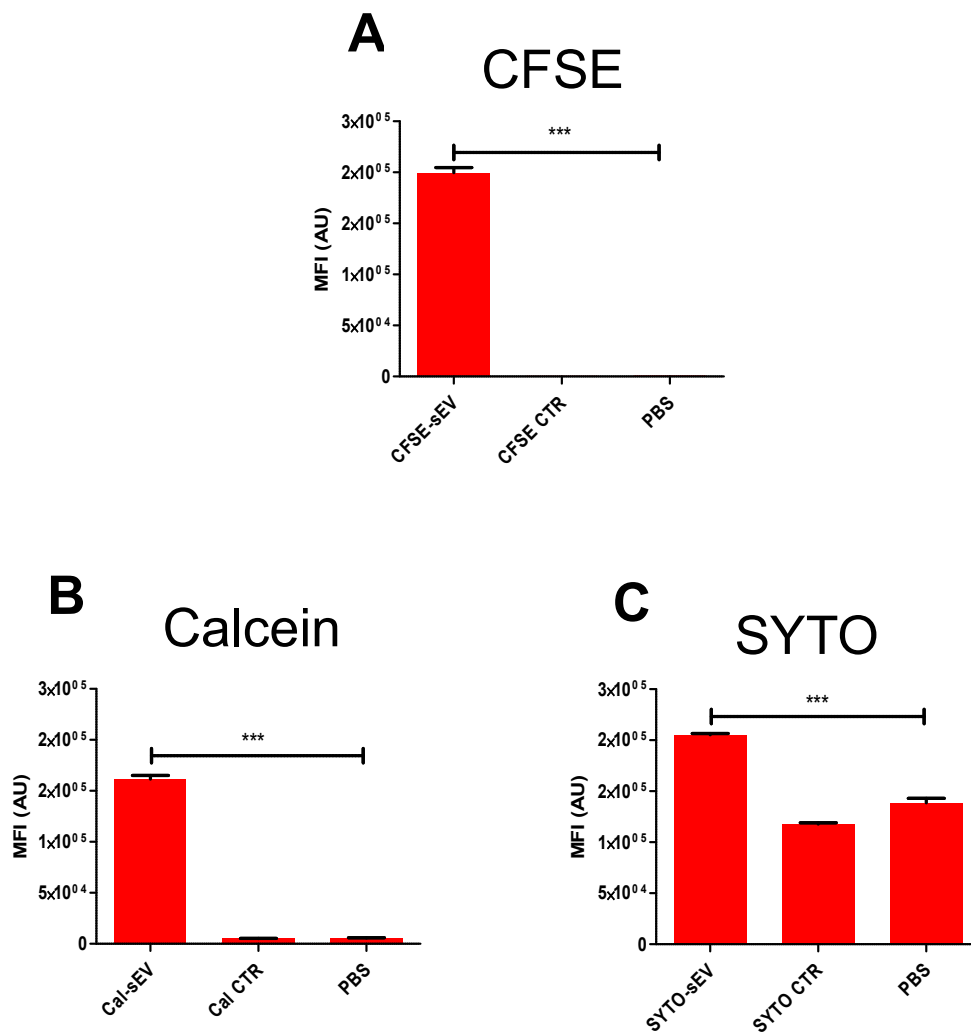


Figure 5.9. Signal of chosen doses of intraluminal dyes for sEV labelling. DU145 derived sEVs were incubated with (A) 200 μ M CFSE, (B) 40 μ M Cal or (C) 200 μ M SYTO for 1 hour at 37°C. Unbound dye was removed and labelled sEVs were diluted 1:6 in PBS and their mean fluorescent intensities measured using PHERAstar FS microplate reader. Respective fluorescence of controls for free dye (Dye CTR) were also measured. Points on graphs represent means \pm SEM, based on triplicate wells, ***P<0.001, one-way ANOVA with Tukey's multiple comparison test.

5.4.2. Characterisation of luminally labelled sEVs

Intraluminal dye labelling of sEVs was optimised and effect of dyes on sEV size was evaluated. Since the dyes are all membrane permeable, we monitored their leakage from the vesicles. As in chapter 4 with Alexa labelled sEVs, sEVs labelled with CFSE/Cal/SYTO were visualised and evaluated by Nanoparticle Tracking Analysis (NTA). It was important to determine whether fluorescent sEVs alone could be visualised microscopically, because this would enable us to monitor the staining pattern of the sEVs before cellular uptake by fibroblasts as well as afterwards. The effect the labelling processes have on the size distribution of the sEV populations was also determined, as there is known fluorescent artificial particulate formation with some exogenous dyes, particularly lipophilic dyes such as PKH (Morales-Kastresana et al., 2017; Pužar Dominkuš et al., 2018).

DU145 derived sEVs labelled with 200 μ M CFSE, 40 μ M Cal or 200 μ M SYTO were diluted 1:60 in PBS and added to glass-bottomed plates, suitable for fluorescence microscopy. Since the sEVs were floating in suspension, Apotome could not be used when capturing images as the sEVs move around between image captures, therefore wide-field fluorescence was used (figure 5.10). In all three samples, many fluorescent puncta can be seen, reminiscent of Alexa488-sEVs (figure 4.4). Figure 5.9 showed that controls for free dye were not detected above background signal using the plate reader, and here there are no visible fluorescent particles observed microscopically (figure 5.10).

NTA was carried out on the labelled sEVs, as well as samples of controls for free dye (CFSE CTR/Cal CTR/SYTO CTR), to observe the effect of the dyes on the size distribution of the sEV population and quantify any nanoparticles in the controls for free dye. Like with the Alexa labelling, the labelling process dilutes the sEVs, therefore histograms of the labelled sEVs are clearly smaller than the undiluted and untreated sEVs (figure 5.11a) and represents roughly a 50% reduction in particle concentration in all the labelled sEV populations from the starting sEV sample. With all three dyes, fluorescent nanoparticles were undetected (figure 5.11b), demonstrating that artificial particulates are not formed by these dyes, in agreement with fluorescent signal data presented in figures 5.9 and 5.10. In relation to labelled sEVs, the portion of the particle population below 200nm (in the range of sEVs) were \approx 80% for CFSE and Cal labelled sEVs, not significantly

different from the unlabelled sEVs (figure 5.11c), in the SYTO-sEV population, there was roughly a further 10% reduction in the portion of the population under 200nm, revealing a possible aggregation of vesicles caused by SYTO dye. The most common sized particle in all samples was $\approx 100\text{nm}$ (figure 5.11d), so whilst the mean size of the SYTO-sEVs was higher than the rest of the samples, its modal size was approximately the same, meaning the SYTO-sEV population had a high proportion of larger particles than the others, but not a shift of the entire histogram up the particle size scale.

Since the selected dyes are able to permeate membranes, thus the reason they were chosen, it is possible that dye does not only enter the sEV lumen upon addition but can also pass through the membrane bi-directionally, escaping the sEV. Cleavage of acetate groups on CFSE by esterases decrease the permeability of the compound (Parish, 1999), and CFSE binds to proteins covalently (Quah and Parish, 2010), so we believe CFSE should remain once bound to sEVs. Once Calcein AM is cleaved by esterase enzymes, it too is considered less membrane permeant (Gray et al., 2015). SYTO would bind RNA molecules once inside the sEV, but we do not know how stable this bond is. Labelled sEVs were diluted 1:6 in PBS and seeded onto a high protein binding sticky ELISA plate for 1 hour before sEVs still in suspension were washed away, leaving sEVs bound to the sticky plate. We then measured fluorescence intensity of these sEVs using the PHERAstar FS microplate reader, then every hour washed and measured the plate again to monitor loss of fluorescent signal over 6 hours. In parallel, fluorescence intensity was also measured in a separate plate which was not washed over the 6 hour time course, to ensure changes in fluorescent signal were due to change in the amount of dye and not photobleaching or deterioration of the dye over 6 hours.

After 6 hours, with washes every hour, fluorescent signal of CFSE-sEV and SYTO-sEV decreases by roughly 5-6% from their starting signal intensities, not significantly different to the decrease in Alexa488-sEV signal over this time (figure 5.12a). Cal-sEV signal however significantly decreases by about 26% over 6 hours, suggesting this dye is being lost from the immobilised vesicles and washed away every hour over this time course. Though we cannot rule out the possibility that the Cal dye is present on the sEV exterior and somehow reduces the stickiness of the vesicles to the plate (although since the plates are designed for high affinity

binding this seems unlikely). When the plate is not washed over 6 hours, Cal-sEV signal only decreases from $\approx 2\%$ (figure 5.12b), showing that the signal decrease in the washed plate is not due to bleaching of the dye, as the signal is almost entirely intact after 6 hours in the unwashed plate. CFSE-sEV and SYTO-sEV signal increases by 5-6% over 6 hours in the unwashed plate, suggesting longer dye-sEV incubation times could increase the fluorescent intensity of the sEVs. It is possible that the sEVs in this experiment contained SYTO unbound to RNA and CFSE which had not been cleaved, the small increase of sEV signal over 6 hours with these dyes could be explained by further RNA binding of SYTO and CFSE cleavage by esterases over this time course.

Fluorescent puncta can be visualised microscopically when sEVs are labelled with CFSE/Cal/SYTO, these puncta are analogous to Alexa-sEVs. Exosome Spin Columns appear to capture unbound dye as no fluorescent particles are detected microscopically in dye CTR samples and the Nanosight does not detect any particles by light scatter in these samples, meaning the dyes do not form aggregates of comparable size to sEVs. Cal-sEV signal is gradually lost over 6 hours compared to sEVs labelled with Alexa, CFSE or Cal. We were concerned that Cal could escape sEVs thus contaminating the solution with unbound Cal. On the other hand, the small decreases in fluorescent signals of CFSE/SYTO-sEVs were comparable to Alexa-sEV signal loss, and since the Alexa-sEV bond is covalent, this small signal loss could be explained by a loss of a small number of sEVs during wash steps. Therefore, we were confident that CFSE and SYTO dyes are retained by the sEVs following the labelling process.

Results

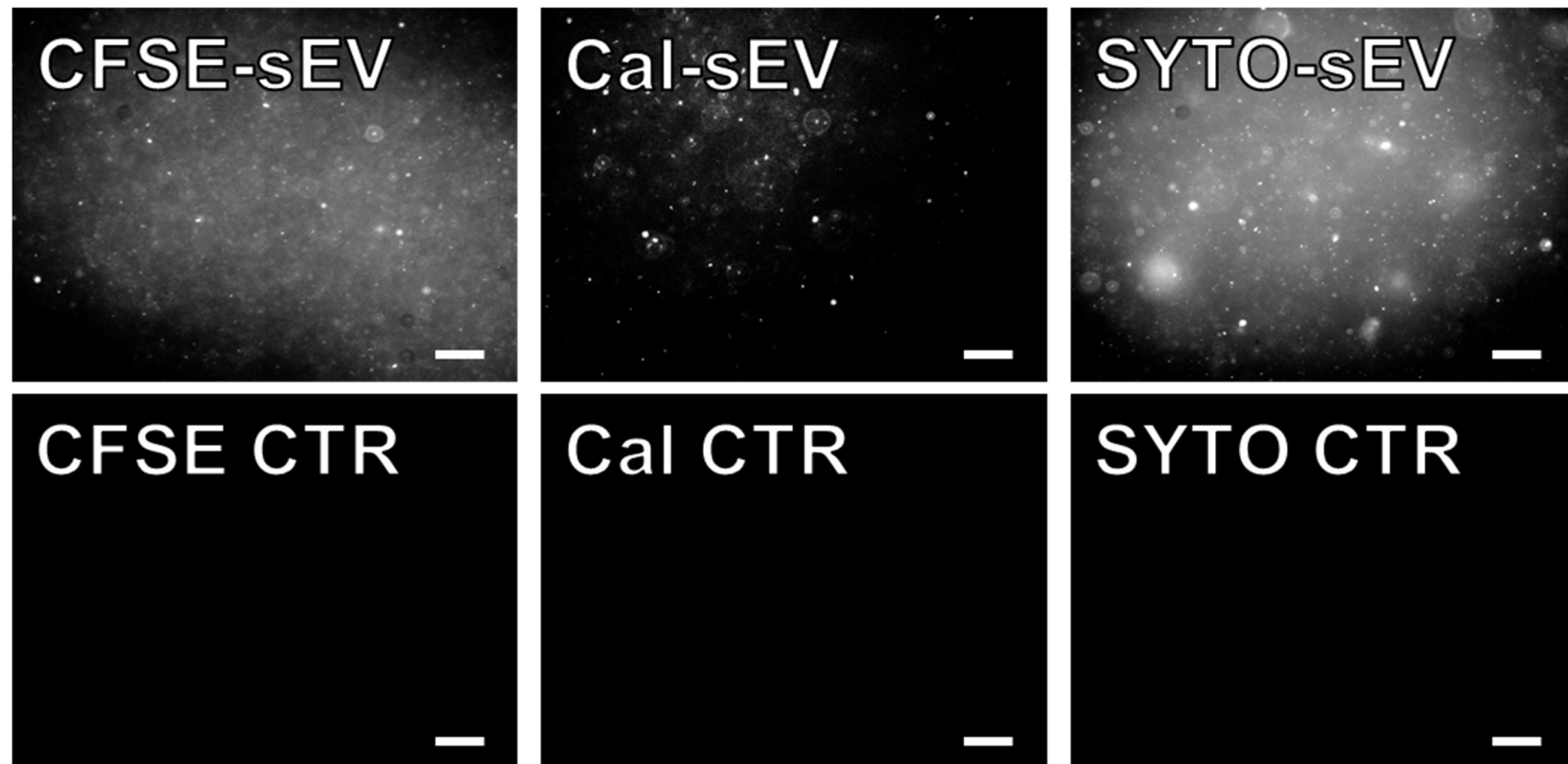


Figure 5.10. Visualisation of sEVs labelled with intraluminal dyes. Labelled sEVs were diluted 1:60 PBS and added to microscopy plates for fluorescent visualisation, respective dye CTR fluorescence was also measured. Images were captured of sEVs floating in suspension. sEVs = white. Images captured by Axio Observer Z1, 63x lens used, scale bar = 20 μ m. Images are representative from an experiment of 9 fields of view across 3 wells

Results

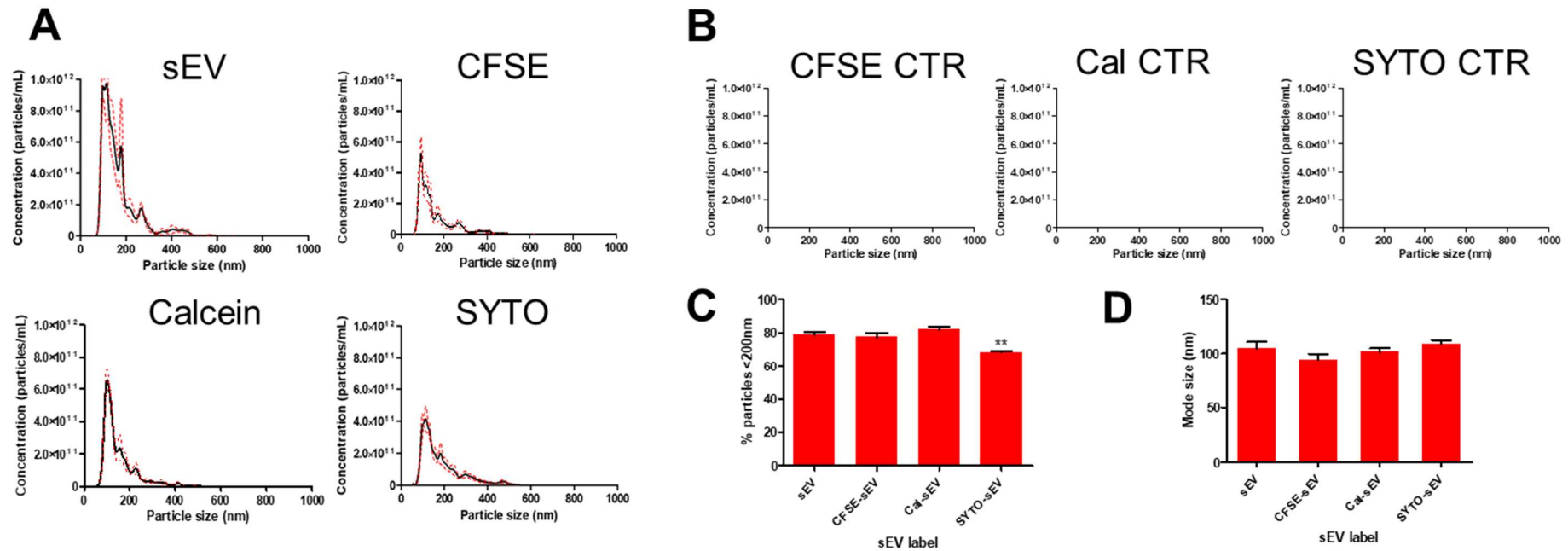


Figure 5.11. NTA of sEVs labelled with intraluminal dyes. NTA histogram demonstrating the size distributions of sEV populations labelled with intraluminal dyes. Histogram represents the concentration of analysed particles against their respective size in nm. Presented histograms are an average of 5 measurements. (A) Histograms of particles detected in unlabelled DU145 derived sEV, CFSE-sEV, Cal-sEV and SYTO-sEV samples. (B) Histograms of particles detected in control for free dye samples. (C) Percentage of measured particles from the histograms in A under 200nm. (D) Modal sizes of measured particles from the histograms in A. Bars represent means +/- SEM, based on the 5 measurements taken per sample, **P<0.01, one-way ANOVA with Tukey's multiple comparison test.

Results

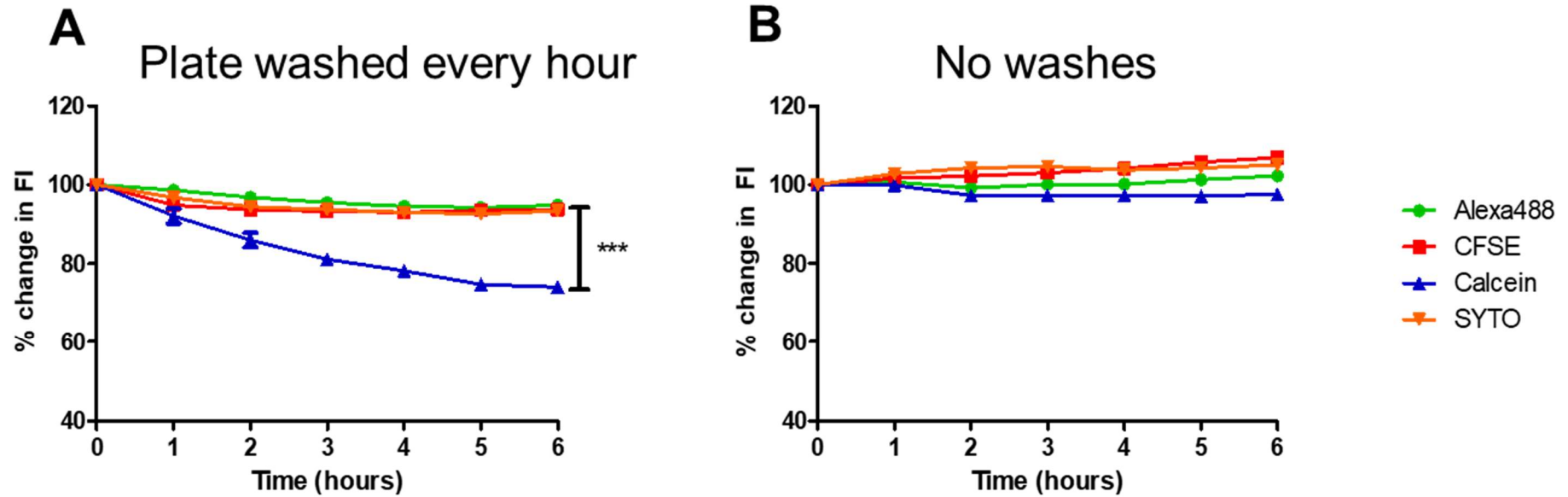


Figure 5.12. Monitoring loss of intraluminal dyes from sEVs over time. DU145 derived sEVs labelled with intraluminal dyes or Alexa488 were diluted 1:6 in PBS and added to sticky ELISA plates and incubated for 1 hour then washed. Change in fluorescent signal of labelled sEVs was measured over 6 hours. (A) Plates were washed, and fluorescent intensities measured by plate reader every hour for 6 hours. (B) Fluorescent intensities measured by plate reader every hour for 6 hours with no wash steps. Points on the graphs represent means +/- SEM, based on triplicate wells, *** $P < 0.001$, two-way ANOVA with Bonferroni post hoc test.

5.4.3. Uptake of labelled sEVs

Following validation of sEV labelling with intraluminal dyes, labelled sEVs were used for cellular uptake studies in fibroblasts to determine whether cellular uptake of the vesicle was required for the dyes to stain the fibroblast, through pharmacological inhibition, as this may clarify whether the intraluminal dyes are still associated with sEVs at the point of sEV internalisation. Similarly, to uptake studies with Alexa-sEVs, fibroblasts were treated with 25µg/mL CFSE/Cal/SYTO-sEVs for 1 hour, in order to image their intracellular location before the sEVs enter lysosomes.

We were unable to fix SYTO stained cells without compromising their staining pattern in the fibroblast, so for all cellular uptake microscopy studies with intraluminal dyes, cells were visualised live in Fluorobrite DMEM. Our aim was to monitor the staining patterns of intraluminal dye labelled sEVs post-uptake by fibroblasts and compare differences seen between dyes, as this could provide clues on sEV cargo delivery.

Fibroblasts treated with 25µg/mL CFSE/Cal/SYTO-sEVs for 1 hour were analysed for fluorescent intensity by live cell flow cytometry to determine expression of these dyes within the fibroblast population. Fibroblasts treated with CFSE-sEVs (figure 5.13a), Cal-sEVs (figure 5.13b) and SYTO-sEVs (figure 5.13c) are highly fluorescent, the signals are significantly above cells treated with media only. Histograms show the distribution of fluorescent intensities across the fibroblast population, revealing positive fluorescent signal in roughly 91% of the CFSE-sEV treated cells, 100% of Cal-sEV treated cells and 99% of SYTO-sEV treated cells. As further evidence that there is no unbound dye in these treatments, fibroblasts treated with CFSE CTR, Cal CTR or SYTO CTR do not express any fluorescent signal above the background of media only treated cells (figure 5.13), reinforcing the evidence that any fluorescent entities added to these fibroblasts are associated with sEVs, and therefore any signal detected in the fibroblast is sEV derived.

When we looked at fibroblasts treated with labelled sEVs using the Axio Observer Z1 microscope, we observed distinct staining patterns between the dyes. Due to the rapid photo bleaching of these dyes, Apotome was not used to capture images in these uptake studies. Fibroblasts treated with 25µg/mL CFSE-sEVs appear similar to those treated with Alexa-sEVs, with a dispersion of green puncta

Results

throughout the cells (figure 5.14a), fluorescent signal cannot be seen in fibroblasts treated with CFSE CTR (figure 5.14a). Fibroblasts treated with 25µg/mL Cal-sEVs exhibit quite a distinct fluorescent staining pattern (figure 5.14b), again signal was not detected in the Cal CTR (figure 5.14b), There is a diffuse staining throughout the cell cytosol, with what appears to be intense nuclear staining. Some bright puncta can be seen over the diffuse staining (figure 5.14b, zoom, white arrows), though these puncta mostly appear close to the nuclei of the cell, rather than the cell-wide puncta seen with CFSE-sEV treatment. SYTO-sEV treated fibroblasts again have their own unique pattern of staining (figure 5.14c). Nuclear staining is observable, single puncta are also present, however much of the bright punctate staining is arranged as a reticular network (figure 5.14c, zoom, white arrows). The staining patterns in these cells appear reminiscent of mitochondria staining in fibroblasts (Burbulla and Krüger, 2012). SYTO CTR, like with CFSE or Cal, does not exhibit a fluorescent signal (figure 5.14c).

As SYTO-sEV staining resulted in mitochondria-like patterns, we tested mitochondria localisation of sEV delivered SYTO. Fibroblasts were treated with 100nM Mitotracker for 1 hour to stain mitochondria in the cells red, then the fibroblasts were treated with 25µg/mL SYTO-sEVs for 1 hour, before cells were visualised live in Fluorobrite DMEM. Overlap of the reticular regions of both SYTO-sEV and Mitotracker staining reveal that SYTO dye is localising to mitochondria after sEV delivery to the cell (figure 5.15a), co-localised regions appear orange/yellow in colour (figure 5.15a, merge). Co-localisation analysis shows that almost all of the Mitotracker is co-stained with SYTO (figure 5.15b), and evidence here shows delivery of sEV cargo to the mitochondrial network in fibroblasts. We are unsure as to why the SYTO-sEVs delivered to fibroblasts almost entirely label the mitochondria, though the SYTO product supplier (ThermoFisher Scientific) note that SYTO does often label mitochondria in SYTO treated cells (ThermoFisher Scientific, 2004). This phenomenon is SYTO related and is not seen with protein binding dye, such as with Alexa488-sEV treated fibroblasts. In marked contrast, Mitotracker does not appear to co-localise with Alexa488-sEV signal at all (figure 16a), all of the Mitotracker appears red as there is no co-localisation, which would generate the orange/yellow colour seen with SYTO. In these cells the Mander's coefficient for Mitotracker co-stained with Alexa488-sEVs is roughly 0.01 (figure 5.16b).

Results

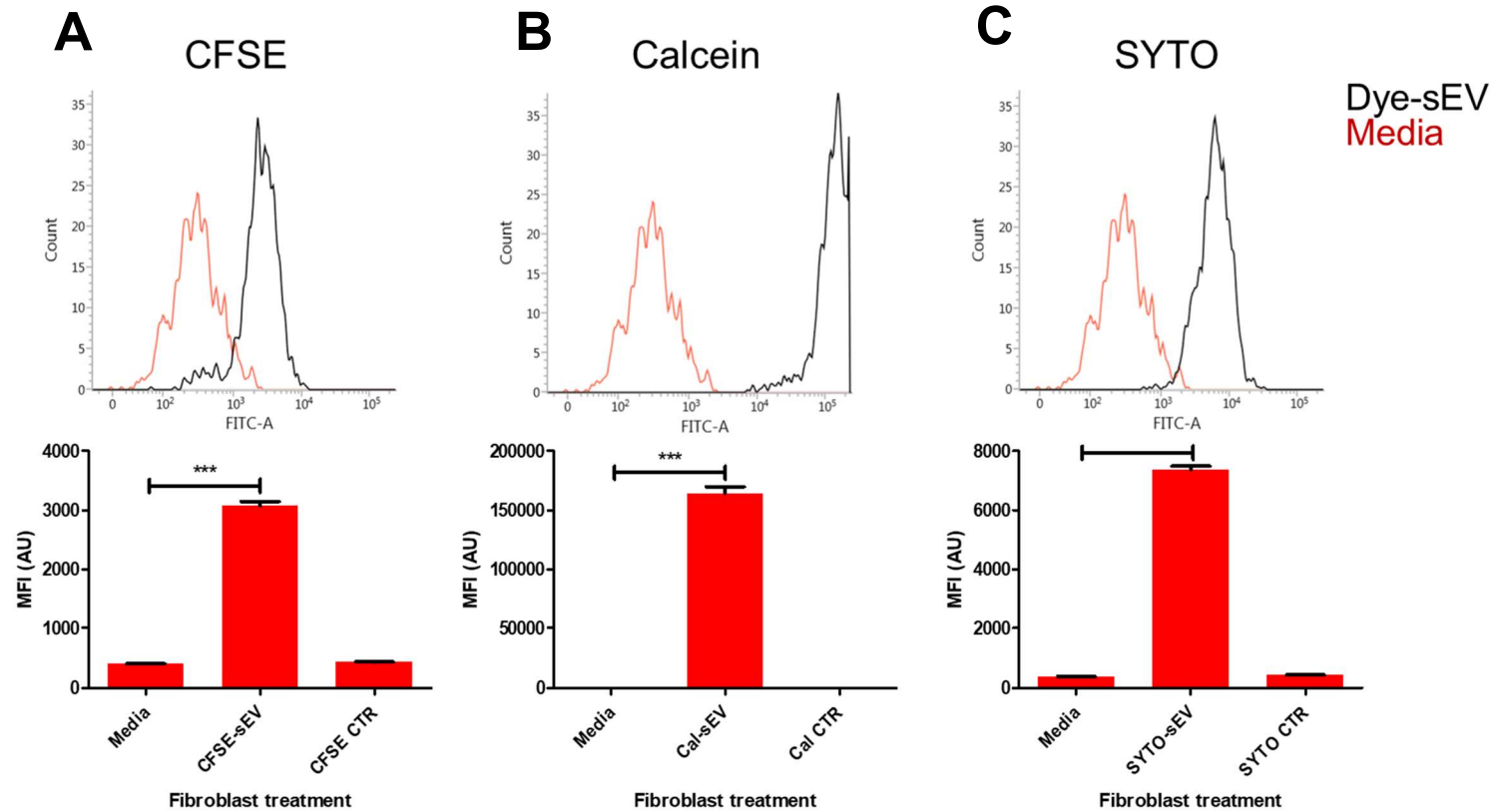


Figure 5.13. Fibroblast uptake of sEVs labelled with intraluminal dyes. Fibroblasts were treated with (A) 25µg/mL CFSE-sEVs, (B) 25µg/mL Cal-sEVs or (C) 25µg/mL SYTO-sEVs for 1 hour, then mean fluorescent intensities were measured by flow cytometry. Histograms show the distribution of fluorescent intensities across the fibroblast population, summarised as mean fluorescent intensities in bar graphs. Respective fluorescent intensities of fibroblasts treated with controls for free dye were also measured. Bars represent means +/- SEM, based on triplicate wells, ***P<0.001, one-way ANOVA with Tukey's multiple comparison test.

Results

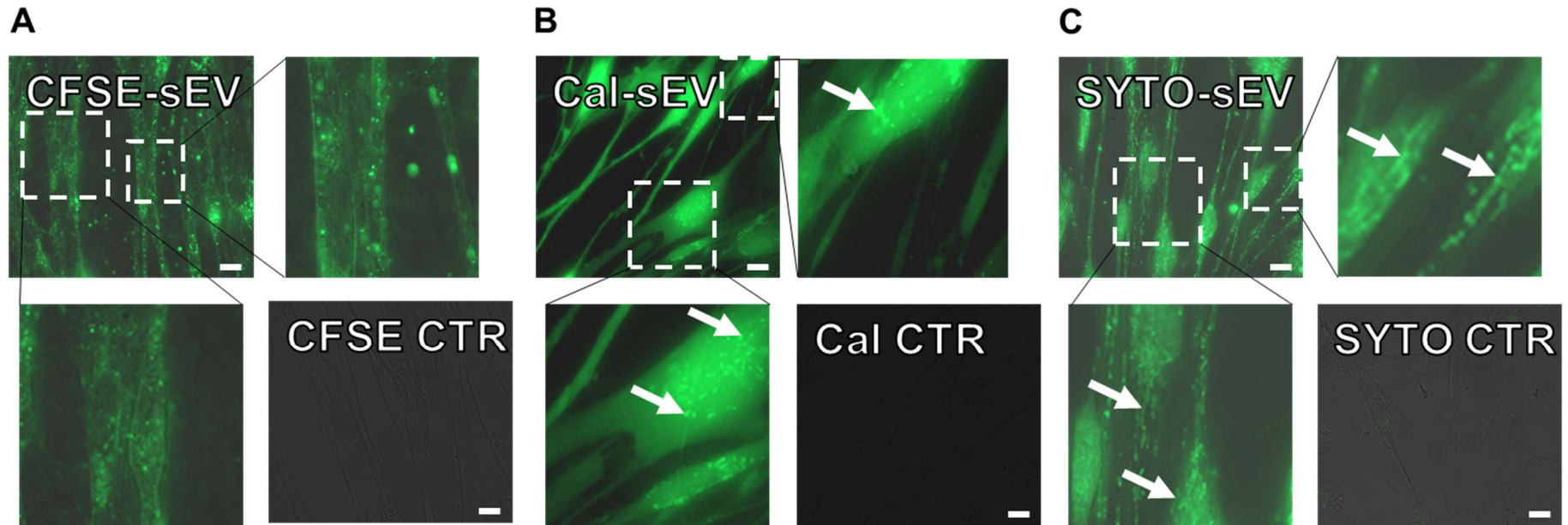


Figure 5.14. Staining patterns of fibroblasts treated with sEVs labelled with intraluminal dyes. Fibroblasts were treated with (A) 25µg/mL CFSE-sEVs, (B) 25µg/mL Cal-sEVs or (C) 25µg/mL SYTO-sEVs for 1 hour, with parallel cells treated with respective controls for free dye. Fibroblasts were visualised for observation of staining patterns exhibited by each respective dye. sEVs = green. Images captured by Axio Observer Z1, 63x lens used, scale bar = 20µm. White arrows represent (B) highly fluorescent puncta and (C) a reticular labelling pattern. Images are representative from an experiment of 9 fields of view across 3 wells.

Results

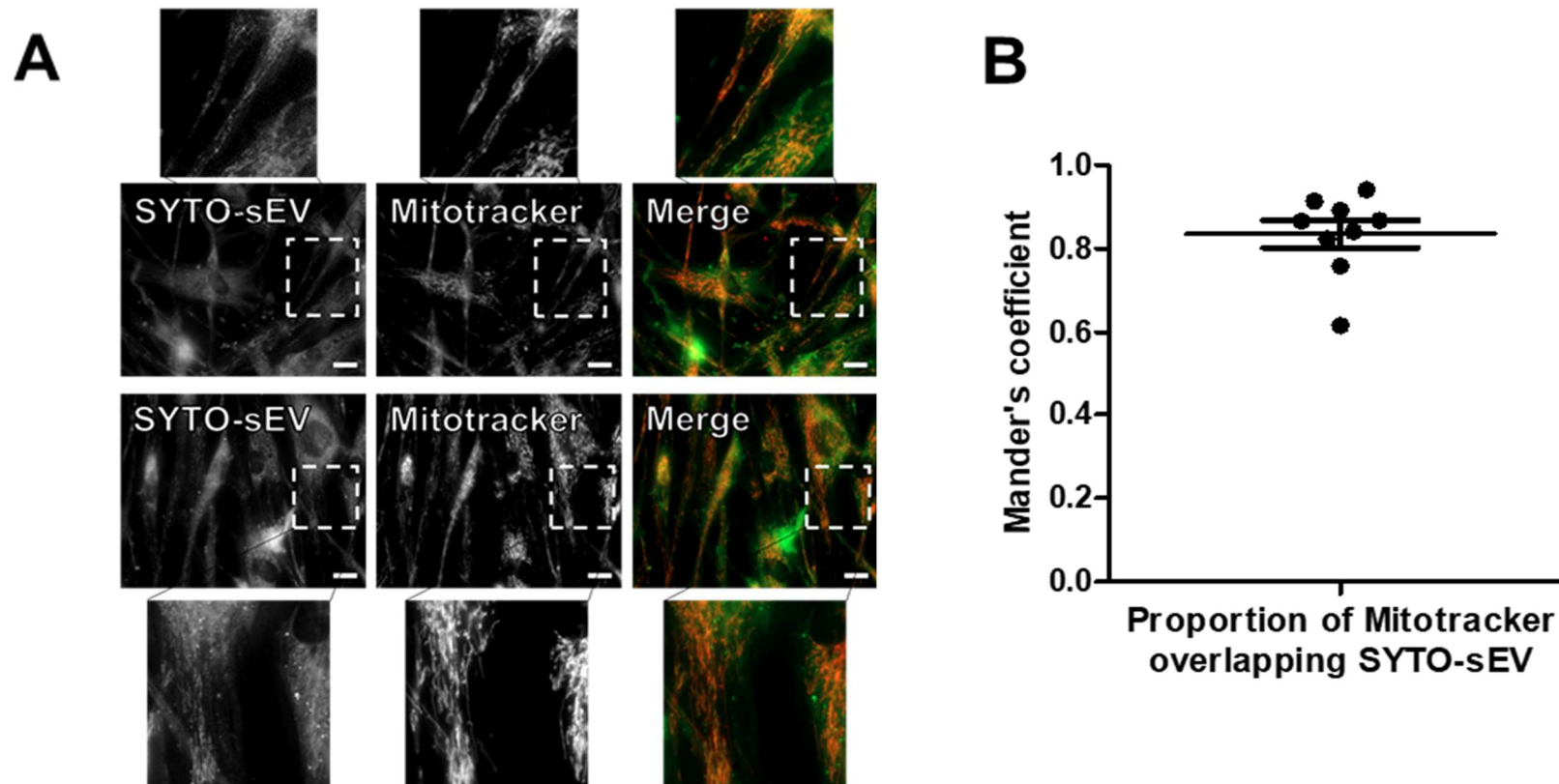


Figure 5.15. Co-localisation of SYTO-sEVs and Mitotracker in fibroblasts. Fibroblasts were treated with 100nM Mitotracker red for 1 hour, then 25 μ g/mL SYTO-sEVs for 1 hour, images were then captured for co-localisation analysis. (A) Representative image of co-localisation between Mitotracker and SYTO. SYTO-sEV = green, Mitotracker = red. Images captured by Axio Observer Z1, 63x lens used, scale bar = 20 μ m. (B) Mander's coefficient analysis to determine co-localisation of SYTO-sEVs and Mitotracker from fields of view taken in A, co-localisation was defined as proportion of red signal (Mitotracker) associated with green signal (SYTO-sEVs), measured by the JACoP plugin on the ImageJ software. Graph represent mean \pm SEM of Mander's coefficients calculated from 9 fields of view across 3 wells (Each point represents 1 field of view).

Results

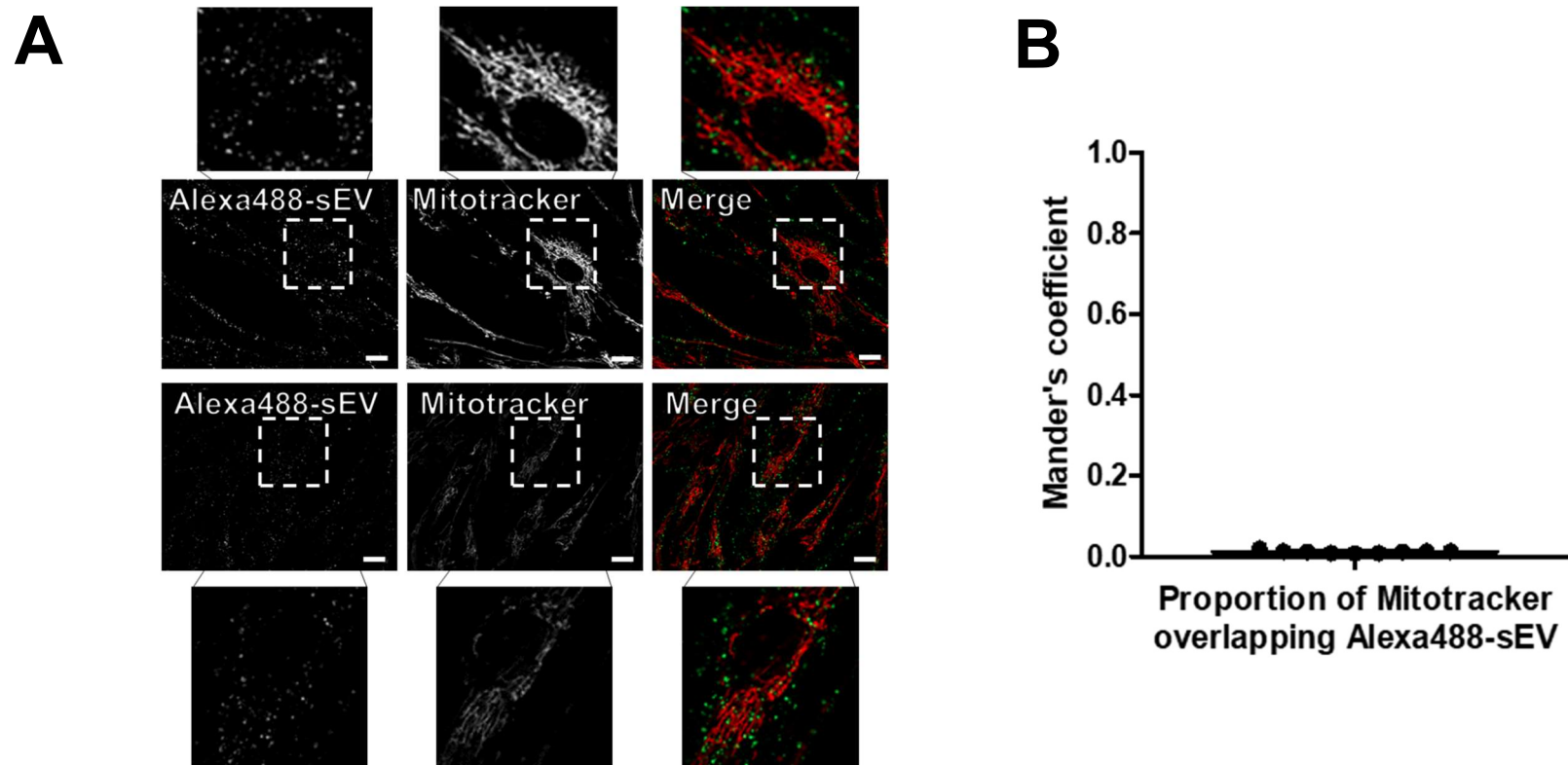


Figure 5.16. Co-localisation of Alexa488-sEVs and Mitotracker in fibroblasts. Fibroblasts were treated with 100nM Mitotracker red for 1 hour, then 25 μ g/mL Alexa488-sEVs for 1 hour, images were then captured for co-localisation analysis. (A) Representative image of co-localisation between Mitotracker and Alexa488. Alexa488-sEV = green, Mitotracker = red. Images captured by Axio Observer Z1, 63x lens used, scale bar = 20 μ m. (B) Mander's coefficient analysis to determine co-localisation of Alexa488-sEVs and Mitotracker from fields of view taken in A, co-localisation was defined as proportion of red signal (Mitotracker) associated with green signal (Alexa488-sEVs), measured by the JACoP plugin on the ImageJ software. Graph represent mean \pm SEM of Mander's coefficients calculated from 9 fields of view across 3 wells (Each point represents 1 field of view).

In relation to the perhaps surprising staining patterns seen here, we wanted to know whether the uptake of the labelled sEV is necessary for fibroblast staining to occur, or whether the dyes can label the cells independent of sEV internalisation. Dynasore, an inhibitor of dynamin, was used in the previous chapter to demonstrate the relevance of dynamin in sEV internalisation and was shown to be a potent inhibitor of sEV uptake by fibroblasts. Dynasore was used again here to abrogate sEV uptake. The signal of CFSE/Cal/SYTO-sEV treated fibroblasts was compared against fibroblasts pre-treated with 10µg/mL Dynasore for 30 minutes prior to sEV treatment together with 10µg/mL Dynasore to determine the role of sEV internalisation for dye delivery. The signal of treated fibroblasts was measured by fluorescence microscopy and flow cytometry (figure 5.17). Dynasore treatment clearly reduces the presence of CFSE-sEVs in the fibroblast (figure 5.17a), to a significant degree, and the fluorescent intensity of the cell populations measured by flow cytometry is also reduced by Dynasore treatment (figure 5.17b), suggesting CFSE uptake therefore requires uptake through a dynamin dependent route. With Cal-sEV treatment, there is disagreement between the two methods, microscopy shows no significant difference in fluorescent signal with Dynasore (figure 5.17c), whereas flow cytometry does show a decrease in signal with Dynasore (figure 5.17d), though to a lesser extent than Dynasore treatment in CFSE-sEV treated fibroblasts, meaning that the inhibition of Cal delivery to fibroblasts in minor and fibroblast staining with Cal occurs partially independently of sEV uptake. Like CFSE, cellular uptake of SYTO-sEVs are significantly inhibited by Dynasore treatment, seen by fluorescent microscopy (figure 5.17e) and measured by flow cytometry (5.17f).

Despite the diverse staining patterns displayed by the three intraluminal dyes, we demonstrated that cellular uptake of the dye by the fibroblast is affected by inhibition of sEV internalisation. Dynasore inhibits uptake of both CFSE and SYTO labelled sEVs, two dyes with distinct staining patterns, with SYTO dyes showing less punctate staining following cellular uptake of the vesicle. It is unclear from the data how much of an impact Dynasore has on internalisation of Cal-sEVs, only showing significant results with flow cytometry analysis. Earlier we presented evidence of Cal escape from the sEV over time (figure 5.12b), and the lesser impact Dynasore has on Cal-sEV uptake compared to the other labelled sEVs could mean that a proportion of Cal uptake is independent of sEV delivery.

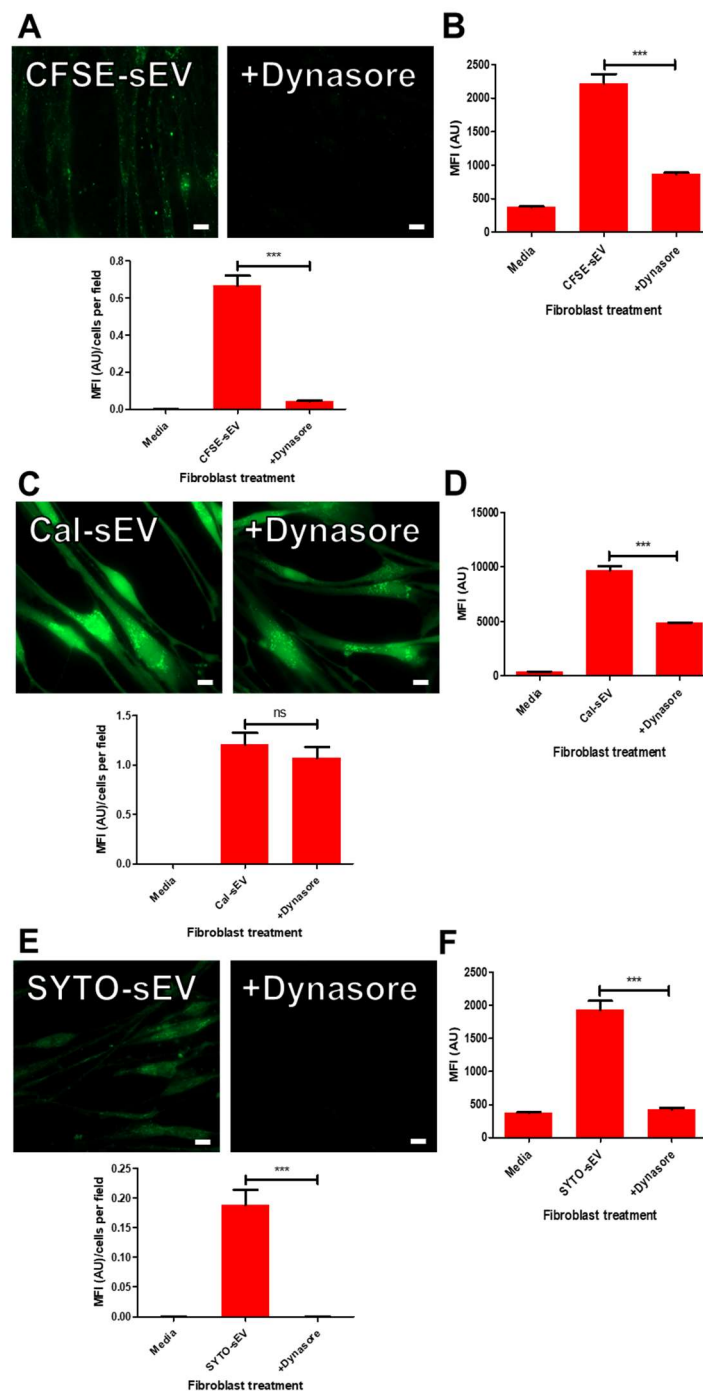


Figure 5.17. Fibroblast uptake inhibition of sEVs labeled with intraluminal dyes.

Fibroblasts were pre-treated with/without 10 μ g/mL Dynasore for 30 minutes, then co-treated with (A, B) 25 μ g/mL CFSE-sEVs, (C, D) 25 μ g/mL Cal-sEVs or (E, F) 25 μ g/mL SYTO-sEVs with/without 10 μ g/mL Dynasore for 1 hour. Mean fluorescent intensities were measured in fibroblasts through images captured by fluorescence microscopy (A, C, E; fluorescent intensity measured using ImageJ software and divided by number of cells per field of view, sEVs = green. Images captured by Axio Observer Z1, 63x lens used, scale bar = 20 μ m), and flow cytometry (B, D, F) to determine the effect of Dynasore on sEV delivery of dye to the fibroblast. Bars represent means \pm SEM, based on 9 fields of view across 3 wells for microscopy experiments, and triplicate wells for flow cytometry, ***P<0.001, one-way ANOVA with Tukey's multiple comparison test.

5.4.4. Dual-labelled sEVs

SYTO and Cal labelled sEVs show a non-punctate staining in fibroblasts, but these signals (more so with SYTO) can be inhibited by abrogation of sEV internalisation. We believe this means that the dyes are released from the sEV after cellular uptake, and given that SYTO in particular does not spontaneously leach out from the sEV, this dye release from the sEV must be a cell directed phenomenon. The Alexa and CFSE labelled sEVs remain punctate following uptake by the fibroblast, as protein labelling dyes, their continued association with the sEV was therefore expected. Co-labelling of sEVs with a protein binding dye and one of our intraluminal dyes may allow us to monitor sorting of the different sEV components after cellular uptake and track escape of Cal/SYTO in real time through monitoring co-localisation of the dual-labelled vesicles. DU145 derived sEVs were first labelled with one of the green intraluminal dyes, using previously stated doses and incubation conditions, then after removal of unbound dye the collected labelled sEVs were then incubated with 200µg/mL red Alexa594 for 1 hour and unbound dye was removed again. The resulting solutions contained sEVs labelled with a green intraluminal dye and a red Alexa dye, and the whole labelling process takes roughly 2.5 hours including the incubation steps. Confirmation of dual-labelling was carried out through co-localisation analysis of sEVs only, following this we would study the cellular uptake of these vesicles.

Dual-labelled sEVs were added to glass-bottomed microscopy plates and incubated for 1 hour at room temperature to allow settling of sEV on the plate surface. Co-localisation analysis would only be possible on sEVs stuck to the plate, as sEVs floating in suspension would move too fast for multi-colour image capture. An Axio Observer Z1 was used to capture images of dual-labelled sEVs, then co-localisation analysis of the two colours was carried out to determine the success of the dual-labelling process. Since CFSE is a protein binding dye, capable of labelling the internal and external sEV surface, we would expect a relatively low number of CFSE labelled sEVs to be co-labelled with Alexa594, whereas Cal and SYTO do not have known protein interactions, therefore we assume Cal/SYTO-sEVs will have a greater degree of Alexa594 labelling. Co-localisation was observed in CFSE-Alexa594 labelling (figure 5.18a, zoom, white arrows) showing sEVs could be labelled with Alexa594 after CFSE incorporation, though the proportion of CFSE-

sEVs which are also Alexa594 positive is low (Mander's coefficient ≈ 0.14). It is possible that the amine binding CFSE labels a greater proportion of the sEV population than the sulphhydryl group labelling Alexa dye, revealing a potential limitation of the Alexa labelling approach. Or, binding of CFSE to proteins causes some steric hindrance, inhibiting binding of Alexa dyes to the proteins.

Surprisingly, practically no co-localisation was observed in Cal-Alexa594 sEVs (figure 5.18), meaning the Cal labelling is perhaps impeding Alexa594 binding, or Cal is exclusively labelling entities which do not express -SH bearing proteins for Alexa labelling. SYTO-Alexa594 co-labelling was more successful, co-labelled vesicles could be detected (figure 5.18c, zoom, white arrows), and the proportion of SYTO labelled sEVs which could be co-labelled with Alexa594 was much higher than with CFSE or Cal labelling (Mander's coefficient ≈ 0.7). With SYTO labelling, there are a large number of Alexa594 positive yet SYTO negative sEVs present, suggesting that SYTO labelling protocols could be further optimised, or a significant portion of the sEV population lacks enough RNA for detection of SYTO. It has been reported that there may actually be a very small amount of RNA per vesicle (Chevillet et al., 2014). Since sEVs could not be co-labelled with Cal and Alexa594, and the earlier evidence that Cal may be leaking from the sEV over time, Cal labelling was abandoned for further experiments. We next investigated cellular uptake of CFSE/SYTO-Alexa594-sEVs.

5.4.5. Uptake of dual-labelled sEVs

Fibroblasts were visualised using the Axio Observer Z1 following 1 hour treatment with 25µg/mL CFSE-Alexa594-sEVs or 25µg/mL SYTO-Alexa594-sEVs. With CFSE-Alexa594-sEV treatment, a high degree of co-localisation is observed 1 hour post-uptake (figure 5.19, zoom, white arrows) seen by the orange/yellow colour. Though CFSE positive sEVs had low Alexa594 positivity (figure 5.18a), the co-localisation in fibroblasts is much higher (Mander's coefficient ≈ 0.66), suggesting sorting of single labelled sEVs into endocytic compartments. This is known to occur after cellular uptake, possibly producing the increase in co-localisation observed. As SYTO staining does not conform to the punctate staining we see with CFSE/Alexa dyes, we observed little co-localisation between SYTO and Alexa594 after sEV internalisation (figure 5.20). The proportion of SYTO co-localising with Alexa594 after sEV internalisation is low (Mander's coefficient ≈ 0.15), which is lower than what was measured in sEVs prior to addition to fibroblasts (figure 5.18c). This demonstrates separation of the two dyes within an hour of sEV uptake by the fibroblast. We showed that sEVs can be co-labelled with SYTO and Alexa594, and after cellular uptake, the Alexa594 remains punctate, whereas the SYTO has largely disassociated and exhibited its own very distinct staining pattern, indicating the SYTO has left the sEV within an hour of internalisation by the fibroblast.

Results

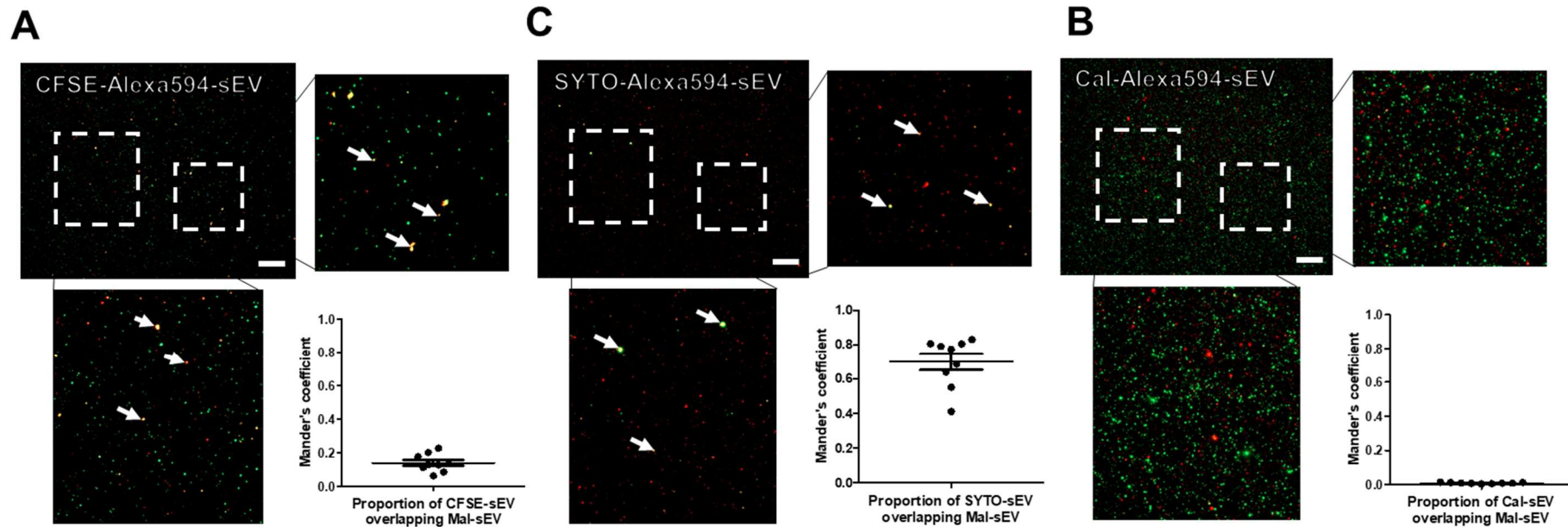


Figure 5.18. Co-localisation of dual-labelled sEVs. DU145 derived sEVs were labelled with (A) 200 μ M CFSE, (B), 40 μ M Cal or (C) 200 μ M SYTO. Labelled sEVs were then dual-labelled with 200 μ g/mL Alexa594. Dual-labelled sEVs were diluted 1:6 in PBS and seeded onto microscopy plates for co-localisation analysis. Representative images are shown, CFSE/Cal/SYTO = green, Alexa 594 = red, white arrows indicate regions of co-localisation. Images captured by Axio Observer Z1, 63x lens used, scale bar = 20 μ m. Mander's coefficient analysis was carried out to determine co-localisation of red/green in dual-labelled sEVs from fields of view taken. Co-localisation was defined as proportion of green signal (CFSE/Cal/SYTO) associated with red signal (Alexa594-sEVs), measured by the JACoP plugin on the ImageJ software. Graphs represent mean +/- SEM of Mander's coefficients calculated from 9 fields of view across 3 wells (Each point represents 1 field of view).

Results

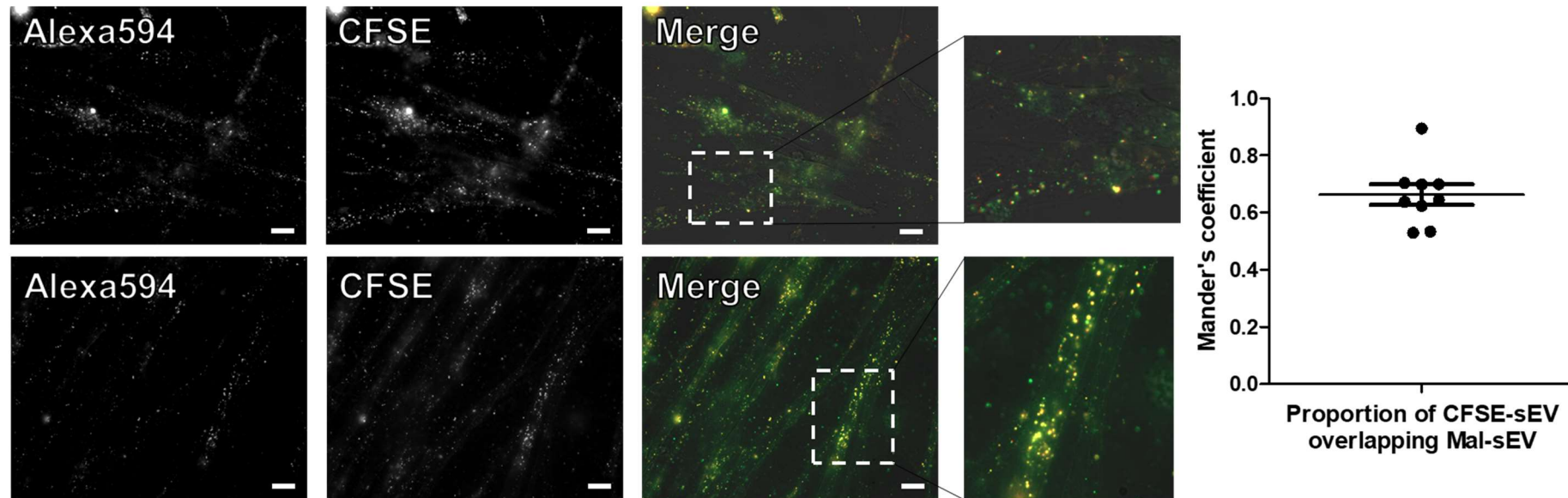


Figure 5.19. Fibroblast uptake of CFSE-Alexa594-sEVs. Fibroblasts were treated with 25 μ g/mL CFSE-Alexa594-sEVs for 1 hour, then visualised by fluorescence microscopy for co-localisation analysis. Representative image of co-localisation between CFSE and Alexa594 in fibroblasts is shown. CFSE = green, Alexa594 = red. Images captured by Axio Observer Z1, 63x lens used, scale bar = 20 μ m. Mander's coefficient analysis to determine co-localisation of CFSE and Alexa594 from fields of view taken. Co-localisation was defined as proportion of green signal (CFSE) associated with red signal (Alexa594), measured by the JACoP plugin on the ImageJ software. Graph represent mean \pm SEM of Mander's coefficients calculated from 9 fields of view across 3 wells (Each point represents 1 field of view).

Results

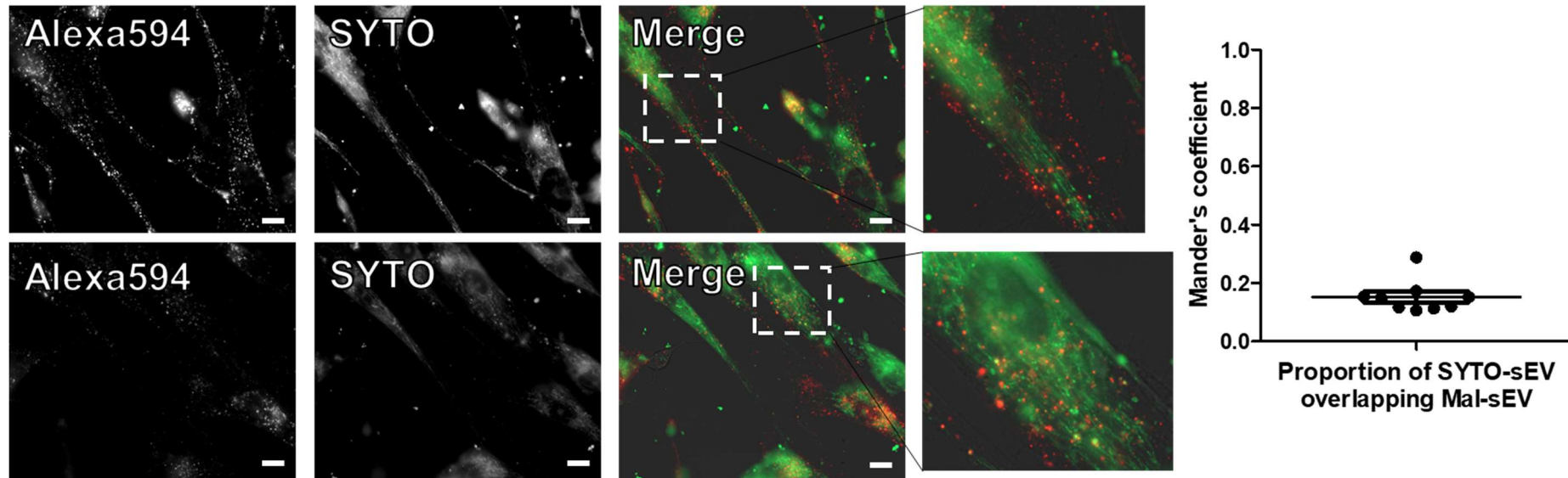


Figure 5.20. Fibroblast uptake of SYTO-Alexa594-sEVs. Fibroblasts were treated with 25 μ g/mL SYTO-Alexa594-sEVs for 1 hour, then visualised by fluorescence microscopy for co-localisation analysis. Representative image of co-localisation between SYTO and Alexa594 in fibroblasts is shown. SYTO = green, Alexa594 = red. Images captured by Axio Observer Z1, 63x lens used, scale bar = 20 μ m. Mander's coefficient analysis to determine co-localisation of SYTO and Alexa594 from fields of view taken. Co-localisation was defined as proportion of green signal (SYTO) associated with red signal (Alexa594), measured by the JACoP plugin on the ImageJ software. Graph represent mean \pm SEM of Mander's coefficients calculated from 9 fields of view across 3 wells (Each point represents 1 field of view).

5.4.6. Tracking sEV intraluminal dye escape

We next attempted to track release of SYTO dye by Alexa594 coated vesicles at the early stages of fibroblast uptake through use of time-lapse microscopy. In using time-lapse microscopy, we thought this would enable us to observe the release of sEV intraluminal dyes in real-time.

Fibroblasts were placed in the black box (used in section 5.2.2) with CO₂ and temperature control, mimicking incubator conditions, and imaged by time-lapse microscopy using the Axiovert 100 microscope, capturing images in the brightfield (to visualise the fibroblasts) and with Alexa488/594 filters every 30 seconds. Time-lapses were initiated, then 25µg/mL SYTO-Alexa594-sEVs were applied directly onto the fibroblast containing wells, to allow real time uptake visualisation of the dual-labelled sEVs by the fibroblasts.

Initially, monitoring dual-labelled sEVs floating in the media around the fibroblasts was challenging; the sEVs move between image capture of each colour, giving the appearance of a red sEV closely following a green sEV (figure 5.21a, zoom, white arrows), though when the sEV is less mobile in a given image capture, it then appears as one co-labelled entity (figure 5.21a, zoom, 2-3min). Over the course of the time-lapse, sEVs begin to stick to the plate in the spaces not covered by fibroblasts, and dual-labelled sEVs can clearly be seen (figure 5.21b, zoom, white arrows). sEVs which are dual-labelled are detectable within the time-lapse set up, though mobile sEVs are difficult to track in two colours. We detected what appeared to be a sEV sticking to the plasma membrane of a fibroblast (figure 5.22a, zoom, white arrows), which we hoped we would be able to observe in large numbers across multiple fields of view, allowing us to track uptake and SYTO escape from the Alexa594 labelled sEV, however we ran into a number of problems. The SYTO dye was sensitive to photobleaching with multiple image captures (figure 5.22b), with the green colour deteriorating minutes into the experiment, making the continuous tracking of the SYTO over time very difficult. Also, since we added the sEVs and imaged immediately, there were a large number of fluorescent sEVs in the media (usually washed off in other experiments), creating a background signal we were unable to overcome in many fields of view and making visualisation of single sEVs problematic. The field of view shown in figures 5.21 and 5.22 was the best we were able to achieve in terms of visualising

dual-labelled sEVs in the presence of fibroblasts, however we were not able to observe cellular uptake of these sEVs.

In conclusion to this set of experiment, DU145 sEVs can be co-labelled with CFSE/SYTO and Alexa594 to produce dual-coloured sEVs, these sEVs were used to demonstrate release of SYTO from the sEV following cellular uptake, whilst sEV proteins remain associated within the fibroblast. Monitoring uptake of co-labelled sEVs by time-lapse microscopy was not entirely successful, and with the current experimental setup it was not possible to effectively detect very early sEV entry events and partition of the two dyes of the dual-labelled sEV. Such a system with an alternate microscopy setup however may be able to discern the separation of the dyes and determine the intracellular location of dye escape from sEVs.

Results

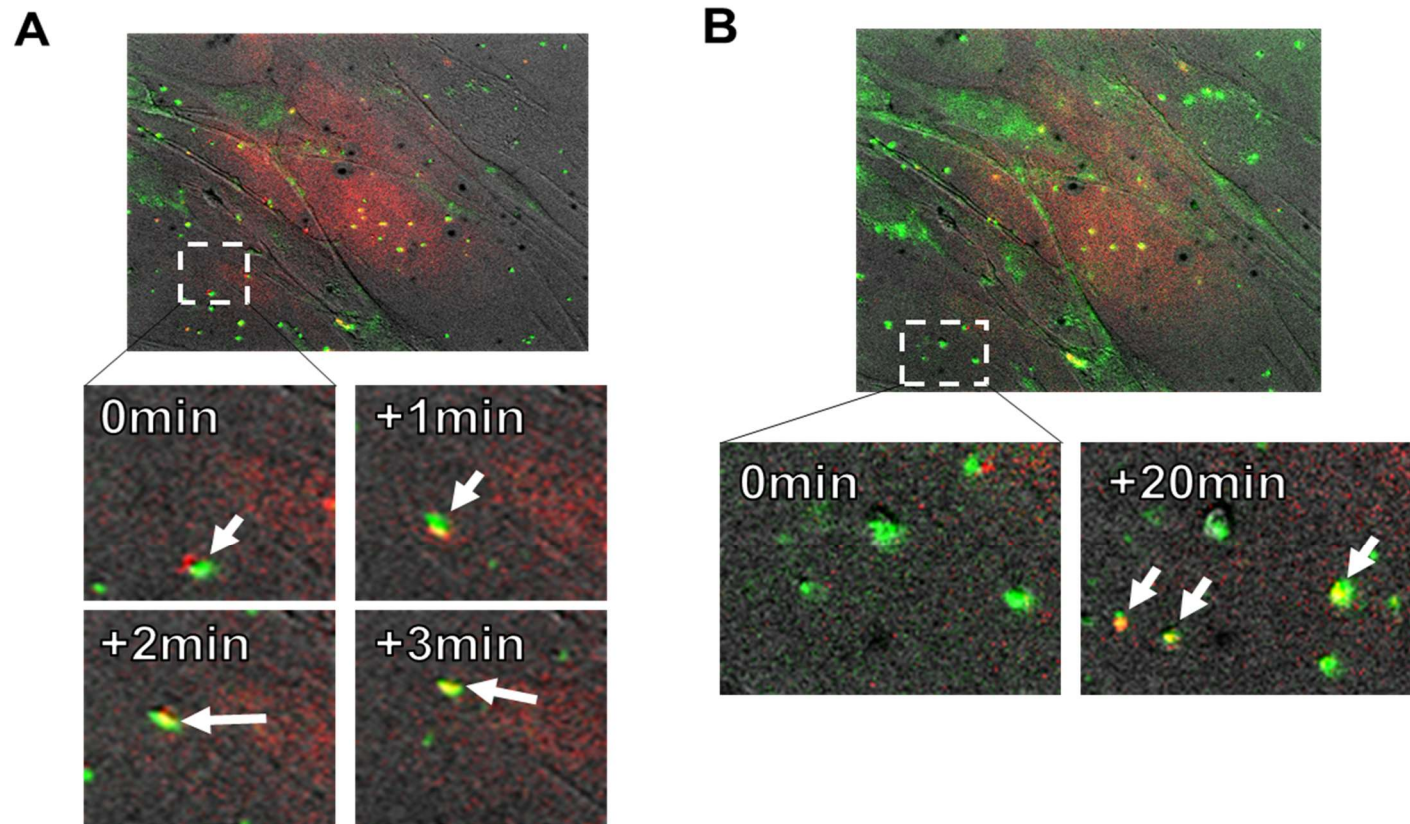


Figure 5.21. Detection of SYTO-Alexa594-sEVs by time-lapse microscopy. Fibroblasts were visualised by time-lapse microscopy, images taken every 30 seconds, after first image capture 25 μ g/mL SYTO-Alexa594-sEVs were added to the fibroblast media, images were captured in the brightfield to detect the fibroblasts, and with Alexa488/594 filters to detect dual labelled sEVs. Time-lapse microscopy was assessed for its ability to detect dual-labelled sEVs. SYTO = green, Alexa594 = red. (A) Visualisation of movement of a dual-labelled sEV in fibroblast media over 3 minutes, with loss of yellow/orange co-localisation signal with the mobile sEV in minutes 0-2. (B) Detection of dual-labelled sEVs settling on the microscopy plate over 20 minutes, white arrows indicate co-localisation of green and red signals. Images were captured using an Axiovert 100 and a 40x lens.

Results

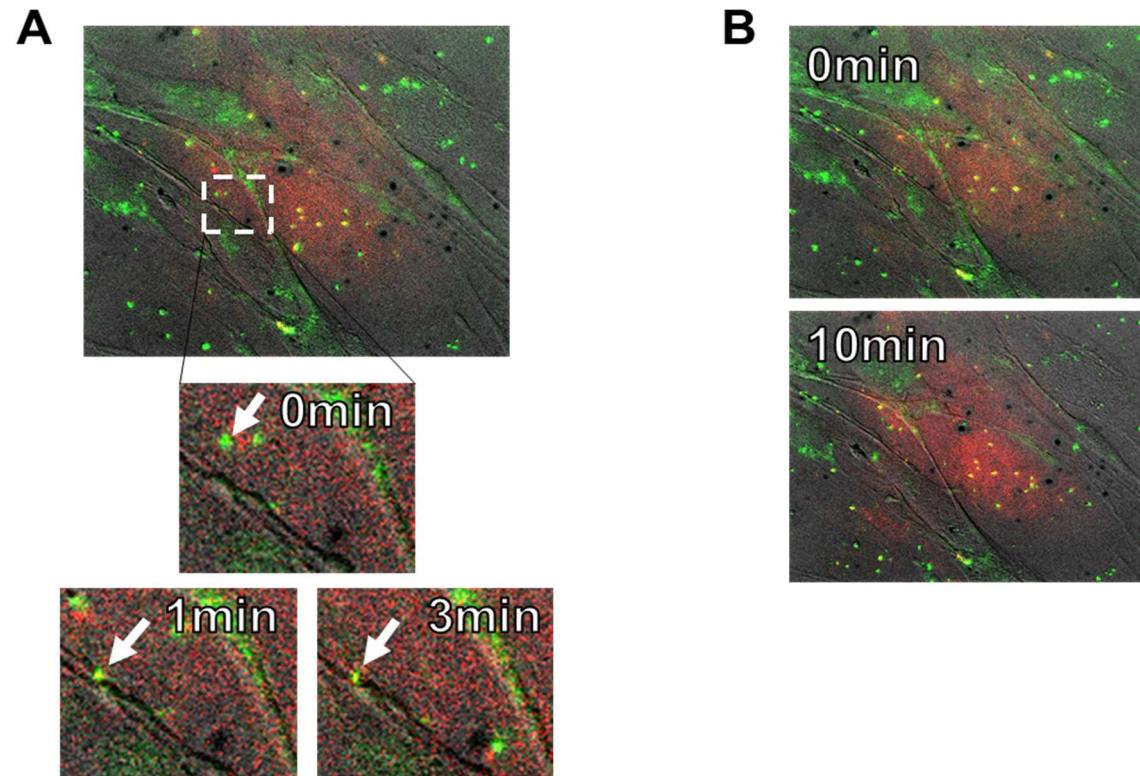


Figure 5.22. Monitoring fibroblast uptake of SYTO-Alexa594-sEVs by time-lapse microscopy. Fibroblasts were visualised by time-lapse microscopy, images taken every 30 seconds, after first image capture 25 μ g/mL SYTO-Alexa594-sEVs were added to the fibroblast media, images were captured in the brightfield to detect the fibroblasts, and with Alexa488/594 filters to detect dual labelled sEVs. Time-lapse microscopy was assessed for its ability to monitor fibroblast uptake of dual-labelled sEVs. SYTO = green, Alexa594 = red. (A) Visualisation of binding of a dual-labelled sEV to the plasma membrane of a fibroblast over 3 minutes. (B) Loss of green fluorescent signal in a field of view over 10 minutes, indicating photobleaching of SYTO fluorophore. Images were captured using an Axiovert 100 and a 40x lens.

5.5. Discussion

The aims of the current chapter were to elucidate the subcellular fate of the PCa sEV in fibroblasts and monitor transfer of sEV luminal cargo to the cell, our findings are summarised in figure 5.23. DU145 derived sEVs are taken up by primary fibroblasts, enter early endosomes and transit the endosomal system, beginning to arrive at lysosomes within 2 hours. We showed we can effectively label sEVs with membrane permeable fluorescent dyes. These dyes require sEV internalisation by fibroblasts to stain the cells, but express distinct patterns, indicating escape from the sEV within an hour of cell entry. A simple method for dual-coloured labelling of sEVs was presented, although we were unable to take full advantage of these sEVs for clarifying cargo transfer to fibroblasts. Overall, the data unveils a complex sorting of PCa sEVs by fibroblasts, and using simple labelling techniques, we demonstrated that we could use fluorescently labelled sEVs to show direct microscopic evidence of intraluminal content delivery shortly after the endocytosis of the vesicle.

DU145 derived sEVs remain within fibroblasts following endocytosis, though after washing the cells of external sEVs, sEV signal in the fibroblast continues to rise over 3 hours. This is not due to the pH of the endosomal compartment of the sEV, as the Alexa dyes are described as insensitive to pH between pH4 and pH10. sEVs not washed off, if stuck to the plasma membrane of the fibroblast or the cell culture plate, could be continued to be taken up after media washing. This would explain rise in fluorescent signal over time. When fibroblasts were treated at 4°C, sEVs could be seen bound to the plasma membrane of the cell (figure 4.12), and this was after washing and fixing the cells, therefore the idea sEVs remain bound to the cell after simple media washing is not unreasonable.

Fibroblasts are positive for Alexa633 signal 72 hours after Alexa633-sEV treatment. The staining pattern does not stay punctate however, a more diffuse staining is observed. Since we showed sEVs traffic to lysosomes over the first few hours post-uptake, it is probable that the Alexa633 dye has been disassociated from the sEV within the lysosome, as enzymes located in lysosomes will break disulphide bonds (Arunachalam et al., 2000). We do not currently know what happens to sEVs within the lysosome, so we can only speculate on how long the sEV survives for in the fibroblast, however it is plausible that the Alexa dyes

survive structurally intact in the fibroblast long after the sEV has been degraded. Grouping of Alexa633-sEVs over 4 hours post-uptake into larger fluorescent entities shows sorting of sEVs, from primary endocytic vesicles, merging into to other endosomal compartments. These fluorescent areas generated by the sEVs are significantly larger 2 hours after uptake, which is also when sEVs begin to reach lysosomes. The mean area size increases further through 4 hours, which correlates with increased lysosomal localisation of sEVs in the same time frame.

Within 2 hours of cellular uptake, sEVs were identified in early endosomes, late endosomes and lysosomes using the Bacmam transduction reagents. Lysosomal fate of sEVs was supported by dextran co-localisation experiments. Even at 4 hours however there were still many sEVs which were not co-localising with dextran loaded lysosomes, though plasma membrane bound sEVs may be continuously entering the cell, which could affect this co-localisation readout.

Due the shape of the fibroblasts, it is difficult to draw around cells for co-localisation analysis, therefore co-localisation was measured on whole fields of view, again this could reduce the end result, as sEVs outside the fibroblasts would also be counted. Optimisation of dextran dose was not carried out either for this study, therefore there may be lysosomes within the fibroblast which are not labelled with dextran. Optimisation and polishing of the co-localisation experiments would have allowed us to determine a more accurate account of the proportion of sEVs which have reached lysosomes at a given time. Cells slowly process endocytosed cargo bound for lysosomes and they can take several hours to sort all of this cargo to its destination (Kielian et al., 1986). All sEVs will likely not reach the lysosomes until several hours post-uptake. Immediately after a 30 minutes pulse of sEVs and transferrin, a proportion of sEVs are present in Tf positive compartments, presumably early endosomes since we did not see evidence of sEV recycling. Tf is recycled rapidly, so the exact proportion of sEVs in early endosomes at a given time is difficult to calculate, though combined with the Bacmam and dextran experiments, sEVs probably transit from early endosome to late endosomes within 1-2 hours after uptake, before reaching lysosomes. Antibody labelling could be explored to elucidate sEV subcellular location, though it would be sensible to demonstrate lack of sEV labelling with antibodies, to avoid false positive signals being generated. If PCa derived sEVs can transfer their

intraluminal cargo to fibroblasts, it is therefore reasonable to propose that this occurs within 2 hours of uptake, prior to lysosome localisation, as we assume that any sEV contents would be degraded at this point.

For determination of intraluminal cargo delivery by sEVs, we used fluorescent dyes which were capable of permeating the sEV membrane and had been shown to label sEVs previously. Other dyes were tested for delivery by sEVs; through cellular uptake experiments (data not shown), we found that we could load sEVs with Hoescht and DRAQ5 (both ThermoFisher Scientific), however we could not carry out all experiments, such as those using the plate reader (detection and dye leakage experiments) due to lack of corresponding filter sets, therefore the dyes we selected for these experiments all emitted green fluorescence, so they could be detected using all instruments.

Validation experiments showed we can fluorescently detect sEVs, and importantly show that what we are detecting is sEV associated and not free unbound dye, as this makes us more confident in later experiments that our observations can be attributed to labelled sEVs. Unlike some of the lipophilic dyes, neither CFSE, Calcein or SYTO produced fluorescent aggregates, SYTO-sEVs had a slightly higher mean size than the other sEVs, though the modal sizes were the same. CFSE and SYTO were shown to be stable in their binding to sEVs, whereas Cal may be leaking out of the sEV steadily over time, this could affect what we observe in cellular uptake studies. The effect dyes have on vesicle structure and the stability of their conjugation is an important aspect to consider, along with unbound dye (discussed in chapter 4), when using these labelled sEVs in experiments. These validation steps are vital for studies in which fluorescent sEVs are utilised, however they are rarely considered in the literature. Further experiments we could have carried out include RNase treatment of sEVs to demonstrate intraluminal localisation of SYTO, though RNA is often reported to be protected by sEVs from RNase and proteinase K treatment suggesting that most RNA is in fact within the sEV (Enderle et al., 2015; Shelke et al., 2014), however this may not be the case for EVs from biofluid sources. Similarly, with CFSE, we did not calculate how much of the CFSE was intraluminal verses surface bound, which perhaps could have been achieved through sEV surface protein digestion experiments.

Results

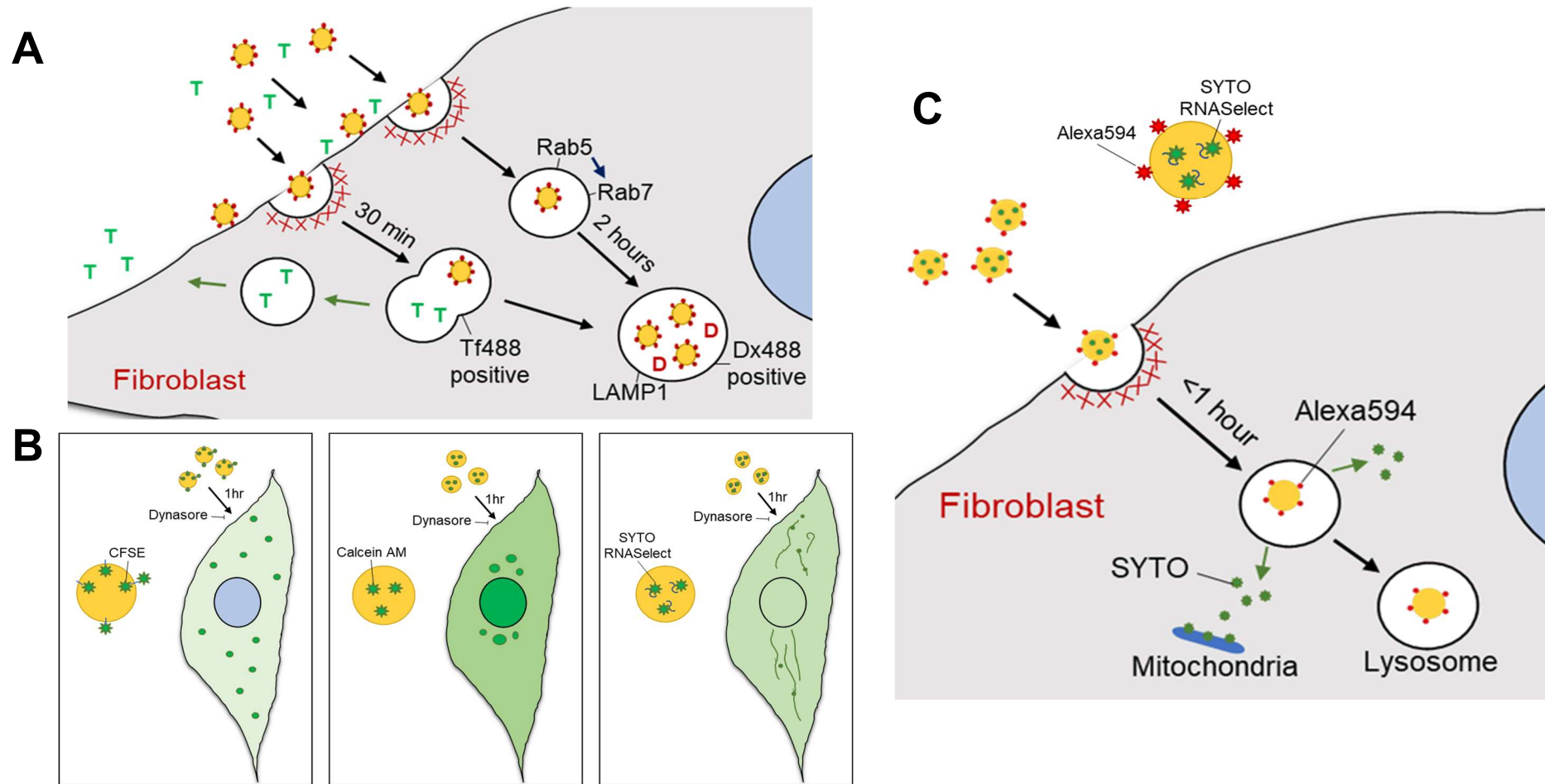


Figure 5.23. Schematic summary of chapter 5. Summary of the data collected in chapter 5. (A) Internalised sEVs enter early endocytic compartments within 30 minutes of uptake, and traffic to lysosomes within 2 hours. (B) sEVs can be labelled with intraluminal dyes, these exhibit distinct staining patterns following fibroblast uptake. (C) sEVs can be dual-labelled with Alexa594 and an intraluminal dye. Within an hour of uptake of SYTO-Alexa594-sEVs, the dyes mostly disassociate, with SYTO staining mitochondria.

Change of both the Cal and SYTO (non-protein binding dyes) staining patterns following cellular uptake of the sEV indicate escape of sEV cargo is possible shortly after endocytosis, when the sEV is in an early endocytic compartment. On the other hand, being a protein labelling dye, CFSE staining remains punctate indicating that sEV proteins remain associated with the rest of the sEV structure. SYTO staining exhibited a clearly different intracellular distribution pattern, which we found was due to mitochondrial labelling. Mitochondrial localisation of sEV dyes has been shown previously. Tian *et al* presented co-localisation of R18 (lipophilic dye) with Mitotracker within 3 hours of sEV uptake (Tian et al., 2013), though they note that R18 can be attracted to the mitochondria due to charge of the R18 dye (Reungpatthanaphong et al., 2003). The SYTO dyes have a positive charge at neutral pH, according to the suppliers (ThermoFisher-Scientific), which likely explains the co-localisation of SYTO and Mitotracker in this study. We did not observe co-localisation between Alexa488-sEVs and Mitotracker, suggesting the SYTO-Mitotracker co-localisation is due to the chemistry of the dye and not necessarily the subcellular location of the sEV itself, however sEV-mitochondria interactions shouldn't be ruled out completely, as sEV have been shown to contain mitochondrial DNA (Sansone et al., 2017a), therefore interaction between endosomes and mitochondria is possible.

The dyes are not escaping the sEV and permeating through the fibroblast plasma membrane before getting an opportunity to be endocytosed, since we showed the uptake blocker Dynasore could significantly reduce the fluorescent signal in the cells. The weakest effect uptake inhibition had was on Cal. This dye appears to be permeating the cell independently of the sEV, supported by our finding that Cal can leak from the sEV following labelling. When studying endocytosis and intracellular trafficking of sEVs, one must take into account the chemistry of the fluorescent dye chosen, because as we have shown, the cellular patterns of the dye depend on how the dye is bound to the sEV. Comparison of the dyes used here with the classical lipophilic dye may be useful to judge the effectiveness of lipophilic dyes and the accuracy of uptake studies which have used these probes.

In dual-labelling the sEVs, we were able to assess how effectively we have labelled sEVs with the intraluminal dyes and extract more information on the delivery of intraluminal cargo to the fibroblast. CFSE seems to have inhibited some Alexa

binding, presumably due to CFSE sequestering sEV surface proteins and/or providing some steric hindrance for Alexa labelling. Or it is possible that amine groups which CFSE binds are more abundant within sEV populations than sulphhydryl groups which the Alexa dye binds to. Despite a low proportion of CFSE-sEVs co-labelling with Alexa594, a high degree of co-localisation is seen an hour after sEV uptake, which points towards the sorting and accumulation of many sEVs into common endocytic compartment. This also underlines the endosomal fate of sEV proteins, and clearly highlights that the proteins are not incorporated into the plasma membrane through sEV-plasma membrane fusion.

How sEVs transfer proteins to recipient cells in a functional manner remains unclear, as with CFSE and the Alexa dyes, all of our data pointed to endocytosis and endosomal traffic to lysosomes. However, we also do not know how long the dyes remain bound to the sEV post-uptake and at what point we are tracking just the dye and not the sEV. SYTO effectively labels sEVs which are coated with Alexa594, and we found that much of this SYTO then labels the mitochondria/cytosol in the fibroblast, whereas Alexa594 remains punctate in a clear distinct fashion. This points to the capacity of SYTO to disassociate from the Alexa594-sEV shell soon following internalisation.

It is unclear why Cal-sEVs could not be co-labelled with Alexa594, though we would assume that there is some interaction between Cal and the sEV surface which we do not understand, or there is a previously undetected population of particles in a sEV sample which do not have proteins available for Alexa binding, yet may incorporate the esterases needed to cleave the Calcein AM in a vesicle lumen. This unexplained effect on the sEV surface, as well as the data showing leakage of Cal from the vesicle, have led us to conclude that Calcein AM is not a suitable compound for the uniform labelling of all sEVs for use in cellular uptake studies. The presented data suggests that perhaps a distinct sub-population of sEVs is labelled by Cal, or that there are aggregates, or binding to other sample constituents during the labelling reaction.

Use of CFSE or SYTO and a non-green Alexa maleimide binding dye was shown here to enable dual-labelling of sEVs, in a process which is straightforward and rapid. Further optimisation of the labelling procedure may have improved the proportion of sEVs which are co-labelled.

Our inability to carry out time-lapse experiments to monitor dual-labelled sEV cellular uptake in real-time reveals some limitations of this study. Whilst the Alexa dyes are insensitive to photobleaching, CFSE and SYTO rapidly bleach and become difficult to detect with constant light exposure. Another issue is the fluorescent state of the dye when it is bound to its target/cleaved by its respective enzyme versus unbound/ not cleaved. It is not clear how much SYTO the labelled sEVs is carrying which is not bound to RNA, and the delivery of this SYTO could suddenly become fluorescent upon cellular delivery. This would make tracking fluorescent dye delivery confusing. Strategies to engineer cells to produce sEVs with desirable intraluminal cargo (soluble protein or fluorescent dye) has been investigated in recent years. An elegant study describes sEV loading “via optically reversible protein-protein interactions” which produces sEVs with fluorescent dyes within their lumen (Yim et al., 2016). This method ensures luminal loading of sEVs during their formation and therefore could be a useful strategy for tracking sEV luminal cargo, particularly in co-culture or *in vivo* studies. Production of sEVs with a stable dye, insensitive to photobleaching and reacting with cellular organelles, would be desirable for tracking delivery of intraluminal sEV contents. Fluorescence microscopy itself is limited in its resolving limit and cannot provide all the answers on the mechanisms of sEV cargo transfer to recipient cells. A few studies have shown sEVs in endocytic vesicles by electron microscopy (Heusermann et al., 2016; Morelli et al., 2004; Svensson et al., 2013). Analysis of sEV structure in different endosomal compartments by electron microscopy could help clarify the fate of sEVs following internalisation. We have begun exploring correlative light and electron microscopy (CLEM) as a means of determining the nature of fluorescently labelled sEV containing endosomes in fibroblasts.

We have shown that fibroblasts process PCa sEVs, transporting them to lysosomes, whilst the sEVs transfer their intraluminal cargo to the cell cytosol shortly after endocytosis. The impact of this in terms of fibroblast differentiation was examined in the next chapter.

Chapter 6- Modulation of small extracellular vesicle uptake by fibroblasts

6.1. Introduction

In the previous chapter, we demonstrated that DU145 derived sEVs can transfer intraluminal cargo to fibroblasts, shortly after cellular uptake. Inhibition of sEV internalisation abrogates the delivery of its luminal contents to the fibroblast. Others have shown that delivery of sEV contents to recipient cells can lead to phenotypic change in the cell (Skog et al., 2008; Valadi et al., 2007), and this is due at least in part to mRNA/miRNA acquisition by the cell and subsequent transcriptome modulation. Blocking cellular uptake of sEVs should therefore prevent phenotypic change driven by delivery of sEV cargo. Previously, the group detailed clear differences in the phenotype of the fibroblast stimulated by DU145 derived sEVs versus soluble TGF β 1, and since the sEV contains a complex cargo made of proteins, lipids and nucleic acids, we hypothesise that the sEV is delivering its contents to the fibroblast, which is responsible for driving the complex and unique form of myofibroblast differentiation. Inhibiting sEV internalisation by the fibroblast and evaluating the markers of differentiation will allow us to determine the role of sEV uptake in driving changes in the fibroblast.

Markers of fibroblast stimulation were assessed in cells induced in the presence/absence of sEV uptake inhibitors. Pharmacological inhibitors are known to have adverse and off target effects in cells (Ivanov, 2008; Vercauteren et al., 2010), therefore specific blockade of the sEV surface to perturb cellular uptake may be a more suitable approach for determining relevance of sEV internalisation in functionality in future studies, as interruption of potentially multiple intracellular processes could be avoided. Use of Heparin resulted in successful blockade of cellular uptake of sEVs in chapter 4, showing that these vesicles were likely reliant on sEV-cell surface interactions for internalisation to occur.

Furthermore, Clathrin mediated endocytosis (CME) is a receptor dependent process, so sEV surface proteins are very likely important factors. Integrins are a family of transmembrane proteins, typically arranged as heterodimers made up of an α and β subunit (Harburger and Calderwood, 2009), these proteins play roles in adhesion and mediating cell signalling related to cell motility and differentiation. Integrins that promote cancer progression are upregulated in tumours (Guo and Giancotti, 2004), enabling cell migration and invasion for example. Integrins are also present on the surface of sEVs in high abundance, though is not fully

appreciated. They have been implicated in cellular internalisation of the vesicles (Atay et al., 2011; Hoshino et al., 2015; Wang et al., 2015). Here we investigated the roles of integrins on the surface of the DU145 derived sEV in the internalisation of the sEV by fibroblasts. Identification of specific PCa derived sEV markers for the blockade of cellular uptake of the vesicle may reveal therapeutic targets.

The aim of this chapter was to determine the role of sEV internalisation on the stimulation of fibroblast differentiation into a form of myofibroblast previously characterised as pro-angiogenic and tumour promoting *in vivo* (Webber et al., 2015b). We attempted to achieve this objective through monitoring the effects of sEV internalisation blockade on sEV functionality, with the use of pharmacological inhibition and specific targeting of sEV surface integrins.

6.2. Effect of endocytosis inhibitors on sEV induced myofibroblast differentiation

The fibroblast phenotype simulated by DU145 derived sEVs is distinct from that generated by soluble TGF β 1 (sTGF β 1), therefore we propose that delivery of the intraluminal cargo from the sEV to the fibroblast is key in invoking additional effects mediated by sEV co-delivered factors. In chapter 2 we demonstrated abrogation of sEV internalisation through use of pharmacological inhibitors. Here, the same pharmacological inhibitors were used to determine the role of sEV internalisation by fibroblasts on markers of fibroblast stimulation; in particular, we examined onset of expression of α SMA and elevated secretion of HGF. Since many fibroblast stimulation experiments were due to be carried out, and we wanted to maximise the effect of our pharmacological inhibitors, we decided to reduce the sEV dose and treatment time used previously to stimulate the fibroblasts. sEV dose can be reduced from 200 μ g/mL whilst still inducing secretion of significant levels of HGF by the fibroblast (Webber et al., 2015b), meaning we could lower the sEV dose used in the current study allowing us to be more economical in our use of sEVs. It was previously shown that there was approximately 7pg of TGF β 1 per 1 μ g of DU145 sEVs (Clayton et al., 2007). Equivalent doses of sTGF β 1 to <200 μ g/mL sEVs were tested on their ability to induce α SMA in fibroblasts following a 48 hour stimulation. 48 hours, rather than 72 hours carried out previously, was the stimulation time here, as this we expected that this would reduce the chance of the pharmacological inhibitors to convey their cytotoxic effects on the fibroblast.

Figure 6.1a shows the expression of α SMA in fibroblasts stimulated with 0.1675, 0.375 or 0.75ng/mL sTGF β 1 (equivalent to 25, 50 and 100 μ g/mL sEVs respectively). Only 0.75ng/mL sTGF β 1 (equivalent to 100 μ g/mL sEVs, half of the previously used dose) was capable of inducing clear cut expression of α SMA positive fibroblasts (figure 6.1a). Following this finding, fibroblasts were treated with 100 μ g/mL sEV for 48 hours, and the supernatants were tested by sandwich ELISA for HGF levels, to confirm whether this dose was capable of inducing HGF secretion by the fibroblast. 100 μ g/mL sEVs could induce secretion of significant levels of HGF above unstimulated fibroblasts (figure 6.1b), and the equivalent dose of sTGF β 1 does not stimulate HGF secretion, as expected. For remaining fibroblast

stimulation experiments in this chapter, the 100 μ g/mL sEVs for 48 hours condition was used.

Next, the effect of pharmacological inhibitors of endocytosis were assessed for their effect on sEV induced fibroblast stimulation. We used the same inhibitors as in chapter 4 to abrogate cellular uptake of sEVs at the previously stated doses: 10 μ g/mL Dynasore, 100ng/mL Cytochalasin D (CytoD), 1 μ g/mL EIPA, 100ng/mL Bafilomycin A1 (BafA). α SMA expression and HGF secretion was assessed in fibroblast stimulated for 48 hours with 100 μ g/mL sEVs with/without an inhibitor. α SMA expression was unaffected by the presence of EIPA or Heparin (figure 6.2), however there was reduced α SMA expression in fibroblasts co-treated with either Dynasore, CytoD or BafA. These results were not entirely comparable to those seen with HGF assays. Again, Dynasore had an inhibitory effect, significantly reducing the detected HGF levels in the stimulated fibroblast supernatant (figure 6.3). No other inhibitor had significant impact on HGF levels. Dynasore, the most potent uptake inhibitor tested in chapter 4, inhibited both α SMA expression and HGF levels, however, whilst all of these inhibitors reduce sEV internalisation to an extent, not all inhibitors perturbed fibroblast differentiation as measured by HGF output. This discrepancy between uptake inhibition and effect on fibroblast stimulation suggests that there may not be a link between the two process.

Pharmacological inhibitors are also limited, in that they can have unintended consequences on the functioning of the cell. CytoD is an inhibitor of actin polymerisation, and polymerisation of the smooth muscle specific α isoform of actin (Kinner et al., 2002), therefore its abrogation of α SMA filament formation in stimulated fibroblasts would be expected, regardless of the inhibitory effect on sEV internalisation. Additionally, Dynamin-2 (target of Dynasore), is involved in actin function (Yamada et al., 2016), and Dynasore itself has been shown to destabilise actin filaments (Yamada et al., 2009). Interestingly, EIPA is reported to cause disassembly of actin filaments (Lagana et al., 2000), though α SMA was still detectable in fibroblasts treated with EIPA or Heparin (figure 6.2). Effects of cellular uptake inhibition of sEVs on HGF secretion by fibroblasts is difficult to determine with these inhibitors too, as we cannot be sure that an interruption to endocytic vesicle transport has no impact on the exocytic pathways for HGF production.

Results

The sEV delivered TGF β 1 mediated response is known to be abrogated by addition of TGF β neutralising antibody to the treatment conditions, inhibiting both α SMA expression and HGF secretion (Webber et al., 2015b). We confirmed functionality of the antibody, through inhibition of α SMA expression, when fibroblasts were treated with 200 μ g/mL sEVs with 10 μ g/mL TGF β neutralising antibody for 72 hours (figure 6.4a). We performed a typical sEV internalisation experiment with the presence of 10 μ g/mL TGF β neutralising antibody to determine the role of TGF β signalling in sEV uptake. By fluorescence microscopy, there does not appear to be any difference in the uptake efficiency of sEVs by fibroblasts (figure 6.4b). A small attenuation in uptake can be detected through measurement by flow cytometry (figure 6.4c), however without an isotype control antibody, we cannot confirm whether this specific impedence of uptake is genuine, or whether steric hindrance of the antibody is at play. Any blockade conveyed from the antibody though however is small, whereas the perturbation of sEV induced differentiation is very clear cut (Webber et al., 2015b), suggesting the two process are unlikely to be linked.

The data here suggests that sEV internalisation is independent of the TGF β 1 mediated changes in fibroblast phenotype. Whether sEV delivered luminal cargo could induce phenotypic change independent of TGF β signalling was therefore worth examining. Due to undesirable effects of pharmacological inhibitors however, we investigated perturbation of highly expressed proteins on the sEV surface to bring about inhibition of sEV internalisation, as alternative to pharmacological inhibition of endocytosis.

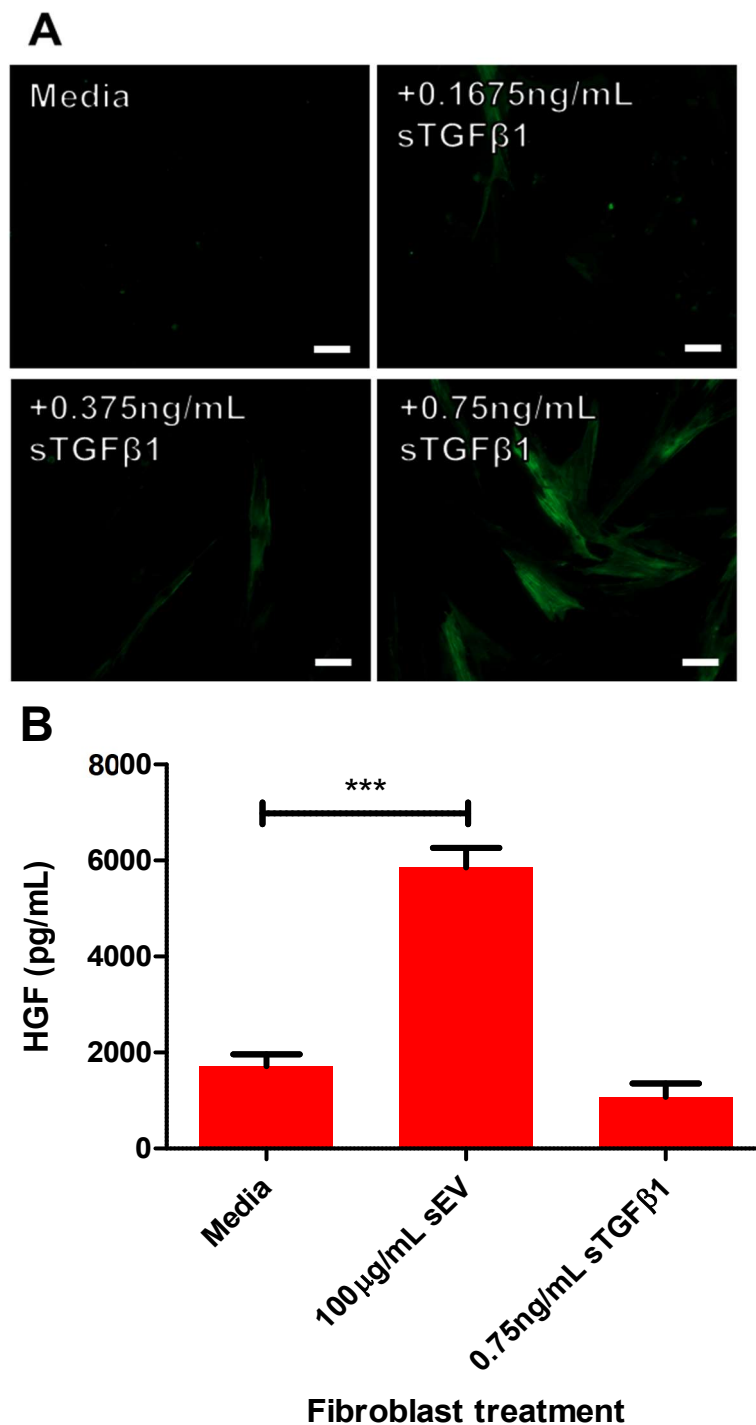


Figure 6.1. Fibroblast stimulation with a reduced Du145 derived sEV dose. (A) Fibroblasts were treated for 48 hours with 0.1675, 0.375 or 0.75ng/mL sTGFβ1 (equivalent to 25, 50, 100μg/mL sEVs respectively) or media, then stained with an antibody against αSMA (green). Images captured by Axio Observer Z1, 20x lens used, scale bar = 50μm. (B) Fibroblasts were treated with 100μg/mL sEVs, 0.75ng/mL sTGFβ1 or media for 48 hours, and HGF in the cell conditioned media was quantified by sandwich ELISA. Bars represent means +/- SEM, based on triplicate wells, ***P<0.001, one-way ANOVA with Tukey's multiple comparison test.

Results

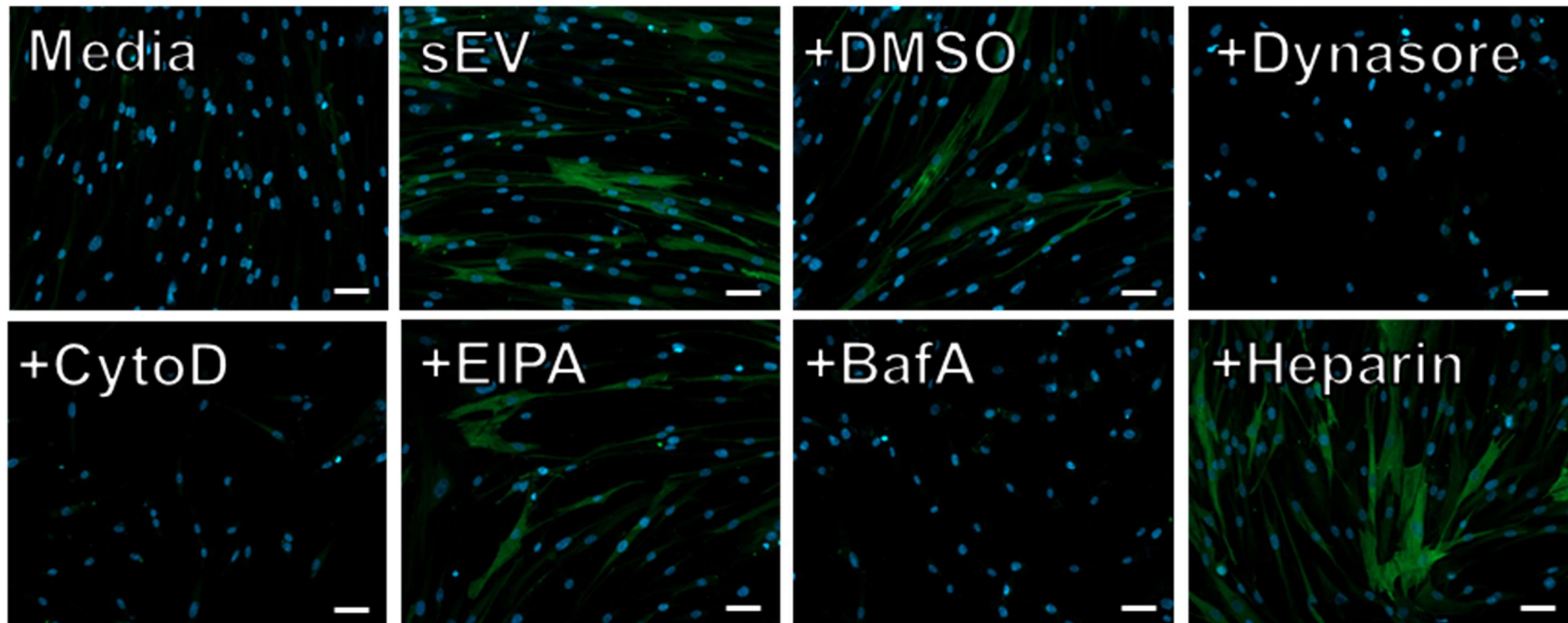


Figure 6.2. Effect of endocytic inhibitors on sEV induced onset of α SMA expression in fibroblasts. Fibroblasts were treated for 48 hours with 100 μ g/mL sEVs in the presence of 10 μ g/mL Dynasore, 100ng/mL CytoD, 1 μ g/mL EIPA, 100ng/mL BafA or 1:1000 DMSO in DMEM/F12. Cells were then stained for α SMA, α SMA = green, nuclei = blue. Images captured by Axio Observer Z1, 20x lens used, scale bar = 50 μ m. Images are representative images from an experiment of 9 fields of view across 3 wells.

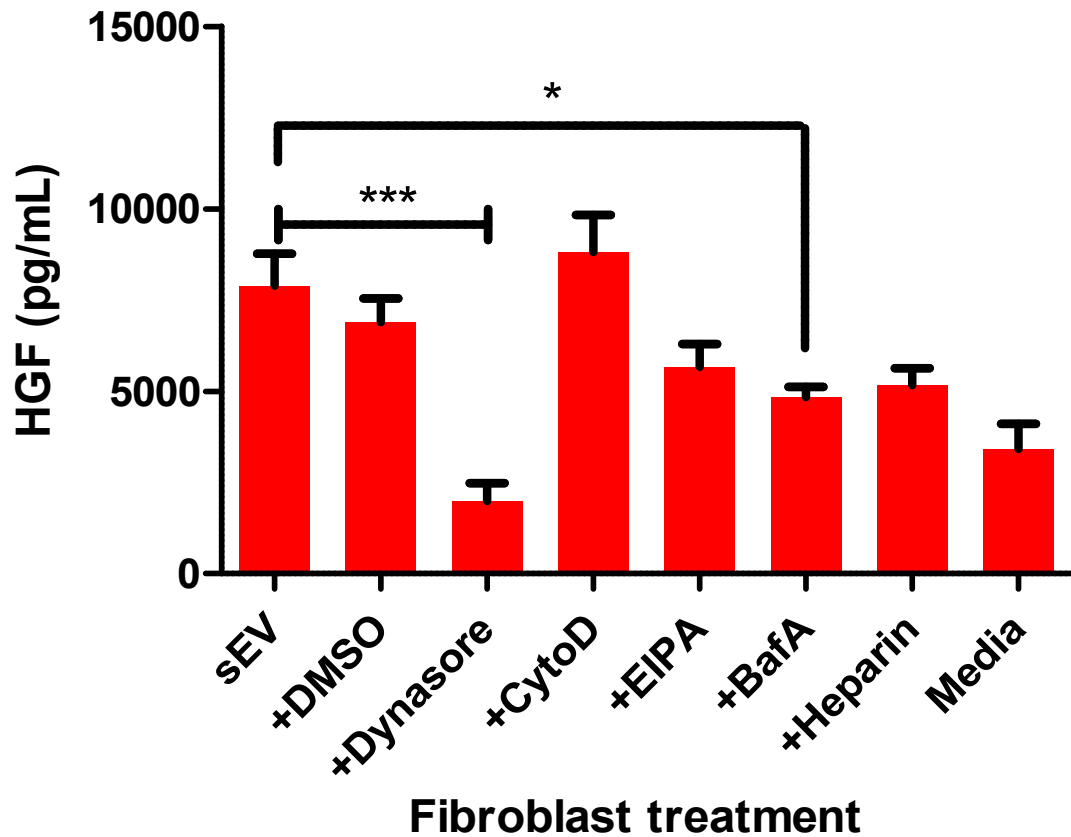


Figure 6.3. Effect of endocytic inhibitors on sEV induced production of HGF by fibroblasts. Fibroblasts were treated for 48 hours with 100 μ g/mL sEVs in the presence of 10 μ g/mL Dynasore, 100ng/mL CytoD, 1 μ g/mL EIPA, 100ng/mL BafA, 50 μ g/mL Heparin or 1:1000 DMSO in DMEM/F12. Cell supernatants were collected and HGF levels were measured by modified DuoSet ELISA. Bars represent means \pm SEM, based on three experiments, *** P <0.001, one-way ANOVA with Tukey's multiple comparison test.

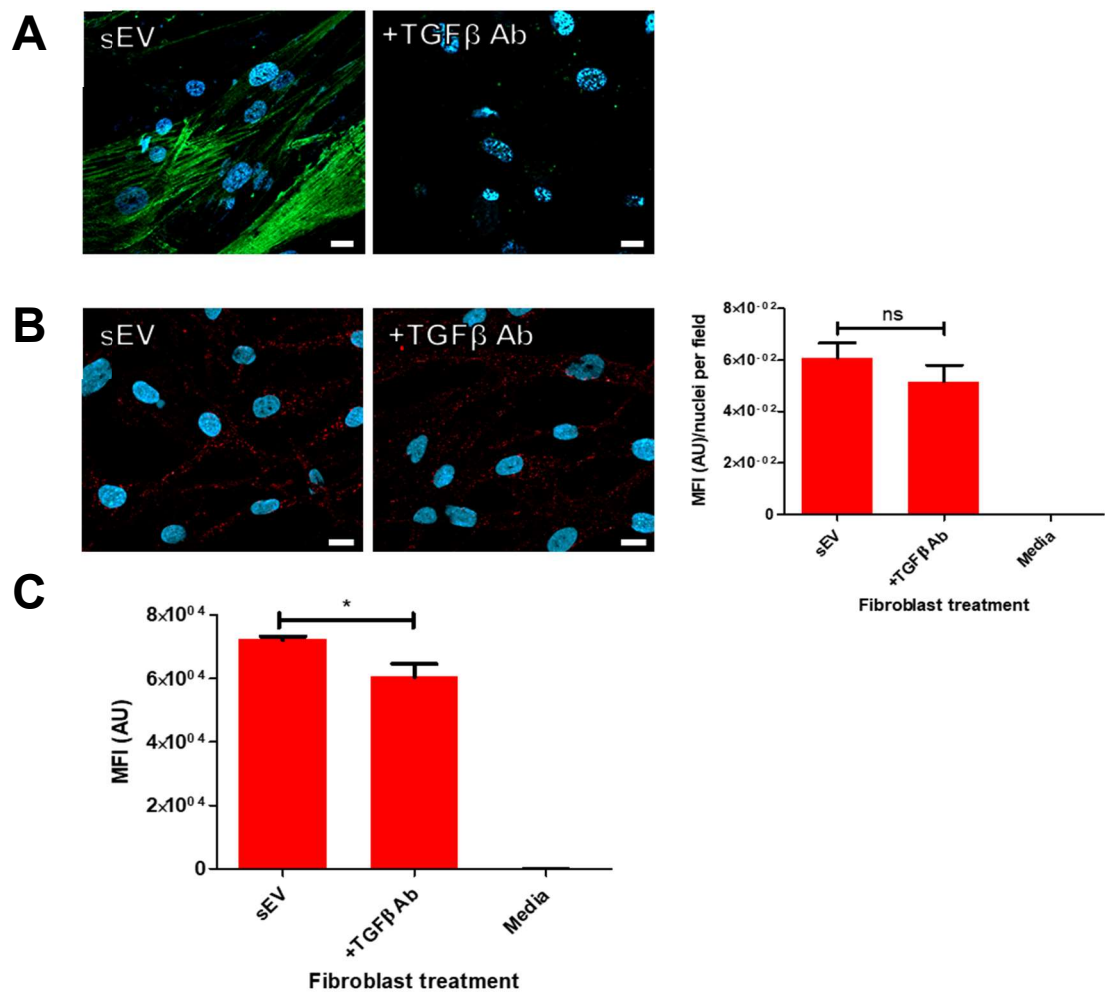


Figure 6.4. Effect of TGFβ neutralising antibody on sEV uptake by fibroblasts. (A) Fibroblasts were treated with 200μg/mL sEVs with/without 10μg/mL TGFβ neutralising antibody for 72 hours, then stained with an αSMA antibody. αSMA = green, nuclei = blue. Images captured by Axio Observer Z1, 63x lens used, scale bar = 20μm. This demonstrates functionality of the TGFβ neutralising antibody as used in previous studies. Fibroblasts were treated with 25μg/mL Alexa594-sEVs (B) or Alexa633-sEVs (C) and 10μg/mL TGFβ neutralising antibody (table 2.1) for 1 hour. (B) Cells were visualised by fluorescence microscopy and their fluorescent intensities quantified by ImageJ, Alexa594-sEVs = red, nuclei = blue. Images captured by Axio Observer Z1, 63x lens used, scale bar = 20μm, Bars represent means +/- SEM, based on 9 fields of view across 3 wells, one-way ANOVA with Tukey's multiple comparison test. (C) Fluorescent intensities of cells were measured by flow cytometry. Bars represent means +/- SEM, based on triplicate wells, *P<0.05, one-way ANOVA with Tukey's multiple comparison test.

6.3. Blockade of sEV surface Integrins

Integrins are shown to be involved in sEV uptake (Atay et al., 2011; Hoshino et al., 2015; Wang et al., 2015), and were therefore a logical target to begin exploring cellular uptake inhibition of sEVs. Enrichment of integrins on DU145 derived sEVs relative to cells has also been described (Webber et al., 2014). We therefore examined whether cellular uptake of sEVs could be perturbed by blockade of sEV integrins.

6.3.1. RGD peptide mediated blocking of sEV uptake by fibroblasts

The RGD peptide has an integrin recognition sequence (Ruoslahti, 1996), and can be used to block interaction of many integrins, such as $\alpha v\beta 1$ and $\alpha IIb\beta 3$, with their RGD motif containing ligands. Other integrins bind domains like the LDV motif, independent of the RGD motif (Humphries et al., 2006). Due to the widely reported use of RGD peptide, and the large number of integrins which interact with RGD motifs, the RGD peptide was used here to demonstrate the role of integrin interactions between sEVs and fibroblasts. In sEV internalisation studies, RGD has been used to demonstrate the role of integrins in sEV-cell adherence (Wang et al., 2015) and subsequent internalisation of the sEV (Atay et al., 2011; Wang et al., 2015). We tested the effect of RGD peptide on internalisation of DU145 derived sEVs by fibroblasts, to identify a potential role for integrins.

Fibroblasts were treated with 25 μ g/mL Alexa labelled sEVs for 1 hour in the presence of 25, 50 or 100 μ g/mL of RGD peptide (Sigma-Aldrich), then fluorescent intensity of the fibroblasts was measured by flow cytometry and in parallel by fluorescence microscopy. Microscopy reveals some, albeit weak inhibition of sEV uptake by fibroblasts. Doses of 25 and 100 μ g/mL significantly reduced fluorescent intensity (figure 6.5a), and whilst intensity is reduced, the dispersion of fluorescent puncta appears the same between conditions. Flow cytometry also showed a dose dependent reduction in MFI in fibroblasts by RGD (figure 6.5b). The highest doses of RGD reduction cellular uptake of sEVs by roughly 29% in the microscopy experiment and 40% in the flow cytometry experiment. Cellular uptake was not fully abrogated, and the data do suggest an integrin binding component is involved in sEV-fibroblast interaction and subsequent uptake.

Results

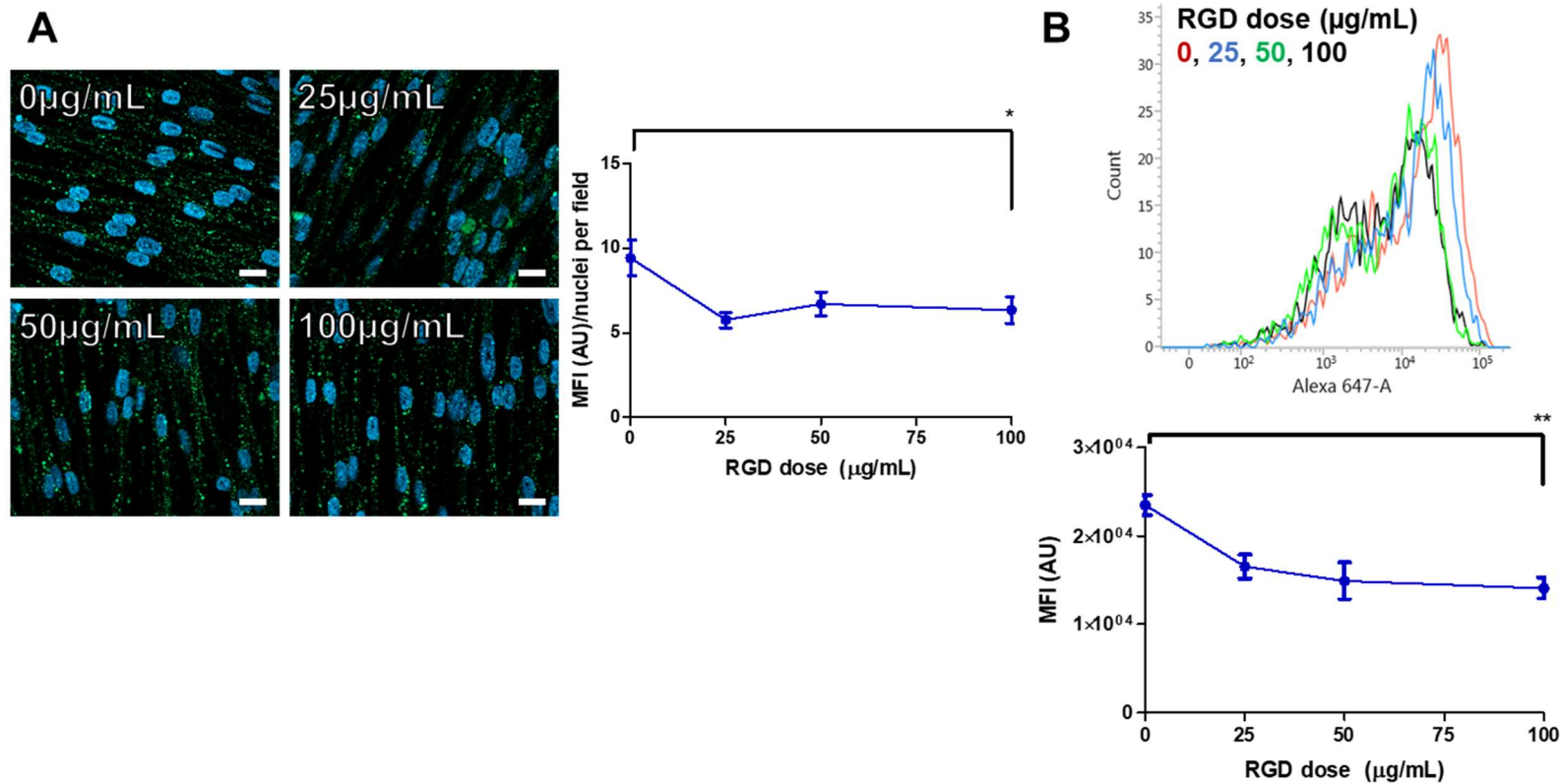


Figure 6.5. RGD mediated blockade of DU145 derived sEV internalisation by fibroblasts. Fibroblasts were treated with (A) 25µg/mL Alexa488-sEVs or (B) 25µg/mL Alexa633-sEVs for 1 hour with 0, 25, 50 or 100µg/mL RGD. (A) Cells were visualised by fluorescence microscopy and their fluorescent intensities quantified by ImageJ, Alexa488-sEVs = green, nuclei = blue. Images captured by Axio Observer Z1, 63x lens used, scale bar = 20µm, Points on graphs represent means +/- SEM, based on 9 fields of view across 3 wells, *P<0.05, one-way ANOVA with Tukey's multiple comparison test. (B) Fluorescent intensities of cells were measured by flow cytometry. Points on graphs represent means +/- SEM, based on triplicate wells, *P<0.05, **P<0.01, one-way ANOVA with Tukey's multiple comparison test.

We next decided to perform a small-scale integrin profiling experiment to identify specific integrin subunits present on the surface of DU145 derived sEVs, which would allow specific targeting of sEV integrins in later experiments.

6.3.2. Detection of integrin subunits on sEV surface

The RGD peptide can block a number of integrins from binding to their ligand, so identifying specific integrins relevant in sEV uptake was carried out. We performed integrin profile assessment through immunophenotyping of sEVs using antibodies against specific integrin subunits. Integrin subunits chosen for detection assays were based on their reported expression by DU145 cells. Not all the integrin subunits subsequently chosen have RGD binding motifs (Ruoslahti, 1996), however they were still evaluated, due to their reported expression on DU145 cells in the literature. Through a literature search of integrins expressed by DU145 cells, we selected 4 subunits for detection assays: $\beta 1$ (Das et al., 2017; Dehghani et al., 2014; Witkowski et al., 1993), $\beta 3$ (Cooper et al., 2002; Witkowski et al., 1993), $\alpha 3$ (Das et al., 2017; Witkowski et al., 1993) and $\alpha 6$ (Das et al., 2017; Witkowski et al., 1993) were all reported to be expressed by DU145 cells, therefore we believed they may also be expressed by DU145 derived sEVs, since sEVs are known to express proteins specific to their parent cell.

1 $\mu\text{g}/\text{mL}$ sEVs were seeded onto high protein binding ELISA plates, and the relative expression levels of the chosen integrin subunits was measured, as performed in chapter 3 for detection of tetraspanins on the sEV surface, described in chapter 2.3.4. 1 $\mu\text{g}/\text{mL}$ anti-integrin primary antibodies (table 2.1) were used here. We detected significant expression of all 4 of the integrin subunits on the DU145 derived sEVs (figure 6.6), these were all detectable above the background levels of non-specific binding of isotype control antibodies. $\beta 1$ and $\alpha 3$ were detected to the highest degrees, with their detections 715-fold and 211-fold above background levels respectively, whereas $\beta 3$ and $\alpha 6$ intensities were only 7.3-fold and 2.4-fold above background stickiness. These results indicate that $\beta 1$ and $\alpha 3$ are likely more abundant on the DU145 derived sEV surface compared to $\beta 3$ and $\alpha 6$, or that their respective antibodies have a greater binding affinity.

Integrin antibodies were to be used to block sEV uptake by fibroblasts; the ability to block cellular uptake of sEVs using anti-integrin antibodies has been shown before, with an anti- $\beta 1$ antibody (Wang et al., 2015). Prior to blocking experiments,

Results

we first carried out titrations with the antibodies to determine whether there was a saturation point with the detection, as a saturating dose would give us as much integrin coverage as possible for sEV internalisation experiments. Titrations were carried out using anti-integrin antibodies at doses of 0.1-10 μ g/mL to determine a saturation point. Saturation of β 1 detection was achieved with 0.5 μ g/mL anti- β 1 and 1 μ g/mL sEVs (figure 6.7), whereas signal of α 3 did not saturate up to the highest dose of 10 μ g/mL anti- α 3. With the two integrins which are not as highly detected, β 3 detection was saturated and detectable above background levels, but only 2.3-fold, and α 6 detection was not significantly different from background stickiness levels at 10 μ g/mL anti- α 6. β 3 and α 6 integrins were excluded from cellular uptake blocking experiments due to their relatively low detection on the sEV surface. For cellular uptake experiments, the highest dose of 10 μ g/mL of anti- β 1 and anti- α 3 were used to ensure as much sEV integrin coverage as possible, whilst α 3 detection was not saturated, even with 1 μ g/mL sEVs being used, β 1 detection could be saturated at a much lower antibody dose. Using higher quantities of antibodies for cellular uptake experiments was impractical due to antibody costs.

Results

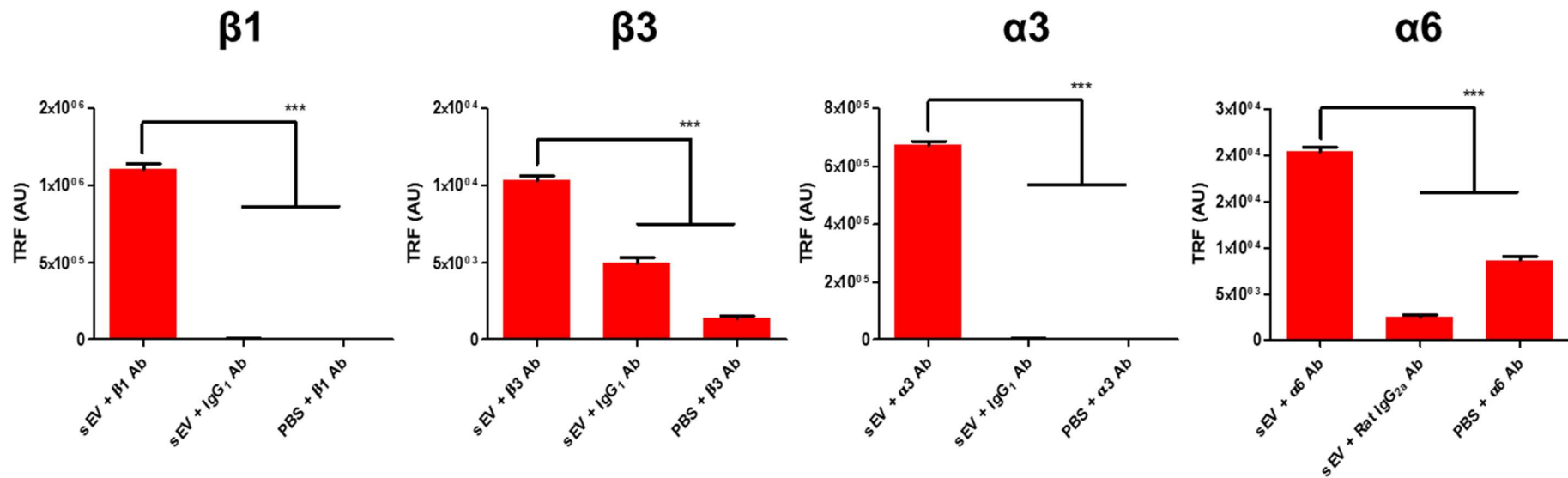


Figure 6.6. Detection of integrin subunits on DU145 derived sEVs by immunophenotyping plate assay. 1 μ g/well of sEVs were seeded onto high protein binding ELISA plates and analysed for the expression of the integrin subunits $\beta 1$, $\beta 3$, $\alpha 3$ and $\alpha 6$, using 1 μ g/mL anti-integrin antibodies, compared with detection of isotype control antibodies and the anti-integrin antibodies in PBS only. Bars represent means \pm SEM, based on triplicate wells, ***P<0.001, one-way ANOVA with Tukey's multiple comparison test.

Results

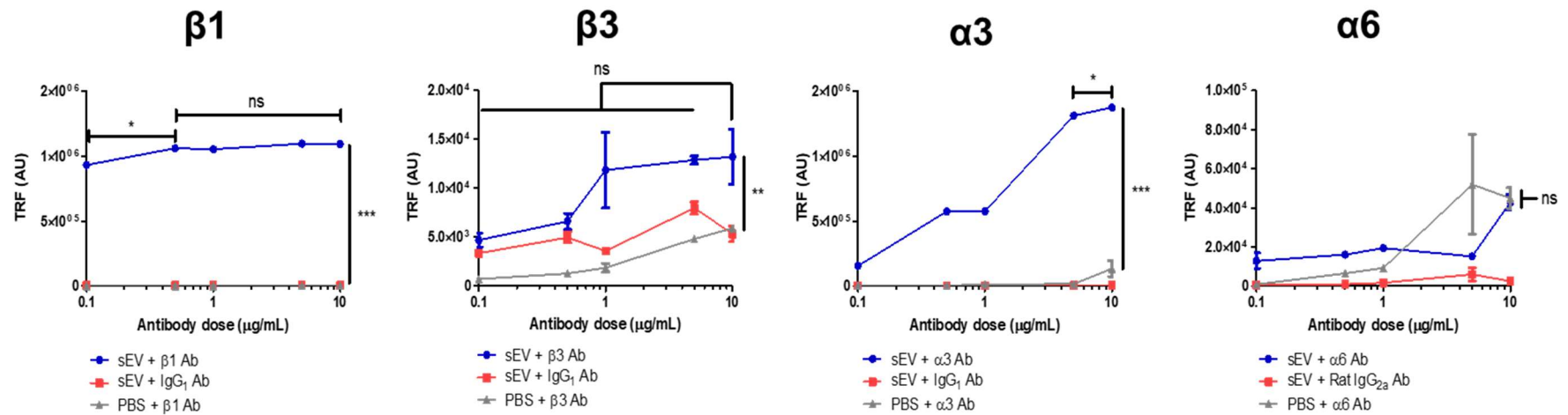


Figure 6.7. Dosing of anti-integrin antibodies for detection saturation of DU145 derived sEV integrins by immunophenotyping plate assay. 1 μg /well of sEVs were seeded onto high protein binding ELISA plates and analysed for the expression of the integrin subunits $\beta 1$, $\beta 3$, $\alpha 3$ and $\alpha 6$, using 0.1, 0.5, 1, 5 or 10 $\mu\text{g/mL}$ anti-integrin antibodies, compared with detection of isotype control antibodies and the integrin antibodies in PBS only. Points on graphs represent means \pm SEM, based on triplicate wells, * $P < 0.05$, ** $P < 0.01$, *** $P < 0.001$, one-way ANOVA with Tukey's multiple comparison test.

6.3.3. Integrin antibody blockade of sEV internalisation by fibroblasts

25µg/mL Alexa633-sEVs were mixed with 10µg/mL anti-β1/anti-α3 or isotype control antibody for 18 hours at room temperature, as we thought this would enable sufficient coating of the sEVs, then fibroblasts were treated with these mixtures for 1 hour. Non-bound antibodies were not removed prior to fibroblast treatment, as we wanted their presence in the media during this 1 hour treatment to help ensure constant blockade of their targets. Fluorescent intensity of the fibroblasts was then measured by flow cytometry, with the aim of being repeated by fluorescence microscopy in later experiments to explore intracellular distribution.

Unexpectedly, we did not observe any attenuation of cellular uptake of sEV with anti-β1 or anti-α3 addition and in fact noted a marked increase in fluorescent signal with either antibody treatments, relative to the sEV only treatment (figure 6.8), this was about a 1.9-fold increase with anti-α3 and 1.7-fold with anti-β1. Also, surprisingly, Isotype control antibody also caused an increase in fluorescent signal in fibroblasts (1.6-fold). These results were opposite to what was expected. Before further experiments with these anti-integrin antibodies, we decided to try antibody blockade experiments using an antibody against an alternative, highly expressed protein to determine whether this result would be repeated, with a non-integrin target. CD9 was shown earlier to be highly detected on the sEV surface (figure 3.4), and so was targeted here with an anti-CD9 antibody. Under the same experimental procedure, Alexa633-sEVs were mixed with 10µg/mL anti-CD9 or IgG_{2b} control antibody, and following incubation were used to treat fibroblasts. Fluorescent intensities were again measured by flow cytometry. In an experiment attempted twice, we again did not find any reduction in fluorescent signal in the fibroblast using these antibodies, in the first attempt we could not detect a significant difference between antibody treated versus sEV only treated fibroblasts (figure 6.9a), but in the second attempt, we saw an increase in fluorescent signal in fibroblasts treated with sEVs and antibodies (figure 6.9b). Interestingly there was also a significant difference in this second experiment between the anti-CD9 and IgG_{2b} control antibody conditions, suggesting the increased fluorescent signal in the anti-CD9 cells was due to the CD9 targeting of the antibody. Due to the unexpected results generated, we did not further investigate the role of integrins

in sEV internalisation in this study, and therefore did not perform microscopy experiments to complement the flow cytometry data. The results collected from these cellular uptake experiments were unexplainable, but our inability to block sEV internalisation by fibroblasts using antibodies against sEV surface proteins meant we were unable to further clarify the role of sEV uptake in the stimulation of the fibroblast.

Here, we demonstrated inconsistencies in using pharmacological inhibitors to determine the role of PCa derived sEV internalisation in driving phenotypic change in the fibroblast, with the inhibitors showing varying impacts on sEV induced marker expression/secretion. And with the off-target effects of the inhibitors found through a literature search, we were unable to confidently use these inhibitors to identify a link between sEV uptake and function in this instance, though we did note case of inhibitors not impeding HGF secretion despite inhibiting sEV internalisation (e.g. CytoD, BafA). Block of sEV internalisation using RGD revealed a role for integrins in this process, and we then showed detection of integrins $\beta 1$ and $\alpha 3$ on the sEV surface, as well as $\beta 3$ and $\alpha 6$, albeit to a lesser extent. Unfortunately, we were unable to block sEV internalisation by fibroblasts using anti-integrin or anti-CD9 antibodies and saw evidence of increased cellular uptake in the presence of these antibodies.

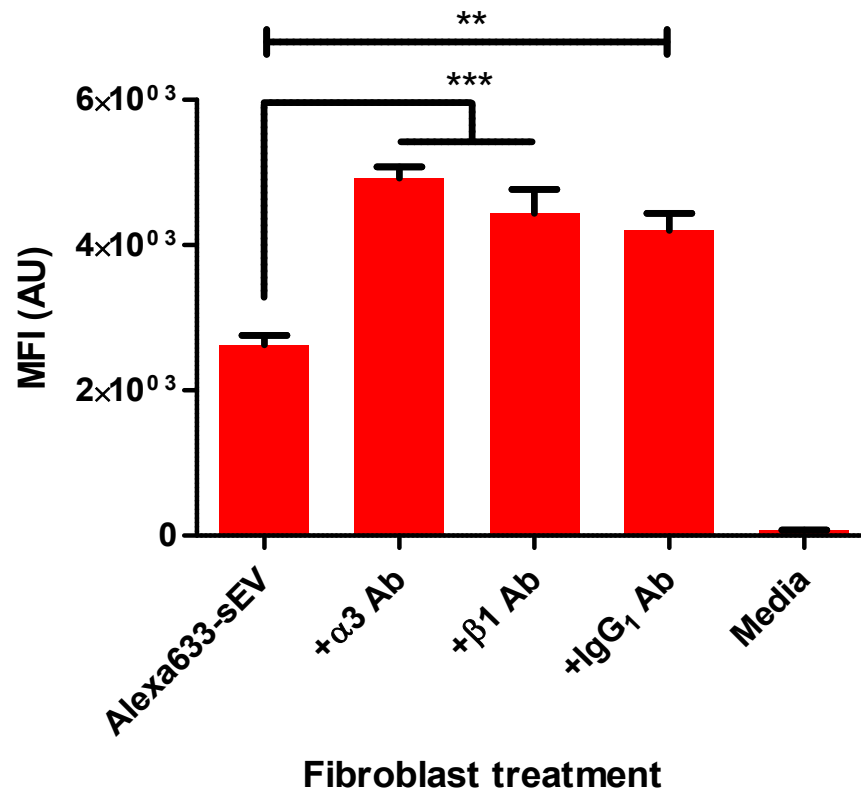


Figure 6.8. Anti-integrin antibody mediated blockade of DU145 derived sEV internalisation by fibroblasts. Fibroblasts were treated with $25 \mu\text{g}/\text{mL}$ Alexa633-sEVs for 1 hour with/without $10 \mu\text{g}/\text{mL}$ anti- $\beta 1$ /anti- $\alpha 3$ /isotype control antibody. Fluorescent intensities of cells were measured by flow cytometry. Bars represent means \pm SEM, based on triplicate wells, ** $P < 0.01$, *** $P < 0.001$, one-way ANOVA with Tukey's multiple comparison test.

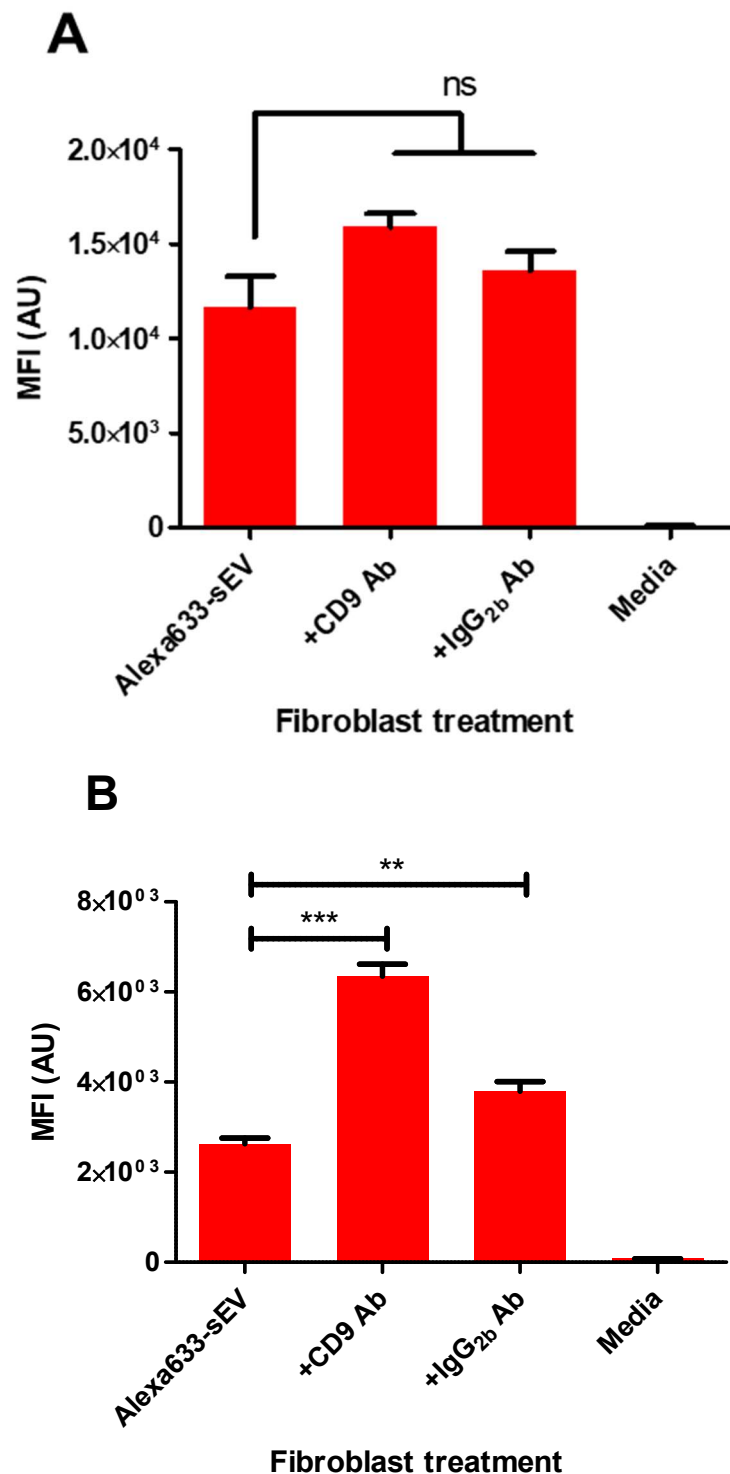


Figure 6.9. Anti-CD9 mediated blockade of DU145 derived sEV internalisation by fibroblasts. Fibroblasts were treated with 25µg/mL Alexa633-sEVs for 1 hour with/without 10µg/mL anti-CD9/isotype control antibody. Fluorescent intensities of cells were measured by flow cytometry. (A) Graph represents experiment one, (B) graph represents experiment two. Bars represent means +/- SEM, based on triplicate wells, **P<0.01, ***P<0.001, one-way ANOVA with Tukey's multiple comparison test.

6.4. Discussion

Here, we sought to determine whether there was a link between endocytosis of DU145 derived sEVs by fibroblasts and the triggering of myofibroblast differentiation into a phenotype that is analogous to a tumour promoting fibroblast. We also investigated inhibition of sEV internalisation through antibody targeting of sEV surface proteins. The data shown in this chapter is summarised in figure 6.10.

Some pharmacological inhibitors, particularly Dynasore (the most potent inhibitor), showed perturbation of fibroblast differentiation, however these compounds are severely limited in that they are reported to have off-target effects on cells which make interpreting results problematic, such that impaired differentiation may not be directly linked to uptake. The inhibitors EIPA and Heparin however, whilst impeding sEV internalisation (modestly with EIPA), showed no effect on fibroblast expression of α SMA or secretion of HGF, other inhibitors, such as CytoD also showed no impact on HGF levels whilst α SMA expression was clearly affected, though CytoD is an inhibitor of actin polymerisation (Flanagan and Lin, 1980). Whilst the inhibitors are severely limited, they did not universally reduce expression of α SMA or secretion of HGF, suggesting there may not be a link between endocytosis of the sEV and the stimulation of the fibroblast. These experiments were also limited in the markers we measured to determine fibroblast differentiation, these myofibroblasts secrete numerous factors and have pro-tumoural effects *in-vivo* (Webber et al., 2015b), assessment of more markers of fibroblast stimulation or *in-vivo* experiments would help elucidate any effect endocytic inhibitors have on sEV function. The sEV-mediated stimulation is dependent on TGF β 1 signalling, which occurs at the plasma membrane of the fibroblast, Webber *et al* demonstrated a role for sEV surface Heparan sulphate proteoglycans (HSPGs) in the handover of TGF β 1 to the fibroblast (Webber et al., 2010). Further investigation of the interaction at the plasma membrane and how HSPGs contribute to sEV induced stimulation of the fibroblast will give us a greater understanding of this process. The minor impedance of sEV uptake in the presence of TGF β neutralising antibody, despite its significant effect on differentiation (Webber et al., 2015b), also strengthens the

likelihood that sEV internalisation is independent of the TGF β signalling process between PCa derived sEVs and fibroblasts.

TGF β blockade, whilst known to inhibit differentiation of the fibroblast, did not appear to have a substantial effect on sEV internalisation, which further demonstrates that the processes of sEV internalisation and sEV delivered TGF β 1 mediated fibroblast differentiation are not linked. Any effect sEV uptake has on determining fibroblast behaviour is therefore likely to be independent of TGF β signalling.

Integrins were a logical target for blocking, since they had been previously been implicated in the internalisation of sEVs (Hoshino et al., 2015; Wang et al., 2015), and some subunits are known to be highly expressed in prostate cancer (Goel et al., 2008). Antibody blockade was presumed to be sufficient to impede endocytosis of the sEV, since integrin antibodies have been used to block sEV internalisation previously (Wang et al., 2015) and antibodies against other proteins, such as the tetraspanins CD9 and CD81 have also been effective (Morelli et al., 2004), though in this case the inhibition of sEV uptake was very modest, only a 5-12% reduction in signal was observed. The results gathered from the flow cytometry experiments were difficult to explain, though in hindsight, further investigation, with complementary microscopy experiments would have been useful to see whether there is an increase in internalised sEV, or if the antibodies cause greater plasma membrane stickiness. Whilst we presume trypsinisation of the fibroblast for flow cytometry strips the cell of surface bound sEVs, we cannot be sure whether the presence of antibodies has any effect in this regard. For the dose of sEVs used for uptake studies, we also cannot be sure whether the dose of antibodies used was sufficiently saturating, though doses used were comparable to previous studies (Morelli et al., 2004). The cost of dramatically increasing antibody doses however was not possible, and even if the doses used were not high enough, this still does not explain the increase in sEV uptake by the fibroblasts. We postulated that increased sEV internalisation in the presence of antibodies could be due to recognition by Fc receptors, however this was not followed up as these receptors are generally reported to be present on cells of the immune system and may not be very abundant on fibroblasts (Ravetch and Kinet, 1991).

In hindsight it may have been more logical to attempt to block specific integrin heterodimers known to interact with RGD motifs, since the RGD peptide is what provided an inhibition of sEV uptake. Instead integrin targeting was based on known expression on DU145 cells, since this was believed to ensure a blocking effect with antibodies, regardless of whether the target integrins were RGD binders. Furthermore, it could have helped to have had a more robust attempt at targeting the chosen integrins, through use of numerous antibodies targeting distinct epitopes, which may have revealed different blocking capabilities between the antibodies. Whilst the results reported in this chapter with regards to the impact of these antibodies on sEV internalisation are unexplained, they are certainly worth further investigation. Washing sEVs of unbound antibodies would be a more elegant approach to examining effects of antibody blockade on sEV uptake, as this would prevent antibody binding to the recipient cell surface allowing us to only consider the role of sEV related integrins and not fibroblast integrins. It is possible fibroblast integrins aid sEV binding through integrin receptors such as ICAM/VCAM/ADAM proteins, which could be expressed on the DU145 sEV surface. Defining the role of fibroblast surface integrins or sEV surface ICAM or ADAM proteins in sEV uptake could be another avenue for future study, as well as whether integrin mediated adhesion of sEVs to extracellular matrix components contributes to their interaction with fibroblasts. This is possible since RGD motifs clearly blocked a sEV-fibroblast interaction here and some matrix components, like vitronectin, contains an RGD motif (Humphries et al., 2006), suggesting sEVs could bind to these components. Ultracentrifugation is reported to wash off excess antibodies from sEVs (Zech et al., 2012). In future studies, a more robust look at the role of PCa derived sEV surface integrins may require a more effective blockade, potentially through knockdown of specific integrins, as described in a study of cancer derived sEVs previously (Hoshino et al., 2015).

In studying the effects of sEV uptake by a recipient cell on its ability to drive phenotypic change in that cell could be alternatively studied through enhancement of sEV internalisation, as opposed to abrogation of endocytosis. Enhancement of sEV internalisation is of particular interest in the area of sEV-based therapeutics, in which sEVs are being explored as carriers of therapeutic molecules, making uptake of these sEVs by target cells desirable. Cell engineering has been employed to attach target tissue specific peptides to sEV-associated membrane proteins to

enhance cellular uptake of the sEV by a specific cell type (Alvarez-Erviti et al., 2011). Others have attached peptides known to induce endocytosis in cells, termed cell penetrating peptides to the surface of sEVs and demonstrated increased internalisation by the recipient cell (Nakase et al., 2016). Taking nanobodies known to target receptors highly expressed on cancer cells (e.g. EGFR) and fusing them with a phospholipid (phosphatidylserine) which will embed itself in a sEV membrane is another elegant example of modification of the sEV surface for increases cellular uptake (Kooijmans et al., 2018). There are numerous described methods for enhancement of sEV internalisation (Johnsen et al., 2014), modification of the sEV surface may be an effective approach for studying the effect of PCa derived sEV uptake by fibroblasts on the phenotype of the cell.

We have identified expression of a number of integrin subunits on the surface of DU145 derived sEVs, however found issues with blocking sEV internalisation using antibodies against integrins as well as the tetraspanin CD9. Use of RGD peptide however revealed a role for integrins in the endocytosis of these PCa derived sEVs and therefore this is worth following up on in the future. Through TGF β blocking and pharmacological inhibition experiments, we show that TGF β signalling between sEV and fibroblast is not linked to the internalisation of the sEV.

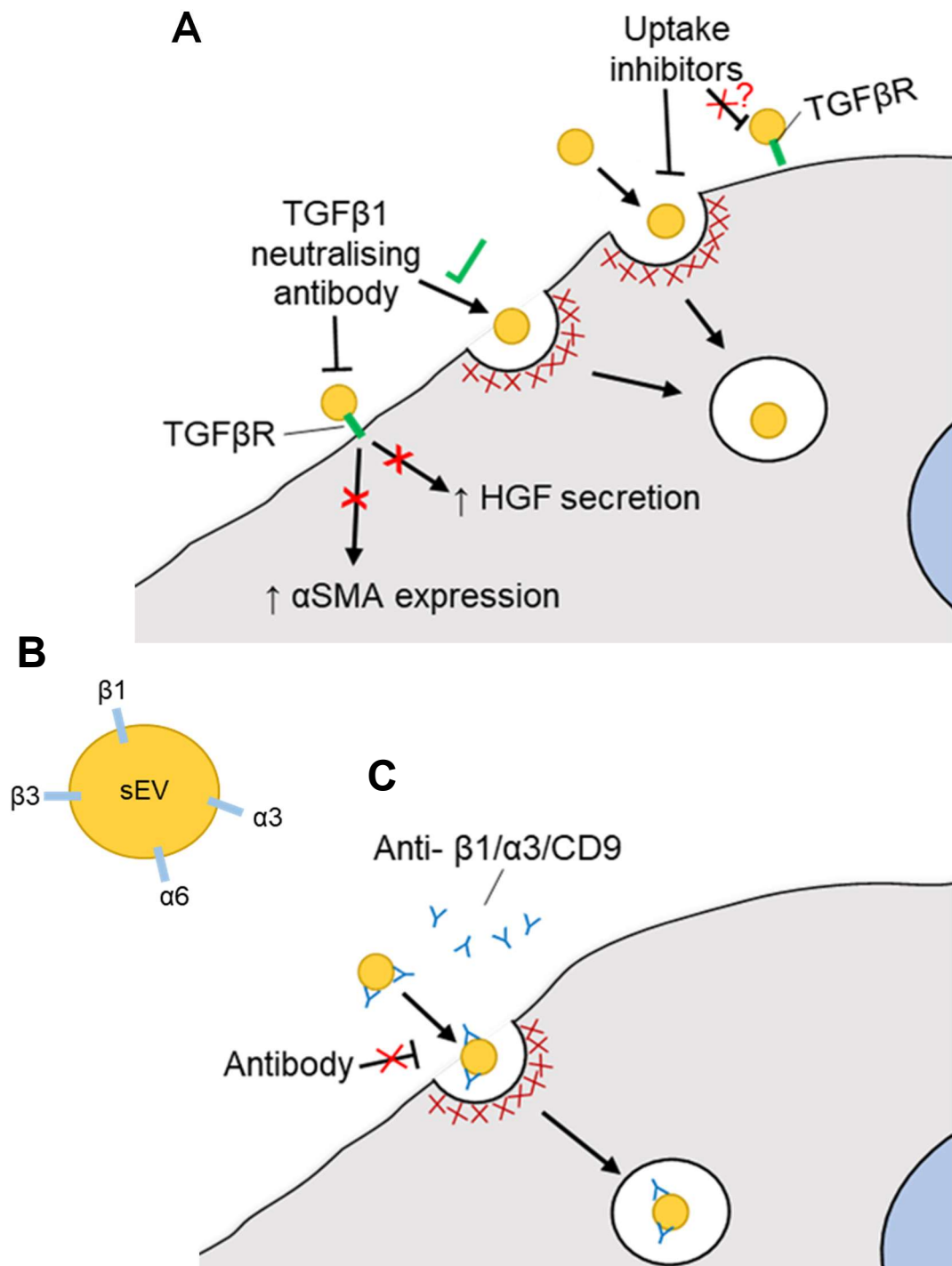


Figure 6.10. Schematic summary of chapter 6. Summary of the data collected in chapter 6. (A) There does not appear to be a link between sEV internalisation by fibroblasts and the ability of the sEV to deliver functional TGFβ1 to the cell. (B) DU145 derived sEVs express integrin subunits β1, β3, α3 and α6. (C) We were unable to impede sEV internalisation by fibroblasts with antibodies against the integrins β1, α3, or the tetraspanin CD9.

Chapter 7- General discussion

7.1. Summarising discussion

sEVs are known to transfer their contents to target cells, how this occurs is not well understood. Here, we studied the cellular uptake and processing of PCa derived sEVs in primary fibroblasts, a biologically relevant cell type in the tumour microenvironment. Through examining this means of sEV-cell communication, we aimed to increase our knowledge of the nature of PCa-fibroblast interactions and the role of sEVs in modulating the stromal component in cancer, but also the mechanisms of sEV cargo delivery to recipient cells in a broader sense.

A schematic summary of the main findings of this study can be seen in figure 7.1, and covers four main points:

1. We have presented novel fluorescent Alexa dye for sEV labelling, Alexa dye labelling does not impede sEV driven TGF β 1-mediated fibroblast stimulation.
2. PCa sEVs are internalised by fibroblasts primarily through Clathrin mediated endocytosis. They are seen in early endosomes after fibroblast uptake and begin to reach lysosomes within 2 hours.
3. sEVs can be labelled with intraluminal fluorescent dyes, RNA binding dye SYTO RNASelect requires sEV internalisation to stain the fibroblast, and the dye escapes within an hour of cellular uptake of the sEV.
4. Cellular uptake of sEVs is independent of sEV mediated delivery of functional TGF β 1 to fibroblasts.

In reporting on studies with sEVs, characterising the sEV sample is important to demonstrate successful purification, and allows one to confidently attribute results to sEV action. We presented data showing sEV isolates, generated through sucrose cushion ultracentrifugation and subsequent pelleting, have the size, structure and protein expression typical of sEVs, and satisfy the ISEV guidelines for defining sEVs (Théry et al., 2018). However, the isolates do not solely contain typical sEV structures, but numerous other membrane bounded or electron dense morphologies. The presence of these structures is rarely discussed, though others have described similar morphologies in their isolates (Zabeo et al., 2017). Whilst

the nature of these structures is unknown, their presence in sEV isolates from different cell types, and generated through different isolation protocols in different studies suggest that these are not artificially created through the isolation process but are real cell derived entities. These structures should be studied further so we can better understand the composition of the sEV population and potential roles of these vesicle subtypes in biological functions.

The widely reported problems with lipophilic dyes in sEV labelling (Morales-Kastresana et al., 2017; Pužar Dominkuš et al., 2018), led us to evaluate an alternative method for fluorescent labelling of sEV for use in cellular uptake studies. Here we proposed the maleimide linked Alexa dyes to label sEV surface proteins. These dyes were stable when bound to sEVs, available in many colours, insensitive to photobleaching and changes in pH, and do not form artificial sEV sized particulates (a common problem with lipophilic dyes). The use of this dye to label sEVs for cellular uptake analysis has now been published (Roberts-Dalton et al., 2017). We carried out experiments to determine the suitability of the dye to label sEVs, we showed that all of the detectable dye in a sEV sample is sEV bound and that the dye does not affect the ability of the sEV to induce fibroblast differentiation. These are important considerations to take into account, to ensure sEVs and not artificial fluorescent particles are being tracked, and that the function of the sEV is not impaired by the labelling process as this could have an unintended knock on effect on the uptake process.

Fibroblasts internalise sEVs, which we can detect fluorescently by microscopy and flow cytometry. Through complimentary use of pharmacological inhibitors and siRNA against distinct endocytic regulators, we identified Clathrin mediated endocytosis as the primary route for cellular uptake of sEVs by fibroblasts.

Interestingly, the main route of uptake in HeLa cells for the same sEVs is macropinocytosis (Roberts-Dalton et al., 2017), revealing an issue with targeting a recipient cell for therapeutic blockade of sEV endocytosis *in vivo*, as sEVs from the same source can be internalised through different routes, dependent on recipient cell type. One should be weary of using pharmacological inhibitors for blockade of endocytosis, we and others warn of the highly cytotoxic nature of the inhibitors, as well as their lack of specificity for their putative target and their off-target effects in the cell (Ivanov, 2008; Vercauteren et al., 2010).

Discussion

Within 30 minutes of cellular uptake, sEVs are present in early endosomes, as shown by their co-localisation with transferrin and Rab5 labelled endosomes, then slowly transit to lysosomes within 2 hours, seen by their increased co-localisation with dextran over this time. Fluorescent signal is still present in cells even at 72 hours post-uptake though less punctate. We do not know however what the fate of the sEV is once it reaches lysosome and at what point the fluorescent signal is disassociated dye following possible degradation of the sEV. We then wanted to see whether the intraluminal cargo of the PCa derived sEV was transferred to fibroblasts sometime after endocytosis. sEVs were labelled with membrane permeable fluorescent dyes and again we carried out experiments determining their suitability for sEV labelling. Calcein AM was found to leak from the sEV and was therefore shown to be undesirable as a sEV label in cellular uptake studies. SYTO dye requires endocytosis of the sEV before staining the fibroblast in its distinctive manner, labelling mitochondria. The SYTO dye disassociates from the sEV within an hour of sEV internalisation, suggesting sEV cargo can escape rapidly, possibly from early endocytic compartments. A platform for fluorescently tracking dual-coloured sEVs was created, in which these sEVs were detectable by wide-field time-lapse microscopy, with the aim of showing intraluminal cargo delivery in real-time. We will likely need higher power microscopy to monitor disassociation of the dyes from one another, as we were unable to achieve this with our current microscopy setup.

Through pharmacological inhibition and TGF β 1 blocking experiments, we found that TGF β 1 dependent sEV induced fibroblast stimulation is not linked with the endocytosis of the sEV, meaning the markers measured following the stimulation of the fibroblast are mediated by sEV-fibroblast membrane surface interactions. Since we demonstrated that PCa derived sEVs can deliver intraluminal cargo to fibroblasts however, it is possible that mRNA/miRNA from these vesicles could induce phenotypic change in the fibroblast. We therefore sought to examine the impact of endocytic inhibition of TGF β 1 independent effects on the fibroblast. To achieve this, we moved away from pharmacological inhibitors, due to previously stated problems, and instead targeted the sEV surface proteins, since we had shown a difference in cellular uptake efficiency between DU145 and LNCaP derived sEVs, plus we had also impeded sEV internalisation through use of Heparin and RGD peptide, blockers of surface interactions. We targeted sEV surface

Discussion

integrins for endocytic blockade, as they had a stated role in cancer progression and in internalisation of sEVs. We successfully identified expression of the subunits $\beta 1$, $\beta 3$, $\alpha 3$ and $\alpha 6$ on the DU145 derived sEVs, but did not achieve abrogation of cellular uptake with use of integrin antibodies to block these sEV proteins and unexpectedly observed heightened uptake in the presence of antibodies, independent of antibody specificity. More sophisticated assessment of the role of integrins in cellular uptake of PCa derived sEVs could be achieved through knockdown of integrins for example (Hoshino et al., 2015), to tease out the importance of specific integrins in uptake.

Our evidence of PCa derived sEV intraluminal cargo transfer to fibroblasts shows this to occur shortly after sEV endocytosis, before they reach lysosomes. We also reveal the importance of the sEV-cell surface interactions in endocytosis of sEVs by fibroblasts. From this study, we also present new questions for consideration:

- What is the mechanism of intraluminal cargo escape from the sEV/endosomal compartment?
- How do sEVs mediate interactions at the cell surface leading to endocytosis of the vesicle and what sEV/fibroblast proteins are important?
- Does PCa derived sEV intraluminal cargo, delivered to fibroblasts, drive TGF β 1 independent phenotypic change in the cell?

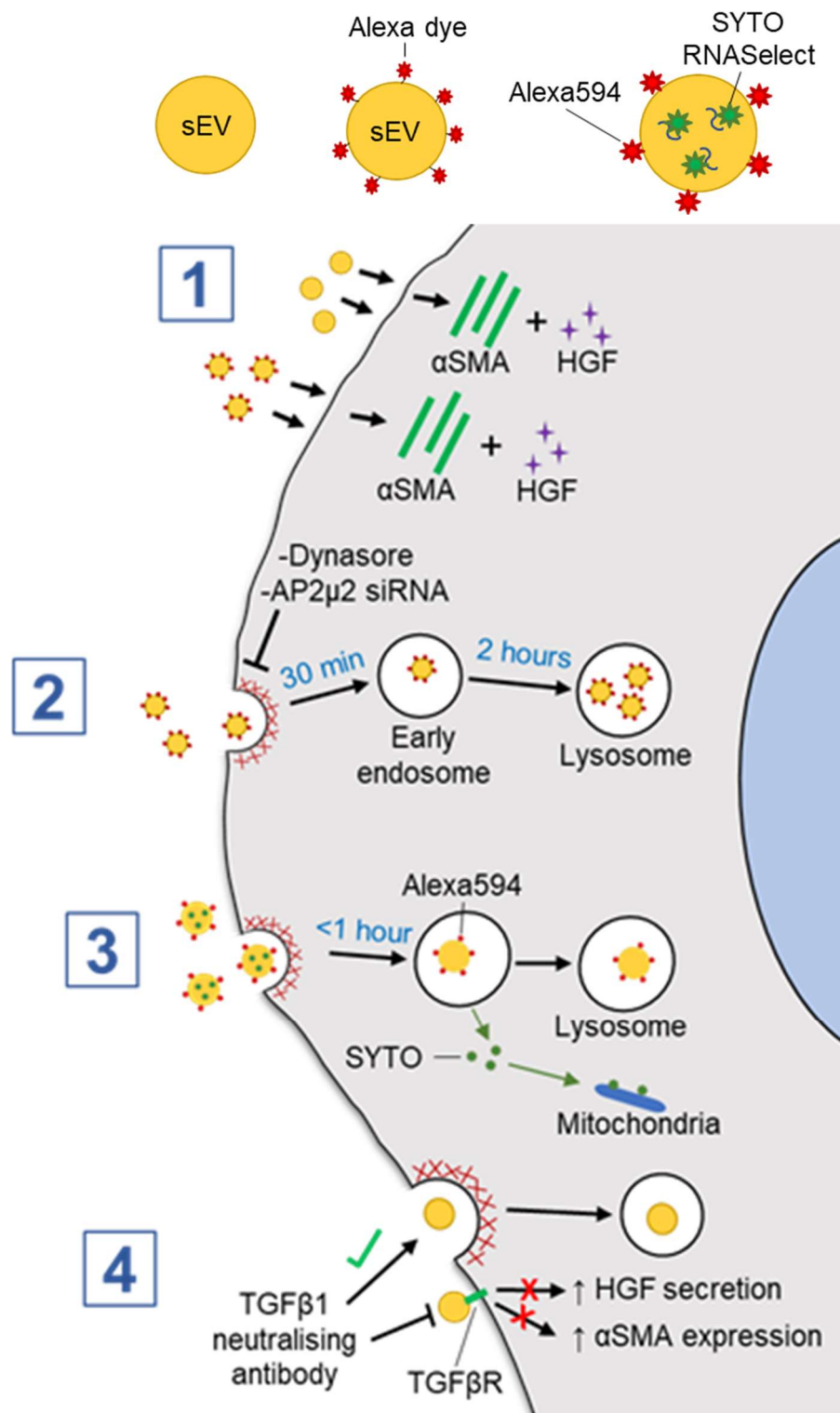


Figure 7.1. Endocytosis and intracellular processing of prostate cancer derived sEVs by fibroblasts. A schematic summary of the primary findings of this study. (1) sEVs can be labelled with Alexa dyes, without perturbing the sEV driven response in fibroblasts. (2) sEVs are taken up by Clathrin mediated endocytosis and are sorted to lysosomes. (3) Intraluminal dye escapes the sEV soon after endocytosis. (4) sEV internalisation is independent of the TGF β 1 response in fibroblasts.

7.2. Future directions

Whilst we reveal the transfer of intraluminal cargo from PCa derived sEVs to fibroblasts soon after endocytosis of the sEV, the mechanism of delivery remains unclear. Elucidating the mechanism of cargo transfer from sEV to the cell cytosol would be an important step in our fundamental understanding of how sEVs operate to communicate with cells.

To escape into the cytosol, intraluminal sEV contents must overcome the sEV and endosomal membranes, but we do not currently know how this occurs. Endosome associated proteins have been implicated in the transfer of sEV contents to target cells (Abrami et al., 2013), further implicating endosomal escape of sEV contents. Examining the sEV structure following endocytosis as it enters different endosomal compartments would clarify the fate of the sEV and could provide information on how its contents are transferred to cells. The study of sEV structure within a recipient cell endosome could be possible using electron microscopy (EM). Intact sEVs have been previously visualised by EM following endocytosis (Heusermann et al., 2016; Morelli et al., 2004). Through use of fluorescently labelled sEVs we have been able to track their subcellular location in fibroblasts, and complimentary use of EM could reveal the state of the sEVs in fluorescently tagged compartments. Correlative light and electron microscopy (CLEM) is a technique combining fluorescence microscopy with EM, which allows image capture of fluorescent entities within cells, followed by clarification of the structure of these entities through EM of the same field of view (de Boer et al., 2015). Cellular uptake and trafficking of our fluorescently labelled sEVs, monitored by CLEM would allow us to identify the sEV structure at the point of intraluminal cargo escape. Furthermore, we could determine the fate of the sEV upon sorting to lysosomes, as well as determine how long protein binding dyes, such as the Alexa and CFSE dyes, remain associated with sEVs during the intracellular sorting process. Use of CLEM to study intracellular processing and fate of sEVs would give us an understanding of sEV-cell interactions not possible with fluorescence microscopy alone.

Discussion

In this study, we found that proteins on the sEV surface were relevant in the internalisation of the sEV by the fibroblast. We also demonstrated intraluminal cargo transfer from sEVs to fibroblasts. Further study of the interaction between PCa derived sEVs and fibroblasts will give us a greater comprehension of the role of sEVs in driving important pathological processes in cancer.

There was a sizeable difference in the cellular uptake efficiencies of DU145 derived sEVs versus LNCaP derived sEVs in fibroblasts, indicating a role of the sEV surface in driving endocytosis. Further, we were able to inhibit endocytosis through use of Heparan sulphate mimetic Heparin and integrin binding blocker RGD. Clearly sEV surface proteins are relevant for the internalisation of PCa derived sEVs by fibroblasts. Since we observed such a marked difference between the cellular uptake of DU145 and LNCaP derived sEVs, examining these differences is an interesting prospect. Proteomic analysis of these two sEV populations could reveal interesting differences in the make-up of the respective sEV surface protein content and identify targets for cellular uptake studies. It would also be intriguing to examine whether the cargo delivery kinetics are different between these sEV populations as well. Pin-pointing specific sEV surface proteins for blockade of endocytosis would be a desirable therapeutic target to perturb sEV mediated actions in the tumour microenvironment.

Although the TGF β 1 mediated response in fibroblasts is not dependent on the cellular uptake of the sEV, we found that these sEVs could nonetheless transfer their cargo to the cell. RNAs are the most commonly reported intraluminal cargo delivered by sEVs. Enrichment of some RNAs in PCa derived sEVs has been reported (Ahadi et al., 2016), supporting the idea that these sEVs could be delivering functional RNAs to cells. Analysis of the RNA content of PCa derived sEVs and evaluation of their effects on fibroblast phenotype is another logical avenue for future study, to further clarify the mechanisms of sEV-fibroblast communication in the growth and survival of tumours.

Concluding remark

In the current study, we showed evidence of transfer of sEV luminal contents to fibroblasts shortly after sEV endocytosis, through use of fluorescent dyes to monitor the sEV interactions with the fibroblast. Determining the functionally relevant cargo and defining the delivery mechanism from sEV to the fibroblast cytosol may present us with novel avenues for intervening and attenuating development of aberrant stromal cells arising due to sEV activities in the tumour microenvironment.

References

- Abrami, L., L. Brandi, M. Moayeri, M. J. Brown, B. A. Krantz, S. H. Leppla, and F. G. van der Goot, 2013, Hijacking multivesicular bodies enables long-term and exosome-mediated long-distance action of anthrax toxin: *Cell Rep*, v. 5, p. 986-96.
- Ahadi, A., S. Brennan, P. J. Kennedy, G. Hutvagner, and N. Tran, 2016, Long non-coding RNAs harboring miRNA seed regions are enriched in prostate cancer exosomes: *Sci Rep*, v. 6, p. 24922.
- Ahmad, I., O. J. Sansom, and H. Y. Leung, 2008, Advances in mouse models of prostate cancer: *Expert Rev Mol Med*, v. 10, p. e16.
- Al Soraj, M., L. He, K. Peynshaert, J. Cousaert, D. Vercauteren, K. Braeckmans, S. C. De Smedt, and A. T. Jones, 2012, siRNA and pharmacological inhibition of endocytic pathways to characterize the differential role of macropinocytosis and the actin cytoskeleton on cellular uptake of dextran and cationic cell penetrating peptides octaarginine (R8) and HIV-Tat: *J Control Release*, v. 161, p. 132-41.
- Al-Nedawi, K., B. Meehan, J. Micallef, V. Lhotak, L. May, A. Guha, and J. Rak, 2008, Intercellular transfer of the oncogenic receptor EGFRvIII by microvesicles derived from tumour cells: *Nat Cell Biol*, v. 10, p. 619-24.
- Al-Soraj, M. H., C. L. Watkins, D. Vercauteren, S. C. De Smedt, K. Braeckmans, and A. T. Jones, 2010, siRNA versus pharmacological inhibition of endocytic pathways for studying cellular uptake of cell penetrating peptides: *J Control Release*, v. 148, p. e86-7.
- Alitalo, K., 2011, The lymphatic vasculature in disease: *Nat Med*, v. 17, p. 1371-80.
- Alvarez-Erviti, L., Y. Seow, H. Yin, C. Betts, S. Lakhali, and M. J. Wood, 2011, Delivery of siRNA to the mouse brain by systemic injection of targeted exosomes: *Nat Biotechnol*, v. 29, p. 341-5.
- Anderson, H. C., 1969, Vesicles associated with calcification in the matrix of epiphyseal cartilage: *J Cell Biol*, v. 41, p. 59-72.
- Arunachalam, B., U. T. Phan, H. J. Geuze, and P. Cresswell, 2000, Enzymatic reduction of disulfide bonds in lysosomes: characterization of a gamma-interferon-inducible lysosomal thiol reductase (GILT): *Proc Natl Acad Sci U S A*, v. 97, p. 745-50.
- Atay, S., S. Banskota, J. Crow, G. Sethi, L. Rink, and A. K. Godwin, 2014, Oncogenic KIT-containing exosomes increase gastrointestinal stromal tumor cell invasion: *Proc Natl Acad Sci U S A*, v. 111, p. 711-6.
- Atay, S., C. Gercel-Taylor, and D. D. Taylor, 2011, Human trophoblast-derived exosomal fibronectin induces pro-inflammatory IL-1 β production by macrophages: *Am J Reprod Immunol*, v. 66, p. 259-69.
- Baravalle, G., D. Schober, M. Huber, N. Bayer, R. F. Murphy, and R. Fuchs, 2005, Transferrin recycling and dextran transport to lysosomes is differentially affected by bafilomycin, nocodazole, and low temperature: *Cell Tissue Res*, v. 320, p. 99-113.
- Bardi, G. T., M. A. Smith, and J. L. Hood, 2018, Melanoma exosomes promote mixed M1 and M2 macrophage polarization: *Cytokine*, v. 105, p. 63-72.
- Barros, F. M., F. Carneiro, J. C. Machado, and S. A. Melo, 2018, Exosomes and Immune Response in Cancer: Friends or Foes?: *Front Immunol*, v. 9, p. 730.
- Barrès, C., L. Blanc, P. Bette-Bobillo, S. André, R. Mamoun, H. J. Gabius, and M. Vidal, 2010, Galectin-5 is bound onto the surface of rat reticulocyte exosomes and modulates vesicle uptake by macrophages: *Blood*, v. 115, p. 696-705.

References

- Bates, G. J., S. B. Fox, C. Han, R. D. Leek, J. F. Garcia, A. L. Harris, and A. H. Banham, 2006, Quantification of regulatory T cells enables the identification of high-risk breast cancer patients and those at risk of late relapse: *J Clin Oncol*, v. 24, p. 5373-80.
- Bergamaschi, A., E. Tagliabue, T. Sørlie, B. Naume, T. Triulzi, R. Orlandi, H. G. Russnes, J. M. Nesland, R. Tammi, P. Auvinen, V. M. Kosma, S. Ménard, and A. L. Børresen-Dale, 2008, Extracellular matrix signature identifies breast cancer subgroups with different clinical outcome: *J Pathol*, v. 214, p. 357-67.
- Bhowmick, N. A., A. Chytil, D. Plieth, A. E. Gorska, N. Dumont, S. Shappell, M. K. Washington, E. G. Neilson, and H. L. Moses, 2004, TGF-beta signaling in fibroblasts modulates the oncogenic potential of adjacent epithelia: *Science*, v. 303, p. 848-51.
- Bobrie, A., M. Colombo, S. Krumeich, G. Raposo, and C. Théry, 2012a, Diverse subpopulations of vesicles secreted by different intracellular mechanisms are present in exosome preparations obtained by differential ultracentrifugation: *J Extracell Vesicles*, v. 1.
- Bobrie, A., S. Krumeich, F. Rey, C. Recchi, L. F. Moita, M. C. Seabra, M. Ostrowski, and C. Théry, 2012b, Rab27a supports exosome-dependent and -independent mechanisms that modify the tumor microenvironment and can promote tumor progression: *Cancer Res*, v. 72, p. 4920-30.
- Boelens, M. C., T. J. Wu, B. Y. Nabet, B. Xu, Y. Qiu, T. Yoon, D. J. Azzam, C. Twyman-Saint Victor, B. Z. Wiemann, H. Ishwaran, P. J. Ter Brugge, J. Jonkers, J. Slingerland, and A. J. Minn, 2014, Exosome transfer from stromal to breast cancer cells regulates therapy resistance pathways: *Cell*, v. 159, p. 499-513.
- Boire, A., L. Covic, A. Agarwal, S. Jacques, S. Sherifi, and A. Kuliopulos, 2005, PAR1 is a matrix metalloprotease-1 receptor that promotes invasion and tumorigenesis of breast cancer cells: *Cell*, v. 120, p. 303-13.
- Bonifacino, J. S., and B. S. Glick, 2004, The mechanisms of vesicle budding and fusion: *Cell*, v. 116, p. 153-66.
- Booth, A. M., Y. Fang, J. K. Fallon, J. M. Yang, J. E. Hildreth, and S. J. Gould, 2006, Exosomes and HIV Gag bud from endosome-like domains of the T cell plasma membrane: *J Cell Biol*, v. 172, p. 923-35.
- Bowman, E. J., A. Siebers, and K. Altendorf, 1988, Bafilomycins: a class of inhibitors of membrane ATPases from microorganisms, animal cells, and plant cells: *Proc Natl Acad Sci U S A*, v. 85, p. 7972-6.
- Brown, E. B., Y. Boucher, S. Nasser, and R. K. Jain, 2004, Measurement of macromolecular diffusion coefficients in human tumors: *Microvasc Res*, v. 67, p. 231-6.
- Bruno, S., F. Collino, M. C. Deregibus, C. Grange, C. Tetta, and G. Camussi, 2013, Microvesicles derived from human bone marrow mesenchymal stem cells inhibit tumor growth: *Stem Cells Dev*, v. 22, p. 758-71.
- Bubendorf, L., A. Schöpfer, U. Wagner, G. Sauter, H. Moch, N. Willi, T. C. Gasser, and M. J. Mihatsch, 2000, Metastatic patterns of prostate cancer: an autopsy study of 1,589 patients: *Hum Pathol*, v. 31, p. 578-83.
- Burbulla, L. F., and R. Krüger, 2012, The use of primary human fibroblasts for monitoring mitochondrial phenotypes in the field of Parkinson's disease: *J Vis Exp*.
- Böing, A. N., E. van der Pol, A. E. Grootemaat, F. A. Coumans, A. Sturk, and R. Nieuwland, 2014, Single-step isolation of extracellular vesicles by size-exclusion chromatography: *J Extracell Vesicles*, v. 3.

References

- Cao, Y., J. Arbiser, R. J. D'Amato, P. A. D'Amore, D. E. Ingber, R. Kerbel, M. Klagsbrun, S. Lim, M. A. Moses, B. Zetter, H. Dvorak, and R. Langer, 2011, Forty-year journey of angiogenesis translational research: *Sci Transl Med*, v. 3, p. 114rv3.
- Carter, S. D., S. K. Mageswaran, Z. J. Farino, J. I. Mamede, C. M. Oikonomou, T. J. Hope, Z. Freyberg, and G. J. Jensen, 2018, Distinguishing signal from autofluorescence in cryogenic correlated light and electron microscopy of mammalian cells: *J Struct Biol*, v. 201, p. 15-25.
- Chadda, R., M. T. Howes, S. J. Plowman, J. F. Hancock, R. G. Parton, and S. Mayor, 2007, Cholesterol-sensitive Cdc42 activation regulates actin polymerization for endocytosis via the GEEC pathway: *Traffic*, v. 8, p. 702-17.
- Challagundla, K. B., P. M. Wise, P. Neviani, H. Chava, M. Murtadha, T. Xu, R. Kennedy, C. Ivan, X. Zhang, I. Vannini, F. Fanini, D. Amadori, G. A. Calin, M. Hadjidaniel, H. Shimada, A. Jong, R. C. Seeger, S. Asgharzadeh, A. Goldkorn, and M. Fabbri, 2015, Exosome-mediated transfer of microRNAs within the tumor microenvironment and neuroblastoma resistance to chemotherapy: *J Natl Cancer Inst*, v. 107.
- Chandrasekar, T., J. C. Yang, A. C. Gao, and C. P. Evans, 2015, Mechanisms of resistance in castration-resistant prostate cancer (CRPC): *Transl Androl Urol*, v. 4, p. 365-80.
- Chen, C. C., L. Liu, F. Ma, C. W. Wong, X. E. Guo, J. V. Chacko, H. P. Farhoodi, S. X. Zhang, J. Zimak, A. Ségaliny, M. Riazifar, V. Pham, M. A. Digman, E. J. Pone, and W. Zhao, 2016, Elucidation of Exosome Migration across the Blood-Brain Barrier Model In Vitro: *Cell Mol Bioeng*, v. 9, p. 509-529.
- Chevillet, J. R., Q. Kang, I. K. Ruf, H. A. Briggs, L. N. Vojtech, S. M. Hughes, H. H. Cheng, J. D. Arroyo, E. K. Meredith, E. N. Gallichotte, E. L. Pogosova-Agadjanyan, C. Morrissey, D. L. Stirewalt, F. Hladik, E. Y. Yu, C. S. Higano, and M. Tewari, 2014, Quantitative and stoichiometric analysis of the microRNA content of exosomes: *Proc Natl Acad Sci U S A*, v. 111, p. 14888-93.
- Cho, J. A., H. Park, E. H. Lim, and K. W. Lee, 2012, Exosomes from breast cancer cells can convert adipose tissue-derived mesenchymal stem cells into myofibroblast-like cells: *Int J Oncol*, v. 40, p. 130-8.
- Chowdhury, R., J. P. Webber, M. Gurney, M. D. Mason, Z. Tabi, and A. Clayton, 2015, Cancer exosomes trigger mesenchymal stem cell differentiation into pro-angiogenic and pro-invasive myofibroblasts: *Oncotarget*, v. 6, p. 715-31.
- Christianson, H. C., K. J. Svensson, T. H. van Kuppevelt, J. P. Li, and M. Belting, 2013, Cancer cell exosomes depend on cell-surface heparan sulfate proteoglycans for their internalization and functional activity: *Proc Natl Acad Sci U S A*, v. 110, p. 17380-5.
- Christoforidis, S., M. Miaczynska, K. Ashman, M. Wilm, L. Zhao, S. C. Yip, M. D. Waterfield, J. M. Backer, and M. Zerial, 1999, Phosphatidylinositol-3-OH kinases are Rab5 effectors: *Nat Cell Biol*, v. 1, p. 249-52.
- Clayton, A., 2012, Cancer cells use exosomes as tools to manipulate immunity and the microenvironment: *Oncoimmunology*, v. 1, p. 78-80.
- Clayton, A., S. Al-Taei, J. Webber, M. D. Mason, and Z. Tabi, 2011, Cancer exosomes express CD39 and CD73, which suppress T cells through adenosine production: *J Immunol*, v. 187, p. 676-83.
- Clayton, A., J. Court, H. Navabi, M. Adams, M. D. Mason, J. A. Hobot, G. R. Newman, and B. Jasani, 2001, Analysis of antigen presenting cell derived exosomes, based on immuno-magnetic isolation and flow cytometry: *J Immunol Methods*, v. 247, p. 163-74.

References

- Clayton, A., C. L. Harris, J. Court, M. D. Mason, and B. P. Morgan, 2003, Antigen-presenting cell exosomes are protected from complement-mediated lysis by expression of CD55 and CD59: *Eur J Immunol*, v. 33, p. 522-31.
- Clayton, A., J. P. Mitchell, J. Court, S. Linnane, M. D. Mason, and Z. Tabi, 2008, Human tumor-derived exosomes down-modulate NKG2D expression: *J Immunol*, v. 180, p. 7249-58.
- Clayton, A., J. P. Mitchell, J. Court, M. D. Mason, and Z. Tabi, 2007, Human tumor-derived exosomes selectively impair lymphocyte responses to interleukin-2: *Cancer Res*, v. 67, p. 7458-66.
- Clayton, A., A. Turkes, S. Dewitt, R. Steadman, M. D. Mason, and M. B. Hallett, 2004, Adhesion and signaling by B cell-derived exosomes: the role of integrins: *FASEB J*, v. 18, p. 977-9.
- Clayton, A., A. Turkes, H. Navabi, M. D. Mason, and Z. Tabi, 2005, Induction of heat shock proteins in B-cell exosomes: *J Cell Sci*, v. 118, p. 3631-8.
- Colombo, M., G. Raposo, and C. Théry, 2014, Biogenesis, secretion, and intercellular interactions of exosomes and other extracellular vesicles: *Annu Rev Cell Dev Biol*, v. 30, p. 255-89.
- Conde-Vancells, J., E. Rodriguez-Suarez, N. Embade, D. Gil, R. Matthiesen, M. Valle, F. Elortza, S. C. Lu, J. M. Mato, and J. M. Falcon-Perez, 2008, Characterization and comprehensive proteome profiling of exosomes secreted by hepatocytes: *J Proteome Res*, v. 7, p. 5157-66.
- Condeelis, J., and J. W. Pollard, 2006, Macrophages: obligate partners for tumor cell migration, invasion, and metastasis: *Cell*, v. 124, p. 263-6.
- Cooper, C. R., C. H. Chay, and K. J. Pienta, 2002, The role of alpha(v)beta(3) in prostate cancer progression: *Neoplasia*, v. 4, p. 191-4.
- Costa Verdera, H., J. J. Gitz-Francois, R. M. Schifferers, and P. Vader, 2017, Cellular uptake of extracellular vesicles is mediated by clathrin-independent endocytosis and macropinocytosis: *J Control Release*, v. 266, p. 100-108.
- CRUK, 2016a, Cancer statistics for the UK, Online.
- CRUK, 2016b, Prostate cancer statistics, Online.
- Curiel, T. J., G. Coukos, L. Zou, X. Alvarez, P. Cheng, P. Mottram, M. Evdemon-Hogan, J. R. Conejo-Garcia, L. Zhang, M. Burow, Y. Zhu, S. Wei, I. Kryczek, B. Daniel, A. Gordon, L. Myers, A. Lackner, M. L. Disis, K. L. Knutson, L. Chen, and W. Zou, 2004, Specific recruitment of regulatory T cells in ovarian carcinoma fosters immune privilege and predicts reduced survival: *Nat Med*, v. 10, p. 942-9.
- Das, L., T. A. Anderson, J. M. Gard, I. C. Sroka, S. R. Strautman, R. B. Nagle, C. Morrissey, B. S. Knudsen, and A. E. Cress, 2017, Characterization of Laminin Binding Integrin Internalization in Prostate Cancer Cells: *J Cell Biochem*, v. 118, p. 1038-1049.
- de Boer, P., J. P. Hoogenboom, and B. N. Giepmans, 2015, Correlated light and electron microscopy: ultrastructure lights up!: *Nat Methods*, v. 12, p. 503-13.
- De Wever, O., Q. D. Nguyen, L. Van Hoorde, M. Bracke, E. Bruyneel, C. Gespach, and M. Mareel, 2004, Tenascin-C and SF/HGF produced by myofibroblasts in vitro provide convergent pro-invasive signals to human colon cancer cells through RhoA and Rac: *FASEB J*, v. 18, p. 1016-8.
- DeClerck, Y. A., 2000, Interactions between tumour cells and stromal cells and proteolytic modification of the extracellular matrix by metalloproteinases in cancer: *Eur J Cancer*, v. 36, p. 1258-68.

References

- Dehghani, M., S. Kianpour, A. Zangeneh, and Z. Mostafavi-Pour, 2014, CXCL12 Modulates Prostate Cancer Cell Adhesion by Altering the Levels or Activities of β 1-Containing Integrins: *Int J Cell Biol*, v. 2014, p. 981750.
- Desgrosellier, J. S., and D. A. Cheresh, 2010, Integrins in cancer: biological implications and therapeutic opportunities: *Nat Rev Cancer*, v. 10, p. 9-22.
- Desmoulière, A., A. Geinoz, F. Gabbiani, and G. Gabbiani, 1993, Transforming growth factor-beta 1 induces alpha-smooth muscle actin expression in granulation tissue myofibroblasts and in quiescent and growing cultured fibroblasts: *J Cell Biol*, v. 122, p. 103-11.
- Dharmawardhane, S., A. Schürmann, M. A. Sells, J. Chernoff, S. L. Schmid, and G. M. Bokoch, 2000, Regulation of macropinocytosis by p21-activated kinase-1: *Mol Biol Cell*, v. 11, p. 3341-52.
- Dimanche-Boitrel, M. T., L. Vakaet, P. Pujuguet, B. Chauffert, M. S. Martin, A. Hammann, F. Van Roy, M. Mareel, and F. Martin, 1994, In vivo and in vitro invasiveness of a rat colon-cancer cell line maintaining E-cadherin expression: an enhancing role of tumor-associated myofibroblasts: *Int J Cancer*, v. 56, p. 512-21.
- Doherty, G. J., and H. T. McMahon, 2009, Mechanisms of endocytosis: *Annu Rev Biochem*, v. 78, p. 857-902.
- Dolman, N. J., J. A. Kilgore, and M. W. Davidson, 2013, A review of reagents for fluorescence microscopy of cellular compartments and structures, part I: BacMam labeling and reagents for vesicular structures: *Curr Protoc Cytom*, v. Chapter 12, p. Unit 12.30.
- Donnarumma, E., D. Fiore, M. Nappa, G. Roscigno, A. Adamo, M. Iaboni, V. Russo, A. Affinito, I. Puoti, C. Quintavalle, A. Rienzo, S. Piscuoglio, R. Thomas, and G. Condorelli, 2017, Cancer-associated fibroblasts release exosomal microRNAs that dictate an aggressive phenotype in breast cancer: *Oncotarget*, v. 8, p. 19592-19608.
- Dragovic, R. A., C. Gardiner, A. S. Brooks, D. S. Tannetta, D. J. Ferguson, P. Hole, B. Carr, C. W. Redman, A. L. Harris, P. J. Dobson, P. Harrison, and I. L. Sargent, 2011, Sizing and phenotyping of cellular vesicles using Nanoparticle Tracking Analysis: *Nanomedicine*, v. 7, p. 780-8.
- Dunn, K. W., M. M. Kamocka, and J. H. McDonald, 2011, A practical guide to evaluating colocalization in biological microscopy: *Am J Physiol Cell Physiol*, v. 300, p. C723-42.
- Dvorak, H. F., 1986, Tumors: wounds that do not heal. Similarities between tumor stroma generation and wound healing: *N Engl J Med*, v. 315, p. 1650-9.
- Enderle, D., A. Spiel, C. M. Coticchia, E. Berghoff, R. Mueller, M. Schlumpberger, M. Sprenger-Haussels, J. M. Shaffer, E. Lader, J. Skog, and M. Noerholm, 2015, Characterization of RNA from Exosomes and Other Extracellular Vesicles Isolated by a Novel Spin Column-Based Method: *PLoS One*, v. 10, p. e0136133.
- Erdogan, B., and D. J. Webb, 2017, Cancer-associated fibroblasts modulate growth factor signaling and extracellular matrix remodeling to regulate tumor metastasis: *Biochem Soc Trans*, v. 45, p. 229-236.
- Escola, J. M., M. J. Kleijmeer, W. Stoorvogel, J. M. Griffith, O. Yoshie, and H. J. Geuze, 1998, Selective enrichment of tetraspan proteins on the internal vesicles of multivesicular endosomes and on exosomes secreted by human B-lymphocytes: *J Biol Chem*, v. 273, p. 20121-7.
- Escrevente, C., S. Keller, P. Altevogt, and J. Costa, 2011, Interaction and uptake of exosomes by ovarian cancer cells: *BMC Cancer*, v. 11, p. 108.

References

- Fabbri, M., A. Paone, F. Calore, R. Galli, E. Gaudio, R. Santhanam, F. Lovat, P. Fadda, C. Mao, G. J. Nuovo, N. Zanesi, M. Crawford, G. H. Ozer, D. Wernicke, H. Alder, M. A. Caligiuri, P. Nana-Sinkam, D. Perrotti, and C. M. Croce, 2012, MicroRNAs bind to Toll-like receptors to induce prometastatic inflammatory response: *Proc Natl Acad Sci U S A*, v. 109, p. E2110-6.
- Falcón-Pérez, J. M., R. Nazarian, C. Sabatti, and E. C. Dell'Angelica, 2005, Distribution and dynamics of Lamp1-containing endocytic organelles in fibroblasts deficient in BLOC-3: *J Cell Sci*, v. 118, p. 5243-55.
- Fedele, C., A. Singh, B. J. Zerlanko, R. V. Iozzo, and L. R. Languino, 2015, The $\alpha v\beta 6$ integrin is transferred intercellularly via exosomes: *J Biol Chem*, v. 290, p. 4545-51.
- Feng, D., W. L. Zhao, Y. Y. Ye, X. C. Bai, R. Q. Liu, L. F. Chang, Q. Zhou, and S. F. Sui, 2010, Cellular internalization of exosomes occurs through phagocytosis: *Traffic*, v. 11, p. 675-87.
- Fitzner, D., M. Schnaars, D. van Rossum, G. Krishnamoorthy, P. Dibaj, M. Bakhti, T. Regen, U. K. Hanisch, and M. Simons, 2011, Selective transfer of exosomes from oligodendrocytes to microglia by macropinocytosis: *J Cell Sci*, v. 124, p. 447-58.
- Flanagan, M. D., and S. Lin, 1980, Cytochalasins block actin filament elongation by binding to high affinity sites associated with F-actin: *J Biol Chem*, v. 255, p. 835-8.
- Folkman, J., E. Merler, C. Abernathy, and G. Williams, 1971, Isolation of a tumor factor responsible for angiogenesis: *J Exp Med*, v. 133, p. 275-88.
- Franke, W. W., E. Schmid, M. Osborn, and K. Weber, 1978, Different intermediate-sized filaments distinguished by immunofluorescence microscopy: *Proc Natl Acad Sci U S A*, v. 75, p. 5034-8.
- Franzen, C. A., P. E. Simms, A. F. Van Huis, K. E. Foreman, P. C. Kuo, and G. N. Gupta, 2014, Characterization of uptake and internalization of exosomes by bladder cancer cells: *Biomed Res Int*, v. 2014, p. 619829.
- Friedman, J. R., J. R. Dibenedetto, M. West, A. A. Rowland, and G. K. Voeltz, 2013, Endoplasmic reticulum-endosome contact increases as endosomes traffic and mature: *Mol Biol Cell*, v. 24, p. 1030-40.
- Frühbeis, C., D. Fröhlich, W. P. Kuo, J. Amphornrat, S. Thilemann, A. S. Saab, F. Kirchhoff, W. Möbius, S. Goebbels, K. A. Nave, A. Schneider, M. Simons, M. Klugmann, J. Trotter, and E. M. Krämer-Albers, 2013, Neurotransmitter-triggered transfer of exosomes mediates oligodendrocyte-neuron communication: *PLoS Biol*, v. 11, p. e1001604.
- Fukumura, D., R. Xavier, T. Sugiura, Y. Chen, E. C. Park, N. Lu, M. Selig, G. Nielsen, T. Taksir, R. K. Jain, and B. Seed, 1998, Tumor induction of VEGF promoter activity in stromal cells: *Cell*, v. 94, p. 715-25.
- Gabbiani, G., G. B. Ryan, and G. Majne, 1971, Presence of modified fibroblasts in granulation tissue and their possible role in wound contraction: *Experientia*, v. 27, p. 549-50.
- Gaggioli, C., S. Hooper, C. Hidalgo-Carcedo, R. Grosse, J. F. Marshall, K. Harrington, and E. Sahai, 2007, Fibroblast-led collective invasion of carcinoma cells with differing roles for RhoGTPases in leading and following cells: *Nat Cell Biol*, v. 9, p. 1392-400.
- Galletta, B. J., and J. A. Cooper, 2009, Actin and endocytosis: mechanisms and phylogeny: *Curr Opin Cell Biol*, v. 21, p. 20-7.
- Gastpar, R., M. Gehrmann, M. A. Bausero, A. Asea, C. Gross, J. A. Schroeder, and G. Multhoff, 2005, Heat shock protein 70 surface-positive tumor exosomes

References

- stimulate migratory and cytolytic activity of natural killer cells: *Cancer Res*, v. 65, p. 5238-47.
- Gilbert, C. A., and J. M. Slingerland, 2013, Cytokines, obesity, and cancer: new insights on mechanisms linking obesity to cancer risk and progression: *Annu Rev Med*, v. 64, p. 45-57.
- Gleason, D. F., and G. T. Mellinger, 1974, Prediction of prognosis for prostatic adenocarcinoma by combined histological grading and clinical staging: *J Urol*, v. 111, p. 58-64.
- Glebov, O. O., N. A. Bright, and B. J. Nichols, 2006, Flotillin-1 defines a clathrin-independent endocytic pathway in mammalian cells: *Nat Cell Biol*, v. 8, p. 46-54.
- Goel, H. L., J. Li, S. Kogan, and L. R. Languino, 2008, Integrins in prostate cancer progression: *Endocr Relat Cancer*, v. 15, p. 657-64.
- Gould, S. J., and G. Raposo, 2013, As we wait: coping with an imperfect nomenclature for extracellular vesicles: *J Extracell Vesicles*, v. 2.
- Gray, W. D., A. J. Mitchell, and C. D. Searles, 2015, An accurate, precise method for general labeling of extracellular vesicles: *MethodsX*, v. 2, p. 360-7.
- Gu, J., H. Qian, L. Shen, X. Zhang, W. Zhu, L. Huang, Y. Yan, F. Mao, C. Zhao, Y. Shi, and W. Xu, 2012, Gastric cancer exosomes trigger differentiation of umbilical cord derived mesenchymal stem cells to carcinoma-associated fibroblasts through TGF- β /Smad pathway: *PLoS One*, v. 7, p. e52465.
- Guo, W., and F. G. Giancotti, 2004, Integrin signalling during tumour progression: *Nat Rev Mol Cell Biol*, v. 5, p. 816-26.
- Hanahan, D., and R. A. Weinberg, 2011, Hallmarks of cancer: the next generation: *Cell*, v. 144, p. 646-74.
- Hanson, P. I., and A. Cashikar, 2012, Multivesicular body morphogenesis: *Annu Rev Cell Dev Biol*, v. 28, p. 337-62.
- Haraszti, R. A., R. Miller, M. Stoppato, Y. Y. Sere, A. Coles, M. C. Didiot, R. Wollacott, E. Sapp, M. L. Dubuke, X. Li, S. A. Shaffer, M. DiFiglia, Y. Wang, N. Aronin, and A. Khvorova, 2018, Exosomes Produced from 3D Cultures of MSCs by Tangential Flow Filtration Show Higher Yield and Improved Activity: *Mol Ther*, v. 26, p. 2838-2847.
- Harburger, D. S., and D. A. Calderwood, 2009, Integrin signalling at a glance: *J Cell Sci*, v. 122, p. 159-63.
- Harding, C., J. Heuser, and P. Stahl, 1983, Receptor-mediated endocytosis of transferrin and recycling of the transferrin receptor in rat reticulocytes: *J Cell Biol*, v. 97, p. 329-39.
- Heidenreich, A., P. J. Bastian, J. Bellmunt, M. Bolla, S. Joniau, T. van der Kwast, M. Mason, V. Matveev, T. Wiegel, F. Zattoni, N. Mottet, and E. A. o. Urology, 2014, EAU guidelines on prostate cancer. part 1: screening, diagnosis, and local treatment with curative intent-update 2013: *Eur Urol*, v. 65, p. 124-37.
- Heijnen, H. F., A. E. Schiel, R. Fijnheer, H. J. Geuze, and J. J. Sixma, 1999, Activated platelets release two types of membrane vesicles: microvesicles by surface shedding and exosomes derived from exocytosis of multivesicular bodies and alpha-granules: *Blood*, v. 94, p. 3791-9.
- Hernandez, D. J., M. E. Nielsen, M. Han, and A. W. Partin, 2007, Contemporary evaluation of the D'amico risk classification of prostate cancer: *Urology*, v. 70, p. 931-5.
- Hess, C., S. Sadallah, A. Hefti, R. Landmann, and J. A. Schifferli, 1999, Ectosomes released by human neutrophils are specialized functional units: *J Immunol*, v. 163, p. 4564-73.

References

- Heusermann, W., J. Hean, D. Trojer, E. Steib, S. von Bueren, A. Graff-Meyer, C. Genoud, K. Martin, N. Pizzato, J. Voshol, D. V. Morrissey, S. E. Andaloussi, M. J. Wood, and N. C. Meisner-Kober, 2016, Exosomes surf on filopodia to enter cells at endocytic hot spots, traffic within endosomes, and are targeted to the ER: *J Cell Biol*, v. 213, p. 173-84.
- Holmgren, L., M. S. O'Reilly, and J. Folkman, 1995, Dormancy of micrometastases: balanced proliferation and apoptosis in the presence of angiogenesis suppression: *Nat Med*, v. 1, p. 149-53.
- Hong, B. S., J. H. Cho, H. Kim, E. J. Choi, S. Rho, J. Kim, J. H. Kim, D. S. Choi, Y. K. Kim, D. Hwang, and Y. S. Gho, 2009, Colorectal cancer cell-derived microvesicles are enriched in cell cycle-related mRNAs that promote proliferation of endothelial cells: *BMC Genomics*, v. 10, p. 556.
- Hood, J. L., R. S. San, and S. A. Wickline, 2011, Exosomes released by melanoma cells prepare sentinel lymph nodes for tumor metastasis: *Cancer Res*, v. 71, p. 3792-801.
- Hoshino, A., B. Costa-Silva, T. L. Shen, G. Rodrigues, A. Hashimoto, M. Tesic Mark, H. Molina, S. Kohsaka, A. Di Giannatale, S. Ceder, S. Singh, C. Williams, N. Soplop, K. Uryu, L. Pharmed, T. King, L. Bojmar, A. E. Davies, Y. Ararso, T. Zhang, H. Zhang, J. Hernandez, J. M. Weiss, V. D. Dumont-Cole, K. Kramer, L. H. Wexler, A. Narendran, G. K. Schwartz, J. H. Healey, P. Sandstrom, K. J. Labori, E. H. Kure, P. M. Grandgenett, M. A. Hollingsworth, M. de Sousa, S. Kaur, M. Jain, K. Mallya, S. K. Batra, W. R. Jarnagin, M. S. Brady, O. Fodstad, V. Muller, K. Pantel, A. J. Minn, M. J. Bissell, B. A. Garcia, Y. Kang, V. K. Rajasekhar, C. M. Ghajar, I. Matei, H. Peinado, J. Bromberg, and D. Lyden, 2015, Tumour exosome integrins determine organotropic metastasis: *Nature*, v. 527, p. 329-35.
- Hosogi, S., H. Miyazaki, K. Nakajima, E. Ashihara, N. Niisato, K. Kusuzaki, and Y. Marunaka, 2012, An inhibitor of Na(+)/H(+) exchanger (NHE), ethyl-isopropyl amiloride (EIPA), diminishes proliferation of MKN28 human gastric cancer cells by decreasing the cytosolic Cl(-) concentration via DIDS-sensitive pathways: *Cell Physiol Biochem*, v. 30, p. 1241-53.
- Hristov, M., W. Erl, S. Linder, and P. C. Weber, 2004, Apoptotic bodies from endothelial cells enhance the number and initiate the differentiation of human endothelial progenitor cells in vitro: *Blood*, v. 104, p. 2761-6.
- Hsieh, C. S., H. M. Lee, and C. W. Lio, 2012, Selection of regulatory T cells in the thymus: *Nat Rev Immunol*, v. 12, p. 157-67.
- Humphries, J. D., A. Byron, and M. J. Humphries, 2006, Integrin ligands at a glance: *J Cell Sci*, v. 119, p. 3901-3.
- Huotari, J., and A. Helenius, 2011, Endosome maturation: *EMBO J*, v. 30, p. 3481-500.
- Hurwitz, H., L. Fehrenbacher, W. Novotny, T. Cartwright, J. Hainsworth, W. Heim, J. Berlin, A. Baron, S. Griffing, E. Holmgren, N. Ferrara, G. Fyfe, B. Rogers, R. Ross, and F. Kabbinavar, 2004, Bevacizumab plus irinotecan, fluorouracil, and leucovorin for metastatic colorectal cancer: *N Engl J Med*, v. 350, p. 2335-42.
- Ivanov, A. I., 2008, Pharmacological inhibition of endocytic pathways: is it specific enough to be useful?: *Methods Mol Biol*, v. 440, p. 15-33.
- Jain, R. K., 2005, Normalization of tumor vasculature: an emerging concept in antiangiogenic therapy: *Science*, v. 307, p. 58-62.
- Jodoin, J., and M. T. Hincke, 2018, Histone H5 is a potent Antimicrobial Agent and a template for novel Antimicrobial Peptides: *Sci Rep*, v. 8, p. 2411.

References

- Johnsen, K. B., J. M. Gudbergsson, M. N. Skov, L. Pilgaard, T. Moos, and M. Duroux, 2014, A comprehensive overview of exosomes as drug delivery vehicles - endogenous nanocarriers for targeted cancer therapy: *Biochim Biophys Acta*, v. 1846, p. 75-87.
- Johnstone, R. M., M. Adam, J. R. Hammond, L. Orr, and C. Turbide, 1987, Vesicle formation during reticulocyte maturation. Association of plasma membrane activities with released vesicles (exosomes): *J Biol Chem*, v. 262, p. 9412-20.
- Kalluri, R., 2016, The biology and function of fibroblasts in cancer: *Nat Rev Cancer*, v. 16, p. 582-98.
- Kalra, H., R. J. Simpson, H. Ji, E. Aikawa, P. Altevogt, P. Askenase, V. C. Bond, F. E. Borràs, X. Breakefield, V. Budnik, E. Buzas, G. Camussi, A. Clayton, E. Cocucci, J. M. Falcon-Perez, S. Gabrielsson, Y. S. Ghossein, D. Gupta, H. C. Harsha, A. Hendrix, A. F. Hill, J. M. Inal, G. Jenster, E. M. Krämer-Albers, S. K. Lim, A. Llorente, J. Lötvall, A. Marcilla, L. Mincheva-Nilsson, I. Nazarenko, R. Nieuwland, E. N. Nolte-'t Hoen, A. Pandey, T. Patel, M. G. Piper, S. Pluchino, T. S. Prasad, L. Rajendran, G. Raposo, M. Record, G. E. Reid, F. Sánchez-Madrid, R. M. Schiffelers, P. Siljander, A. Stensballe, W. Stoorvogel, D. Taylor, C. Thery, H. Valadi, B. W. van Balkom, J. Vázquez, M. Vidal, M. H. Wauben, M. Yáñez-Mó, M. Zoeller, and S. Mathivanan, 2012, Vesiclepedia: a compendium for extracellular vesicles with continuous community annotation: *PLoS Biol*, v. 10, p. e1001450.
- Karimi, N., A. Cvjetkovic, S. C. Jang, R. Crescitelli, M. A. Hosseinpour Feizi, R. Nieuwland, J. Lötvall, and C. Lässer, 2018, Detailed analysis of the plasma extracellular vesicle proteome after separation from lipoproteins: *Cell Mol Life Sci*, v. 75, p. 2873-2886.
- Keller, S., J. Ridinger, A. K. Rupp, J. W. Janssen, and P. Altevogt, 2011, Body fluid derived exosomes as a novel template for clinical diagnostics: *J Transl Med*, v. 9, p. 86.
- Kielian, M. C., M. Marsh, and A. Helenius, 1986, Kinetics of endosome acidification detected by mutant and wild-type Semliki Forest virus: *EMBO J*, v. 5, p. 3103-9.
- Kim, D. K., J. Lee, S. R. Kim, D. S. Choi, Y. J. Yoon, J. H. Kim, G. Go, D. Nhung, K. Hong, S. C. Jang, S. H. Kim, K. S. Park, O. Y. Kim, H. T. Park, J. H. Seo, E. Aikawa, M. Baj-Krzyworzeka, B. W. van Balkom, M. Belting, L. Blanc, V. Bond, A. Bongiovanni, F. E. Borràs, L. Buée, E. I. Buzás, L. Cheng, A. Clayton, E. Cocucci, C. S. Dela Cruz, D. M. Desiderio, D. Di Vizio, K. Ekström, J. M. Falcon-Perez, C. Gardiner, B. Giebel, D. W. Greening, J. C. Gross, D. Gupta, A. Hendrix, A. F. Hill, M. M. Hill, E. Nolte-'t Hoen, D. W. Hwang, J. Inal, M. V. Jagannadham, M. Jayachandran, Y. K. Jee, M. Jørgensen, K. P. Kim, Y. K. Kim, T. Kislinger, C. Lässer, D. S. Lee, H. Lee, J. van Leeuwen, T. Lener, M. L. Liu, J. Lötvall, A. Marcilla, S. Mathivanan, A. Möller, J. Morhayim, F. Mullier, I. Nazarenko, R. Nieuwland, D. N. Nunes, K. Pang, J. Park, T. Patel, G. Pocsfalvi, H. Del Portillo, U. Putz, M. I. Ramirez, M. L. Rodrigues, T. Y. Roh, F. Royo, S. Sahoo, R. Schiffelers, S. Sharma, P. Siljander, R. J. Simpson, C. Soekmadji, P. Stahl, A. Stensballe, E. Stępień, H. Tahara, A. Trummer, H. Valadi, L. J. Vella, S. N. Wai, K. Witwer, M. Yáñez-Mó, H. Youn, R. Zeidler, and Y. S. Ghossein, 2015, EVpedia: a community web portal for extracellular vesicles research: *Bioinformatics*, v. 31, p. 933-9.
- King, H. W., M. Z. Michael, and J. M. Gleadle, 2012, Hypoxic enhancement of exosome release by breast cancer cells: *BMC Cancer*, v. 12, p. 421.

References

- Kinner, B., J. M. Zaleskas, and M. Spector, 2002, Regulation of smooth muscle actin expression and contraction in adult human mesenchymal stem cells: *Exp Cell Res*, v. 278, p. 72-83.
- Kirchhausen, T., 2000, Clathrin: *Annu Rev Biochem*, v. 69, p. 699-727.
- Kirkham, M., A. Fujita, R. Chadda, S. J. Nixon, T. V. Kurzchalia, D. K. Sharma, R. E. Pagano, J. F. Hancock, S. Mayor, and R. G. Parton, 2005, Ultrastructural identification of uncoated caveolin-independent early endocytic vehicles: *J Cell Biol*, v. 168, p. 465-76.
- Klibi, J., T. Niki, A. Riedel, C. Pioche-Durieu, S. Souquere, E. Rubinstein, S. Le Moulec, S. L. Moulec, J. Guigay, M. Hirashima, F. Guemira, D. Adhikary, J. Mautner, and P. Busson, 2009, Blood diffusion and Th1-suppressive effects of galectin-9-containing exosomes released by Epstein-Barr virus-infected nasopharyngeal carcinoma cells: *Blood*, v. 113, p. 1957-66.
- Kooijmans, S. A. A., J. J. M. Gitz-Francois, R. M. Schiffelers, and P. Vader, 2018, Recombinant phosphatidylserine-binding nanobodies for targeting of extracellular vesicles to tumor cells: a plug-and-play approach: *Nanoscale*, v. 10, p. 2413-2426.
- Koumangoye, R. B., A. M. Sakwe, J. S. Goodwin, T. Patel, and J. Ochieng, 2011, Detachment of breast tumor cells induces rapid secretion of exosomes which subsequently mediate cellular adhesion and spreading: *PLoS One*, v. 6, p. e24234.
- Kumar, V. L., and P. K. Majumder, 1995, Prostate gland: structure, functions and regulation: *Int Urol Nephrol*, v. 27, p. 231-43.
- Lagacé, R., J. A. Grimaud, W. Schürch, and T. A. Seemayer, 1985, Myofibroblastic stromal reaction in carcinoma of the breast: variations of collagenous matrix and structural glycoproteins: *Virchows Arch A Pathol Anat Histopathol*, v. 408, p. 49-59.
- Lagana, A., J. Vadnais, P. U. Le, T. N. Nguyen, R. Laprade, I. R. Nabi, and J. Noël, 2000, Regulation of the formation of tumor cell pseudopodia by the Na(+)/H(+) exchanger NHE1: *J Cell Sci*, v. 113 (Pt 20), p. 3649-62.
- Lai, C. P., E. Y. Kim, C. E. Badr, R. Weissleder, T. R. Mempel, B. A. Tannous, and X. O. Breakefield, 2015, Visualization and tracking of tumour extracellular vesicle delivery and RNA translation using multiplexed reporters: *Nat Commun*, v. 6, p. 7029.
- Lai, R. C., T. S. Chen, and S. K. Lim, 2011, Mesenchymal stem cell exosome: a novel stem cell-based therapy for cardiovascular disease: *Regen Med*, v. 6, p. 481-92.
- Lamaze, C., L. M. Fujimoto, H. L. Yin, and S. L. Schmid, 1997, The actin cytoskeleton is required for receptor-mediated endocytosis in mammalian cells: *J Biol Chem*, v. 272, p. 20332-5.
- Lamparski, H. G., A. Metha-Damani, J. Y. Yao, S. Patel, D. H. Hsu, C. Ruegg, and J. B. Le Pecq, 2002, Production and characterization of clinical grade exosomes derived from dendritic cells: *J Immunol Methods*, v. 270, p. 211-26.
- Lee, H. D., B. H. Koo, Y. H. Kim, O. H. Jeon, and D. S. Kim, 2012, Exosome release of ADAM15 and the functional implications of human macrophage-derived ADAM15 exosomes: *FASEB J*, v. 26, p. 3084-95.
- Leitzmann, M. F., and S. Rohrmann, 2012, Risk factors for the onset of prostatic cancer: age, location, and behavioral correlates: *Clin Epidemiol*, v. 4, p. 1-11.
- Li, M., E. Zeringer, T. Barta, J. Schageman, A. Cheng, and A. V. Vlassov, 2014, Analysis of the RNA content of the exosomes derived from blood serum and

References

- urine and its potential as biomarkers: *Philos Trans R Soc Lond B Biol Sci*, v. 369.
- Lin, E. Y., J. F. Li, L. Gnatovskiy, Y. Deng, L. Zhu, D. A. Grzesik, H. Qian, X. N. Xue, and J. W. Pollard, 2006, Macrophages regulate the angiogenic switch in a mouse model of breast cancer: *Cancer Res*, v. 66, p. 11238-46.
- Linares, R., S. Tan, C. Gounou, N. Arraud, and A. R. Brisson, 2015, High-speed centrifugation induces aggregation of extracellular vesicles: *J Extracell Vesicles*, v. 4, p. 29509.
- Liu, A. Y., 2000, Differential expression of cell surface molecules in prostate cancer cells: *Cancer Res*, v. 60, p. 3429-34.
- Liu, A. Y., L. D. True, L. LaTray, W. J. Ellis, R. L. Vessella, P. H. Lange, C. S. Higano, L. Hood, and G. van den Engh, 1999, Analysis and sorting of prostate cancer cell types by flow cytometry: *Prostate*, v. 40, p. 192-9.
- Llorente, A., T. Skotland, T. Sylvänne, D. Kauhanen, T. Róg, A. Orłowski, I. Vattulainen, K. Ekroos, and K. Sandvig, 2013, Molecular lipidomics of exosomes released by PC-3 prostate cancer cells: *Biochim Biophys Acta*, v. 1831, p. 1302-9.
- Lobb, R. J., M. Becker, S. W. Wen, C. S. Wong, A. P. Wiegman, A. Leimgruber, and A. Möller, 2015, Optimized exosome isolation protocol for cell culture supernatant and human plasma: *J Extracell Vesicles*, v. 4, p. 27031.
- Longatti, A., C. Schindler, A. Collinson, L. Jenkinson, C. Matthews, L. Fitzpatrick, M. Blundy, R. Minter, T. Vaughan, M. Shaw, and N. Tigue, 2018, High affinity single-chain variable fragments are specific and versatile targeting motifs for extracellular vesicles: *Nanoscale*, v. 10, p. 14230-14244.
- Lu, P., K. Takai, V. M. Weaver, and Z. Werb, 2011, Extracellular matrix degradation and remodeling in development and disease: *Cold Spring Harb Perspect Biol*, v. 3.
- Ludwig, N., and T. L. Whiteside, 2018, Potential roles of tumor-derived exosomes in angiogenesis: *Expert Opin Ther Targets*, v. 22, p. 409-417.
- Luzio, J. P., P. R. Pryor, and N. A. Bright, 2007, Lysosomes: fusion and function: *Nat Rev Mol Cell Biol*, v. 8, p. 622-32.
- Lázaro-Ibáñez, E., M. Neuvonen, M. Takatalo, U. Thanigai Arasu, C. Capasso, V. Cerullo, J. S. Rhim, K. Rilla, M. Yliperttula, and P. R. Siljander, 2017, Metastatic state of parent cells influences the uptake and functionality of prostate cancer cell-derived extracellular vesicles: *J Extracell Vesicles*, v. 6, p. 1354645.
- Lötvall, J., A. F. Hill, F. Hochberg, E. I. Buzás, D. Di Vizio, C. Gardiner, Y. S. Ghossein, I. V. Kurochkin, S. Mathivanan, P. Quesenberry, S. Sahoo, H. Tahara, M. H. Wauben, K. W. Witwer, and C. Théry, 2014, Minimal experimental requirements for definition of extracellular vesicles and their functions: a position statement from the International Society for Extracellular Vesicles: *J Extracell Vesicles*, v. 3, p. 26913.
- Maida, Y., M. Takakura, T. Nishiuchi, T. Yoshimoto, and S. Kyo, 2016, Exosomal transfer of functional small RNAs mediates cancer-stroma communication in human endometrium: *Cancer Med*, v. 5, p. 304-14.
- Marks, B., M. H. Stowell, Y. Vallis, I. G. Mills, A. Gibson, C. R. Hopkins, and H. T. McMahon, 2001, GTPase activity of dynamin and resulting conformation change are essential for endocytosis: *Nature*, v. 410, p. 231-5.
- Martin, M., P. Pujuguet, and F. Martin, 1996, Role of stromal myofibroblasts infiltrating colon cancer in tumor invasion: *Pathol Res Pract*, v. 192, p. 712-7.

References

- Mathivanan, S., J. W. Lim, B. J. Tauro, H. Ji, R. L. Moritz, and R. J. Simpson, 2010, Proteomics analysis of A33 immunoaffinity-purified exosomes released from the human colon tumor cell line LIM1215 reveals a tissue-specific protein signature: *Mol Cell Proteomics*, v. 9, p. 197-208.
- Maxfield, F. R., and D. J. Yamashiro, 1987, Endosome acidification and the pathways of receptor-mediated endocytosis: *Adv Exp Med Biol*, v. 225, p. 189-98.
- Mayle, K. M., A. M. Le, and D. T. Kamei, 2012, The intracellular trafficking pathway of transferrin: *Biochim Biophys Acta*, v. 1820, p. 264-81.
- Mayor, S., and R. E. Pagano, 2007, Pathways of clathrin-independent endocytosis: *Nat Rev Mol Cell Biol*, v. 8, p. 603-12.
- Mellman, I., 1996, Endocytosis and molecular sorting: *Annu Rev Cell Dev Biol*, v. 12, p. 575-625.
- Midgley, A. C., M. Rogers, M. B. Hallett, A. Clayton, T. Bowen, A. O. Phillips, and R. Steadman, 2013, Transforming growth factor- β 1 (TGF- β 1)-stimulated fibroblast to myofibroblast differentiation is mediated by hyaluronan (HA)-facilitated epidermal growth factor receptor (EGFR) and CD44 co-localization in lipid rafts: *J Biol Chem*, v. 288, p. 14824-38.
- Mitchell, J. P., J. Court, M. D. Mason, Z. Tabi, and A. Clayton, 2008, Increased exosome production from tumour cell cultures using the Integra CELLine Culture System: *J Immunol Methods*, v. 335, p. 98-105.
- Miyamoto, H., T. Murakami, K. Tsuchida, H. Sugino, H. Miyake, and S. Tashiro, 2004, Tumor-stroma interaction of human pancreatic cancer: acquired resistance to anticancer drugs and proliferation regulation is dependent on extracellular matrix proteins: *Pancreas*, v. 28, p. 38-44.
- Montecalvo, A., A. T. Larregina, W. J. Shufesky, D. B. Stolz, M. L. Sullivan, J. M. Karlsson, C. J. Baty, G. A. Gibson, G. Erdos, Z. Wang, J. Milosevic, O. A. Tkacheva, S. J. Divito, R. Jordan, J. Lyons-Weiler, S. C. Watkins, and A. E. Morelli, 2012, Mechanism of transfer of functional microRNAs between mouse dendritic cells via exosomes: *Blood*, v. 119, p. 756-66.
- Montironi, R., R. Mazzucchelli, F. Algaba, and A. Lopez-Beltran, 2000, Morphological identification of the patterns of prostatic intraepithelial neoplasia and their importance: *J Clin Pathol*, v. 53, p. 655-65.
- Moorman, A. M., R. Vink, H. J. Heijmans, J. van der Palen, and E. A. Kouwenhoven, 2012, The prognostic value of tumour-stroma ratio in triple-negative breast cancer: *Eur J Surg Oncol*, v. 38, p. 307-13.
- Morales-Kastresana, A., B. Telford, T. A. Musich, K. McKinnon, C. Clayborne, Z. Braig, A. Rosner, T. Demberg, D. C. Watson, T. S. Karpova, G. J. Freeman, R. H. DeKruyff, G. N. Pavlakis, M. Terabe, M. Robert-Guroff, J. A. Berzofsky, and J. C. Jones, 2017, Labeling Extracellular Vesicles for Nanoscale Flow Cytometry: *Sci Rep*, v. 7, p. 1878.
- Morelli, A. E., A. T. Larregina, W. J. Shufesky, M. L. Sullivan, D. B. Stolz, G. D. Papworth, A. F. Zahorchak, A. J. Logar, Z. Wang, S. C. Watkins, L. D. Faló, and A. W. Thomson, 2004, Endocytosis, intracellular sorting, and processing of exosomes by dendritic cells: *Blood*, v. 104, p. 3257-66.
- Mudhakar, D., and H. Harashima, 2009, Learning from the viral journey: how to enter cells and how to overcome intracellular barriers to reach the nucleus: *AAPS J*, v. 11, p. 65-77.
- Mulcahy, L. A., R. C. Pink, and D. R. Carter, 2014, Routes and mechanisms of extracellular vesicle uptake: *J Extracell Vesicles*, v. 3.

References

- Muralidharan-Chari, V., J. Clancy, C. Plou, M. Romao, P. Chavrier, G. Raposo, and C. D'Souza-Schorey, 2009, ARF6-regulated shedding of tumor cell-derived plasma membrane microvesicles: *Curr Biol*, v. 19, p. 1875-85.
- Murphy, G. P., C. Mettlin, H. Menck, D. P. Winchester, and A. M. Davidson, 1994, National patterns of prostate cancer treatment by radical prostatectomy: results of a survey by the American College of Surgeons Commission on Cancer: *J Urol*, v. 152, p. 1817-9.
- Nabi, I. R., and P. U. Le, 2003, Caveolae/raft-dependent endocytosis: *J Cell Biol*, v. 161, p. 673-7.
- Nakase, I., N. B. Kobayashi, T. Takatani-Nakase, and T. Yoshida, 2015, Active macropinocytosis induction by stimulation of epidermal growth factor receptor and oncogenic Ras expression potentiates cellular uptake efficacy of exosomes: *Sci Rep*, v. 5, p. 10300.
- Nakase, I., K. Noguchi, I. Fujii, and S. Futaki, 2016, Vectorization of biomacromolecules into cells using extracellular vesicles with enhanced internalization induced by macropinocytosis: *Sci Rep*, v. 6, p. 34937.
- Nanbo, A., E. Kawanishi, R. Yoshida, and H. Yoshiyama, 2013, Exosomes derived from Epstein-Barr virus-infected cells are internalized via caveola-dependent endocytosis and promote phenotypic modulation in target cells: *J Virol*, v. 87, p. 10334-47.
- Nazarenko, I., S. Rana, A. Baumann, J. McAlear, A. Hellwig, M. Trendelenburg, G. Lochnit, K. T. Preissner, and M. Zöller, 2010, Cell surface tetraspanin Tspan8 contributes to molecular pathways of exosome-induced endothelial cell activation: *Cancer Res*, v. 70, p. 1668-78.
- Newton, A. J., T. Kirchhausen, and V. N. Murthy, 2006, Inhibition of dynamin completely blocks compensatory synaptic vesicle endocytosis: *Proc Natl Acad Sci U S A*, v. 103, p. 17955-60.
- Nielsen, E., F. Severin, J. M. Backer, A. A. Hyman, and M. Zerial, 1999, Rab5 regulates motility of early endosomes on microtubules: *Nat Cell Biol*, v. 1, p. 376-82.
- Nishio, R., Y. Furuya, O. Nagakawa, and H. Fuse, 2003, Metastatic prostate cancer with normal level of serum prostate-specific antigen: *Int Urol Nephrol*, v. 35, p. 189-92.
- Nolte-'t Hoen, E. N., E. J. van der Vlist, M. Aalberts, H. C. Mertens, B. J. Bosch, W. Bartelink, E. Mastrobattista, E. V. van Gaal, W. Stoorvogel, G. J. Arkesteijn, and M. H. Wauben, 2012, Quantitative and qualitative flow cytometric analysis of nanosized cell-derived membrane vesicles: *Nanomedicine*, v. 8, p. 712-20.
- O'Keefe, M. B., A. H. Devlin, A. J. Burns, T. A. Gardiner, I. D. Logan, D. G. Hirst, and S. R. McKeown, 2008, Investigation of pericytes, hypoxia, and vascularity in bladder tumors: association with clinical outcomes: *Oncol Res*, v. 17, p. 93-101.
- Oesterling, J. E., S. J. Jacobsen, C. G. Chute, H. A. Guess, C. J. Girman, L. A. Panser, and M. M. Lieber, 1993, Serum prostate-specific antigen in a community-based population of healthy men. Establishment of age-specific reference ranges: *JAMA*, v. 270, p. 860-4.
- Ohno, S., M. Takanashi, K. Sudo, S. Ueda, A. Ishikawa, N. Matsuyama, K. Fujita, T. Mizutani, T. Ohgi, T. Ochiya, N. Gotoh, and M. Kuroda, 2013, Systemically injected exosomes targeted to EGFR deliver antitumor microRNA to breast cancer cells: *Mol Ther*, v. 21, p. 185-91.

References

- Olumi, A. F., G. D. Grossfeld, S. W. Hayward, P. R. Carroll, T. D. Tlsty, and G. R. Cunha, 1999, Carcinoma-associated fibroblasts direct tumor progression of initiated human prostatic epithelium: *Cancer Res*, v. 59, p. 5002-11.
- Osteikoetxea, X., A. Balogh, K. Szabó-Taylor, A. Németh, T. G. Szabó, K. Pálóczi, B. Sódar, Á. Kittel, B. György, É. Pállinger, J. Matkó, and E. I. Buzás, 2015, Improved characterization of EV preparations based on protein to lipid ratio and lipid properties: *PLoS One*, v. 10, p. e0121184.
- Ostrowski, M., N. B. Carmo, S. Krumeich, I. Fanget, G. Raposo, A. Savina, C. F. Moita, K. Schauer, A. N. Hume, R. P. Freitas, B. Goud, P. Benaroch, N. Hacohen, M. Fukuda, C. Desnos, M. C. Seabra, F. Darchen, S. Amigorena, L. F. Moita, and C. Thery, 2010, Rab27a and Rab27b control different steps of the exosome secretion pathway: *Nat Cell Biol*, v. 12, p. 19-30; sup pp 1-13.
- Pan, B. T., K. Teng, C. Wu, M. Adam, and R. M. Johnstone, 1985, Electron microscopic evidence for externalization of the transferrin receptor in vesicular form in sheep reticulocytes: *J Cell Biol*, v. 101, p. 942-8.
- Pan, Q., V. Ramakrishnaiah, S. Henry, S. Fouraschen, P. E. de Ruiter, J. Kwekkeboom, H. W. Tilanus, H. L. Janssen, and L. J. van der Laan, 2012, Hepatic cell-to-cell transmission of small silencing RNA can extend the therapeutic reach of RNA interference (RNAi): *Gut*, v. 61, p. 1330-9.
- Panchuk-Voloshina, N., R. P. Haugland, J. Bishop-Stewart, M. K. Bhalgat, P. J. Millard, F. Mao, and W. Y. Leung, 1999, Alexa dyes, a series of new fluorescent dyes that yield exceptionally bright, photostable conjugates: *J Histochem Cytochem*, v. 47, p. 1179-88.
- Parasassi, T., R. Brunelli, G. Costa, M. De Spirito, E. Krasnowska, T. Lundeberg, E. Pittaluga, and F. Ursini, 2010, Thiol redox transitions in cell signaling: a lesson from N-acetylcysteine: *ScientificWorldJournal*, v. 10, p. 1192-202.
- Parish, C. R., 1999, Fluorescent dyes for lymphocyte migration and proliferation studies: *Immunol Cell Biol*, v. 77, p. 499-508.
- Parolini, I., C. Federici, C. Raggi, L. Lugini, S. Palleschi, A. De Milito, C. Coscia, E. Iessi, M. Logozzi, A. Molinari, M. Colone, M. Tatti, M. Sargiacomo, and S. Fais, 2009, Microenvironmental pH is a key factor for exosome traffic in tumor cells: *J Biol Chem*, v. 284, p. 34211-22.
- Parton, R. G., and K. Simons, 2007, The multiple faces of caveolae: *Nat Rev Mol Cell Biol*, v. 8, p. 185-94.
- Payne, C. K., S. A. Jones, C. Chen, and X. Zhuang, 2007, Internalization and trafficking of cell surface proteoglycans and proteoglycan-binding ligands: *Traffic*, v. 8, p. 389-401.
- Pegtel, D. M., K. Cosmopoulos, D. A. Thorley-Lawson, M. A. van Eijndhoven, E. S. Hopmans, J. L. Lindenberg, T. D. de Gruijl, T. Würdinger, and J. M. Middeldorp, 2010, Functional delivery of viral miRNAs via exosomes: *Proc Natl Acad Sci U S A*, v. 107, p. 6328-33.
- Peinado, H., M. Alečković, S. Lavotshkin, I. Matei, B. Costa-Silva, G. Moreno-Bueno, M. Hergueta-Redondo, C. Williams, G. García-Santos, C. Ghajar, A. Nitadori-Hoshino, C. Hoffman, K. Badal, B. A. Garcia, M. K. Callahan, J. Yuan, V. R. Martins, J. Skog, R. N. Kaplan, M. S. Brady, J. D. Wolchok, P. B. Chapman, Y. Kang, J. Bromberg, and D. Lyden, 2012, Melanoma exosomes educate bone marrow progenitor cells toward a pro-metastatic phenotype through MET: *Nat Med*, v. 18, p. 883-91.
- Petersen, O. W., H. L. Nielsen, T. Gudjonsson, R. Villadsen, F. Rank, E. Niebuhr, M. J. Bissell, and L. Rønnov-Jessen, 2003, Epithelial to mesenchymal transition in

References

- human breast cancer can provide a nonmalignant stroma: *Am J Pathol*, v. 162, p. 391-402.
- Pienta, K. J., 2001, Preclinical mechanisms of action of docetaxel and docetaxel combinations in prostate cancer: *Semin Oncol*, v. 28, p. 3-7.
- Plebanek, M. P., R. K. Mutharasan, O. Volpert, A. Matov, J. C. Gatlin, and C. S. Thaxton, 2015, Nanoparticle Targeting and Cholesterol Flux Through Scavenger Receptor Type B-1 Inhibits Cellular Exosome Uptake: *Sci Rep*, v. 5, p. 15724.
- Pospichalova, V., J. Svoboda, Z. Dave, A. Kotrbova, K. Kaiser, D. Klemova, L. Ilkovics, A. Hampl, I. Crha, E. Jandakova, L. Minar, V. Weinberger, and V. Bryja, 2015, Simplified protocol for flow cytometry analysis of fluorescently labeled exosomes and microvesicles using dedicated flow cytometer: *J Extracell Vesicles*, v. 4, p. 25530.
- Prajapati, P., and D. W. Lambert, 2016, Cancer-associated fibroblasts - Not-so-innocent bystanders in metastasis to bone?: *J Bone Oncol*, v. 5, p. 128-131.
- Pužar Dominkuš, P., M. Stenovec, S. Sitar, E. Lasič, R. Zorec, A. Plemenitaš, E. Žagar, M. Kreft, and M. Lenassi, 2018, PKH26 labeling of extracellular vesicles: Characterization and cellular internalization of contaminating PKH26 nanoparticles: *Biochim Biophys Acta Biomembr*, v. 1860, p. 1350-1361.
- Qian, B. Z., and J. W. Pollard, 2010, Macrophage diversity enhances tumor progression and metastasis: *Cell*, v. 141, p. 39-51.
- Quah, B. J., and C. R. Parish, 2010, The use of carboxyfluorescein diacetate succinimidyl ester (CFSE) to monitor lymphocyte proliferation: *J Vis Exp*.
- Rao, S. K., C. Huynh, V. Proux-Gillardeaux, T. Galli, and N. W. Andrews, 2004, Identification of SNAREs involved in synaptotagmin VII-regulated lysosomal exocytosis: *J Biol Chem*, v. 279, p. 20471-9.
- Raposo, G., H. W. Nijman, W. Stoorvogel, R. Liejendekker, C. V. Harding, C. J. Melief, and H. J. Geuze, 1996, B lymphocytes secrete antigen-presenting vesicles: *J Exp Med*, v. 183, p. 1161-72.
- Raposo, G., and W. Stoorvogel, 2013, Extracellular vesicles: exosomes, microvesicles, and friends: *J Cell Biol*, v. 200, p. 373-83.
- Ravetch, J. V., and J. P. Kinet, 1991, Fc receptors: *Annu Rev Immunol*, v. 9, p. 457-92.
- Reungpatthanaphong, P., S. Dechsupa, J. Meesungnoen, C. Loetchutinat, and S. Mankhetkorn, 2003, Rhodamine B as a mitochondrial probe for measurement and monitoring of mitochondrial membrane potential in drug-sensitive and -resistant cells: *J Biochem Biophys Methods*, v. 57, p. 1-16.
- Richards, K. E., A. E. Zeleniak, M. L. Fishel, J. Wu, L. E. Littlepage, and R. Hill, 2017, Cancer-associated fibroblast exosomes regulate survival and proliferation of pancreatic cancer cells: *Oncogene*, v. 36, p. 1770-1778.
- Rink, J., E. Ghigo, Y. Kalaidzidis, and M. Zerial, 2005, Rab conversion as a mechanism of progression from early to late endosomes: *Cell*, v. 122, p. 735-49.
- Roberts-Dalton, H. D., A. Cocks, J. M. Falcon-Perez, E. J. Sayers, J. P. Webber, P. Watson, A. Clayton, and A. T. Jones, 2017, Fluorescence labelling of extracellular vesicles using a novel thiol-based strategy for quantitative analysis of cellular delivery and intracellular traffic: *Nanoscale*, v. 9, p. 13693-13706.
- Ronquist, K. G., C. Sanchez, L. Dubois, D. Chioureas, P. Fonseca, A. Larsson, A. Ullén, J. Yachnin, G. Ronquist, and T. Panaretakis, 2016, Energy-requiring uptake

References

- of prostasomes and PC3 cell-derived exosomes into non-malignant and malignant cells: *J Extracell Vesicles*, v. 5, p. 29877.
- Rove, K. O., and E. D. Crawford, 2014, Traditional androgen ablation approaches to advanced prostate cancer: new insights: *Can J Urol*, v. 21, p. 14-21.
- Runz, S., S. Keller, C. Rupp, A. Stoeck, Y. Issa, D. Koensgen, A. Mustea, J. Sehouli, G. Kristiansen, and P. Altevogt, 2007, Malignant ascites-derived exosomes of ovarian carcinoma patients contain CD24 and EpCAM: *Gynecol Oncol*, v. 107, p. 563-71.
- Ruoslahti, E., 1996, RGD and other recognition sequences for integrins: *Annu Rev Cell Dev Biol*, v. 12, p. 697-715.
- Rønnov-Jessen, L., and O. W. Petersen, 1993, Induction of alpha-smooth muscle actin by transforming growth factor-beta 1 in quiescent human breast gland fibroblasts. Implications for myofibroblast generation in breast neoplasia: *Lab Invest*, v. 68, p. 696-707.
- Rønnov-Jessen, L., O. W. Petersen, and M. J. Bissell, 1996, Cellular changes involved in conversion of normal to malignant breast: importance of the stromal reaction: *Physiol Rev*, v. 76, p. 69-125.
- Sabharanjak, S., P. Sharma, R. G. Parton, and S. Mayor, 2002, GPI-anchored proteins are delivered to recycling endosomes via a distinct cdc42-regulated, clathrin-independent pinocytotic pathway: *Dev Cell*, v. 2, p. 411-23.
- Safaei, R., B. J. Larson, T. C. Cheng, M. A. Gibson, S. Otani, W. Naerdemann, and S. B. Howell, 2005, Abnormal lysosomal trafficking and enhanced exosomal export of cisplatin in drug-resistant human ovarian carcinoma cells: *Mol Cancer Ther*, v. 4, p. 1595-604.
- Sagar, G., R. P. Sah, N. Javeed, S. K. Dutta, T. C. Smyrk, J. S. Lau, N. Giorgadze, T. Tchkonja, J. L. Kirkland, S. T. Chari, and D. Mukhopadhyay, 2016, Pathogenesis of pancreatic cancer exosome-induced lipolysis in adipose tissue: *Gut*, v. 65, p. 1165-74.
- Salehi, M., and M. Sharifi, 2018, Exosomal miRNAs as novel cancer biomarkers: Challenges and opportunities: *J Cell Physiol*, v. 233, p. 6370-6380.
- Samaeekia, R., B. Rabiee, I. Putra, X. Shen, Y. J. Park, P. Hematti, M. Eslani, and A. R. Djalilian, 2018, Effect of Human Corneal Mesenchymal Stromal Cell-derived Exosomes on Corneal Epithelial Wound Healing: *Invest Ophthalmol Vis Sci*, v. 59, p. 5194-5200.
- Samuel, P., L. A. Mulcahy, F. Furlong, H. O. McCarthy, S. A. Brooks, M. Fabbri, R. C. Pink, and D. R. F. Carter, 2018, Cisplatin induces the release of extracellular vesicles from ovarian cancer cells that can induce invasiveness and drug resistance in bystander cells: *Philos Trans R Soc Lond B Biol Sci*, v. 373.
- Sansone, P., C. Savini, I. Kurelac, Q. Chang, L. B. Amato, A. Strillacci, A. Stepanova, L. Iommarini, C. Mastroleo, L. Daly, A. Galkin, B. K. Thakur, N. Soplop, K. Uryu, A. Hoshino, L. Norton, M. Bonafé, M. Cricca, G. Gasparre, D. Lyden, and J. Bromberg, 2017a, Packaging and transfer of mitochondrial DNA via exosomes regulate escape from dormancy in hormonal therapy-resistant breast cancer: *Proc Natl Acad Sci U S A*, v. 114, p. E9066-E9075.
- Sansone, P., C. Savini, I. Kurelac, Q. Chang, L. B. Amato, A. Strillacci, A. Stepanova, L. Iommarini, C. Mastroleo, L. Daly, A. Galkin, B. K. Thakur, N. Soplop, K. Uryu, A. Hoshinob, L. Norton, M. Bonafé, M. Cricca, G. Gasparre, D. Lyden, and J. Bromberg, 2017b, Packaging and transfer of mitochondrial DNA via exosomes regulate escape from dormancy in hormonal therapy-resistant breast cancer: *Proc Natl Acad Sci U S A*, v. 114, p. E9066-E9075.

References

- Sheldon, H., E. Heikamp, H. Turley, R. Dragovic, P. Thomas, C. E. Oon, R. Leek, M. Edelmann, B. Kessler, R. C. Sainson, I. Sargent, J. L. Li, and A. L. Harris, 2010, New mechanism for Notch signaling to endothelium at a distance by Delta-like 4 incorporation into exosomes: *Blood*, v. 116, p. 2385-94.
- Shelke, G. V., C. Lässer, Y. S. Ghossein, and J. Lötvald, 2014, Importance of exosome depletion protocols to eliminate functional and RNA-containing extracellular vesicles from fetal bovine serum: *J Extracell Vesicles*, v. 3.
- Shree, T., O. C. Olson, B. T. Elie, J. C. Kester, A. L. Garfall, K. Simpson, K. M. Bell-McGuinn, E. C. Zabor, E. Brogi, and J. A. Joyce, 2011, Macrophages and cathepsin proteases blunt chemotherapeutic response in breast cancer: *Genes Dev*, v. 25, p. 2465-79.
- Singh, A., C. Fedele, H. Lu, M. T. Nevalainen, J. H. Keen, and L. R. Languino, 2016, Exosome-mediated Transfer of $\alpha\beta 3$ Integrin from Tumorigenic to Nontumorigenic Cells Promotes a Migratory Phenotype: *Mol Cancer Res*, v. 14, p. 1136-1146.
- Singh, P. P., L. Li, and J. S. Schorey, 2015, Exosomal RNA from *Mycobacterium tuberculosis*-Infected Cells Is Functional in Recipient Macrophages: *Traffic*, v. 16, p. 555-71.
- Skog, J., T. Würdinger, S. van Rijn, D. H. Meijer, L. Gainche, M. Sena-Esteves, W. T. Curry, B. S. Carter, A. M. Krichevsky, and X. O. Breakefield, 2008, Glioblastoma microvesicles transport RNA and proteins that promote tumour growth and provide diagnostic biomarkers: *Nat Cell Biol*, v. 10, p. 1470-6.
- Skotland, T., N. P. Hessvik, K. Sandvig, and A. Llorente, 2019, Exosomal lipid composition and the role of ether lipids and phosphoinositides in exosome biology: *J Lipid Res*, v. 60, p. 9-18.
- Soo, C. Y., Y. Song, Y. Zheng, E. C. Campbell, A. C. Riches, F. Gunn-Moore, and S. J. Powis, 2012, Nanoparticle tracking analysis monitors microvesicle and exosome secretion from immune cells: *Immunology*, v. 136, p. 192-7.
- Stamey, T. A., N. Yang, A. R. Hay, J. E. McNeal, F. S. Freiha, and E. Redwine, 1987, Prostate-specific antigen as a serum marker for adenocarcinoma of the prostate: *N Engl J Med*, v. 317, p. 909-16.
- Stenmark, H., 2009, Rab GTPases as coordinators of vesicle traffic: *Nat Rev Mol Cell Biol*, v. 10, p. 513-25.
- Stone, K. R., D. D. Mickey, H. Wunderli, G. H. Mickey, and D. F. Paulson, 1978, Isolation of a human prostate carcinoma cell line (DU 145): *Int J Cancer*, v. 21, p. 274-81.
- Stoorvogel, W., G. J. Strous, H. J. Geuze, V. Oorschot, and A. L. Schwartz, 1991, Late endosomes derive from early endosomes by maturation: *Cell*, v. 65, p. 417-27.
- Svensson, K. J., H. C. Christianson, A. Wittrup, E. Bourseau-Guilmain, E. Lindqvist, L. M. Svensson, M. Mörgelin, and M. Belting, 2013, Exosome uptake depends on ERK1/2-heat shock protein 27 signaling and lipid Raft-mediated endocytosis negatively regulated by caveolin-1: *J Biol Chem*, v. 288, p. 17713-24.
- Swanson, J. A., 2008, Shaping cups into phagosomes and macropinosomes: *Nat Rev Mol Cell Biol*, v. 9, p. 639-49.
- Tannock, I. F., R. de Wit, W. R. Berry, J. Horti, A. Pluzanska, K. N. Chi, S. Oudard, C. Théodore, N. D. James, I. Turesson, M. A. Rosenthal, M. A. Eisenberger, and T. Investigators, 2004, Docetaxel plus prednisone or mitoxantrone plus prednisone for advanced prostate cancer: *N Engl J Med*, v. 351, p. 1502-12.

- ThermoFisher-Scientific, Nucleic Acid Stains - Section 8.1.
- ThermoFisher-Scientific, 2004, SYTO RNASelect Green Fluorescent Cell Stain, Online.
- ThermoFisher-Scientific, 2019, Alexa Fluor™ 488 C 5 Maleimide.
- Théry, C., S. Amigorena, G. Raposo, and A. Clayton, 2006, Isolation and characterization of exosomes from cell culture supernatants and biological fluids: *Curr Protoc Cell Biol*, v. Chapter 3, p. Unit 3.22.
- Théry, C., M. Boussac, P. Véron, P. Ricciardi-Castagnoli, G. Raposo, J. Garin, and S. Amigorena, 2001, Proteomic analysis of dendritic cell-derived exosomes: a secreted subcellular compartment distinct from apoptotic vesicles: *J Immunol*, v. 166, p. 7309-18.
- Théry, C., A. Regnault, J. Garin, J. Wolfers, L. Zitvogel, P. Ricciardi-Castagnoli, G. Raposo, and S. Amigorena, 1999, Molecular characterization of dendritic cell-derived exosomes. Selective accumulation of the heat shock protein hsc73: *J Cell Biol*, v. 147, p. 599-610.
- Théry, C., K. W. Witwer, E. Aikawa, M. J. Alcaraz, J. D. Anderson, R. Andriantsitohaina, A. Antoniou, T. Arab, F. Archer, G. K. Atkin-Smith, D. C. Ayre, J.-M. Bach, D. Bachurski, H. Baharvand, L. Balaj, S. Baldacchino, N. N. Bauer, A. A. Baxter, M. Bebawy, C. Beckham, A. Bedina Zavec, A. Benmoussa, A. C. Berardi, P. Bergese, E. Bielska, C. Blenkiron, S. Bobis-Wozowicz, E. Boilard, W. Boireau, A. Bongiovanni, F. E. Borràs, S. Bosch, C. M. Boulanger, X. Breakefield, A. M. Breglio, M. Á. Brennan, D. R. Brigstock, A. Brisson, M. L. D. Broekman, J. F. Bromberg, P. Bryl-Górecka, S. Buch, A. H. Buck, D. Burger, S. Busatto, D. Buschmann, B. Bussolati, E. I. Buzás, J. B. Byrd, G. Camussi, D. R. F. Carter, S. Caruso, L. W. Chamley, Y.-T. Chang, C. Chen, S. Chen, L. Cheng, A. R. Chin, A. Clayton, S. P. Clerici, A. Cocks, E. Cocucci, R. J. Coffey, A. Cordeiro-da-Silva, Y. Couch, F. A. W. Coumans, B. Coyle, R. Crescitelli, M. F. Criado, C. D'Souza-Schorey, S. Das, A. Datta Chaudhuri, P. de Candia, E. F. De Santana, O. De Wever, H. A. del Portillo, T. Demaret, S. Deville, A. Devitt, B. Dhondt, D. Di Vizio, L. C. Dieterich, V. Dolo, A. P. Dominguez Rubio, M. Dominici, M. R. Dourado, T. A. P. Driedonks, F. V. Duarte, H. M. Duncan, R. M. Eichenberger, K. Ekström, S. El Andaloussi, C. Elie-Caille, U. Erdbrügger, J. M. Falcón-Pérez, F. Fatima, J. E. Fish, M. Flores-Bellver, A. Försonits, A. Frelet-Barrand, et al., 2018, Minimal information for studies of extracellular vesicles 2018 (MISEV2018): a position statement of the International Society for Extracellular Vesicles and update of the MISEV2014 guidelines: *Journal of Extracellular Vesicles*, v. 7, p. 1535750.
- Tian, J. Y., F. J. Guo, G. Y. Zheng, and A. Ahmad, 2018, Prostate cancer: updates on current strategies for screening, diagnosis and clinical implications of treatment modalities: *Carcinogenesis*, v. 39, p. 307-317.
- Tian, T., Y. Wang, H. Wang, Z. Zhu, and Z. Xiao, 2010, Visualizing of the cellular uptake and intracellular trafficking of exosomes by live-cell microscopy: *J Cell Biochem*, v. 111, p. 488-96.
- Tian, T., Y. L. Zhu, F. H. Hu, Y. Y. Wang, N. P. Huang, and Z. D. Xiao, 2013, Dynamics of exosome internalization and trafficking: *J Cell Physiol*, v. 228, p. 1487-95.
- Tian, T., Y. L. Zhu, Y. Y. Zhou, G. F. Liang, Y. Y. Wang, F. H. Hu, and Z. D. Xiao, 2014a, Exosome uptake through clathrin-mediated endocytosis and macropinocytosis and mediating miR-21 delivery: *J Biol Chem*, v. 289, p. 22258-67.

References

- Tian, Y., S. Li, J. Song, T. Ji, M. Zhu, G. J. Anderson, J. Wei, and G. Nie, 2014b, A doxorubicin delivery platform using engineered natural membrane vesicle exosomes for targeted tumor therapy: *Biomaterials*, v. 35, p. 2383-90.
- Tkach, M., and C. Théry, 2016, Communication by Extracellular Vesicles: Where We Are and Where We Need to Go: *Cell*, v. 164, p. 1226-1232.
- Tomasek, J. J., G. Gabbiani, B. Hinz, C. Chaponnier, and R. A. Brown, 2002, Myofibroblasts and mechano-regulation of connective tissue remodelling: *Nat Rev Mol Cell Biol*, v. 3, p. 349-63.
- Trajkovic, K., C. Hsu, S. Chiantia, L. Rajendran, D. Wenzel, F. Wieland, P. Schwille, B. Brügger, and M. Simons, 2008, Ceramide triggers budding of exosome vesicles into multivesicular endosomes: *Science*, v. 319, p. 1244-7.
- Trams, E. G., C. J. Lauter, N. Salem, and U. Heine, 1981, Exfoliation of membrane ecto-enzymes in the form of micro-vesicles: *Biochim Biophys Acta*, v. 645, p. 63-70.
- Tuxhorn, J. A., G. E. Ayala, and D. R. Rowley, 2001, Reactive stroma in prostate cancer progression: *J Urol*, v. 166, p. 2472-83.
- Tuxhorn, J. A., G. E. Ayala, M. J. Smith, V. C. Smith, T. D. Dang, and D. R. Rowley, 2002, Reactive stroma in human prostate cancer: induction of myofibroblast phenotype and extracellular matrix remodeling: *Clin Cancer Res*, v. 8, p. 2912-23.
- Ullal, A. J., D. S. Pisetsky, and C. F. Reich, 2010, Use of SYTO 13, a fluorescent dye binding nucleic acids, for the detection of microparticles in in vitro systems: *Cytometry A*, v. 77, p. 294-301.
- Vader, P., E. A. Mol, G. Pasterkamp, and R. M. Schiffelers, 2016, Extracellular vesicles for drug delivery: *Adv Drug Deliv Rev*, v. 106, p. 148-156.
- Valadi, H., K. Ekström, A. Bossios, M. Sjöstrand, J. J. Lee, and J. O. Lötvall, 2007, Exosome-mediated transfer of mRNAs and microRNAs is a novel mechanism of genetic exchange between cells: *Nat Cell Biol*, v. 9, p. 654-9.
- Van Deun, J., P. Mestdagh, R. Sormunen, V. Cocquyt, K. Vermaelen, J. Vandesompele, M. Bracke, O. De Wever, and A. Hendrix, 2014, The impact of disparate isolation methods for extracellular vesicles on downstream RNA profiling: *J Extracell Vesicles*, v. 3.
- van Niel, G., G. Raposo, C. Candalh, M. Boussac, R. Hershberg, N. Cerf-Bensussan, and M. Heyman, 2001, Intestinal epithelial cells secrete exosome-like vesicles: *Gastroenterology*, v. 121, p. 337-49.
- Vercauteren, D., M. Piest, L. J. van der Aa, M. Al Soraj, A. T. Jones, J. F. Engbersen, S. C. De Smedt, and K. Braeckmans, 2011, Flotillin-dependent endocytosis and a phagocytosis-like mechanism for cellular internalization of disulfide-based poly(amido amine)/DNA polyplexes: *Biomaterials*, v. 32, p. 3072-84.
- Vercauteren, D., R. E. Vandenbroucke, A. T. Jones, J. Rejman, J. Demeester, S. C. De Smedt, N. N. Sanders, and K. Braeckmans, 2010, The use of inhibitors to study endocytic pathways of gene carriers: optimization and pitfalls: *Mol Ther*, v. 18, p. 561-9.
- Verona, E. V., A. G. Elkahloun, J. Yang, A. Bandyopadhyay, I. T. Yeh, and L. Z. Sun, 2007, Transforming growth factor-beta signaling in prostate stromal cells supports prostate carcinoma growth by up-regulating stromal genes related to tissue remodeling: *Cancer Res*, v. 67, p. 5737-46.
- Verweij, F. J., M. P. Bebelman, C. R. Jimenez, J. J. Garcia-Vallejo, H. Janssen, J. Neefjes, J. C. Knol, R. de Goeij-de Haas, S. R. Piersma, S. R. Baglio, M. Verhage, J. M. Middeldorp, A. Zomer, J. van Rheenen, M. G. Coppolino, I. Hurbain, G. Raposo, M. J. Smit, R. F. G. Toonen, G. van Niel, and D. M. Pegtel, 2018,

References

- Quantifying exosome secretion from single cells reveals a modulatory role for GPCR signaling: *J Cell Biol*, v. 217, p. 1129-1142.
- Wang, M., J. Zhao, L. Zhang, F. Wei, Y. Lian, Y. Wu, Z. Gong, S. Zhang, J. Zhou, K. Cao, X. Li, W. Xiong, G. Li, Z. Zeng, and C. Guo, 2017, Role of tumor microenvironment in tumorigenesis: *J Cancer*, v. 8, p. 761-773.
- Wang, R., Q. Ding, U. Yaqoob, T. M. de Assuncao, V. K. Verma, P. Hirsova, S. Cao, D. Mukhopadhyay, R. C. Huebert, and V. H. Shah, 2015, Exosome Adherence and Internalization by Hepatic Stellate Cells Triggers Sphingosine 1-Phosphate-dependent Migration: *J Biol Chem*, v. 290, p. 30684-96.
- Webber, J., and A. Clayton, 2013, How pure are your vesicles?: *J Extracell Vesicles*, v. 2.
- Webber, J., R. Steadman, M. D. Mason, Z. Tabi, and A. Clayton, 2010, Cancer exosomes trigger fibroblast to myofibroblast differentiation: *Cancer Res*, v. 70, p. 9621-30.
- Webber, J., T. C. Stone, E. Katilius, B. C. Smith, B. Gordon, M. D. Mason, Z. Tabi, I. A. Brewis, and A. Clayton, 2014, Proteomics analysis of cancer exosomes using a novel modified aptamer-based array (SOMAscan™) platform: *Mol Cell Proteomics*, v. 13, p. 1050-64.
- Webber, J., V. Yeung, and A. Clayton, 2015a, Extracellular vesicles as modulators of the cancer microenvironment: *Semin Cell Dev Biol*, v. 40, p. 27-34.
- Webber, J. P., L. K. Spary, A. J. Sanders, R. Chowdhury, W. G. Jiang, R. Steadman, J. Wymant, A. T. Jones, H. Kynaston, M. D. Mason, Z. Tabi, and A. Clayton, 2015b, Differentiation of tumour-promoting stromal myofibroblasts by cancer exosomes: *Oncogene*, v. 34, p. 290-302.
- Weigelt, B., and M. J. Bissell, 2008, Unraveling the microenvironmental influences on the normal mammary gland and breast cancer: *Semin Cancer Biol*, v. 18, p. 311-21.
- Weston, S. A., and C. R. Parish, 1990, New fluorescent dyes for lymphocyte migration studies. Analysis by flow cytometry and fluorescence microscopy: *J Immunol Methods*, v. 133, p. 87-97.
- Wieckowski, E. U., C. Visus, M. Szajnik, M. J. Szczepanski, W. J. Storkus, and T. L. Whiteside, 2009, Tumor-derived microvesicles promote regulatory T cell expansion and induce apoptosis in tumor-reactive activated CD8+ T lymphocytes: *J Immunol*, v. 183, p. 3720-30.
- Witkowski, C. M., I. Rabinovitz, R. B. Nagle, K. S. Affinito, and A. E. Cress, 1993, Characterization of integrin subunits, cellular adhesion and tumorigenicity of four human prostate cell lines: *J Cancer Res Clin Oncol*, v. 119, p. 637-44.
- Wolf, T., S. R. Baier, and J. Zempleni, 2015, The Intestinal Transport of Bovine Milk Exosomes Is Mediated by Endocytosis in Human Colon Carcinoma Caco-2 Cells and Rat Small Intestinal IEC-6 Cells: *J Nutr*, v. 145, p. 2201-6.
- Wolfers, J., A. Lozier, G. Raposo, A. Regnault, C. Théry, C. Masurier, C. Flament, S. Pouzieux, F. Faure, T. Tursz, E. Angevin, S. Amigorena, and L. Zitvogel, 2001, Tumor-derived exosomes are a source of shared tumor rejection antigens for CTL cross-priming: *Nat Med*, v. 7, p. 297-303.
- Wubbolts, R., R. S. Leckie, P. T. Veenhuizen, G. Schwarzmann, W. Möbius, J. Hoernschemeyer, J. W. Slot, H. J. Geuze, and W. Stoorvogel, 2003, Proteomic and biochemical analyses of human B cell-derived exosomes. Potential implications for their function and multivesicular body formation: *J Biol Chem*, v. 278, p. 10963-72.
- Wymann, M. P., G. Bulgarelli-Leva, M. J. Zvelebil, L. Pirola, B. Vanhaesebroeck, M. D. Waterfield, and G. Panayotou, 1996, Wortmannin inactivates

References

- phosphoinositide 3-kinase by covalent modification of Lys-802, a residue involved in the phosphate transfer reaction: *Mol Cell Biol*, v. 16, p. 1722-33.
- Xin, X., S. Yang, G. Ingle, C. Zlot, L. Rangell, J. Kowalski, R. Schwall, N. Ferrara, and M. E. Gerritsen, 2001, Hepatocyte growth factor enhances vascular endothelial growth factor-induced angiogenesis in vitro and in vivo: *Am J Pathol*, v. 158, p. 1111-20.
- Yamada, H., T. Abe, S. A. Li, Y. Masuoka, M. Isoda, M. Watanabe, Y. Nasu, H. Kumon, A. Asai, and K. Takei, 2009, Dynasore, a dynamin inhibitor, suppresses lamellipodia formation and cancer cell invasion by destabilizing actin filaments: *Biochem Biophys Res Commun*, v. 390, p. 1142-8.
- Yamada, H., T. Takeda, H. Michiue, T. Abe, and K. Takei, 2016, Actin bundling by dynamin 2 and cortactin is implicated in cell migration by stabilizing filopodia in human non-small cell lung carcinoma cells: *Int J Oncol*, v. 49, p. 877-86.
- Yanagisawa, N., R. Li, D. Rowley, H. Liu, D. Kadmon, B. J. Miles, T. M. Wheeler, and G. E. Ayala, 2007, Stromogenic prostatic carcinoma pattern (carcinomas with reactive stromal grade 3) in needle biopsies predicts biochemical recurrence-free survival in patients after radical prostatectomy: *Hum Pathol*, v. 38, p. 1611-20.
- Yeo, R. W., R. C. Lai, B. Zhang, S. S. Tan, Y. Yin, B. J. Teh, and S. K. Lim, 2013, Mesenchymal stem cell: an efficient mass producer of exosomes for drug delivery: *Adv Drug Deliv Rev*, v. 65, p. 336-41.
- Yeung, V., J. P. Webber, E. A. Dunlop, H. Morgan, J. Hutton, M. Gurney, E. Jones, J. Falcon-Perez, Z. Tabi, R. Errington, and A. Clayton, 2018, Rab35-dependent extracellular nanovesicles are required for induction of tumour supporting stroma: *Nanoscale*, v. 10, p. 8547-8559.
- Yim, N., S. W. Ryu, K. Choi, K. R. Lee, S. Lee, H. Choi, J. Kim, M. R. Shaker, W. Sun, J. H. Park, D. Kim, W. D. Heo, and C. Choi, 2016, Exosome engineering for efficient intracellular delivery of soluble proteins using optically reversible protein-protein interaction module: *Nat Commun*, v. 7, p. 12277.
- Yu, X., S. L. Harris, and A. J. Levine, 2006, The regulation of exosome secretion: a novel function of the p53 protein: *Cancer Res*, v. 66, p. 4795-801.
- Yáñez-Mó, M., P. R. Siljander, Z. Andreu, A. B. Zavec, F. E. Borràs, E. I. Buzas, K. Buzas, E. Casal, F. Cappello, J. Carvalho, E. Colás, A. Cordeiro-da Silva, S. Fais, J. M. Falcon-Perez, I. M. Ghobrial, B. Giebel, M. Gimona, M. Graner, I. Gursel, M. Gursel, N. H. Heegaard, A. Hendrix, P. Kierulf, K. Kokubun, M. Kosanovic, V. Kralj-Iglic, E. M. Krämer-Albers, S. Laitinen, C. Lässer, T. Lener, E. Ligeti, A. Linē, G. Lipps, A. Llorente, J. Lötval, M. Manček-Keber, A. Marcilla, M. Mittelbrunn, I. Nazarenko, E. N. Nolte-'t Hoen, T. A. Nyman, L. O'Driscoll, M. Olivan, C. Oliveira, É. Pállinger, H. A. Del Portillo, J. Reventós, M. Rigau, E. Rohde, M. Sammar, F. Sánchez-Madrid, N. Santarém, K. Schallmoser, M. S. Ostenfeld, W. Stoorvogel, R. Stukelj, S. G. Van der Grein, M. H. Vasconcelos, M. H. Wauben, and O. De Wever, 2015, Biological properties of extracellular vesicles and their physiological functions: *J Extracell Vesicles*, v. 4, p. 27066.
- Zabeo, D., A. Cvjetkovic, C. Lässer, M. Schorb, J. Lötval, and J. L. Höög, 2017, Exosomes purified from a single cell type have diverse morphology: *J Extracell Vesicles*, v. 6, p. 1329476.
- Zech, D., S. Rana, M. W. Büchler, and M. Zöller, 2012, Tumor-exosomes and leukocyte activation: an ambivalent crosstalk: *Cell Commun Signal*, v. 10, p. 37.

References

- Zeisberg, E. M., S. Potenta, L. Xie, M. Zeisberg, and R. Kalluri, 2007, Discovery of endothelial to mesenchymal transition as a source for carcinoma-associated fibroblasts: *Cancer Res*, v. 67, p. 10123-8.
- Zhou, W., M. Y. Fong, Y. Min, G. Somlo, L. Liu, M. R. Palomares, Y. Yu, A. Chow, S. T. O'Connor, A. R. Chin, Y. Yen, Y. Wang, E. G. Marcusson, P. Chu, J. Wu, X. Wu, A. X. Li, Z. Li, H. Gao, X. Ren, M. P. Boldin, P. C. Lin, and S. E. Wang, 2014, Cancer-secreted miR-105 destroys vascular endothelial barriers to promote metastasis: *Cancer Cell*, v. 25, p. 501-15.
- Zhu, W., L. Huang, Y. Li, X. Zhang, J. Gu, Y. Yan, X. Xu, M. Wang, H. Qian, and W. Xu, 2012, Exosomes derived from human bone marrow mesenchymal stem cells promote tumor growth in vivo: *Cancer Lett*, v. 315, p. 28-37.
- Zitvogel, L., A. Regnault, A. Lozier, J. Wolfers, C. Flament, D. Tenza, P. Ricciardi-Castagnoli, G. Raposo, and S. Amigorena, 1998, Eradication of established murine tumors using a novel cell-free vaccine: dendritic cell-derived exosomes: *Nat Med*, v. 4, p. 594-600.